Faculty of Science and Engineering,
Department of Chemistry

Novel Techniques in Organic Geochemistry applied to Australian Resources

Hendrik Grotheer

This thesis is presented for the Degree of
Doctor of Philosophy
of
Curtin University

January 2017

Declaration

To the best of my knowledge and belief this thesis contains no material previously published by any other person except where due acknowledgement has been made.
This thesis contains no material that has been accepted for the award of any other degree or diploma in any University.

Hendrik Grotheer
Bremen, March 23, 2017

Abstract

Organic geochemistry has evolved with continual technological and analytical advancements which have increased the window through which we can explore carbon cycles and organic processes of the past. This process has enabled a more robust investigation of the Earth's history and the evolution of life on it. We now also have a greater understanding of the global nexus between the biosphere and the geosphere. Underpinning this progress has been much application development with new analytical instruments and methods and evaluation of their reliability, including robust scrutiny of any subjectivity or limitations. The present research project shows such concern for the organic geochemical application of several new analytical technologies including the use of novel biomarkers to reconstruct microbial dynamics during past periods of ecological stress and subsequent recovery, and sophisticated instruments which recently became available commercially (hydropyrolysis) or as prototype assemblies (compound specific sulfur isotope analysis).

Hydropyrolysis (HyPy) and compound specific sulfur isotope analysis (CS-S-IA) of organosulfur compounds (OSC) were used to help characterise the organic sulfur of selected organic sediments from geologic sections reflecting dynamic periods of the Earth's evolution and the deposition of valuable hydrocarbon or mineral resources. A commercial HyPy facility was evaluated for its capability to access the sequestered PAH composition of high maturity OM associated with high temperature mineral deposits (e.g., orogenic Au-deposits), and to assist the δ^{34}S measurement of OSCs in these systems and sediments representative of other S-dynamic paleoenvironments. The new analytical capability of continuous-flow sulfur isotope analysis was used to measure δ^{34}S values of sediment-hosted OSCs and to investigate the isotopic impacts on organic S during times of great environmental stress and changes to the global C- and S-cycle (e.g., the Permian-Triassic extinction).

In **Chapter 2** a series of HyPy experiments were conducted on a small suite of authentic polycyclic aromatic hydrocarbons (PAHs; coronene, pyrene and perylene) to investigate the HyPy behaviour of PAH compounds. The results helped to assess the structural significance of aromatic products previously detected by HyPy analysis of metamorphosed kerogens associated with high temperature orogenic Au-deposits. HyPy treated PAH compounds were all varyingly prone to structural hydrogenation. Perylene was observed to be much less stable to the HyPy conditions than more con-

densed PAHs (i.e. coronene and pyrene) and decomposed to low molecular weight aromatic products. Total product concentrations (wt.% of starting PAH) from all HyPy experiments were consistently less than 100 wt.%, probably due to either the condensation of semi-volatile products on walls of the transfer line prior to reaching the HyPy trap or the inefficient cold trapping of highly volatile products – and reflect the challenges of mass balance evaluation of HyPy experiments. The hydrogenation of PAHs was prevalent and very sensitive to the addition of a Mo-S based catalyst, but end temperatures of either 520 °C or 550 °C showed little difference. Fully aromatised and hydrogenated products for any stable ring system can provide a general indication of the size distribution of aromatic units within highly mature kerogen structures.

CS-S-IA of OSCs has the potential to provide great advancements in the field of S-biogeochemistry and in paleoenvironmental reconstructions. However, sample throughput and quality of isotopic information obtained by the newly developed gas chromatography inductively coupled plasma mass spectrometry (GC-ICP-MS) approach is dependent on a number of factors including sample treatment, analytical conditions and subsequent processing of the mass spectral signals measured. The laborious processing of Neptune$^+$ raw data requires it to be exported to a data processing package such as Microsoft Excel, MatLab or ThermoFisher IsoDat. In **Chapter 3** a routine procedure for the auto-processing of raw Neptune$^+$ signals to δ^{34}S values was developed to speed data processing time and also overcome user induced biases and uncertainties. The favourable performance of the auto-processing system was evaluated on standard laboratory samples.

Chapter 4 presents the integration of HyPy to release kerogen bound OSCs and GC-ICP-MS to measure their stable S-isotopic composition. The effect of HyPy on the δ^{34}S signature of an authentic dibenzothiophene (DBT) standard was tested and showed negligible fractionation during the hydropyrolysis process. The HyPy treatment of two S-rich, oil-mature kerogens from different geologic settings (Permian-Triassic Hovea-3 well, Perth Basin, Western Australia; Late Cretaceous Toolebuc Formation, Queensland) released significantly higher concentrations of OSCs compared to their free occurrence in the corresponding bitumen fractions. Kerogen bound DBT and methyldibenzothiophenes (mDBTs) showed a distinct ^{34}S depletion, with δ^{34}S values up to 12 ‰ lighter, compared to their bitumen occurrence. Isotopically distinct kerogen and bitumen fractions likely reflect differences in timing of production, reduced sulfur sources or organic sulfurisation mechanism.

The Permian Triassic (P-Tr) mass extinction, the greatest of such events during the Phanerozoic, was caused by catastrophic environmental stress and major changes to the global C- and S-cycle. **Chapter 5** presents the first description of the δ^{34}S evolution of OSCs during this time in Earth's history, and correlates it with the δ^{34}S of total organic sulfur (i.e., represented by the kerogen fraction of the sediment) and the δ^{34}S of total

inorganic sulfur (i.e., total reducible inorganic sulfur; TRIS). A suite of sedimentary rocks spanning the Permian Triassic Boundary (PTB) at the Global Stratotype and Point Section (GSSP) in Meishan-1 (South China) and Hovea-3 (Perth Basin, Western Australia) were analysed. Distinct δ^{34}S variations between kerogen S and individual OSCs (e.g., DBTs) reflect the occurrence of multiple pools of isotopically distinct organic sulfur within the sediments. Further, the Meishan-1 δ^{34}S profiles suggested a kinetic relationship between organic sulfurisation and inorganic sulfidisation processes during times of low S-flux. In contrast, Hovea-3 reflected a high S-flux system and evidence for isotopic exchange between organic and inorganic S-pools. This further suggests, that TRIS and OSCs were sensitive to water column conditions or local basin environmental controls. At Meishan-1 fluctuation in δ^{34}S values indicate the onset of an event horizon caused by a complex combination of geologic processes leading up to the P-Tr extinction, whereas in Hovea-3 S isotopic variations were related to progressive oxygen depletion to euxinic water column conditions.

Environmental stresses during the P-Tr extinction gave rise to the development of unique microbial communities during the later recovery phase that left distinctive biomarker traces in global rock records. In **Chapter 6** two of these biomarkers (phytanyl benzene and phytanyl toluene) were identified in mudstones from several key P-Tr extinction horizons from mid-northern palaeolatitudes (Spitsbergen and Eastern Greenland), as well as mid-southern palaeolatitudes (Hovea-3 well, Western Australia), but notably not from the Meishan section (South China). Their occurrence was related to the presence of C_{33} *n*-alkyl cyclohexane, suggesting their parent organisms shared a similar ecological niche. Furthermore, their detection at mid-southern and -northern hemisphere localities suggest a widespread occurrence during the recovery. Yet, these compounds were not detected in the carbonate-dominated palaeoequatorial Meishan-1 section which suggests a temperature or climate control on their source.

Acknowledgments

First of all, I want to thank my family and friends back home, especially my parents Gudrun and Bruno for their unconditional believe in me, their support during this challenging journey and always having been the safe haven I needed to refill my energy.

Special thanks to Prof. Kliti Grice, for being my supervisor, helpful meetings, scientific guidance and feedback throughout this PhD. I further want to thank Kliti for giving me the opportunity and funding to attend conferences in Sacramento (Goldschmidt 2014), Boston (GRC 2014), Adelaide (AOGC 2014) and Prague (IMOG 2015). Sincere thanks to A/Prof Paul Greenwood. Paul was not just my supervisor, he always tried to make me feel home in Australia, shared ice-cold beers in warm summer days, did his best to share his passion for Australian Football (did not work) and always provided good and warm advice, not always work related. Thank you for the productive, sometimes intense discussions and most of all for your countless and vital edits on manuscripts, abstracts, posters, talks and this thesis.

I further want to thank the wonderful people I had the pleasure to work with. The co-authors of my manuscripts: Aileen Robert, Prof. Michael Böttcher, Prof. Malcolm McCulloch, Dr. Matthew Piggott and Prof. Richard Twitchett. The staff and researchers at WA-OIGC: Geoff Chidlow, Peter Hopper, Dr. Alex Holman, Dr. Alan Scarlett, Dr. Svenja Tulipani, Dr. Jeff Dick, Dr. Alison Blyth, Dr. Sabine Lengger, Dr. Robert Lockhart, Dr. Ines Melendez, Dr. Sebastian Naeher, Dr. Anais Pages and Dr. Martijn Woltering. And of course the PhD and honors students that I shared some good times with: Chloe Plet, Robert Clegg, Jaime Cesar Colmenares, Matthew Cambell, Calum Fox, Gemma Spaak, Bettina Schaefer, Nannan He, Shirley Hu, Sureyya Kose, Kuldeep Dilip More and Sharon Shan. The funding for my project has been provided by the CSIRO Organic Geochemistry of Mineral Systems Cluster and the Curtin University Department of Chemistry.

Primary and related Publications

This thesis is assembled by publications, either accepted, published, submitted and in preparation, which form the individual chapters and are listed below.

Chapter 2

Grotheer, Hendrik, Robert, Aileen M., Greenwood, Paul F., Grice, Kliti (2015). Stability and hydrogenation of polycyclic aromatic hydrocarbons during hydropyrolysis (HyPy)– Relevance for high maturity organic matter. *Organic Geochemistry*, 86, pp. 45 - 54

Chapter 4

Grotheer, Hendrik, Greenwood, Paul F., McCulloch, Malcolm, Böttcher, Michael E., Grice, Kliti (*in review*). δ^{34}S character of organosulfur compounds in kerogen and bitumen fractions of sedimentary rocks. *Organic Geochemistry*

Chapter 5

Grotheer, Hendrik, Greenwood, Paul F., McCulloch, Malcolm, Böttcher, Michael E., Summons, Roger E., Grice, Kliti. Global significance of the sulfur isotope composition of sedimentary inorganic and organic sulfur phases across the Permian-Triassic transition.

Chapter 6

Grotheer, Hendrik, LeMétayer, Pierre, Piggott, Matthew J., Lindeboom, Erik J., Holman, Alex I., Twitchett, Richard J., Grice, Kliti (2017). Occurrence and significance of phytanyl arenes across the Permian-Triassic boundary interval. *Organic Geochemistry*, 104, pp. 42 - 52

Statement of Contribution of Others

The work presented in this thesis was primarily designed, experimentally executed, interpreted, and individual manuscripts were prepared by the first author (Hendrik Grotheer). Contributions by co-authers are described below.

Chapter 2

Aileen M. Robert assisted with the experiments, Paul F. Greenwood and Kliti Grice assisted with the experimental design and the preperation of the manuscript.

Chapter 4

Macolm T. McCulloch provided the ICP-MS infrastructure and techniqual expertise. Michael E. Böttcher provided C-irmMS data and assisted in the preparation of the manuscript. Paul F. Greenwood and Kliti Grice assisted with the experimental design and the preperation of the manuscript.

Chapter 5

Macolm T. McCulloch provided the ICP-MS infrastructure and techniqual experise. Michael E. Böttcher provided C-irmMS data and assisted in the preparation of the manuscript. Roger E. Summons provided sample material and assisted in the preperation of the manuscript. Paul F. Greenwood and Kliti Grice assisted with the experimental design and the preperation of the manuscript.

Chapter 6

Matthew J. Piggott and Erik J. Lindeboom synthesised the phytanyl arene standards. Pierre LeMétayer and Alex I. Holman assisted with the sample extraction and data

collection. Kliti Grice and Richard J. Twitchett assisted with the experimental design and the preperation of the mansucript.

Secondary Publications

Manuscripts and abstracts based on research that was conducted during the preperation of this thesis.

Peer reviewed journal articles not part of thesis research

Robert, A.M., **Grotheer, H.**, Bourdet, J., Suvorova, A., Grice, K., McCuaig, T.C., Greenwood, P.F. (*in review*). Evidence and origin of the different types of sedimentary organic matter and its implications on Paleoproterozoic orogenic gold mineralisation. *Precambrian Research*

Robert, A.M., **Grotheer, H.**, Greenwood, P.F., McCuaig, T.C., Bourdet, J., Grice K. (2016). The hydropyrolysis (HyPy) release of hydrocarbon products from a high maturity kerogen associated with an orogenic Au deposit and their relationship to the mineral matrix. *Chemical Geology*, 425, pp. 127-144

Conference abstracts

* directly related to this thesis

*__Grotheer, H.__, Greenwood, P.F., Böttcher, M.E., Summons, R.E., Grice, K. (2016). δ^{34}S of DBT, mDBTs and pyrite in the Permian-Triassic boundary. Australian Organic Geochemistry Conference, 4 - 7 December 2016 in Fremantle, Australia. Poster presentation

*__Grotheer, H.__, Robert, A.M., Greenwood, P.F., Grice, K. (2015). Hydrogenation of PAHs by hydropyrolysis (HyPy) – Implications for HyPy analysis of high maturity OM. International Meeting of Organic Geochemistry, 13 - 18 September 2015 in Prague, Czech Republic. Poster presentation

Robert, A.M., **Grotheer, H.**, Greenwood, P.F., Grice, K., McCuaig, T.C. (2015). The mineral matrix effects on hydropyrolysis released hydrocarbon products from high maturity carbonaceous material associated with orogenic Au. International

Meeting of Organic Geochemistry, 13 - 18 September 2015 in Prague, Czech Republic.

Robert, A.M., **Grotheer, H.**, Greenwood, P.F., Schwark, L., Bourdet, J., Grice, K., McCuaig, T.C. (2015). Carbonaceous and Organic Matter in Orogenic Gold (Au) Systems: Investigating the role of organics in Au mineralisation. International Meeting of Organic Geochemistry, 13 - 18 September 2015 in Prague, Czech Republic.

*__Grotheer, H.__, Robert, A.M., Greenwood, P.F., Grice, K. (2014). Hydrogenation of PAHs by hydropyrolysis (HyPy) – Implications for the use of HyPy for geologically old and over mature samples. Australian Organic Geochemistry Conference, 30 November - 2 December 2014 in Adelaide, Australia. Oral presentation

Robert, A.M., **Grotheer, H.**, Greenwood, P.F., Schwark, L., Bourdet, J., Grice, K., Jaraula, J., Bagas, L., McCuaig, T.C. (2014). Carbonaceous and other forms of Organic Matter in Orogenic Gold (Au) Systems: Investigating the role of organics in Au mineralisation. Australian Organic Geochemistry Conference, 30 November - 2 December 2014 in Adelaide, Australia.

Robert, A.M., **Grotheer, H.**, Greenwood, P.F., Schwark, L., Bourdet, J., Grice, K., Jaraula, J., Bagas, L., McCuaig, T.C. (2014). Carbonaceous and Organic Matter in Orogenic Gold (Au) Systems: Investigating the role of organics in Au Mineralisation. Gold14@Kalgoorlie International Symposium, 8-10 October 2014 in Kalgoorlie, Australia.

*__Grotheer, H.__, Robert, A.M., Lockhart, R., Li, K., Large, R., Greenwood, P.F., Dick, J., Yeats, C., Grice, K (2014). The role of Organics in Au Systems: Relationship between Sedimentary Organic Matter, Black Carbon and Mineralisation. Gordon Research Conference/Seminar Organic Geochemistry, 2-8 August 2014 in Holderness, New Hamphsire, USA. Poster/Oral presentation

Robert, A.M., **Grotheer, H.**, Greenwood, P.F., Bourdet, J., McCuaig, T.C., Jaraula, J., Grice, K., Bagas, L., Schwark, L. (2014). Organic and Carbonaceous Matter in Orogenic Gold systems: Investigating the role of organics in Au mineralisation. Gordon Research Conference/Seminar Organic Geochemistry, 2-8 August 2014 in Holderness, New Hamphsire, USA.

Robert, A.M., **Grotheer, H.**, Jaraula, C., McCuaig, T.C., Bagas, L., Greenwood, P.F., Bourdet, J., Schwark, L., Grice, K. (2014). Organic Matter in Orogenic Gold (Au) Systems. Australian Earth Science Convention, 7-10 July 2014 in Newcastle, Australia.

*__Grotheer, H.__, Robert, A.M., Lockhart, R., Greenwood, P.F., Dick, J., Yeats, C., Grice, K (2014). The Role of Organics in Au Systems: Relationships between Black Carbon and Mineralisation. Goldschmidt 2014, 8-13 June 2014 in Sacramento, California, USA. Poster presentation

Robert, A.M., __Grotheer, H.__, Lockhart, R., Greenwood, P.F., McCuaig, T.C., Jaraula, C., Grice, K., Bagas, L., Schwark, L. (2014). Organics in Orogenic Gold Systems: Characterisation of Organic Matter Associated with Gold (Au) Deposits. Goldschmidt 2014, 8-13 June 2014 in Sacramento, California, USA.

List of Figures

List of Tables

Contents

1. Introduction

Organic Geochemistry

Organic geochemistry includes the study of chemical reactions, transformations and the fate of biomolecules or organic matter (OM) deposited in aquatic and terrestrial environments. Major areas of interest include an understanding of the elements and dynamics of the global carbon cycle (past and present); the evolution of our planet and the life it supports, including periods of great stress and adaptation (e.g., mass extinction events); the exploration for petroleum resources which sustain the energy demand of contemporary human societies. Scientific research addressing these interests and indeed the organic geochemistry discipline have largely evolved with the availability of increasingly more powerful analytical methods to characterise the molecular structures or stable isotopic nature of OM. This evolution gained much impetus with the groundbreaking discovery of Eglinton and colleagues in the 1960's that crude oil could be separated into several different hydrocarbon components by pushing it through newly invented chromatography columns. The rather cumbersome packed columns used in these pioneering studies of petroleum composition have evolved into the sophisticated capillary columns of today which are able to resolve oils into thousands of different compounds.

OG is a scientific discipline driven by technological and analytical advancements that almost on a decadal level revolutionise our understanding of the global nexus between the biosphere and the geosphere. This has enabled a more robust investigation and understanding of the Earth's history. The exciting potential of novel analytical techniques often raise hopes for significant scientific discovery, but always need to be carefully tested for their real applicability, their reliability, biases and limitations.

1.1. The global carbon and sulfur cycle

1.1.1. Carbon

The carbon cycle – the transfer of carbon between different carbon-pools on Earth – has been active since the Archean and has been strongly influenced by historical changes in atmospheric and paleooceanic redox conditions (Des Marais, 1997). OM primarily

consists of carbon (C), hydrogen (H), oxygen (O) and in lower abundance nitrogen (N) and sulfur (S), which form the essential elements for all life on Earth. Organic carbon is strongly linked to inorganic carbon, as the majority of organic carbon is fixated through photosynthesis from largely atmospheric CO_2 or dissolved CO_2/HCO_3^- in the photic zones of oceans or lakes. The major sinks and sources of carbon are: i) atmospheric CO_2, ii) biomass; iii) sedimentary OM; iv) petroleum; v) carbonates; vi) dissolved carbon (inorganic and organic) and vii) carbonates that can also be deeply buried in metamorphic rocks and the Earth's mantle (Hedges, 1992; Killops & Killops, 2005).

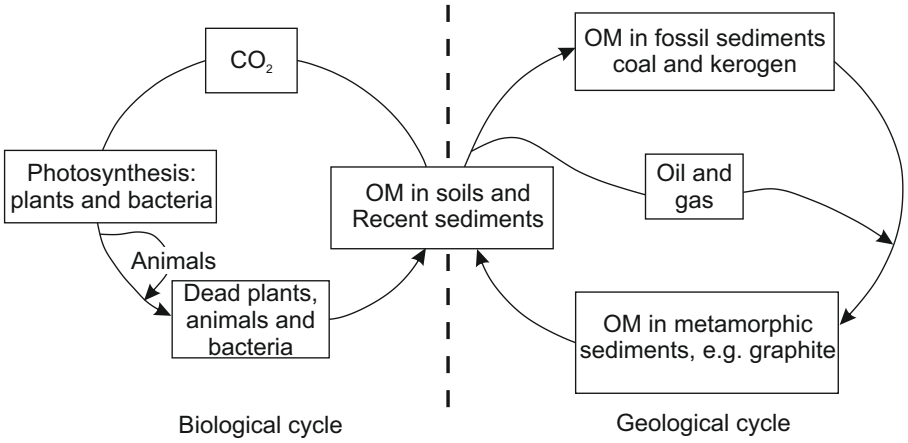

Figure 1.1.: Organic carbon cycle on Earth (redrawn from Tissot and Welte, 1984). OM= Organic matter

The global C-cycle can be divided into two interlinked parts, the biological and the geological C-cycles (Figure 1.1; Tissot & Welte, 1984). The biologic cycle starts with the photosynthetic fixation of CO_2 into biogenic molecules which upon decay of living biomass undergoes metabolic and chemical oxidation back to CO_2. A small fraction of C from the biologic cycle, thus, is buried in sediments and forms the starting point of the geologic C-cycle (Littke *et al.*, 1997). Typically only 0.1 % of biogenic C is geologically preserved in oxic environments (Moodley *et al.*, 2005), but under anoxic and reducing conditions preservation this can be higher than 5 % (Peters *et al.*, 2005a). Burial of the deposited sediments over long geological times leads to the formation of petroleum and coals or over-mature metamorphic forms of C (e.g., graphite or diamond). Geological C may be subsequently returned to CO_2 following erosion of sedimentary rocks or combustion of fossil fuels and once released to the atmosphere becomes available for photosynthesis thus refueling the biologic cycle (Tissot & Welte, 1984). The transformation of biogenic to fossil organic carbon starts with the decay of the living cell and is followed by numerus alterations in the water column or upon deposition on the sea floor or lake bottom, where a broad range of microbes contribute to its degradation and mineralisation (Schulz & Zabel, 2006). The alterations that

OM undergoes in the upper layers of sediments are referred to as diagenesis. During diagenesis the OM undergoes either microbial mediated defunctionalisation and condensation reactions resulting in the formation of macromolecular and organic solvent insoluble OM – i.e. the kerogen fraction (Tissot & Welte, 1984; Vandenbroucke & Largeau, 2007). Alternatively, kerogen formation is partly due to selective preservation of, possibly sulfur cross-linked, biomacromolecules during diagenesis (e.g. Tegelaar *et al.*, 1989; Gelin *et al.*, 1996). The increased temperatures and pressures with burial can result in the catagenic break down of kerogen (Killops & Killops, 2005) leading to the formation of petroleum.

Today, organic geochemists study the closely linked biologic and geologic cycle as it forms the basis for paleoenvironmental reconstructions. Although biomolecules undergo structural changes (e.g., defunctionalisation, saturation, condensation or aromatisation) during sedimentary burial, the carbon skeleton of the biomolecule may be preserved. Fossil molecules found in ancient rocks which resemble their biomolecular precursor(s) are referred to as biomarkers (Peters *et al.*, 2005a; Brocks & Grice, 2011). The occurrence and relative abundances of biomarkers detected in ancient sediments thus allow qualitative interpretations such as the environmental conditions during OM deposition.

1.1.2. Isotope Geochemistry

The stable isotopic measurement of various Earth systems represents a powerful tool for organic geochemists to unravel the global cycle of key elements. Isotopes of a given element have the same number of protons but differ by the number of neutrons per atom. For instance, C has two stable ($^{12}_{6}$C, $^{13}_{6}$C) and 13 known radioactive isotopes (for example $^{14}_{6}$C) each containing 6 protons but any of 6, 7, or 8+ neutrons. S on the other hand has four stable isotopes ($^{32}_{16}$S, $^{33}_{16}$S, $^{34}_{16}$S, $^{36}_{16}$S) each containing 16 protons and 16, 17, 18 or 20 neutrons. C, S, H, O and N isotopes are of particular interest to organic geochemists. The natural abundances of stable isotopes varies for every element, for instance ^{12}C accounts for 98.899 atom % and ^{13}C for only 1.111 atom % (Table 1.1; Hoefs, 2009). The stable isotopes and their natural abundance are listed in Table 1.1. Variations from the natural abundance occur in nature due to isotopic fractionation (ε) during chemical, biological or physical processes (Hoefs, 2009). The magnitude of fractionation can also vary for different compounds, depending on relative bond strengths.

Table 1.1.: The stable isotopes and their natural abundances (in atom %) of the major elements of living systems.

Carbon	Sulfur	Hydrogen	Oxygen	Nitrogen
	^{34}S (4.215)		^{18}O (0.204)	
^{12}C (98.899)	^{32}S (95.018)	^{1}H (99.985)	^{16}O (99.759)	^{14}N (99.963)
^{13}C (1.111)	^{33}S (0.75)	^{2}D (4.215)	^{17}O (0.037)	^{15}N (0.366)
	^{36}S (0.02)			

The stable isotopic composition is expressed as the ratio of two isotopes normalised to the same ratio measured for an international standard. For S the ratio of ^{34}S/^{32}S is normalised to the conventional δ^{34}S notation as a per mil (‰) deviation from the international standard Vienna Canyon Diablo Troilite (VCDT) according to the following equation:

$$\delta^{34}S(‰) = \left(\frac{R_a}{R_s}\right) - 1 \tag{1.1}$$

Where R_a is the ^{34}S/^{32}S ratio of the analyte and R_s is the ^{34}S/^{32}S ratio of the VCDT standard ($\equiv$ 0.044151; Werner & Brand, 2001). For C, R is the measured ratio of ^{13}C/^{12}C for the sample and standard, respectively, and the δ^{13}C is expressed relative to the international marine carbonate standard Vienna Pee Dee Belemnite (VPDB; Hoefs, 2009).

Stable isotopic values of individual compounds, measured by compound specific isotope analysis (CSIA), can provide information about specific biosynthetic pathways and sources and has been widely and successfully used by organic geochemists for applications such as biogeochemistry, paleoenvironmental reconstructions or energy resource exploration (Freeman *et al.*, 1990; Grice & Brocks, 2011; Brocks & Summons, 2013; Greenwood *et al.*, 2014).

1.1.3. Sulfur

The main S inputs to the oceans are continental dissolution of evaporate minerals and the oxidative weathering of sulfites. Oxidised S, in form of sulfate (SO_4^{2-}), from these sources are transported *via* rivers to marine shelf systems (Hurtgen, 2012). In the marine system, sulfur is largely stored as reduced sulfur from microbial mediated sulfate reduction, which can react with iron (Fe) to form (and be buried as) pyrite or react with organic substances during early diagenesis, where the S- and C-cycle closely interlink, to form organosulfur compounds (OSCs). Sulfate reduction in organic matter-rich environments follows two pathways: a) abiotic assimilatory reduction of SO_4^{2-} followed

by biosynthetic incorporation of S into microbial cell material (e.g. cysteine, biotin) with minor δ^{34}S reduction (ε = -1 ‰ to -3 ‰; Kaplan & Rittenberg 1964; Amrani 2014); and b) microbial dissimilatory reduction of SO_4^{2-} to HS^- (Figure 1.2) characterised by a relatively large ^{34}S depletion (typically δ^{34}S $\varepsilon \leq$ -20 ‰).

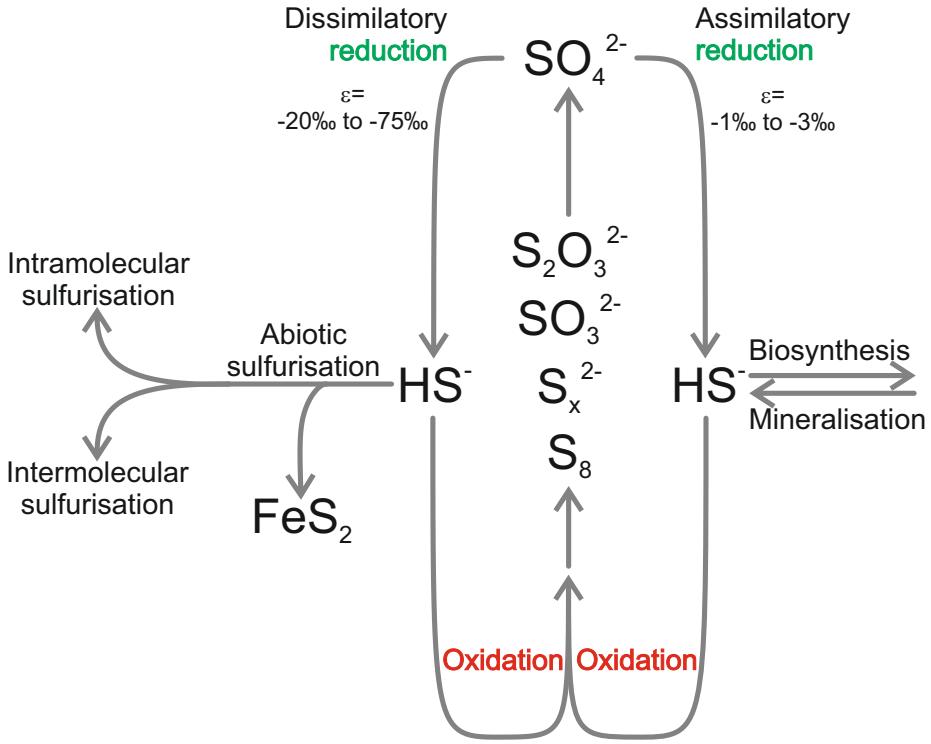

Figure 1.2.: Early diagenetic sulfur cycle on Earth (modified from Amrani, 2014)

During dissimilatory sulfate reduction microbes use sulfate as electron acceptor for the oxidation of OM, when other electron acceptors (e.g., O_2 or NO_3^-) are depleted within the sediment or water column (Jørgensen, 1982; Berner, 1989; Canfield *et al.*, 2010). This reaction is termed microbial sulfate reduction (MSR) and is expressed by the following chemical equation:

$$CH_4 + SO_4^{2-} \rightleftharpoons CO_3^{2-} + H_2S + H_2O$$

Environmental observation and theoretical modelling have shown MSR, being a kinetically driven and microbial mediated reaction, can result in large isotopic fractionation. The H_2S produced can be up to 75 ‰ depleted in ^{34}S relative to the sulfate reactant (Wortmann *et al.*, 2001; Brunner & Bernasconi, 2005; Canfield *et al.*, 2010). Most laboratory experiments on pure MSR cultures, however, could not replicate the large fractions observed in nature. The δ^{34}S fractionation measured from these biochemical simulations has not exceeded –47 ‰ (Kaplan & Rittenberg, 1964; Fry *et al.*, 1988; Peterson, 1999; Canfield, 2001; Detmers *et al.*, 2001). The δ^{34}S fractionation of laboratory experiments were mechanistically recognised as the repeated cycle of abiotic sulfide oxidation followed by microbial disproportionation of S^0 to HS^- and SO_4^{2-}, whereas produced sulfate becomes relatively enriched and the sulfide depleted

in ^{34}S (Canfield & Thamdrup, 1994; Canfield & Teske, 1996). The oxidative sedimentary recycling of sulfur requires an aerobic water column and takes place along the sediment-water interface, hence, this model has been widely used to track the progressive oxygenation of the atmosphere (Canfield & Teske, 1996; Parnell *et al.*, 2010) and subsequent changes in oceanic redox conditions (Kajiwara *et al.*, 1994; Passier *et al.*, 1999; Grice *et al.*, 2005c).

Sulfurisation

Pore-water sulfide, and other reduced sulfur species can react with iron and other metals to form monosulfides such as mackinawite (FeS), greigite (Fe_3S_4) and pyrite (FeS_2) (Goldhaber, 2004; Rickard & Luther, 2007; Amrani, 2014). Pyrite is the most stable sulfide mineral on Earth. The precipitation of pyrite occurs with a negligible 1 ‰ fractionation of the source sulfide (Butler *et al.*, 2004), thus, the isotopic composition of sulfide minerals are thought to be representative of ancient pore-water sulfide and have been used to reconstruct the atmospheric composition and redox conditions over Earth's history (Canfield *et al.*, 2000; Fike *et al.*, 2006).

Reduced sulfur species can also react with organic molecules to form OSCs – a process termed sulfurisation (Sinninghe Damste & de Leeuw, 1990). Despite decades of research, the process of organic matter sulfurisation remains ill-constrained due to the large variety of OSCs found in nature and the multitude of potential reaction pathways (Werne *et al.*, 2004). Two prominent pathways are thought to be i) intramolecular addition of HS^- to reactive sides of organic molecules (e.g., double bonds, functional groups) resulting in the formation of cyclic-S groups such as thiolane, thiane or thiophene; and ii) intermolecular addition of sulfide and polysulfides (S_x^{2-}) resulting in the formation of geo-macromolecules cross-linked via C-S_x-C bridges (e.g., Kohnen *et al.*, 1990; Sinninghe Damste & de Leeuw, 1990; Werne *et al.*, 2004; Raven *et al.*, 2015; Figure 1.3).

Organic sulfur, in the form of kerogen or proto-kerogen, has been shown to be isotopically enriched in ^{34}S relative to polysulfides or bisulfide sources (Anderson & Pratt, 1995; Bottrell & Raiswell, 2000). This isotopic enrichment in ^{34}S was not evident in either laboratory controlled sulfurisation experiments (Amrani & Aizenshtat, 2004) or early compound specific $\delta^{34}S$ analysis of OSCs in recent sediments (Werne *et al.*, 2008). However, recently Raven *et al.* (2015) presented $\delta^{34}S$ data of individual OSCs in recent sediments from the Cariaco Basin including volatile OSCs with a distinctively depleted $\delta^{34}S$ composition relative to the bulk organic sulfur pool. They concluded there must be two (or more) isotopically distinctive sulfurisation pathways. For example intermolecular S addition, forming the bulk organic S-pool, was suggested to be a reversible reaction and to be in equilibrium with co-existing S_x^{2-}, whereas intramolecular S addition, forming volatile OSCs, was suggested to be a non-reversible

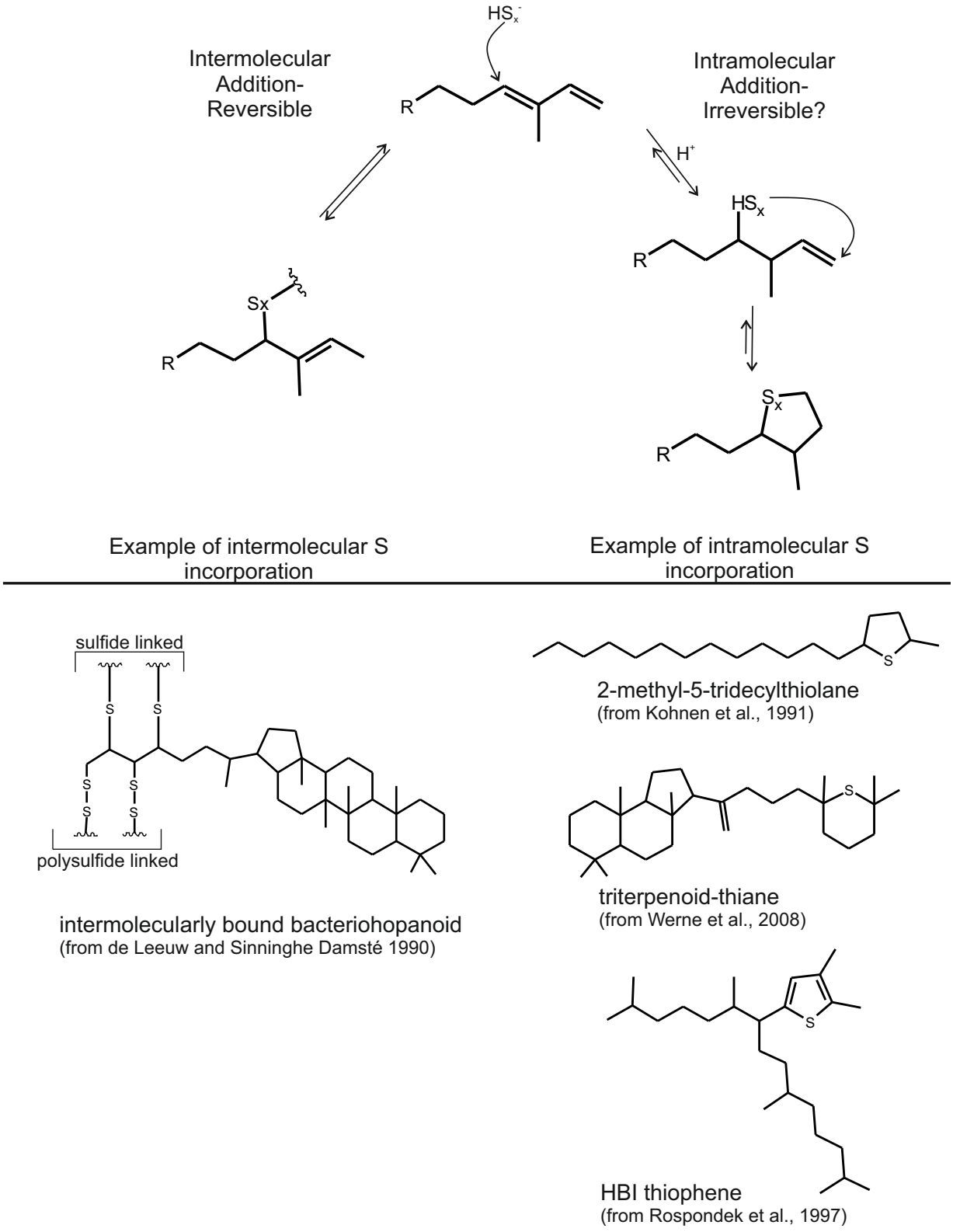

Figure 1.3.: Reaction pathways of organic sulfurisation (top; redrawn from Kohnen *et al.*, 1990 and Raven *et al.*, 2015). Examples of OSCs formed during sulfurisation (bottom; from de Leeuw & Sinninghe Damsté, 1990; Kohnen *et al.*, 1991; Rospondek *et al.*, 1997; Werne *et al.*, 2008)

reaction and S addition from pore-water sulfide resulted in a significant ^{34}S depletion (Figure 1.3).

The results presented by Raven *et al.* (2015) demonstrated that compound-specific $\delta^{34}S$ analysis of OSCs was a powerful tool that could help illuminate complex sulfurisation and kerogen formation processes. Furthermore, they provided evidence that sedimentary OSCs preserved the isotopic signals of early diagenetic sources. This approach might therefor be useful for paleoenvironmental reconstructions of ancient sediments.

1.2. Mass extinction

Mass extinctions represent dynamic periods of Earth's history that saw the widespread and rapid reduction of life on our planet, and specifically involved the loss of more than one paleogeographically widespread higher taxon. They typically result in a transient decline in abundance of marine as well as terrestrial species (Sepkoski Jr., 1986; Bambach, 2006; Whiteside & Grice, 2016) and are responsible for some of the most intense changes in biotic evolution in Earth's history (e.g., Twitchett *et al.*, 2001; Benton & Twitchett, 2003; Bambach, 2006; Twitchett, 2006).

Over the last 600 Ma the planet experienced 5 major extinction events i) during the end Ordovician; or associated with the ii) Frasnian/Famennian (F/F); iii) Permian/Triassic (P/Tr); iv) Triassic/Jurassic (Tr/J); and v) Cretaceous/Tertiary (K/T) boundaries (Wiese & Reitner, 2011; Figure 1.4). Most extinctions, with exception of the end Ordovician event, are associated with periods of increased volcanic activity related to the tectonic evolution of the planet (Bambach, 2006). The K/T extinction, the best-known of all mass extinctions, was due to massive volcanic activity and a coinciding meteoroid impact (Becker *et al.*, 2000; Kring, 2007). Biomarker reconstructions of paleoenvironments have confirmed that mass extinctions were times of severe biotic stress, triggered by hydrothermal and volcanic processes resulting in global warming, sea level rise and fall, intensified global anoxia and eutrophic oceans (Hallam & Wignall, 1997; Benton & Twitchett, 2003; Grice *et al.*, 2005c; Bond & Wignall, 2008; Nabbefeld *et al.*, 2010).

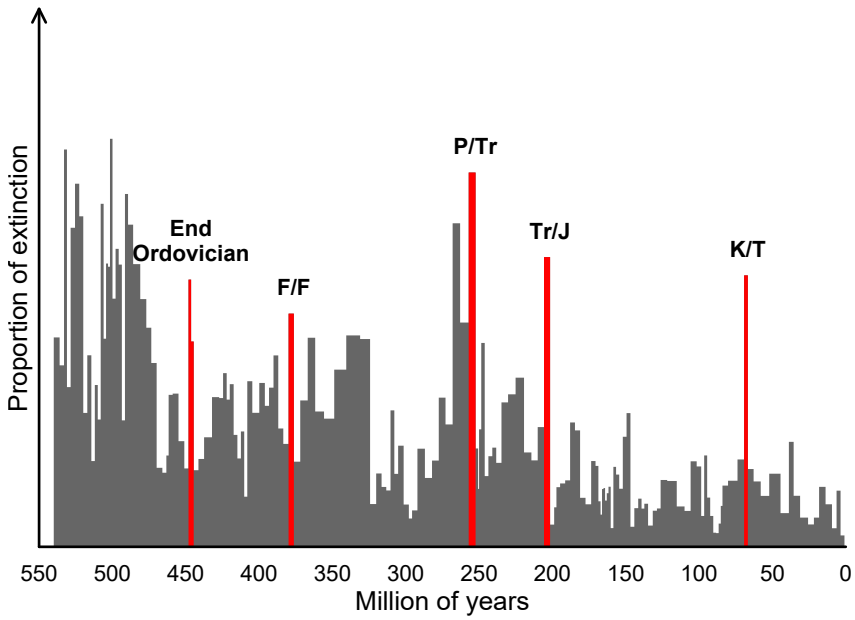

Figure 1.4.: Mass extinction events in Earth's history (modified after Bambach *et al.*, 2006)

Permian-Triassic (P/Tr) mass extinction

The end Permian extinction is regarded as the most severe extinction event during the Phanerozoic, showing a disappearance of 95 % of marine and 70 % of terrestrial species (e.g., Erwin *et al.*, 2002) during a very short interval of 60 ± 48 kyr, about 252 Ma, based on uranium-lead zircon ages from the Global Stratotype Section and Point (GSSP) at Meishan, South China (Burgess *et al.*, 2014). The cause for this extreme extinction remains controversial due to a lack of compelling evidence. It was likely caused by a complex interplay of rapid environmental changes related to co-occurring volcanic activity (Erwin, 1994; Racki & Wignall, 2005), although a few have suggested a bolide impact might also have been responsible (Koeberl *et al.*, 2004).

The P-Tr extinction coincided with the eruption of the Siberian flood basalts (Kamo *et al.*, 2003) and greenhouse gases (e.g., CH_4, CO_2, H_2S) potentially released (Ryskin, 2003) may have caused global warming (e.g., Wignall, 2001; Sephton *et al.*, 2005; Reichow *et al.*, 2009; Svensen *et al.*, 2009). Global warming in return could have led to the thawing of gas hydrates and CH_4 fixated on oceanic shelves may have been released into the atmosphere, intensifying the global warming trend (Krull & Retallack, 2000). Intensive and rapid global warming would have led to sea level rise, continental shelf expansion, reduction of oceanic circulation and elevated terrestrial weathering and nutrient fluxes, oceanic O_2 depletion and global euxinic conditions, where toxic H_2S reached the photic zone possibly serving as a kill mechanism for oceanic biota (Grice *et al.*, 2005a,b,c; Kaiho *et al.*, 2006a,b; Riccardi *et al.*, 2006; Meyer *et al.*, 2008; Algeo & Twitchett, 2010; Nabbefeld *et al.*, 2010).

Globally, one or more drivers of the extinction resulted in major turbulences of the carbon and sulfur cycles, indicated by co-eval negative shifts in the $\delta^{13}C$ records of carbonates and organic carbon, as well as the $\delta^{34}S$ composition of various inorganic sulfur species (Holser *et al.*, 1989; Cao *et al.*, 2002; Korte *et al.*, 2004; Newton *et al.*, 2004; Berner, 2005; Grice *et al.*, 2005c; Riccardi *et al.*, 2006; Algeo *et al.*, 2008). Fluctuations in the S-cycle have previously been identified by changes in the $\delta^{34}S$ composition of carbonate associated sulfates (CAS; e.g., Newton *et al.*, 2004; Riccardi *et al.*, 2006; Gorjan & Kaiho, 2007) or the abundance, morphology and $\delta^{34}S$ composition of pyrite (e.g., Fenton *et al.*, 2007; Gorjan *et al.*, 2007; Bond & Wignall, 2010). Further, due to the close coupling of the C- and S-cycle during early diagenesis it appears likely that fluctuations in the respective cycles can be observed in the organic S fractions of sediments, however, difficulties in measuring $\delta^{34}S$ of organic S have to date largely prevented such investigations.

1.3. Novel Techniques

1.3.1. Compound specific $\delta^{34}S$

The stable S isotopic ($\delta^{34}S$) compositing of organic sulfur has traditionally been limited to the bulk analysis of whole sediments or isolated fractions (e.g., humic acids; Nissenbaum *et al.*, 1972; Francois, 1987). Werne *et al.* (2008) first demonstrated the $\delta^{34}S$ measurement of individual OSC, but only after the use of a very labor-intensive and time-consuming preparative high-performance liquid chromatography (HPLC) to isolate individual OSC. Once the major compounds had been isolated in sufficient quantities their $\delta^{34}S$ values were subsequently measured by elemental analyzer isotope ratio mass spectrometry (EA-IRMS). This study successfully demonstrated the concept of CS-S-IA and the exciting application possibilities relating to sulfur biogeochemical studies.

Continuous-flow compound specific sulfur isotope analysis using a gas chromatograph coupled to an inductively coupled plasma mass spectrometer (GC-ICP-MS) was first reported by researchers at the California Institute of Technology (CalTech, Pasadena, CA, USA; Amrani *et al.*, 2009). Two similar facilities have since been developed at The University of Western Australia (Perth, Australia; Greenwood *et al.*, 2013) and at the Hebrew University (Jerusalem, Israel; Said-Ahmad & Amrani, 2013).

For $\delta^{34}S$ analysis the GC-ICP-MS system offers several important advantages over the traditional gas-source isotope ratio mass spectrometry (IRMS) widely used for $\delta^{13}C$ or δD analysis of hydrocarbon compounds. A traditional GC-IRMS system would require the continuous oxidation of OSCs to SO_2 and their separation from other oxidation products (e.g., CO_2 or H_2O). The ICP-MS system overcomes this issue by directly transforming OSCs in the argon plasma source to atomic sulfur and other ions. The use of multi-collector faraday detectors allows the separate and simultaneous measurement of monoatomic sulfur isotopes (i.e., $^{32}S^+$ and $^{34}S^+$), which require no correction for oxygen isotopes (Greenwood *et al.*, 2014). The very high mass-resolving power (m/Δm) of modern multicollector ICP-MS (MC-ICP-MS) systems can importantly detect $^{32}S^+$ (31.9721 Da) and $^{34}S^+$ (33.9678 Da) in isolation from oxygen isotopolouges $^{16}O_2{}^+$ (31.9898 Da) and $^{16}O^{18}O^+$ (33.9940 Da) of the same nominal mass.

Setup

The work of this thesis was conducted on the GC-ICP-MS facility at The University of Western Australia (UWA), which essentially replicated the prototype facility developed at the California Institute of Technology. The setup and a schematic layout of the UWA GC-ICP-MS system is shown in Figure 1.5. It uses an Agilent 6890 GC, interfaced

to a Thermo Fisher Scientific Neptune^{+} MC-ICP-MS. The grounded interface of this ICP-MS supports the high mass resolution (~15 mDa) required to clearly separate the monoatomic sulfur and diatomic oxygen ions (Greenwood *et al.*, 2014).

GC (top-front) - ICP- MS

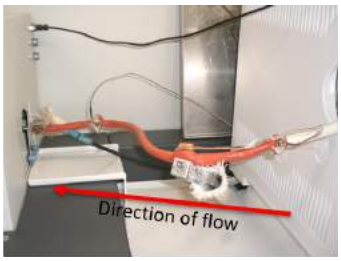

Transfer line from GC (right) and ICP-MS (left). High Temp. (320 °C) maintained by low-V resistive heating in heating tube

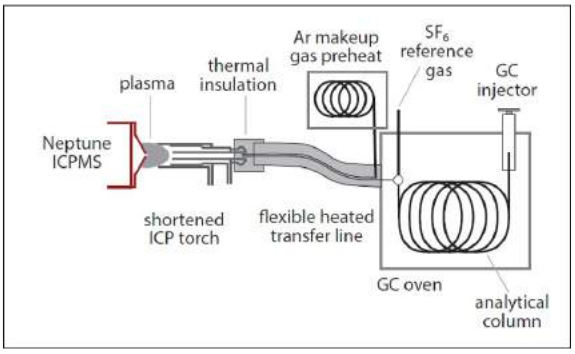

Schematic prototype instrument (after Amrani et al. 2009). GC carrier gas and Ar sample gas flow coaxially through the transfer line and into the injector, where they mix. SF_6 reference gas is introduced at the end of analytical column.

Figure 1.5.: GC-ICP-MS facility at UWA and schematic layout of the first GC-ICP-MS instrument at Caltech (modified after Greenwood *et al.*, 2014)

The extension of the analytical column from inside the GC oven to the ICP torch was achieved by passing a capillary column through a 1/8" (3.175 mm) stainless steel tube maintained at high temperature *via* low-voltage resistive heating. This transfer line (Figure 1.5), coupling the GC to the ICP-MS, was kept at high temperature to maintain GC-resolved analytes in the gas phase during their transfer to the ICP torch. Flexibility of the transfer line is essential in order to 'tune' the torch position relative to the cone/skimmer orifice (Greenwood *et al.*, 2014).

The argon makeup gas (~ 1-2 L/min) of the ICP was pre-heated by passing through a coil of 1/8" SS tubing wrapped in heating tape and maintained 300 °C to minimise the condensation of analytes as they elute from the capillary column into the torch.

Instrument tuning and subsequent calibration of δ^{34}S values was achieved by the injection of sulfur hexafluoride (SF_6) reference gas. The inert, odorless and inexpensive gas was introduced at the end of the analytical column *via* a simple gas inlet system. The system provides for either pulsed or continuous flow of SF_6 diluted in helium to

the mass spectrometer (Amrani *et al.*, 2009). A continuous flow of SF_6 is required for the tuning of the mass spectrometer. Pulsed injections of SF_6 are injected *via* micro-volume capillary loops to the carrier gas stream and result in discrete peaks during the analysis of samples which can be used for the calibration of $\delta^{34}S$ values.

Applications

Early applications of compound specific sulfur isotope research include an investigation of the mechanism and timeframes of diagenetic organic sulfurisation (Werne *et al.*, 2008; Raven *et al.*, 2015, 2016). In geologic systems, most sulfur is incorporated into the kerogen matrix on < 1000 Y timescales so kerogen $\delta^{34}S$ values may be indicative of sedimentary and early diagenetic processes. Individual OSCs generated during early sulfurisation of OM thus potentially carry $\delta^{34}S$ signals that provide insights into sulfurisation and the complex interplay between the sulfur, carbon and oxygen cycles through Earth's history.

Werne *et al.* (2008) were the first to apply CSIA to sulfur rich sediments from the Cariaco Basin. However, there were some difference in the $\delta^{34}S$ values they reported from EA-IRMS measurements of individual OSCs isolated by preparative HPLC to the $\delta^{34}S$ values of some of the same compounds later measured by the GC-ICP-MS approach (Raven *et al.*, 2015). These differences may have been due to the presence of elemental sulfur in HPLC separated OSCs (Raven *et al.*, 2015), a problem that does not occur on well separated peaks during the flow through GC-ICP-MS approach. The formation of individual OSCs, similar to pyrite, has been shown to occur either syngenetic in the water column or diagenetic in the sediment. Raven *et al.* (2015) showed that OSCs (i.e., highly branched isoprenoid thiolanes and triterpenoid thianes) detected in the upper 5 m of the sediment were ^{34}S-depleted relative to co-existing pyrite suggesting a diagenetic formation, whereas residual non extractable organic S was isotopically enriched. This observation led to the conclusion that OSCs may arise from different reaction pathways (and organic sulfurisation processes) with distinct isotopic effects. It was suggested that OSCs formed either *via* intermolecular addition of HS^-, a possibly non-reversible reaction leading to a kinetically driven ^{34}S depletion of OSCs relative to their likely S source from pore-water dissolved HS^-. Whereas syngenetic sulfurisation, possibly *via* intramolecular S addition in the water column was a reversible reaction that would reflect equilibrium isotope effects (Greenwood *et al.*, 2014). This observation was later confirmed by Raven *et al.* (2016) showing fast abiotic OM sulfurisation in particles in the Cariaco Basin water column on the timescale of days and a clear $\delta^{34}S$ link between i) proto-kerogen and syngenetically formed C_{20} thiophene; and ii) elemental sulfur (S^0) and polysulfides ($S_x{}^{2-}$, $HS_x{}^-$).

The GC-ICP-MS approach has also recently been used for the characterisation of ocean derived sulfur aerosols (Amrani *et al.*, 2013a; Said-Ahmad & Amrani, 2013)

and OSCs present in oils (Amrani *et al.*, 2012; Greenwood *et al.*, 2015; Gvirtzman *et al.*, 2015; Li *et al.*, 2015). It has proven especially useful for oil exploration related applications. Unlike hydrocarbon biomarkers, OSCs (e.g., parent and alkylated benzothiophenes (BT), dibenzothiophenes (DBT) and thiodiamandoids (TD)) detected in oils and source rocks provide very limited information about specific sources or environmental conditions during formation or deposition of the oil (Greenwood *et al.*, 2014). Geologically, the bulk amount of sulfur is incorporated into OM *via* secondary processes (e.g., diagenesis, catagenesis and thermogenic sulfate reduction (TSR)) following deposition (Peters *et al.*, 2005b). δ^{34}S values may help distinguish the impact and extent of these processes. Furthermore, the broad isotopic variance of different sources and depositional environments suggest δ^{34}S data will be particularly useful for oil-oil and oil-source rock correlations.

GC-ICP-MS has already been used in several oil-oil correlation studies. Large differences have been seen in the δ^{34}S values of BTs and DBTs reported from non-altered oils of several formations including Smackover Formation (Gulf of Mexico; Amrani *et al.*, 2012); Oman (Amrani *et al.*, 2012); Tarim Basin (north-west China; Greenwood *et al.*, 2013); Jinxian Sag (northern China; Greenwood *et al.*, 2013); and north-east Iraq (Greenwood *et al.*, 2015). For instance, the mBT, DBT and mDBT δ^{34}S values from the Smackover Formation (~ -5 ‰; Amrani *et al.*, 2012) are over 20 ‰ depleted relative to their counterparts in the Tarim Basin (+15 to +20 ‰; Greenwood *et al.*, 2013). The difference is much larger than any change anticipated from varying degrees of maturity (Greenwood *et al.*, 2014). In fact, a laboratory controlled maturation experiment on an immature source rock (Amrani *et al.*, 2013b) showed only minor variation in the δ^{34}S composition of OSCs (i.e., BTs and DBTs) detected from samples of increasing thermal maturity. Increased isotope mixing during maturation may result in S isotopic homogeneity. If secondary processes (i.e., TSR or BSR) can be excluded, isotopic differences can then be attributed to other, possibly paleoenvironmental, factors. These observations raise confidence in using CS-S-IA of OSCs for oil-oil and oil-source rock correlations.

The effect of TSR on individual OSCs was extensively investigated by Amrani *et al.* (2012). TSR is a high-temperature redox process in which sulfates such as gypsum ($CaSO_4 \cdot 2H_2O$) or anhydrite ($CaSO_4$) are reduced and organic matter oxidised (Machel *et al.*, 1995; Machel, 2001). The reaction primarily involves the destruction of easily oxidised short chain normal and branched alkanes (Rooney, 1996; Manzano *et al.*, 1997; Cross *et al.*, 2004), and the formation of extensive amounts of CO_2 and H_2S resulting in sour gas reservoirs with oil of poor quality and low economic value (Greenwood *et al.*, 2014). The TSR reaction also results in the formation of aromatic sulfur compounds (e.g., BTs and DBTs). Amrani *et al.* (2012) investigated the effect of TSR on individual parent and methyl BTs and DBTs in a set of Upper Jurassic oils

from the TSR impacted Smackover Formation (southern USA) and complimented the investigation with artificial TSR gold tube experiments. They showed that both mBTs and BTs in the natural and pyrolysed oils quickly adopted the δ^{34}S signature of the sulfate source at low levels of TSR. Furthermore, the higher molecular weight DBTs which form less rapidly than BTs, did not adopt the δ^{34}S signature of the source as quickly as BTs (Amrani *et al.*, 2012). This observation led to the proposed TSR index $\Delta\delta^{34}S_{\text{BT-DBT}}$. Such an easily measurable parameters to assess the extent of TSR will be a useful tool for oil and gas exploration.

The novel use of GC-ICP-MS to analyse δ^{34}S values of individual OSCs has real potential to answer many contemporary questions in organic and biogeochemistry relating to taphonomy, unconventional petroleum systems or microbial and global sulfur cycling. The global S-cycle has experienced major disturbances in the past triggered by combinations of tectonically driven hydrothermal and volcanic activity, which led to the eutrophication of oceans, sea-level rises, global warming and wide spread global oceanic anoxia (Grice *et al.*, 2005c). These conditions are believed to be responsible for the most severe ecologic crisis of the Phanerozoic, the End Permian mass extinction and the subsequent formation of large petroleum systems. Some of the changes in the S-cycle during major mass extinctions have already been identified by disturbances in the inorganic S isotopic record of pyrites (e.g., Fenton *et al.*, 2007; Nabbefeld *et al.*, 2010).

1.3.2. Hydropyrolysis

Hydropyrolysis (HyPy) was developed in the mid-20th century to directly produce methane and light aromatic feedstocks (benzene) from coal under very high temperature (800 °C) and pressure (300 bar) conditions (Hiteshue *et al.*, 1957; Finn *et al.*, 1980; Fynes *et al.*, 1980). The subsequent addition of dispersed catalysts such as sulfide molybdenum to the sample achieved higher conversion rates at pressures of only 150 bar (Bolton *et al.*, 1988; Snape *et al.*, 1989). Hydrotreatment of primary oil vapors to remove heteroatoms from polar species led to further increase in hydrocarbon yields (Bolton *et al.*, 1989). These early developments formed the basis for the subsequent use of HyPy as an analytical pyrolysis procedure for the characterisation of OM-rich sediments.

Setup

The analytical HyPy apparatus now commercially marketed by STRATA Technology Ltd is schematically illustrated in Figure 1.6. It consists of a reactor unit connected to an external dry ice cooled silica trap. Conventionally, the catalyst mixed sample is placed on top of a steel wool plug in the center of the reactor. The reactor unit is resis-

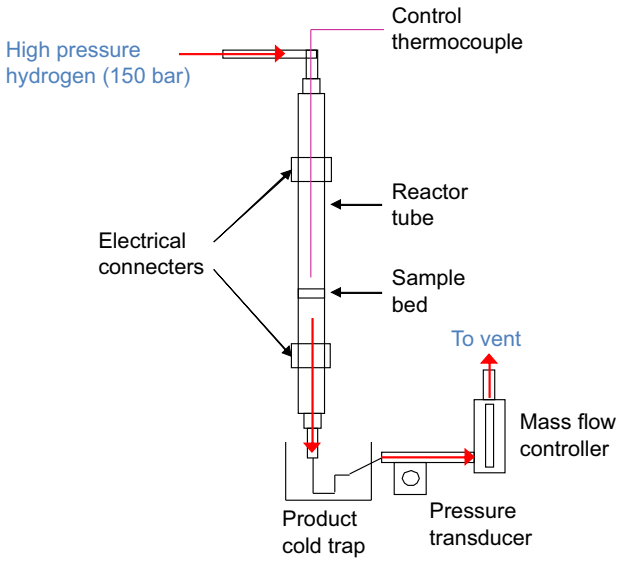

Figure 1.6.: Schematic illustration of the Strata manufactured HyPy setup.

tively heated *via* the electrical connectors following pre-defined temperature programs and the system is operated under constant hydrogen pressure of 150 bar with a flow of 5 L/min. The constant flow and high H_2 pressure ensure rapid flushing of pyrolysis products out of the heating zone and subsequent trapping on the dry ice cooled silica bed. Optimum operating conditions have been identified in various studies (e.g., Love *et al.*, 1997) of different standard compounds and organic sediments across a range of thermal maturities and are further discussed in subsequent chapters.

Applications of HyPy

HyPy has proven a useful analytic tool which can support a vast number of organic geochemical applications. The broad demonstration of HyPy as a valuable complement to traditional online pyrolysis or chemical degradation methods was presented by Love *et al.* (1995). They showed the aliphatic HyPy fraction from an immature type I kerogen (Göynük oil shale, Miocene age) was primarily composed of a bimodal, homologous distribution of *n*-alkanes and *n*-alk-1-ene doublets extending beyond *n*-C_{35}. Triterpanes were also dominated by biologically inherited 17β(H), 21β(H) isomers of C_{27} to C_{35} hopanes, with the major C_{29}-C_{33} hopanes detected at 3-10 times greater their solvent extractable concentrations. Furthermore, C_{34} and C_{35} hopanes were detected in HyPy fractions where they were absent in corresponding bitumen fractions. These product distributions demonstrated the unique ability of HyPy to maximise the yield of hydrocarbon biomarkers covalently bound to the kerogen matrix with minimal stereochemical alteration. Robinson *et al.* (1991) had also shown that many of the hopanes released *via* HyPy from a lignite retained the biologically inherited, but thermodynamically unstable, 17β(H), 21β(H) stereochemistry.

HyPy has been used to analyse the hydrocarbon biomarker compositions of a large range of petroleum and related samples and to support a number of exploration applications. For instance, aliphatic biomarker ratios measured by HyPy can provide a reliable measure of the thermal maturity of source rocks across a broad maturity range from the beginning (Love *et al.*, 1996; Bishop *et al.*, 1998; Murray *et al.*, 1998; Bowden *et al.*, 2006) to post oil window maturities (Lockhart *et al.*, 2008). This innovative pyrolysis method has also proven useful for distinguishing the indigenous composition of rocks from secondary charged or migrating oils (Russell *et al.*, 2004); and evaluating the extent of alterations such as biodegradation (Sonibare *et al.*, 2009). HyPy is typically applied to the kerogen fraction of source rocks, first isolated from the solvent removed bitumen fraction in which migrated oils, drilling fluids or external contamination will be captured. The hydrocarbon products subsequently released by HyPy treatment of the kerogen fraction will be representative of indigenous OM from syn-sedimentary deposition.

The effectiveness of HyPy in releasing hydrocarbon biomarkers had also been used to detect the trace OM preserved in very old or high maturity geological sediments, such as 2.5-3.4 Ga old Archean rocks. The bitumen fraction of such ancient samples are vulnerable to secondary alterations or OM from exogenous sources. Brocks *et al.* (2003) and Marshall *et al.* (2007) reported pyrene, phenanthrene and other polycyclic aromatic hydrocarbons (PAHs) in the 2.5 Ga Mt. McRae shale and 3.4-3.5 Ga Strelley Pool cherts, respectively, both from the Pilbara Craton (Western Australia). The $\delta^{13}C$ values of the more abundant PAHs were measured to be similar to the ~ - 30 ‰ of the bulk kerogen (Brocks *et al.*, 2003; Marshall *et al.*, 2007). These studies demonstrated how organic geochemical analyses of HyPy treated kerogen fractions can provide valuable biological source information from overmature rocks.

The PhD candidate was also involved in the informative application of HyPy and Raman spectroscopy to meta-sedimentary rocks associated with an orogenic Au-deposit (Robert *et al.*, 2016). The study site was the Paleoproterozoic Koolpin Formation in Cosmo Howley, Pine Creek Orogen, Northern Territory Australia, which mainly consists of carbonaceous mudstones, mudstone and siltstone hosting the Au mineralisation (Needham *et al.*, 1988). The Au mineralisation is believed to have been introduced by a high temperature magmatic fluid (500 °C) from granite intrusions with the carbonaceous meta-sedimentary rocks providing a secondary host rock control (Matthaei *et al.*, 1995a,b). HyPy was successfully able to release organic molecules even from these samples exposed to severe thermal stress (Robert *et al.*, 2014) and furthermore revealed intimate mineral-kerogen relationships thought to reflect the active role of the OM in the mineralisation process (Robert *et al.*, 2016). Certain mineral groups (e.g., carbonates, clays, quarts) were shown to be closely bound to organic moieties of similar but subtly varying hydrocarbon composition. The major HyPy products were PAHs,

dominated by pyrene and hydrogenated four ringed analogues, whilst some *n*-alkanes thought to be indigenous were also surprisingly detected (Robert *et al.*, 2014, 2016). The HyPy/Laser Raman data distinguished two types of carbonaceous material, one of which was associated with the hydrothermal fluid important to Au transportation, precipitation and accumulation.

The unusual high abundance of pyrene and hydro-pyrenes raised questions about their origin and whether they truly reflected the composition of the sedimentary OM of these deposits, or alternatively whether they were a by-product of the HyPy procedure. The uncertainties about chemical reactions at high temperature and pressure during HyPy have only been superficially addressed. Meredith *et al.* (2006) did report the chemical behaviour, reactions and breakup products of model compounds treated by HyPy. Experiments with such simple reactants are necessary to fully interpret the chemical composition of the HyPy extract and their molecular relationship to the precursor kerogen. The Meredith *et al.* study, however, was limited to functionalised compounds like carboxylic acids, stearic and oleic acids as well as saturated and unsaturated C_{27} sterols. These compounds are vulnerable to thermal stress so are unlikely relevant to high maturity geological sediments.

1.4. Aims of this thesis

This PhD project researched several novel applications of new organic geochemical analytical technologies. HyPy and CS-S-IA were used to characterise selected sediments relevant to the exploration of valuable resources or to sensitive periods of the Earth's evolution. A commercial HyPy facility was evaluated for its capability to measure the sequestered PAH composition of high maturity OM associated with high temperature mineral deposits, and to assist the δ^{34}S measurement of OSCs in these systems and other S-dynamic paleoenvironments. The recently developed analytical capacity of CS-S-IA was used to measure the compound specific δ^{34}S composition of sediment hosted OSCs.

To address a gap in basic knowledge of aromatic hydrocarbon behaviour during HyPy, **Chapter 2** investigated the HyPy reactivity of three PAHs (pyrene, perylene and coronene) under different experimental conditions. PAHs are some of the most thermally stable organic molecules found in nature and were shown to be the major organic molecules isolated from HyPy treatments of severely thermally altered sedimentary rocks associated with high temperature orogenic Au-deposits (Robert *et al.*, 2016). A sophisticated understanding of the stability and reactivity of PAHs under HyPy conditions is needed to accurately interpret the origin and reaction history of the HyPy products of such rocks.

CS-S-IA of OSCs promise to provide great advancements in the field of S-biogeochemistry

and in paleoenvironmental reconstructions. The sample throughput and quality of isotopic information obtained by the newly developed GC-ICP-MS approach is dependent on a number of factors including sample treatment, analytical conditions and subsequent processing of the raw data. With respect to data processing, the Neptune$^+$ software unfortunately is unable to proces transient signals. For this the raw data must be exported and processed separately by either Microsoft Excel, MatLab or ThermoFisher IsoDat. This cumbersome procedure is time consuming and vulnerable to operator subjectivities. To help overcome these problems a routine procedure for the auto-processing of raw Neptune$^+$ signals into δ^{34}S values was developed and tested in **Chapter 3**.

In **Chapter 4** HyPy was used to release kerogen bound OSCs from selected S-rich sediments and along with the OSCs in the bitumen fraction their δ^{34}S values were measured to investigate sources, sulfurisation pathways and bonding types of organic S. The effect of HyPy on the δ^{34}S signatures of an authentic standard was first tested to evaluate for any S-isotope fractionation on OSCs during the pyrolysis treatment. The HyPy approach was then used to release OSCs from the kerogens of S-rich sediments from the P-Tr Hovea-3 well (Western Australia, Australia) and the Late Cretaceous Toolebuc Formation (Queensland, Australia).

The P-Tr extinction and subsequent recovery is a period of great interest and despite decades of research there is still on-going conjecture about the major controls and consequences of this major extinction. The Earth encountered highly dynamic S-cycles during the P and Tr periods, with previous reports of fluctuating inorganic S-isotope incursions during the extinction event. A large portion of organically bound sulfur has also been detected in P-Tr sedimentary sequences and it is now possible to measure the δ^{34}S composition of bitumen OSCs in ancient sedimentary rocks by GC-ICP-MS. In **Chapter 5**, the δ^{34}S of OSCs present across two P-Tr sections: i) Hovea-3 (Perth Basin, Western Australia); and ii) GSSP at Meishan-1 (South China) were measured. The isotopic behaviour individual OSCs as well as of pyritic and kerogen bound sulfur during the P-Tr extinction were assessed to better understand the organic and inorganic S-cycles during this environmentally dynamic time in the history of the Earth.

In order to gain a better understanding of environmental conditions and microbial flora following the extinction, **Chapter 6** presents the distribution and discusses the significance of new microbial biomarkers (i.e., phytanyl arenes) in three PTB sections: i) the Perth Basin, Western Australia; ii) Lusitaniadalen, Spitsbergen; and iii) Jameson's Land, East Greenland. The occurrence of phytanyl arenes was confirmed by co-injection of synthesised phytanyl benzene, phytanyl toluene and phytanyl naphthalene standards. Their abundance and distribution was discussed in the light of previous biomarker records and the site specific lithology, in order to assess environmental factors forcing the development of a unique microbial community following the P-Tr

extinction.

References

Algeo, T., Shen, Y., Zhang, T., Lyons, T., Bates, S., Rowe, H., & Nguyen, T. K T. 2008. Association of 34S-depleted pyrite layers with negative carbonate d13C excursions at the Permian-Triassic boundary: Evidence for upwelling of sulfidic deep-ocean water masses. *Geochemistry, Geophysics, Geosystems*, **9**(4), 1–10.

Algeo, T. J., & Twitchett, R. J. 2010. Anomalous early Triassic sediment fluxes due to elevated weathering rates and their biological consequences. *Geology*, **38**(11), 1023–1026.

Amrani, A. 2014. Organosulfur Compounds: Molecular and Isotopic Evolution from Biota to Oil and Gas. *Annual Review of Earth and Planetary Sciences*, **42**(1), 733–768.

Amrani, A., & Aizenshtat, Z. 2004. Mechanisms of sulfur introduction chemically controlled: δ34S imprint. *Organic Geochemistry*, **35**(11-12), 1319–1336.

Amrani, A., Sessions, A. L., & Adkins, J. F. 2009. Compound-specific δ34S analysis of volatile organics by coupled GC/multicollector-ICPMS. *Analytical Chemistry*, **81**(21), 9027–9034.

Amrani, A., Deev, A., Sessions, A. L., Tang, Y., Adkins, J. F., Hill, R. J., Moldowan, M. J., & Wei, Z. 2012. The sulfur-isotopic compositions of benzothiophenes and dibenzothiophenes as a proxy for thermochemical sulfate reduction. *Geochimica et Cosmochimica Acta*, **84**, 152–164.

Amrani, A., Said-Ahmad, W., Shaked, Y., & Kiene, R. P. 2013a. Sulfur isotope homogeneity of oceanic DMSP and DMS. *Proceedings of the National Academy of Sciences*, **110**(46), 18413–8.

Amrani, A., Dror, G., Said-Ahmad, W., Feinstein, S., & Reznik, I. J. 2013b. The distribution and sulfur isotope ratios of specific organic sulfur compounds during pyrolysis of thermally immature kerogen. *Pages 561–562 of: 26th International Meeting of Organic Geochemistry, Book of Abstracts*.

Anderson, T. F., & Pratt, L. M. 1995. Isotopic evidence for the origin of organic sulfur and elemental sulfur in marine sediments. *Pages 378–396 of: Geochemical Transformations of Sedimentary Sulfur*. Washington D. C.: ACS Symposium Series 612.

Bambach, R. K. 2006. Phanerozoic Biodiversity Mass Extinctions. *Annual Review of Earth and Planetary Sciences*, **34**(1), 127–155.

Becker, L., Poreda, R. J., & Bunch, T. E. 2000. Fullerenes: an extraterrestrial carbon carrier phase for noble gases. *Proceedings of the National Academy of Sciences*, **97**(7), 2979–83.

Benton, M. J., & Twitchett, R. J. 2003. How to kill (almost) all life: the end-Permian extinction event. *Trends in Ecology & Evolution*, **18**(7), 358–365.

Berner, R. A. 1989. Biogeochemical cycles of carbon and sulfur and their effect on atmospheric oxygen over phanerozoic time. *Global and Planetary Change*, **1**(1-2), 97–122.

Berner, R. A. 2005. The carbon and sulfur cycles and atmospheric oxygen from middle Permian to middle Triassic. *Geochimica et Cosmochimica Acta*, **69**(13), 3211–3217.

Bishop, A. N., Love, G. D., McAulay, A. D., Snape, C. E., & Farrimond, P. 1998. Release of kerogen-bound hopanoids by hydropyrolysis. *Organic Geochemistry*, **29**(4), 989–1001.

Bolton, C., Riemer, C., Snape, C. E., Derbushire, F. J., & Terrer, M.T. 1988. Effect of low temperature catalytic hydrogenation on pyrolysis and hydropyrolysis of a bituminous coal. *Fuel*, **67**, 901–905.

Bolton, C., Snape, C. E., & Stephens, H. P. 1989. Hydrocracking of hydropyrolysis tar with hydrous titanium oxide catalysts. *Fuel*, **68**(2), 161–167.

Bond, D. P. G., & Wignall, P. B. 2008. The role of sea-level change and marine anoxia in the Frasnian-Famennian (Late Devonian) mass extinction. *Palaeogeography, Palaeoclimatology, Palaeoecology*, **263**(3-4), 107–118.

Bond, D. P. G., & Wignall, P. B. 2010. Pyrite framboid study of marine Permian-Triassic boundary sections: A complex anoxic event and its relationship to contemporaneous mass extinction. *Bulletin of the Geological Society of America*, **122**(7-8), 1265–1279.

Bottrell, S. H., & Raiswell, R. 2000. Sulphur isotopes and microbial sulphur cycling in sediments. *Pages 96–104 of:* Riding, R., & Awramik, S. (eds), *Microbial Sediments*. Springer Berlin / Heidelberg.

Bowden, S. A., Farrimond, P., Snape, C. E., & Love, G. D. 2006. Compositional differences in biomarker constituents of the hydrocarbon, resin, asphaltene and kerogen fractions: An example from the Jet Rock (Yorkshire, UK). *Organic Geochemistry*, **37**(3), 369–383.

Brocks, J. J., & Grice, K. 2011. Biomarkers (molecular fossils). *Pages 147–167 of:* Reitner, J., & Thiel, V. (eds), *Encyclopedia of Geobiology*. Dordrecht, The Netherlands: Springer.

Brocks, J. J., & Summons, R. E. 2013. Sedimentary Hydrocarbons, Biomarkers for Early Life. *Pages 61–103 of:* Holland, H., & Turekian, K. (eds), *Treatise on Geochemistry: Second Edition*, vol. 10. Elsevier Ltd.

Brocks, J. J., Love, G. D., Snape, C. E., Logan, G. A., Summons, R. E., & Buick, R. 2003. Release of bound aromatic hydrocarbons from late Archean and Mesoproterozoic kerogens via hydropyrolysis. *Geochimica et Cosmochimica Acta*, **67**(8), 1521–1530.

Brunner, B., & Bernasconi, S. M. 2005. A revised isotope fractionation model for dissimilatory sulfate reduction in sulfate reducing bacteria. *Geochimica et Cosmochimica Acta*, **69**(20), 4759–4771.

Burgess, S. D., Bowring, S. A., & Shen, S. Z. 2014. High-precision timeline for Earth's most severe extinction. *Proceedings of the National Academy of Sciences*, **111**(9), 3316–3321.

Butler, I. B., Böttcher, M. E., Rickard, D., & Oldroyd, A. 2004. Sulfur isotope partitioning during experimental formation of pyrite via the polysulfide and hydrogen sulfide pathways: Implications for the interpretation of sedimentary and hydrothermal pyrite isotope records. *Earth and Planetary Science Letters*, **228**(3-4), 495–509.

Canfield, D. E. 2001. Biogeochemistry of Sulfur Isotopes. *Reviews in Mineralogy and Geochemistry*, **43**(1), 607–636.

Canfield, D. E., & Teske, A. 1996. Late Proterozoic rise in atmospheric oxygen concentration inferred from phylogenetic and sulphur-isotope studies. *Nature*, **382**(6587), 127–132.

Canfield, D. E., & Thamdrup, B. 1994. The production of 34S-depleted sulfide during bacterial disproportionation of elemental sulfur. *Science*, **266**, 1973–1975.

Canfield, D. E., Habicht, K. S., & Thamdrup, B. 2000. The Archean Sulfur Cycle and the early history of Atmospheric Oxygen. *Science*, **288**(5466), 658–661.

Canfield, D. E., Stewart, F. J., Thamdrup, B., De Brabandere, L., Dalsgaard, T., Delong, E. F., Revsbech, N. P., & Ulloa, O. 2010. A cryptic sulfur cycle in oxygen-minimum-zone waters off the Chilean coast. *Science*, **330**(6009), 1375–1378.

Cao, C., Wang, W., & Jin, Y. 2002. Carbon isotope excursions across the Permian-Triassic bound- ary in the Meishan section, Zhejiang Province, China. *Chinese Science Bulletin*, **47**(13), 1125.

Cross, M. M., Manning, D. A. C., Bottrell, S. H., & Worden, R. H. 2004. Thermochemical sulphate reduction (TSR): Experimental determination of reaction kinetics and implications of the observed reaction rates for petroleum reservoirs. *Organic Geochemistry*, **35**(4), 393–404.

de Leeuw, J. W., & Sinninghe Damsté, J. S. 1990. Organic sulphur compounds and other biomarkers as indicators of Palaeosalinity: A critical evaluation. *Pages 417–443 of:* Orr, W L., & White, C. M. (eds), *Geochemistry of sulfur in fossil fuels*. Washington, D.C.: American Chemical Society Symposium Series 249.

Des Marais, D. J. 1997. Long-term evolution of the biogeochemical carbon cycle. *Reviews in Mineralogy and Geochemistry*, **35**, 429–448.

Detmers, J., Brüchert, V., Habicht, K. S., & Kuever, J. 2001. Diversity of sulfur isotope fractionations by sulfate reducing prokaryotes. *Applied and Environmental Microbiology*, **67**(2), 888–894.

Erwin, D. H. 1994. The Permo-Triassic Extinction. *Nature*, **367**(6460), 231–236.

Erwin, D. H., Bowring, S. A., & Yugan, J. 2002. End-Permian mass extinctions: A review. *Geological Society of America Special Paper*, **365**, 363–383.

Fenton, S., Grice, K., Twitchett, R., Bottcher, M., Looy, C., & Nabbefeld, B. 2007. Changes in biomarker abundances and sulfur isotopes of pyrite across the Permian–Triassic (P/Tr) Schuchert Dal section (East Greenland). *Earth and Planetary Science Letters*, **262**(1-2), 230–239.

Fike, D. A., Grotzinger, J. P., Pratt, L. M., & Summons, R. E. 2006. Oxidation of the Ediacaran ocean. *Nature*, **444**(7120), 744–7.

Finn, M. J., Fynes, G., Ladner, W. R., & Newman, J. O. H. 1980. Light aromatics from the hydropyrolysis of coal. *Fuel*, **59**(6), 397–404.

Francois, R. 1987. A study of sulfur enrichment in the humic fraction of marine sediments during early diagenesis. *Geochimica et Cosmochimica Acta*, **51**(1), 17–27.

Freeman, K. H., Hayes, J. M., Trendel, J.-M., & Albrecht, P. 1990. Evidence from carbon isotope measurements for diverse origins of sedimentary hydrocarbons. *Nature*, **343**.

Fry, B., Ruf, W., Gest, H., & Hayes, J. M. 1988. Sulphur isotope effects associated with oxidation of sulphide by O2 in aqueous solution. *Chemical Geology*, **73**, 205–210.

Fynes, G., Ladner, W. R., & Newman, J. O. H. 1980. The hydropyrolysis of coal to BTX. *Progress in Energy and Combustion Science*, **6**(3), 223–232.

Gelin, F., Sinninghe Damsté, J. S., Harrison, W. N., Reiss, C., Maxwell, J. R., & De Leeuw, J. W. 1996. Variations in origin and composition of kerogen constituents as revealed by analytical pyrolysis of immature kerogens before and after desulphurization. *Organic Geochemistry*, **24**(6-7), 705–714.

Goldhaber, M. B. 2004. Sulfur-rich sediments. *Pages 257–288 of: Sediments, Diagenesis, and Sedimentary Rocks*. Elsevier.

Gorjan, P., & Kaiho, K. 2007. Correlation and comparison of seawater δ34Ssulfate records at the permian-triassic transition. *Chemical Geology*, **243**(3-4), 275–285.

Gorjan, P., Kaiho, K., Kakegawa, T., Niitsuma, S., Chen, Z. Q., Kajiwara, Y., & Nicora, A. 2007. Paleoredox, biotic and sulfur-isotopic changes associated with the end-Permian mass extinction in the western Tethys. *Chemical Geology*, **244**(3-4), 483–492.

Greenwood, P. F., McCulloch, M., Grice, K., Holman, A., Hong, L., Ling, H., & Jin, S. 2013. Compound specific d34S analysis - Development and applications. *Pages 146–147 of: 26th International Meeting of Organic Geochemistry, Book of Abstracts*.

Greenwood, P. F., Amrani, A., Sessions, A., Raven, M. R., Holman, A., Dror, G., Grice, K., McCulloch, M. T., & Adkins, J. F. 2014. Development and Initial Biogeochemical Applications of Compound-Specific Sulfur Isotope Analysis. *Chap. 10, pages 285–312 of:* Grice, K. (ed), *Principles and Practice of Analytical Techniques in Geosciences*. UK: Royal Society of Chemistry.

Greenwood, P. F., Schwark, L., Mohammed, L., Zhu, G., Grice, K., & McCulloch, M. 2015. Compound-specific sulfur isotope analysis of oils using GC-MC-ICPMS. *Pages 113–114 of: 27th International Meeting of Organic Geochemistry, Book of Abstracts*.

Grice, K., & Brocks, J. J. 2011. Biomarkers (organic, compound specific isotopes). *Pages 167–182 of:* Reitner, J., & Thiel, V. (eds), *Encyclopedia of Geobiology*. Dordrecht, The Netherlands: Springer.

Grice, K., Twitchett, R. J., Alexander, R., Foster, C. B., & Looy, C. 2005a. A potential biomarker for the Permian–Triassic ecological crisis. *Earth and Planetary Science Letters*, **236**(1-2), 315–321.

Grice, K., Summons, R. E., Grosjean, E., Twitchett, R. J., Dunning, W., Wang, S. X., & Böttcher, Michael E. 2005b. Depositional conditions of the northern onshore Perth Basin (basal Triassic). *APPEA Journal*, **45**(1), 263–274.

Grice, K., Cao, C., Love, G. D., Böttcher, M. E., Twitchett, R. J., Grosjean, E., Summons, R. E., Turgeon, S. C., Dunning, W., & Jin, Y. 2005c. Photic zone euxinia during the Permian-triassic superanoxic event. *Science*, **307**, 706–709.

Gvirtzman, Z., Said-Ahmad, W., Ellis, G. S., Hill, R. J., Moldowan, J. M., Wei, Z., & Amrani, A. 2015. Compound-specific sulfur isotope analysis of thiadiamondoids of oils from the Smackover Formation, USA. *Geochimica et Cosmochimica Acta*, **167**, 144–161.

Hallam, A., & Wignall, P. B. 1997. *Mass Extinctions and their Aftermath*. Oxford University Press.

Hedges, J. I. 1992. Global biogeochemical cycles: progress and problems. *Marine Chemistry*, **39**(1-3), 67–93.

Hiteshue, R. W., Anderson, R. B., & Schlesinger, M. D. 1957. Hydrogenating Coal at 800 C. *Industrial & Engineering Chemistry*, 1–3.

Hoefs, J. 2009. *Stable isotope geochemistry*. 9th edn. Springer Berlin.

Holser, W. T., Schönlaub, H. P., Attrep Jr, M., Boeckelmann, K., Klein, P., Magaritz, M., Orth, C. J., Fenninger, A., Jenny, C., Kralik, M., Mauritsch, H., Pak, E., Schramm, J. M., Stattegger, K., & Schmöller, R. 1989. A unique geochemical record at the Permian/Triassic boundary. *Nature*, **337**(5), 39–44.

Hurtgen, M. T. 2012. The Marine Sulfur Cycle, Revisited. *Science*, **337**(6092), 305–306.

Jørgensen, B. B. 1982. Mineralization of organic matter in the sea bed - the role of sulphate reduction. *Nature*, **296**(5858), 643–645.

Kaiho, K., Kajiwara, Y., Chen, Z.-Q., & Gorjan, P. 2006a. A sulfur isotope event at the end of the Permian. *Chemical Geology*, **235**(1-2), 33–47.

Kaiho, K., Chen, Z. Q., Kawahata, H., Kajiwara, Y., & Sato, H. 2006b. Close-up of the end-Permian mass extinction horizon recorded in the Meishan section, South China: Sedimentary, elemental, and biotic characterization and a negative shift of sulfate

sulfur isotope ratio. *Palaeogeography, Palaeoclimatology, Palaeoecology*, **239**(3-4), 396–405.

Kajiwara, Y., Yamakita, S., Ishida, K., Ishiga, H., & Imai, A. 1994. Development of a largely anoxic stratified ocean and its temporary massive mixing at the Permian/Triassic boundary supported by the sulfur isotopic record. *Palaeogeography, Palaeoclimatology, Palaeoecology*, **111**(3-4), 367–379.

Kamo, S. L., Czamanske, G. K., Amelin, Y., Fedorenko, V. A., Davis, D. W., & Trofimov, V. R. 2003. Rapid eruption of Siberian flood-volcanic rocks and evidence for coincidence with the Permian-Triassic boundary and mass extinction at 251 Ma. *Earth and Planetary Science Letters*, **214**(1-2), 75–91.

Kaplan, I. R., & Rittenberg, S. C. 1964. Microbiological Fractionation of Sulphur Isotopes. *Journal of general Microbiology*, **34**(1958), 195–212.

Killops, S. D., & Killops, V. J. 2005. *Introduction to Organic Geochemistry*. Oxford: Blackwell Publishing.

Koeberl, C., Farley, K. A., Peucker-Ehrenbrink, B., & Sephton, M. A. 2004. Geochemistry of the end-Permian extinction event in Austria and Italy: No evidence for an extraterrestrial component. *Geology*, **32**(12), 1053–1056.

Kohnen, M. E. L., Sinninghe Damsté, J. S., Kock-Van Dalen, A. C., Ten Havens, H. L., Rullkötter, J., & de Leeuw, J. W. 1990. Origin and diagenetic transformations of C 25 and C 30 highly branched isoprenoid sulphur compounds: Further evidence for the formation of organically bound sulphur during early diagenesis. *Geochimica et Cosmochimica Acta*, **54**, 3053–3063.

Kohnen, M. E. l., Sinninghe Damsté, J. S., Kock-van Dalen, A. c., & de Leeuw, J. W. 1991. Di- or polysulphide-bound biomarkers in sulphur-rich geomacromolecules as revealed by selective chemolysis. *Geochimica et Cosmochimica Acta*, **55**(5), 1375–1394.

Korte, C., Kozur, H. W., Joachimski, M. M., Strauss, H., Veizer, J., & Schwark, L. 2004. Carbon, sulfur, oxygen and strontium isotope records, organic geochemistry and biostratigraphy across the Permian/Triassic boundary in Abadeh, Iran. *International Journal of Earth Sciences*, **93**(4), 565–581.

Kring, D. A. 2007. The Chicxulub impact event and its environmental consequences at the Cretaceous-Tertiary boundary. *Palaeogeography, Palaeoclimatology, Palaeoecology*, **255**(1-2), 4–21.

Krull, E. S., & Retallack, G. J. 2000. d13C depth profiles from paleosols across the Permian-Triassic boundary: Evidence for methane release. *Bulletin of the Geological Society of America*, **112**(9), 1459–1472.

Li, S., Amrani, A., Pang, X., Yang, H., Said-Ahmad, W., Zhang, B., & Pang, Q. 2015. Origin and quantitative source assessment of deep oils in the Tazhong Uplift, Tarim Basin. *Organic Geochemistry*, **78**, 1–22.

Littke, R., Baker, D. R., & Rullkötter, J. 1997. Deposition of petroleum source rocks. *Pages 271–333 of:* Welte, D. H, Horsfield, B., & Baker, D. R. (eds), *Petroleum and basin evolution.*

Lockhart, R. S., Meredith, W., Love, G. D., & Snape, C. E. 2008. Release of bound aliphatic biomarkers via hydropyrolysis from Type II kerogen at high maturity. *Organic Geochemistry*, **39**(8), 1119–1124.

Love, G. D, Snape, C. E., Carr, A. D., & Houghton, R. C. 1995. Release of covalently-bound alkane biomarkers in high yields from kerogen via catalytic hydropyrolysis. *Organic Geochemistry*, **23**(10), 981–986.

Love, G. D., Snape, C. E., Carr, A. D., & Houghton, R. C. 1996. Changes in Molecular Biomarker and Bulk Carbon Skeletal Parameters of Vitrinite Concentrates as a Function of Rank. *Energy & Fuels*, **10**(1), 149–157.

Love, G. D., McAulay, A., Snape, C. E., & Bishop, A. N. 1997. Effect of Process Variables in Catalytic Hydropyrolysis on the Release of Covalently Bound Aliphatic Hydrocarbons from Sedimentary Organic Matter. *Energy & Fuels*, **11**(3), 522–531.

Machel, H. G. 2001. Bacterial and thermochemical sulfate reduction in diagenetic settings – old and new insights. *Sedimentary Geology*, **140**, 143–175.

Machel, H. G., Krouse, H. R., & Sassen, R. 1995. Products and distinguishing criteria of bacterial and thermochemical sulfate reduction. *Applied Geochemistry*, **10**(4), 373–389.

Manzano, B. K., Fowler, M. G., & Machel, H. G. 1997. The influence of thermochemical sulphate reduction on hydrocarbon composition in Nisku reservoirs, Brazeau river area, Alberta, Canada. *Organic Geochemistry*, **27**(7-8), 507–521.

Marshall, C. P., Love, G. D., Snape, C. E., Hill, A. C., Allwood, A. C., Walter, M. R., Van Kranendonk, M. J., Bowden, S. A., Sylva, S. P., & Summons, R. E. 2007. Structural characterization of kerogen in 3.4Ga Archaean cherts from the Pilbara Craton, Western Australia. *Precambrian Research*, **155**(1-2), 1–23.

Matthaei, S. K., Henley, R. W., & Heinrich, C. A. 1995a. Gold precipitation by fluid mixing in bedding-parallel fractures near carbonaceous slates at the Cosmopolitan Howley gold deposit, northern Australia. *Economic Geology*, **90**, 2123–2142.

Matthaei, S. K., Henley, R. W., Bacigalupo-Rose, S., Binns, R. A., Andrew, A. S., Carr, G. R., French, DH, McAndrew, J, & Kananagh, M. 1995b. Intrusion-related, high-temperature gold quartz veining in the Cosmopolitan Howley metasedimentary rock-hosted gold deposit, Northern Territory, Australia. *Economic Geology*, **90**, 1012–1045.

Meredith, W., Sun, C.-G., Snape, C. E., Sephton, M. A., & Love, G. D. 2006. The use of model compounds to investigate the release of covalently bound biomarkers via hydropyrolysis. *Organic Geochemistry*, **37**(12), 1705–1714.

Meyer, K. M., Kump, L. R., & Ridgwell, A. 2008. Biogeochemical controls on photic-zone euxinia during the end-Permian mass extinction. *Geology*, **36**(9), 747–750.

Moodley, L., Middelburg, J. J., Herman, P. M. J., Soetaert, K. E. R., & de Lange, G. J. 2005. Oxygenation and organic-matter preservation in marine sediments: direct experimental evidence from ancient organic carbon-rich deposits. *Geology*, **33**, 889–892.

Murray, I. P., Love, G. D., Snape, C. E., & Bailey, N. J. L. 1998. Comparison of covalently-bound aliphatic biomarkers released via hydropyrolysis with their solvent-extractable counterparts for a suite of Kimmeridge clays. *Organic Geochemistry*, **29**(5-7), 1487–1505.

Nabbefeld, B., Grice, K., Twitchett, R. J., Summons, R. E., Hays, L., Böttcher, M. E., & Asif, M. 2010. An integrated biomarker, isotopic and palaeoenvironmental study through the Late Permian event at Lusitaniadalen, Spitsbergen. *Earth and Planetary Science Letters*, **291**(1-4), 84–96.

Needham, R. S., Stuart-Smith, P. G., & Page, R. W. 1988. Tectonic evolution of the Pine Creek Inlier, Northern Territory. *Precambrian Research*, **41**, 543–564.

Newton, R. J., Pevitt, E. L., Wignall, P. B., & Bottrell, S. H. 2004. Large shifts in the isotopic composition of seawater sulphate across the Permo-Triassic boundary in northern Italy. *Earth and Planetary Science Letters*, **218**(3-4), 331–345.

Nissenbaum, A., Baedecker, M. J., & Kaplan, I. R. 1972. Organic geochemistry of Dead Sea sediments. *Geochimica et Cosmochimica Acta*, **36**(7), 709–727.

Parnell, J., Boyce, A. J., Mark, D., Bowden, S., & Spinks, S. 2010. Early oxygenation of the terrestrial environment during the Mesoproterozoic. *Nature*, **468**(7321), 290–293.

Passier, H. F., Bosch, H.-J., Nijenhuis, I. A., Lourens, L. J., Böttcher, M. E., Leenders, A., Damsté, J. S. S., de Lange, G. J., & de Leeuw, J. W. 1999. Sulphidic Mediterranean surface waters during Pliocene sapropel formation. *Nature*, **397**(6715), 146–149.

Peters, K. E., Walters, C. C., & Moldowan, J. M. 2005a. *The biomarker guide Volume 1: biomarkers and isotopes in the environment and human history*. Cambridge: Cambridge University Press.

Peters, K. E., Walters, C. C., & Moldowan, J. M. 2005b. *The biomarker guide, Volume 2. Biomarkers and isotopes in petroleum exploration and Earth history*. Cambridge: Cambridge University Press.

Peterson, B. J. 1999. Stable isotopes as tracers of organic matter input and transfer in benthic food webs: A review. *Acta Oecologica*, **20**(4), 479–487.

Racki, G., & Wignall, P. B. 2005. Late permian double-phased mass extinction and volcanism: an oceanographic perspective. *Developments in Palaeontology and Stratigraphy*, **20**, 263–297.

Raven, M. R., Adkins, J. F., Werne, J. P., Lyons, T. W., & Sessions, A. L. 2015. Sulfur isotopic composition of individual organic compounds from Cariaco Basin sediments. *Organic Geochemistry*, **80**, 53–59.

Raven, M. R., Sessions, A. L., Adkins, J. F., & Thunell, R. C. 2016. Rapid organic matter sulfurization in sinking particles from the Cariaco Basin water column. *Geochimica et Cosmochimica Acta*, **190**, 175–190.

Reichow, M. K., Pringle, M. S., Al'Mukhamedov, A. I., Allen, M. B., Andreichev, V. L., Buslov, M. M., Davies, C. E., Fedoseev, G. S., Fitton, J. G., Inger, S., Medvedev, A. Y., Mitchell, C., Puchkov, V. N., Safonova, I. Y., Scott, R. A., & Saunders, A. D. 2009. The timing and extent of the eruption of the Siberian Traps large igneous province: Implications for the end-Permian environmental crisis. *Earth and Planetary Science Letters*, **277**(1-2), 9–20.

Riccardi, A. L., Arthur, M. A., & Kump, L. R. 2006. Sulfur isotopic evidence for chemocline upward excursions during the end-Permian mass extinction. *Geochimica et Cosmochimica Acta*, **70**(23), 5740–5752.

Rickard, D., & Luther, G. W. 2007. Chemistry of iron sulfides. *Chemical Reviews*, **107**, 514–562.

Robert, A. M., Grotheer, H., Lockhart, R., Greenwood, P. F., McCuaig, T.C., Jaraula, C. M.B., Grice, K., Bagas, L., & Schwark, L. 2014. Organics in orogenic gold systems: Characterisation of organic matter associated with gold (Au) deposits. *Page 2092 of: Goldschmidt 2014, book of abstracts*.

Robert, A. M., Grotheer, H., Greenwood, P. F., McCuaig, T. C., Bourdet, J., & Grice, K. 2016. The hydropyrolysis (HyPy) release of hydrocarbon products from a high maturity kerogen associated with an orogenic Au deposit and their relationship to the mineral matrix. *Chemical Geology*, **425**, 127–144.

Robinson, N., Eglinton, G., Lafferty, C. J., & Snape, C. E. 1991. Comparison of alkanes released from a bituminous coal via hydropyrolysis and low temperature hydrogenation. *Fuel*, **70**(2), 249–253.

Rooney, M. A. 1996. Carbon isotopic evidence for the accelerated destruction of light hydrocarbons by thermochemical sulfate reduction. *In: Abstract of the NSERC Thermochemical Sulphate Reduction (TSR) and Bacterial Sulphate Reduction (BSR) Workshop*.

Rospondek, M. J., Köster, J., & Sinninghe Damsté, J. S. 1997. Novel C26 highly branched isoprenoid thiophenes and alkane from the menilite formation, outer Carpathians, SE Poland. *Organic Geochemistry*, **26**(5-6), 295–304.

Russell, C. A., Snape, C. E., Meredith, W., Love, G. D., Clarke, E., & Moffatt, B. 2004. The potential of bound biomarker profiles released via catalytic hydropyrolysis to reconstruct basin charging history for oils. *Organic Geochemistry*, **35**, 1441–1459.

Ryskin, G. 2003. Methane-driven oceanic eruptions and mass extinctions. *Geology*, **31**(9), 741–744.

Said-Ahmad, W., & Amrani, A. 2013. A sensitive method for the sulfur isotope analysis of dimethyl sulfide and dimethylsulfoniopropionate in seawater. *Rapid Communications in Mass Spectrometry*, **27**(24), 2789–2796.

Schulz, H. D., & Zabel, M. 2006. *Marine Geochemistry*. Springer.

Sephton, M. A., Looy, C. V., Brinkhuis, H., Wignall, P. B., de Leeuw, J. W., & Visscher, H. 2005. Catastrophic soil erosion during the end-Permian biotic crisis. *Geology*, **33**(12), 941–944.

Sepkoski Jr., J. J. 1986. Phanerozoic overview of mass extinction. *Pages 277–295 of: Patterns and Processes in the History of Life*. Springer Berlin / Heidelberg.

Sinninghe Damste, J. S., & de Leeuw, J. W. 1990. Analysis, structure and geochemical significance of organically-bound sulphur in the geosphere: State of the art and future research. *Organic Geochemistry*, **16**(4-6), 1077–1101.

Snape, C. E., Bolton, C., Dosch, R. G., & Stephens, H. P. 1989. High liquid yields from bituminous coal via hydropyrolysis with dispersed catalysts. *Energy & Fuels*, 421–425.

Sonibare, O. O., Snape, C. E., Meredith, W., Uguna, C. N., & Love, G. D. 2009. Geochemical characterisation of heavily biodegraded tar sand bitumens by catalytic hydropyrolysis. *Journal of Analytical and Applied Pyrolysis*, **86**(1), 135–140.

Svensen, H., Planke, S., Polozov, A. G., Schmidbauer, N., Corfu, F., Podladchikov, Y. Y., & Jamtveit, B. 2009. Siberian gas venting and the end-Permian environmental crisis. *Earth and Planetary Science Letters*, **277**(3-4), 490–500.

Tegelaar, E. W., de Leeuw, J. W., Derenne, S., & Largeau, C. 1989. A reappraisal of kerogen formation. *Geochimica et Cosmochimica Acta*, **53**(11), 3103–3106.

Tissot, B., & Welte, D. 1984. *Petroleum Formation and Occurrence*. 2nd edn. Heidelberg: Springer.

Twitchett, R. J. 2006. The palaeoclimatology, palaeoecology and palaeoenvironmental analysis of mass extinction events. *Palaeogeography, Palaeoclimatology, Palaeoecology*, **232**(2-4), 190–213.

Twitchett, R. J., Looy, C. V., Morante, R., Visscher, H., & Wignall, P. B. 2001. Rapid and synchronous collapse of marine and terrestrial ecosystems during the end-Permian biotic crisis. *Geology*, **29**(4), 351–354.

Vandenbroucke, M., & Largeau, C. 2007. Kerogen origin, evolution and structure. *Organic Geochemistry*, **38**(5), 719–833.

Werne, J. P., Hollander, D. J., Lyons, T. W., & Sinninghe Damsté, J. S. 2004. Organic sulfur biogeochemistry: Recent advances and future research directions. *Pages 135–150 of: Special paper 379: Sulfur biogeochemistry - past and present*. Geological Society of America.

Werne, J. P., Lyons, T. W., Hollander, D. J., Schouten, S., Hopmans, E. C., & Sinninghe Damsté, J. S. 2008. Investigating pathways of diagenetic organic matter sulfurization using compound-specific sulfur isotope analysis. *Geochimica et Cosmochimica Acta*, **72**(14), 3489–3502.

Werner, R. A., & Brand, W. A. 2001. Referencing strategies and techniques in stable isotope ratio analysis. *Rapid Communications in Mass Spectrometry*, **15**(7), 501–519.

Whiteside, J. H., & Grice, K. 2016. Biomarker Records Associated with Mass Extinction Events. *Annual Review of Earth and Planetary Sciences*, **44**, 581–612.

Wiese, F., & Reitner, J. 2011. Critical intervals in Earth's history. *In: Encyclopedia of geobiology*. Springer Netherlands.

Wignall, P. B. 2001. Large igneous provinces and mass extinctions. *Earth Science Reviews*, **53**(1-2), 1–33.

Wortmann, U. G., Bernasconi, S. M., & Böttcher, M. E. 2001. Hypersulfidic deep biosphere indicates extreme sulfur isotope fractionation during single-step microbial sulfate reduction. *Geology*, **29**(7), 647–650.

2. Stability and hydrogenation of PAH during hydropyrolysis (HyPy) – Relevance for high maturity organic matter

Hendrik Grotheer, Aileen M. Robert,
Paul F. Greenwood and Kliti Grice

Organic Geochemistry 2015, 86, pp 45-54

Abstract

A series of hydropyrolysis (HyPy) experiments have been conducted on a small suite of authentic polycyclic aromatic hydrocarbons (PAHs: coronene, pyrene and perylene) to investigate the HyPy behaviour of these PAHs. This information may help in the interpretation of the structural significance of aromatic HyPy products, often detected in high abundance, from high maturity kerogens. The PAHs were separately treated by HyPy and were all susceptible to some extent of hydrogenation. Perylene also decomposed into low molecular weight aromatics (e.g., methylbiphenyls). Structurally, perylene is much less stable than the more condensed PAHs coronene and pyrene. The total product concentrations (wt.% of starting PAH) from all HyPy experiments were consistently less than 100 wt.%, probably due to either the condensation of semi-volatile products on walls of the transfer line prior to reaching the HyPy trap or the inefficient cold trapping of highly volatile products. Hydrogenation of PAHs was prevalent and was found to be significantly influenced by the addition of a Mo-S based catalyst and potentially the C/Mo ratio, but largely independent of the two final temperatures used (520 °C and 550 °C). The fully aromatised and hydrogenated products for any stable ring system may provide a general indication of the size distribution of aromatic units within the kerogen structure.

2.1. Introduction

Hydropyrolysis (HyPy), an analytical process conducted at high temperature (up to 550 °C) and hydrogen pressure (150 bar) in the presence of a dispersed sulfided molybdenum catalyst, has been widely used to characterise coals and oil shales (Snape *et al.*, 1989, 1994). An important attribute of catalytically assisted HyPy cracking is the release of macromolecularly bound hydrocarbons with minimal isomeric alteration (Love *et al.*, 1995, 1997). In addition to structural characterisation, HyPy has proven to be a useful tool for a broad range of organic geochemical applications, including authentication of the organic composition of geological materials compromised by oil or migrated bitumen or extreme levels of biodegradation (Murray *et al.*, 1998; Russell *et al.*, 2004); evaluation of organic matter (OM) composition of meteorites (Sephton *et al.*, 2004); the detection of indigenous hydrocarbons in Archean rocks with implication to the evolution of early life (Brocks *et al.*, 2003; Marshall *et al.*, 2007; French *et al.*, 2015); and to investigate the role of sulfur in contemporary toxic oozes (Lockhart *et al.*, 2013).

Most HyPy studies have focused on aliphatic products, yet polycyclic aromatic hydrocarbons (PAHs) have also been detected following HyPy treatment of a range of high thermal maturity samples. PAHs were the major products from the HyPy treat-

ment of the black carbon fraction of soils (Meredith *et al.*, 2013), charcoals (Ascough *et al.*, 2010) and Archean rocks (Brocks *et al.*, 2003; Marshall *et al.*, 2007; French *et al.*, 2015). We also recently observed a relatively high abundance of parent and hydrogenated PAHs from the HyPy treatment of high maturity organic sediments host to a large orogenic gold deposit (Robert *et al.*, 2014). The products of the Au-associated organic matter (OM) were dominated by pyrene which had previously been reported to be a major HyPy product released from charcoals (Ascough *et al.*, 2010).

Here we describe a series of HyPy experiments with three pure PAH compounds: pyrene [A.1a], perylene [A.2a] and coronene [A.3a]. The extent of their thermal degradation and the type and abundance of products from these experiments may prove helpful in the interpretation of the aromatic-rich HyPy profiles typical of high maturity kerogens.

Systematic investigation of the isolated behaviour of different compounds is a fundamental step in establishing their behaviour and reactivity under new analytical conditions, and the results from such basic but essential experiments often help to interpret the analysis of more complex materials (i.e., organic sediments). Indeed, model compounds have often been analysed to improve our understanding of pyrolysis reaction mechanisms (Smith *et al.*, 1989; Mukherjee *et al.*, 1994; Abbott *et al.*, 1995; Rushdi *et al.*, 2003; Nkansah *et al.*, 2011) or to monitor their behaviour under simulated hydrothermal petroleum conditions (McCollom *et al.*, 1999). The HyPy behaviour of PAHs, however, has not previously been studied. Model compound-based HyPy studies have so far been largely limited to functionalised compounds like carboxylic acids, stearic and oleic acids as well as saturated and unsaturated C_{27} sterols (Meredith *et al.*, 2006).

2.2. Materials and Methods

Three model PAHs were used to investigate the effect of HyPy treatment at selected temperatures and catalyst loads. Individual stock solutions of pyrene (~70 ppm; $C_{16}H_{10}$, 99 %, Sigma Aldrich [A.1a]), perylene (~130 ppm; $C_{20}H_{12}$, $\geq$ 99.5 %, Sigma Aldrich [A.2a]) and coronene (~ 130 ppm; $C_{24}H_{12}$, 97 %, Sigma Aldrich [A.3a]) were produced and stored in a freezer at -20 °C. Roman numbers refer to the chemical structures shown in the appendix, where [A.1a–A.1h] represent pyrene-, [A.2a–A.2e] perylene- and [A.3a–A.3f] coronene-related structures. Structures [A.4a–A.4d] show additional PAHs. Silica gel (high purity, 40 Å, 35-70 mesh, Sigma Aldrich) was annealed at 550 °C for 16 h and stored at 160 °C prior to preparation of the following beds: (a) pure silica gel; and (b) silica gel loaded with 5 wt.% sulfided molybdenum catalyst ($(NH_4)MoO_2S_2$) as previously described by Love *et al.* (1995). Sub aliquots (0.5 ml) of the respective PAH solutions were separately adsorbed onto the catalyst and non-

catalyst loaded silica beds (0.5 g).

The samples were pyrolysed using a commercial apparatus (STRATA Technology Ltd) and following traditional operating procedures (Snape *et al.*, 1994; Love *et al.*, 1995; Meredith *et al.*, 2004; Aboglila *et al.*, 2011; Lockhart *et al.*, 2013). Briefly, the samples were pyrolysed with resistive heating from 25 °C to 250 °C at 300 °C/min, and then from 250 °C to the final temperature of either 520 °C or 550 °C at 8 °C/min with the final temperature held for 2 min. A constant pressure (150 bar) and flow rate (5 L/min) of ultra-high purity hydrogen (BOC Group) was maintained throughout thermal treatment. The released compounds were cold trapped on a silica-filled trap, chilled with dry ice. Products adsorbed on the silica trap were eluted with DCM (40 ml) on a large chromatographic column; elemental sulfur was removed with HCl-activated copper turnings.

The reactor and trap were cleaned after each analysis by: (i) 2 x 30 min ultrasonication in DCM: MeOH 9:1; and (ii) thermal conditioning of the sample-free HyPy reactor at 300 °C/min from 25 °C to 300 °C then 10 °C/min to 550 °C held for 10 min under constant pressure (150 bar) and H_2 flow rate (5 L/min) and confirmed to be contaminant free by HyPy treatment of clean silica gel (loaded with or without catalyst dependent on next analysis type to be run).

The HyPy released products were analysed by gas chromatography-mass spectrometry (GC-MS). A HP 6890 GC fitted with a ZB-5MS capillary column (30 m x 0.25 mm i.d. x 1 μm film thickness) was used. Ultra high purity helium (BOC) was employed as a carrier gas at constant flow rate (1.3 ml/min), with a GC oven temperature programme of 40 °C (1 min hold) to 330 °C (25 min hold) at 10 °C/min. The mass spectrometer was an Agilent 5975 inert mass selective detector (MSD) with the transfer line temperature maintained at 320 °C. Mass spectra (70 eV) were acquired in full scan mode (30-530 Da) at ~4 scans per second and at a source temperature of 230 °C.

HyPy products were quantified based on external calibration established by analysing the PAHs at several different concentrations. Duplicates were conducted of all HyPy treatments: PAH compounds, catalyst or non-catalyst; 520 °C or 550 °C final temperature. Product yields (wt.% reactant) are reported as the average value of duplicate analysis, with their variability expressed as standard variation (SV±).

2.3. Results

Hydropyrolysis product yields

In the absence of a catalyst, HyPy product yields were highest from pyrene (68 wt.% at 520 °C and 72 wt.% at 550 °C), moderate from coronene (47 wt.%; 46 wt.%) and lowest from perylene (39 wt.%; 37 wt.%) (Figure 2.1; Table 2.1). The addition of the catalyst significantly reduced the HyPy yield of products from pyrene and perylene, but had little effect on coronene product yields. For example, at 520 °C the yield of pyrene products dropped from 68 wt.% without the catalyst to 50 wt.% with the catalyst. A similar reduction was evident at 550 °C and the pyrolysis temperature generally had less of an effect compared to the catalyst.

With the exception of the catalyst-free coronene experiments the reproducibility of the total yield was generally reasonable ($\leq \pm$ 3 wt.%). The duplicate coronene non-catalyst experiments showed relatively larger variabilities of ± 17 wt.% at 520 °C and ± 7 wt.% at 550 °C.

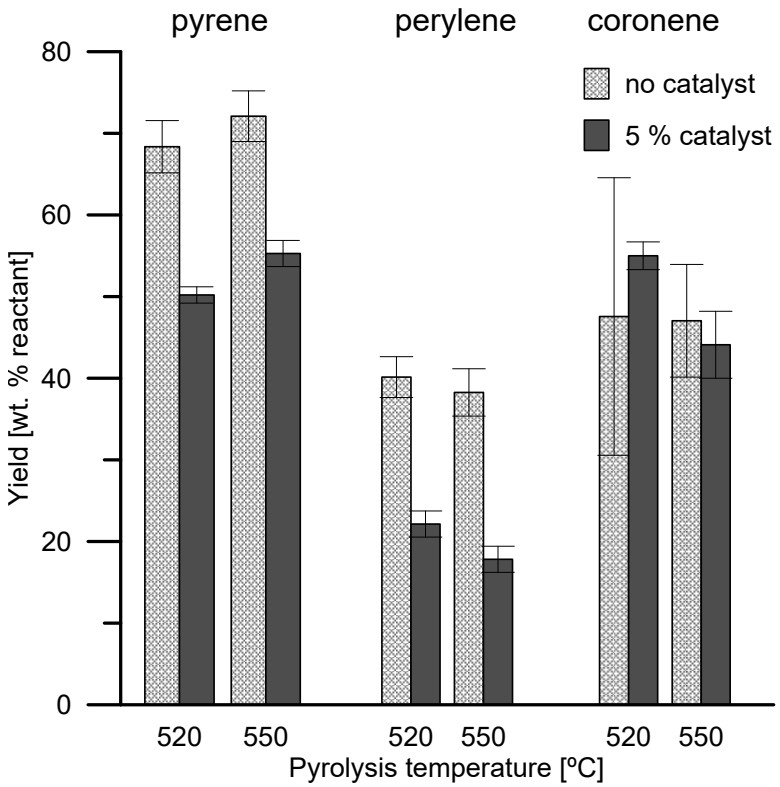

Figure 2.1.: Total product yield (wt.% reactant) generated from the hydropyrolysis of pyrene, perylene and coronene adsorbed onto pure silica (dashed bars) and silica mixed with 5 wt.% catalyst (grey bars) at a final temperature of 520 °C and 550 °C. Error bars indicate the variability between duplicates.

Pyrene

Total ion chromatograms (TICs) showing distributions of products from the HyPy treatments of pyrene are illustrated in Figure 2.2 and product abundances are listed in Table 2.1. A range of hydrogenated products were detected. The relative abundance differed significantly in the presence or absence of the catalyst, but less so between the final pyrolysis temperatures investigated (Figure 2.5). HyPy released products at 550 °C and without the catalyst included pyrene [A.1a] (21 wt.%), 2H- [A.1b] (24 wt.%), 4H- [A.1c] (21 wt.%), 6H- [A.1d–A.1e] (4 wt.%) and 10H-[pyrenes] [A.1f–A.1g] (2 wt.%). The corresponding 520 °C pyrolysis showed a similar distribution of products. Whilst the addition of the catalyst reduced overall product yields (by 17 wt.% at 550 °C) – particularly of 2H-[pyrene] (reduced by ~half to 9 wt.%) and 4H-[pyrene] (by ~three quarters to 5 wt.%) – there was an increase in the degree of hydrogenation exemplified by the detection of fully hydrogenated 16H-[pyrene] [A.1h] isomers (13 wt.%). No products indicative of the breakdown of the four ringed pyrene structure were detected.

Perylene

TICs showing the distribution of products from the HyPy treatments of perylene are shown in Figure 2.3 and product abundances are shown in Table 2.1. Catalyst-free 550 °C HyPy products included 14H-[perylene] [A.2d] (20 wt.%) and 6H-[perylene] [A.2b] (16 wt.%) as well as traces of perylene [A.2a] and 2H-[4H-benz[*de*]anthracene] [A.4c]. Product yields were lower with the catalyst (by 20 wt.% at 550 °C) – particularly 6H- and 14H-[perylene] which had reduced to < 2 wt.% - although there was an increase in abundance of the fully hydrogenated 20H-[perylene] [A.2e] (7 wt.%; Figure 2.5). No perylene was recovered, but several products were indicative of the breakdown of the perylene ring system and additional rearrangement in some cases. In the presence of the catalyst, perylene breaks down to 2-Me-1,1'-biphenyl [A.4a] (3 wt.%), 2H-[4-Me-naphthalene] [A.4b] (1 wt.%), 2H-[4H-benz[*de*]anthracene] [A.4c] (1 wt.%), with traces of pyrene [A.1a] and 2H-[pyrene] [A.1b] also detected.

Coronene

TICs from the HyPy treatments of coronene are shown in Figure 2.4 and product abundances in Table 2.1. HyPy at 550 °C with and without the catalyst gave mostly coronene [A.3a] (40 - 42 wt.%) and only traces of hydrogenated and methylated coronene. Similar product profiles were obtained with both final pyrolysis temperature and with the presence or absence of the catalyst (Figure 2.5). Coronene yield (52 wt.%) was highest at 520 °C and with the catalyst.

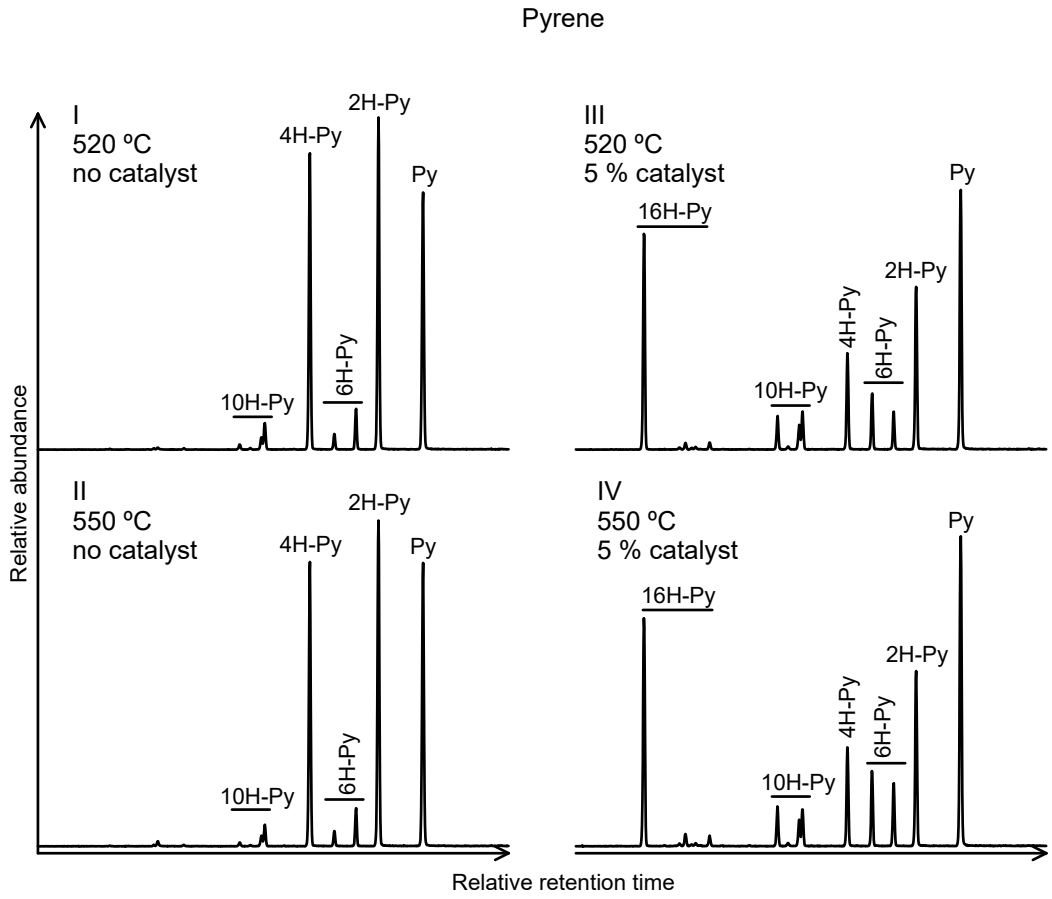

Figure 2.2.: Partial gas chromatograms of the products generated from pyrene in the absence of the catalyst at 520 °C (I) and 550 °C (II) and in the presence of the catalyst at 520 °C (III) and 550 °C (IV) final hydropyrolysis temperature. Key: Py, pyrene; XH-Py, X-hydropyrene.

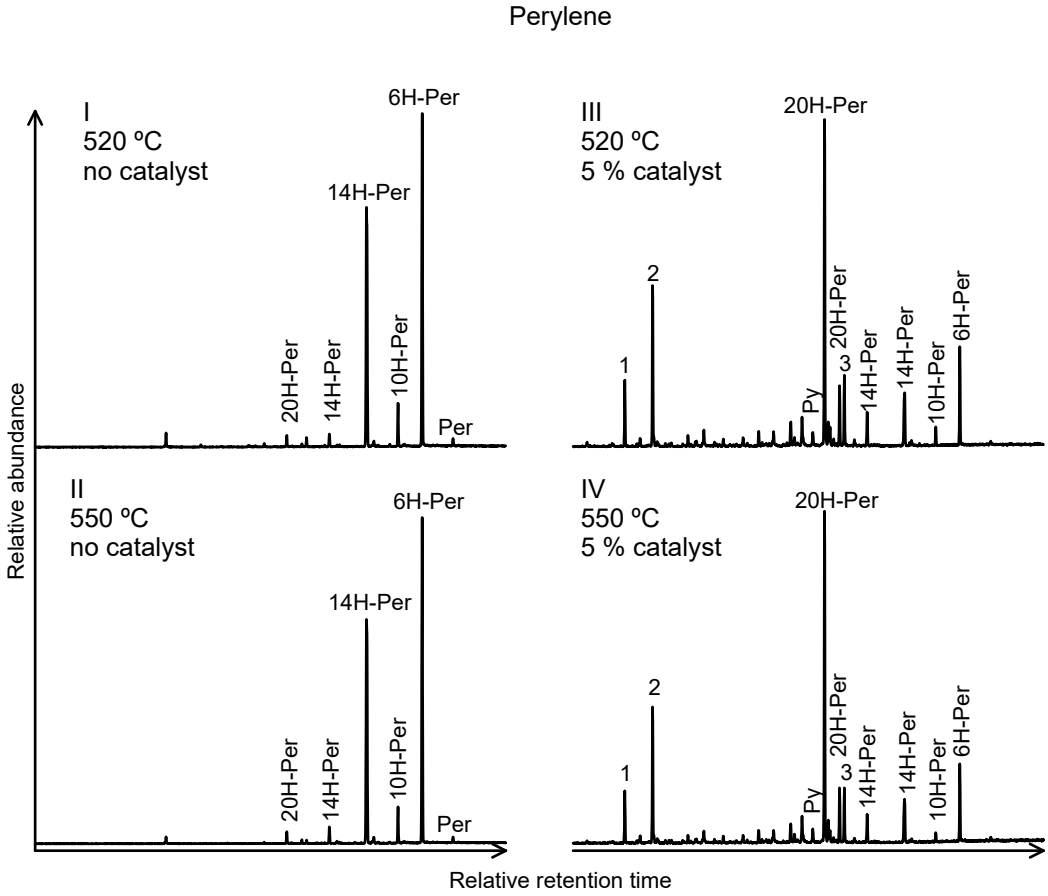

Figure 2.3.: Partial gas chromatograms of the products generated from perylene in the absence of the catalyst at 520 °C (I) and 550 °C (II) and in the presence of the catalyst at 520 °C (III) and 550 °C (IV) final hydropyrolysis temperature. Key: Per, perylene; XH-Per, X-hydroperylene; Py, pyrene; 1, 2H-4-methyl-nephthalene; 2, 2-methyl-1.1'-biphenyl; 3, 2H-4H-benz[*de*]anthracene.

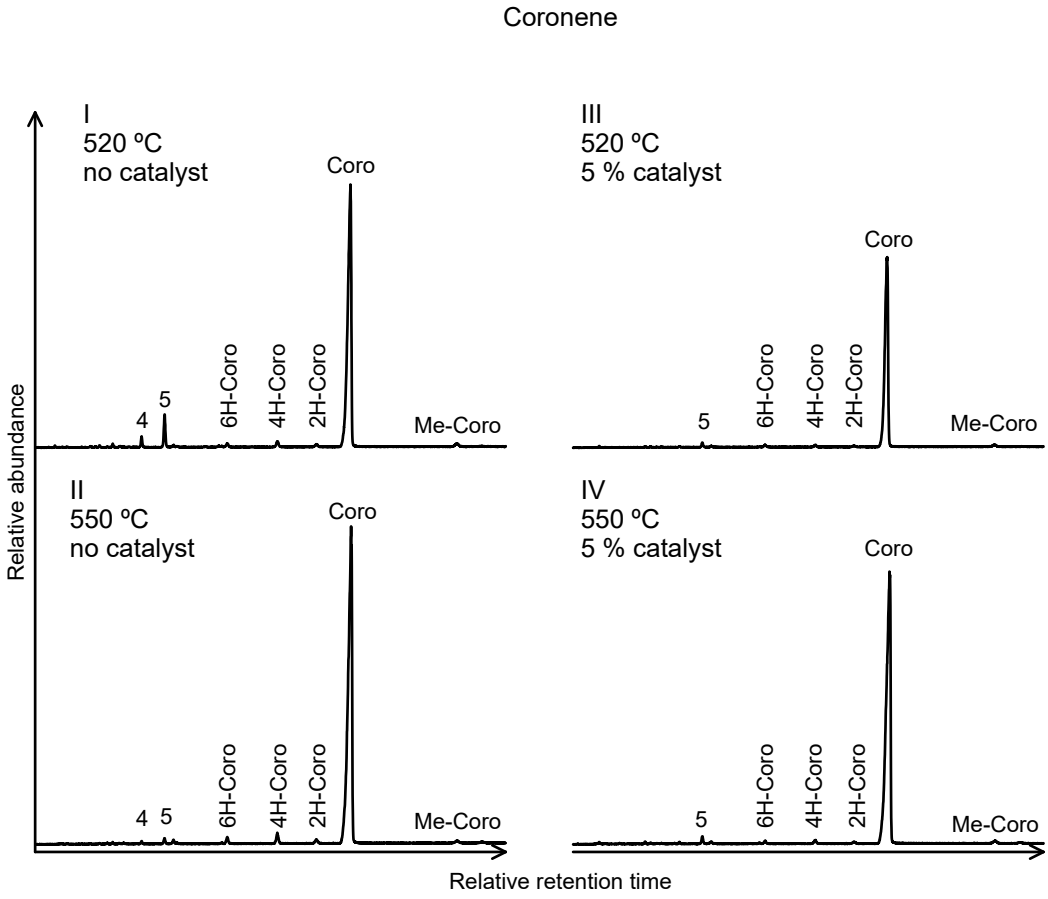

Figure 2.4.: Partial gas chromatograms of the products generated from coronene in the absence of the catalyst at 520 °C (I) and 550 °C (II) and in the presence of the catalyst at 520 °C (III) and 550 °C (IV) final hydropyrolysis temperature. Key: Coro, coronene; XH-Coro, X-hydrocoronene; Me-Coro, methyl-coronene; 4, 2H-benzo[*ghi*]perylene; 5, benzo[*ghi*]perylene.

Table 2.1.: Total yields (wt.% reactant) of HyPy products at 520 °C and 550 °C final pyrolysis temperature in the presence and absence of the catalyst from pyrene, perylene and coronene. The SV ± range indicates variability between duplicates. Roman numbers refer to chemical structures (see appendix).

			no catalyst				5 wt.% catalyst			
			temperature [°C]				temperature [°C]			
			520	SV	550	SV	520	SV	550	SV
reactant	product	structure	[wt.%]	±	[wt.%]	±	[wt.%]	±	[wt.%]	±
pyrene	pyrene	[A.1a]	19.7	1.2	20.8	0.9	14.5	0.6	16.9	0.4
	2H-[pyrene]	[A.1b]	23.0	0.4	24.3	0.6	8.8	0.0	9.2	0.0
	4H-[pyrene]	[A.1c]	20.0	0.5	20.8	1.1	4.9	0.1	5.1	0.1
	6H-[pyrene]	[A.1d–A.1e]	3.3	0.4	3.7	0.3	4.7	0.1	6.0	1.0
	10H-[pyrene]	[A.1f–A.1g]	2.4	0.8	2.4	0.2	4.9	0.2	5.4	0.0
	16H-[pyrene]	[A.1h]	⋯	⋯	⋯	⋯	12.5	0.5	12.7	0.8
	total		68.4	3.2	72.1	3.1	50.2	1.0	55.3	1.6
perylene	perylene	[A.2a]	trace		trace		—	—	—	—
	6H-[perylene]	[A.2b]	16.0	1.8	15.5	2.2	1.7	0.4	1.2	0.0
	10H-[perylene]	[A.2c]	2.1	0.1	1.6	0.2	trace		trace	
	14H-[perylene]	[A.2d]	20.5	0.3	19.5	0.2	2.1	0.5	1.7	0.1
	20H-[perylene]	[A.2e]	0.6	0.0	0.8	0.1	8.9	0.1	7.2	0.0
	pyrene	[A.1a]	⋯	⋯	⋯	⋯	trace		trace	

Table 2.1.: Total yields (wt.% reactant) of HyPy products at 520 °C and 550 °C final pyrolysis temperature in the presence and absence of the catalyst from pyrene, perylene and coronene. The SV ± range indicates variability between duplicates. Roman numbers refer to chemical structures (see appendix).

			no catalyst temperature [°C]				5 wt.% catalyst temperature [°C]			
reactant	product	structure	520 [wt.%]	SV ±	550 [wt.%]	SV ±	520 [wt.%]	SV ±	550 [wt.%]	SV ±
	2H-[pyrene]	[A.1b]	···	···	···	···	trace		trace	
	2-Me-1,1'-biphenyl	[A.4a]	···	···	···	···	3.3	0.2	2.9	0.7
	2H-[4-Me-naphthalene]	[A.4b]	···	···	···	···	1.3	0.1	1.1	0.2
	2H-[4H-benz[*de*]anthracene]	[A.4c]	trace		trace		1.5	0.1	1.0	0.1
	others		···	···	···	···	2.4	0.0	2.0	0.4
	total		39.2	2.2	37.4	2.7	21.2	1.4	17.1	1.5
coronene	coronene	[A.3a]	41.0	14.2	42.4	6.3	52.6	1.5	40.4	3.3
	Me-coronene	[A.3b]	0.8	0.1	0.5	0.1	0.6	0.1	0.6	0.1
	2H-[coronene]	[A.3c]	0.7	0.3	0.7	0.1	trace		trace	
	4H-[coronene]	[A.3d]	1.1	0.3	1.3	0.1	0.4	0.0	0.7	0.1
	6H-[coronene]	[A.3e]	0.7	0.2	0.7	0.1	0.3	0.0	0.5	0.0
	24H-[coronene]	[A.3f]	···	···	···	···	trace		trace	
	benzo[*ghi*]perylene	[A.4d]	2.2	1.4	0.7	0.0	0.5	0.1	0.9	0.1
	total		46.5	16.5	46.3	6.7	54.5	1.7	43.9	3.6

2.4. Discussion

2.4.1. Relative stability of PAHs

The product yields from the separate HyPy treatment of the three PAHs were consistently < 100 wt.% relative to the starting material. The product yields were much more dependent on the use or not of the catalyst than the final pyrolysis temperature. Perylene gave much lower yields than pyrene despite having similar boiling points (BP pyrene = 404 °C, perylene = 400 °C), hence also their volatilisation temperatures. Furthermore, little difference was evident in the products at the 520 °C and 550 °C pyrolysis temperatures. The addition of the Mo-S based catalyst reduced the product yields from both perylene and pyrene, but had little effect on the product yields from the less thermally labile coronene (BP = 525 °C). This suggests that the generation of products was controlled by factors other than the boiling point of the PAHs.

HyPy of coronene showed lower abundances of hydrogenated products than the other two PAHs, which probably also reflects its higher thermal stability during the HyPy treatment. PAH stability is dependent on the number of complete and isolated aromatic rings as described by the qualitative "aromatic sextet" theory (Clar, 1972). Coronene [A.3a] has 3 isolated aromatic rings, or sextets, and 3 non-reactive π-double bonds in the outer six rings. The outer sextets are believed to migrate into the neighbouring rings, thus creating an additional ring current making coronene highly stable and non-reactive (Clar *et al.*, 1968). Pyrene [A.1a] is also relatively stable with two sextets and two fixed π-double bonds (Clar *et al.*, 1963; Clar, 1972). This is one less of each than occurs in coronene, potentially indicative of lower stability which probably accounts for the higher degree of hydrogenated pyrenes than coronenes. Perylene [A.2a], especially in the presence of the catalyst, was the most unstable of the three PAHs surviving the HyPy treatment in relatively low abundances and yielding HyPy products reflecting ring structure break-up. The perylene structure can be considered as two naphthalene complexes connected by two single bonds, resulting in two sextets and 4 non-fixated and reactive π-double bounds (Clar, 1972). This π-double bond configuration makes perylene more reactive and therefore less stable than pyrene, despite its similar BP. The relative stabilities shown in our experiments (coronene > pyrene > perylene) are also in agreement with thermodynamic calculations (Stein & Fahr, 1985; Stein, 1991; Stein & Brown, 1991).

The relatively low stability and high reactivity of perylene might account for the low HyPy product yields from this PAH, but relatively high product losses were also encountered for HyPy treatment of pyrene (50 wt.% product loss) and coronene (65 wt.% loss). The high unaccounted wt.% of PAH reactant consumed during the HyPy experiments could be attributed to any of the following: (i) condensation of semi-

volatiles in the HyPy apparatus prior to adsorption on the silica trap; (ii) production of polyaromatic macromolecules in the reactor which could not be extracted with organic solvents; and (iii) loss of highly volatile products (e.g., hydrocarbon gases).

Some of the semi-volatile products generated from the PAHs, especially the structurally condensed high BP coronene reactant, could condense within the HyPy system (e.g., reactor tube, transfer pathway to the trap, upper part of the trap tube) preventing their complete transfer to the silica trap.

Some of the PAH reactant may have also been converted into a non-labile residue. Meredith *et al.* (2006) associated the low HyPy yields from pure stearic and oleic acids (~70 wt%) to the formation of stable Si-O-C linkages between the acids and the silica substrate retarding volatilisation. Si-O-C linkages are thought to be stable up to HyPy temperatures of 600 °C (Mitchell *et al.*, 1993) and may similarly influence the volatilisation of pyrene, perylene and coronene. Solvent extraction of the present HyPy residues showed no GC-MS products, indicating that no free PAH reactant survived the thermal treatment. Mukherjee *et al.* (1994) furthermore reported the formation of bipyrenes (*m/z* = 402) and soot from the pyrolysis of pyrene in a laminar flow drop tube furnace between 1200 and 1500 K, but within the *m/z* range of the GC-MSD we employed such high MW, coupled structures could not be measured.

At the other end of the volatility spectrum, highly mobile gaseous range products (e.g., CO_2, CH_4) may have escaped adsorption onto the silica trap or have been lost with subsequent preparation (i.e., elution from the trap silica). However, no decomposition products, smaller than the starting reactant, could be identified from the pyrene and coronene reactants. Volatile generation from these PAHs would thus have required rapid collapse of the whole ring structure on reaching a critical point temperature, producing just highly volatile, low MW hydrocarbons (e.g., CH_4). Efficient gasification of such stable structures would seem unlikely, although Mitchell *et al.* (1993) reported extensive secondary hydrocracking of benzene into volatile units (e.g., CH_4, C_4H_8 and C_5H_8) during HyPy in the presence of a Mo-S catalyst.

The experimental procedure used here did not allow for the exhaustive capture of all products (volatiles, residue and solid products) or a robust mass balance assessment of reactions. The PAH reactants (~35 µg pyrene, ~65 µg perylene, ~65 µg coronene) were orders of magnitude lower in mass than the silica substrate (0.5 g) making reliable measurements of the mass variation or characterisation (e.g., EA) of small amounts of any insoluble soot formed during the HyPy treatment unfeasible. It remains unclear to what extant potential sinks influenced the detection of HyPy products, but modified experimental setup could be used in the future to account for all possibilities.

The outcomes of these relatively simple experiments with isolated PAHs are not directly translatable to the corresponding analysis of complex natural systems. Indeed, an observed increase of HyPy yield from coals by the addition of the catalyst (Bolton

et al., 1988; Snape *et al.*, 1989) and high thermal stability of pyrene shown by Ascough *et al.* (2010) during the hydropyrolysis of charcoals contrasts the relatively low HyPy yields and the decrease in yield by the addition of the catalyst for our model compound experiments. This quantitative difference is likely due to the different nature of respective sample types. In our experiments the PAHs were adsorbed on the silica surface, but the hydrocarbon structural units within coals are covalently bound within a larger organic network, and with varying functionalities, which may help protect them from thermal degradation. Addition of the catalyst to the coals (typically in lower or equal abundance as the organic carbon) increased HyPy product yields (Bolton *et al.*, 1988; Snape *et al.*, 1989) by lowering the activation energies for the cracking of C-C bonds. In the presented PAH experiments, however, the catalyst was in excess to the PAH reactant (C/Mo = 0.02 for the pyrene experiment) which may have increased the rates of decomposition reactions.

Nevertheless, some observations from the present PAH experiments may provide useful insight into the HyPy behaviour of more complex systems. The negligible abundances of low MW products from the HyPy of pyrene and coronene suggests all parent and hydrogenated products of a particular condensed ring system may be indicative of the kerogen concentrations of the parent PAH. Such a correlation might also partially extend to non-condensed PAHs like perylene. Whilst these PAHs might produce smaller ringed products, the combined abundance of the fully aromatised and hydrogenated analogues of a particular ringed system might provide a general indication of the corresponding PAH in high maturity kerogens. Of course these interpretations would be complicated by difficulties in reliably accounting for all smaller ringed products of larger ringed systems (e.g., methyl-biphenyl products of perylene). But perhaps some of these difficulties could be lessened by careful consideration of the nature of the sample being analysed. For instance, the natural occurrence of perylene has been correlated to the evolutionary rise of vascular plants (Grice *et al.*, 2009) so this structure could be assumed to be absent in ancient organic-rich sediments.

It has been proposed that higher molecular weight PAHs can form by the condensation of low molecular weight precursors through the addition of C_2 and C_4 units to the existing ring structure (Stein, 1978). The present HyPy experiments showed no evidence for any polycyclic structure larger than the starting PAH reactant. HyPy of coronene did produce a low abundance of methyl-coronene [A.3b] suggesting that methylation of some PAHs may occur and the prevalence and controls on this reaction during HyPy warrants further investigation. Interestingly, pyrene which showed the highest hydrogenation reactivity gave no methylated products. The controls on PAH methylation during HyPy treatment remain unclear, and if some structural systems were particularly prone to these reactions they may compromise the use of traditional parameters which compare the relative abundance of parent and methylated PAHs.

For instance, similar methylation of phenanthrene during HyPy analysis would potentially distort thermal maturity indices based on phenanthrene and methyl-phenanthrene abundances (Radke *et al.*, 1982; Dick *et al.*, 2013; Holman *et al.*, 2014; Le Métayer *et al.*, 2014).

2.4.2. Hydrogenation of pyrene

The HyPy detection of 2H-[pyrene] and also 2H- and 4H-[phenanthrenes] were reported in the analysis of high maturity OM from Archean sediments (Marshall *et al.*, 2007). The 2H-[pyrene] was in much lower abundance than pyrene, although this may have been influenced by the high carbon to molybdenum ratio (C/Mo = 1.5 - 2.1; cf. 0.02 in our experiments) resulting from analysis of samples of low TOC (Cf. our model compound analysis). No explanation for the production or significance of the hydrogenated products of Archean kerogens was given. We have previously detected unusually high concentrations of pyrene and hydrogenated pyrenes from the HyPy treatment of high maturity OM in sediments associated with orogenic gold deposits (Robert *et al.*, 2014); and Ascough *et al.* (2010) similarly observed high abundances of pyrene from HyPy of charcoal. Few PAHs have been reported from HyPy studies of low maturity OM samples. This suggests they derived from similar aromatic structures within high maturity kerogens which can be released by HyPy. High abundances of hydrogenated aromatic products were also detected, so released PAHs are evidently susceptible to hydrogenation in the HyPy reactor, probably promoted by the high hydrogen atmosphere and Mo-S catalyst.

Hydrogenation of the reactant PAHs was evident for all treatments regardless of pyrolysis temperature or inclusion of the catalyst. It was clearly more extensive, however, for pyrene than the other PAHs (Figure 2.5). In the absence of the catalyst, hydrogenation occurs predominantly on the carbons at position 4 and 5 to form 4,5-dihydropyrene [A.1b] and also additionally on carbons 9 and 10 forming 4,5,9,10-tetrahydropyrene [A.1c]. This observation is in agreement with density functional theory in which calculated hydrogen bonding energies for a series of PAHs predict highest energies for twofold coordinated carbon atoms within PAH structures (Rasmussen, 2013). Table 2.2 shows the hydrogenation ratios for pyrene. The ratios of [pyrene/(2H-[pyrene]+pyrene)] and [pyrene/([4H-pyrene]+pyrene)] in the absence of the catalyst show the parent pyrene was equally abundant as the 2H- and 4H-[pyrene] products. Furthermore the ratio of [pyrene/ (∑XH-[pyrene]+pyrene)] (i.e. where ∑XH-[pyrene] is the sum of all hydrogenated pyrene analogues), is 0.3. The ratio indicates the relative % of pyrene over all produced analogues. Therefore, the release and persistence of intact (fully aromatised) pyrene was only 30 % of all products with this 4 ringed structure. The degree of hydrogenation was similar at 520 and 550 °C, reflecting little

differences at these temperatures.

The catalyst intensifies the hydrogenation and even contributed complete hydrogenation of some of the pyrene reactant to form 16H-[pyrene]. This fully saturated product was detected in almost equal abundance as the fully aromatised pyrene. Simultaneously, the relative abundance of 2H- and 4H-[pyrene] to pyrene decreases significantly (Table 2.1; Table 2.2; Figure 2.5), thus identifying these as likely intermediates in a progressive hydrogenation mechanism. Furthermore the ratio of [pyrene/ (∑XH-[pyrene]+pyrene)] is 0.3. This is exactly the same ratio obtained for the catalyst-free experiment.

The activation temperature of the catalyst is approximately 400 °C (Meredith *et al.*, 2014), similar to the BP of pyrene and perylene, but significantly lower than the BP of coronene. Hydrogenation probably occurs following volatilisation in the gaseous phase and is directly influenced by the catalyst. This observation supports the idea that hydrogenated analogues derive directly from a parent PAH and so could be used to predict the PAH composition of kerogens.

The hydrogenation of PAHs at low pressure and ambient temperature has previously been shown to be regioselective in the presence of palladium or platinum catalysts (Fu *et al.*, 1980) and highly selective under elevated temperature and pressure in the presence of a cobalt carbonyl catalyst (Feder & Halpern, 1975). Hence, hydrogenation of PAHs in the presence of the Mo-S catalyst might have also been expected, and as the present HyPy experiments show.

Hydrogenated PAH products might ultimately provide valuable information about the structures and cracking behaviour of very high maturity kerogens, or related high temperature phenomena such as the reaction of sedimentary OM with hydrothermal fluids. However, much better understanding of the controls on their HyPy generation will be needed.

Table 2.2.: Hydrogenation ratios for pyrene depending on final pyrolysis temperature and catalyst load. The ± range indicates the variability between duplicates following error propagation.

	no catalyst				5 wt% catalyst			
	temperature [°C]				temperature [°C]			
ratio	520	±	550	±	520	±	550	±
$pyrene/(2H-[pyrene]+pyrene)$	0.46	0.05	0.46	0.04	0.62	0.04	0.65	0.03
$pyrene/(4H-[pyrene]+pyrene)$	0.50	0.05	0.50	0.05	0.75	0.06	0.77	0.04
$pyrene/(16H-[pyrene]+pyrene)$	···	···	···	···	0.54	0.04	0.57	0.04
$pyrene/(\Sigma H-[pyrene]+pyrene)$	0.29	0.03	0.29	0.02	0.29	0.02	0.31	0.02

2.5. Conclusions

The HyPy treatment of three different PAH structures showed the extent of product generation including the persistence of free PAH reactant. Hydrogenation and smaller ringed products was largely controlled by the relative structural stability of the PAHs (coronene > pyrene > perylene). Unlike perylene, the more condensed ringed aromatics (e.g., pyrene and coronene) did not break down into smaller ringed structures adsorbed on the silica trap or analysed by GC-MS. However, total product recoveries were less than the reactant losses, possibly due to analytical limitations such as condensation of products prior to reaching the trap. All PAHs showed a vulnerability to hydrogenation, the extent of these reactions was influenced to varying degrees by the metal catalyst. The combined abundance of hydrogenated and fully aromatic systems sharing the same polycyclic frame may provide a general indication of the kerogen concentrations of the corresponding PAH.

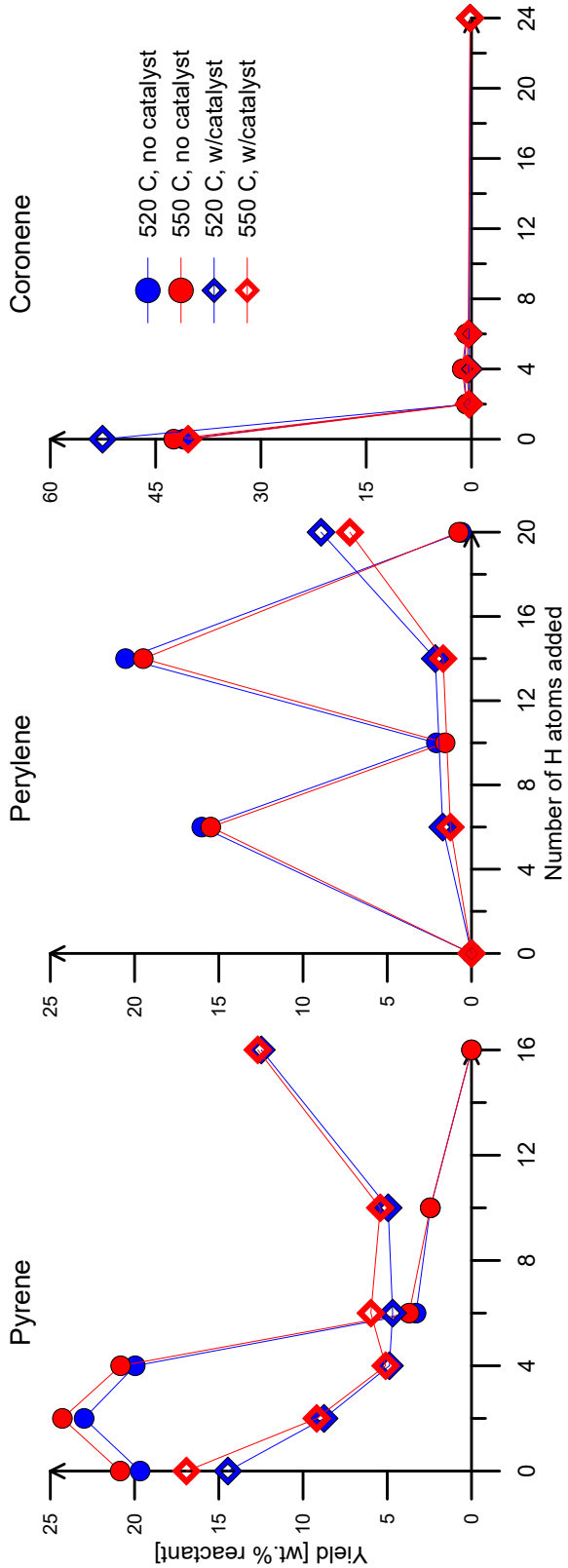

Figure 2.5: Product yield (wt% reactant) relative to the amount of hydrogen atoms added to parent pyrene (left), perylene (middle) and coronene (right) structure at 520 °C (blue lines), 550 °C (red lines), in the absence of the catalyst (closed circles) and with catalyst (open diamonds).

Acknowledgments

This study was conducted as part of the CSIRO Flagship Collaboration Fund Cluster for Organic Geochemistry of Mineral Systems, led by Curtin University and thanks are provided by all authors of this paper. HG thanks CSIRO and the Department of Chemistry, Curtin University for a joint scholarship as well as WA-OIGC and TIGeR for top-up scholarships. Geoff Chidlow is thanked for providing technical support for GC-MS analysis and HyPy maintenance. We thank Will Meredith and an anonymous reviewer for their helpful and constructive comments.

References

Abbott, G. D., Bennett, B., & Petch, G. S. 1995. The thermal degradation of 5a (H)-cholestane during closed-system pyrolysis. *Geochimica et Cosmochimica Acta*, **59**(11), 2259–2264.

Aboglila, S., Grice, K., Trinajstic, K., Snape, C., & Williford, K. H. 2011. The significance of 24-norcholestanes, 4-methylsteranes and dinosteranes in oils and source-rocks from East Sirte Basin (Libya). *Applied Geochemistry*, **26**(9-10), 1694–1705.

Ascough, P., Bird, M.I., Meredith, W., Wood, R.E., Snape, C.E., Brock, F., Higham, T.F., Large, D.J., & Apperley, D.C. 2010. Hydropyrolysis: implications for radiocarbon pre-treatment and characterization of Black Carbon. *Radiocarbon*, **52**(2), 1336–1350.

Bolton, C., Riemer, C., Snape, C. E., Derbushire, F. J., & Terrer, M.T. 1988. Effect of low temperature catalytic hydrogenation on pyrolysis and hydropyrolysis of a bituminous coal. *Fuel*, **67**, 901–905.

Brocks, J. J., Love, G. D., Snape, C. E., Logan, G. A., Summons, R. E., & Buick, R. 2003. Release of bound aromatic hydrocarbons from late Archean and Mesoproterozoic kerogens via hydropyrolysis. *Geochimica et Cosmochimica Acta*, **67**(8), 1521–1530.

Clar, E. 1972. *The Aromatic Sextet*. London: J. Wiley.

Clar, E., Guye-Vuillème, J. F., McCallum, S., & Macpherson, I. A. 1963. Annellation effects in the pyrene series and the classification of absorption spectra. *Tetrahedron*, **19**(1954), 2185–2197.

Clar, E., Sanigök, Ü., & Zander, M. 1968. NMR studies of perylene and coronene derivatives. *Tetrahedron*, **24**, 2817–2823.

Dick, J. M., Evans, K. A., Holman, A. I., Jaraula, C. M. B., & Grice, K. 2013. Estimation and application of the thermodynamic properties of aqueous phenanthrene and isomers of methylphenanthrene at high temperature. *Geochimica et Cosmochimica Acta*, **122**(dec), 247–266.

Feder, H. M., & Halpern, J. 1975. Mehanism of the cobalt carbonyl-catalyzed homogenous hydrogenation of aromatic hydrocarbons. *Journal of the American Chemical Society*, **97**, 7186–7188.

French, K. L., Hallmann, C., Hope, J. M., Schoon, P. L., Zumberge, J. A., Hoshino, Y., Peters, C. A., George, S. C., Love, G. D., Brocks, J. J., Buick, R., & Summons,

R. E. 2015. Reappraisal of hydrocarbon biomarkers in Archean rocks. *Proceedings of the National Academy of Sciences*, **112**(19), 5915–5920.

Fu, P. P., Lee, H. M., & Harvey, R. G. 1980. Regioselective catalytic hydrogenation of polycyclic aromatic hydrocarbons under mild conditions. *Journal of Organic Chemistry*, **45**, 2797–2803.

Grice, K., Lu, H., Atahan, P., Asif, M., Hallmann, C., Greenwood, P., Maslen, E., Tulipani, S., Williford, K., & Dodson, J. 2009. New insights into the origin of perylene in geological samples. *Geochimica et Cosmochimica Acta*, **73**(21), 6531–6543.

Holman, A. I., Greenwood, P. F., Brocks, J. J., & Grice, K. 2014. Effects of sulfide minerals on aromatic maturity parameters: Laboratory investigation using micro-scale sealed vessel pyrolysis. *Organic Geochemistry*, **76**, 270–277.

Le Métayer, P., Grice, K., Chow, C. N., Caccetta, L., Maslen, E., Dawson, D., & Fusetti, L. 2014. The effect of origin and genetic processes of low molecular weight aromatic hydrocarbons in petroleum on their stable carbon isotopic compositions. *Organic Geochemistry*, **72**, 23–33.

Lockhart, R. S., Berwick, L. J., Greenwood, P. F., Grice, K., Kraal, P., & Bush, R. 2013. Analytical pyrolysis for determining the molecular composition of contemporary monosulfidic black ooze. *Journal of Analytical and Applied Pyrolysis*, **104**, 640–652.

Love, G. D, Snape, C. E., Carr, A. D., & Houghton, R. C. 1995. Release of covalently-bound alkane biomarkers in high yields from kerogen via catalytic hydropyrolysis. *Organic Geochemistry*, **23**(10), 981–986.

Love, G. D., McAulay, A., Snape, C. E., & Bishop, A. N. 1997. Effect of Process Variables in Catalytic Hydropyrolysis on the Release of Covalently Bound Aliphatic Hydrocarbons from Sedimentary Organic Matter. *Energy & Fuels*, **11**(3), 522–531.

Marshall, C. P., Love, G. D., Snape, C. E., Hill, A. C., Allwood, A. C., Walter, M. R., Van Kranendonk, M. J., Bowden, S. A., Sylva, S. P., & Summons, R. E. 2007. Structural characterization of kerogen in 3.4Ga Archaean cherts from the Pilbara Craton, Western Australia. *Precambrian Research*, **155**(1-2), 1–23.

McCollom, T. M., Simoneit, B. R. T., & Shock, E. L. 1999. Hydrous pyrolysis of polycyclic aromatic hydrocarbons and implications for the origin of PAH in hydrothermal petroleum. *Energy and Fuels*, **13**(6), 401–410.

Meredith, W., Russell, C. A., Cooper, M., Snape, C. E., Love, G. D., Fabbri, D., & Vane, C. H. 2004. Trapping hydropyrolysates on silica and their subsequent thermal desorption to facilitate rapid fingerprinting by GC-MS. *Organic Geochemistry*, **35**(1), 73–89.

Meredith, W., Sun, C.-G., Snape, C. E., Sephton, M. A., & Love, G. D. 2006. The use of model compounds to investigate the release of covalently bound biomarkers via hydropyrolysis. *Organic Geochemistry*, **37**(12), 1705–1714.

Meredith, W., Ascough, P. L., Bird, M. I., Large, D. J., Snape, C. E., Song, J., Sun, Y., & Tilston, E. L. 2013. Direct evidence from hydropyrolysis for the retention of long alkyl moieties in black carbon fractions isolated by acidified dichromate oxidation. *Journal of Analytical and Applied pyrolysis*, **103**, 232–239.

Meredith, W., Snape, C. E., & Love, G. D. 2014. Development and use of catalytic hydropyrolysis (HyPy) as an analytical tool for organic geochemical application. *Chap. 6, pages 171–203 of:* Grice, Kliti (ed), *Principles and Practice of Analytical Techniques in Geosciences*. UK: Royal Society of Chemistry.

Mitchell, S. C., Lafferty, C. J., Garcia, R., Snape, C. E., Buchanan, A. C., Britt, P. F., & Klavetter, E. 1993. Silica-Immobilized Compounds As Models For Probing Coal Pyrolysis and Hydropyrolysis Phenomena. *Energy & Fuels*, **7**(11), 331–333.

Mukherjee, J., Sarofim, A. F., & Longwell, J. P. 1994. Polycyclic aromatic hydrocarbons from the high-temperature pyrolysis of pyrene. *Combustion and Flame*, **96**, 191–200.

Murray, I. P., Love, G. D., Snape, C. E., & Bailey, N. J. L. 1998. Comparison of covalently-bound aliphatic biomarkers released via hydropyrolysis with their solvent-extractable counterparts for a suite of Kimmeridge clays. *Organic Geochemistry*, **29**(5-7), 1487–1505.

Nkansah, M. A., Christy, A. A., & Barth, T. 2011. The use of anthracene as a model compound in a comparative study of hydrous pyrolysis methods for industrial waste remediation. *Chemosphere*, **84**(4), 403–408.

Radke, M., Willsch, H., Leythaeuser, D., & Teichmüller, M. 1982. Aromatic components of coal: relation of distribution pattern to rank. *Geochimica et Cosmochimica Acta*, **46**, 1831–1848.

Rasmussen, J. A. 2013. Polycyclic aromatic hydrocarbons: Trends for bonding hydrogen. *Journal of Physical Chemistry A*, **117**, 4279–4285.

Robert, A. M., Grotheer, H., Lockhart, R., Greenwood, P. F., McCuaig, T.C., Jaraula, C. M.B., Grice, K., Bagas, L., & Schwark, L. 2014. Organics in orogenic gold systems: Characterisation of organic matter associated with gold (Au) deposits. *Page 2092 of: Goldschmidt 2014 Book of Abstracts*.

Rushdi, A. I., Ritter, G., Grimalt, J. O., & Simoneit, B. R. T. 2003. Hydrous pyrolysis of cholesterol under various conditions. *Organic Geochemistry*, **34**, 799–812.

Russell, C. A., Snape, C. E., Meredith, W., Love, G. D., Clarke, E., & Moffatt, B. 2004. The potential of bound biomarker profiles released via catalytic hydropyrolysis to reconstruct basin charging history for oils. *Organic Geochemistry*, **35**, 1441–1459.

Sephton, M. A., Love, G. D., Watson, J. S., Verchovsky, A. B., Wright, I. P., Snape, C. E., & Gilmour, I. 2004. Hydropyrolysis of insoluble carbonaceous matter in the Murchison meteorite: new insights into its macromolecular structure. *Geochimica et Cosmochimica Acta*, **68**(6), 1385–1393.

Smith, J. W., Batts, B. D., & Gilbert, T. D. 1989. Hydrous pyrolysis of model compounds. *Organic Geochemistry*, **14**(4), 365–373.

Snape, C. E., Bolton, C., Dosch, R. G., & Stephens, H. P. 1989. High liquid yields from bituminous coal via hydropyrolysis with dispersed catalysts. *Energy & Fuels*, 421–425.

Snape, C. E., Lafferty, C. J., Eglinton, G., Robinson, N., & Collier, R. 1994. The potential of hydropyrolysis as a route for coal liquefaction. *International Journal of Energy Research*, **18**, 233–242.

Stein, S. E. 1978. On the High Temperature Chemical Equilibria of Polycyclic Aromatic Hydrocarbons. *The Journal of Physical Chemistry*, **82**(5), 566–571.

Stein, S. E. 1991. Thermal reactions and properties of polycyclic aromatic hydrocarbons. *Accounts of Chemical Research*, **24**(6), 350–356.

Stein, S. E., & Brown, R. L. 1991. Prediction of carbon-hydrogen bond dissociation energies for polycyclic aromatic hydrocarbons of arbitrary size. *Journal of the American Chemical Society*, **113**(12), 787–793.

Stein, S. E., & Fahr, A. 1985. High-Temperature Stabillties of Hydrocarbons. *American Chemical Society*, 3114–3125.

Appendix

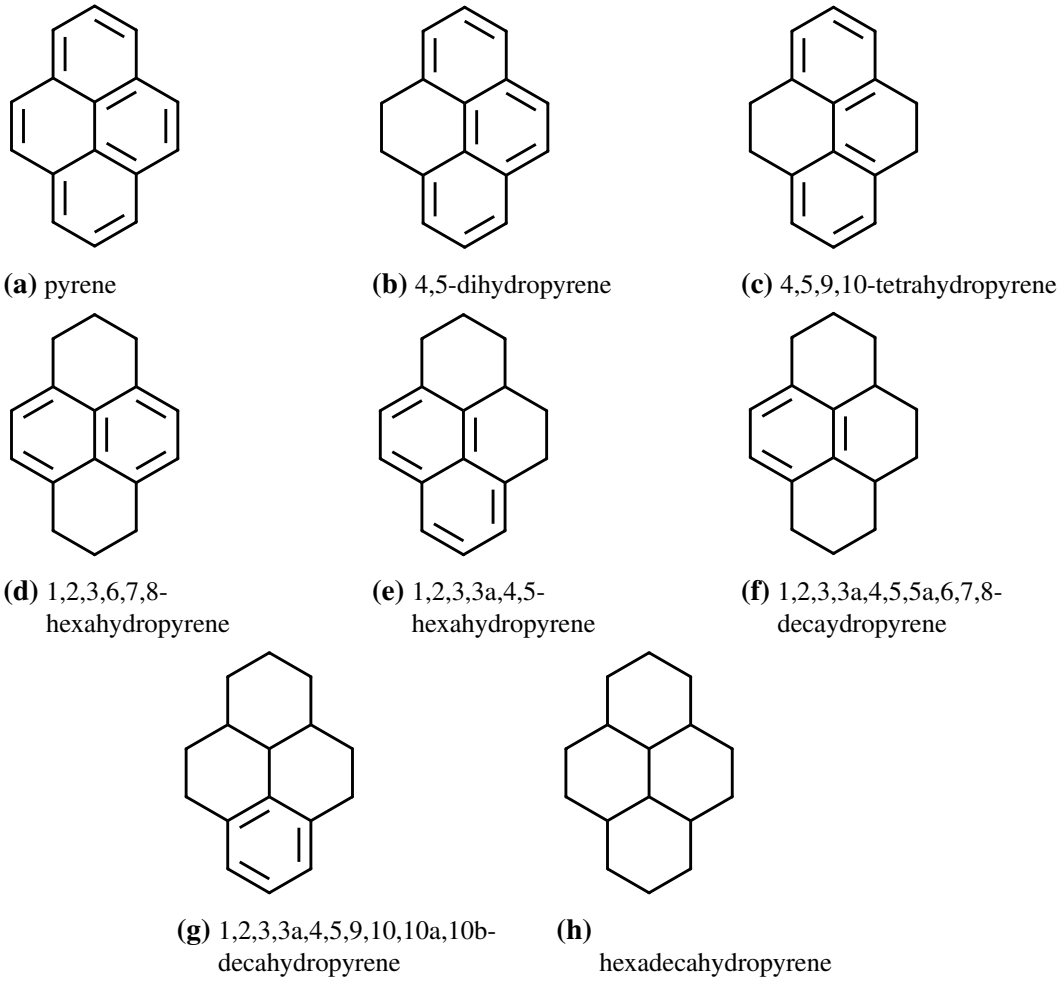

(a) pyrene

(b) 4,5-dihydropyrene

(c) 4,5,9,10-tetrahydropyrene

(d) 1,2,3,6,7,8-hexahydropyrene

(e) 1,2,3,3a,4,5-hexahydropyrene

(f) 1,2,3,3a,4,5,5a,6,7,8-decaydropyrene

(g) 1,2,3,3a,4,5,9,10,10a,10b-decahydropyrene

(h) hexadecahydropyrene

Figure A.1.: Pyrene analouges

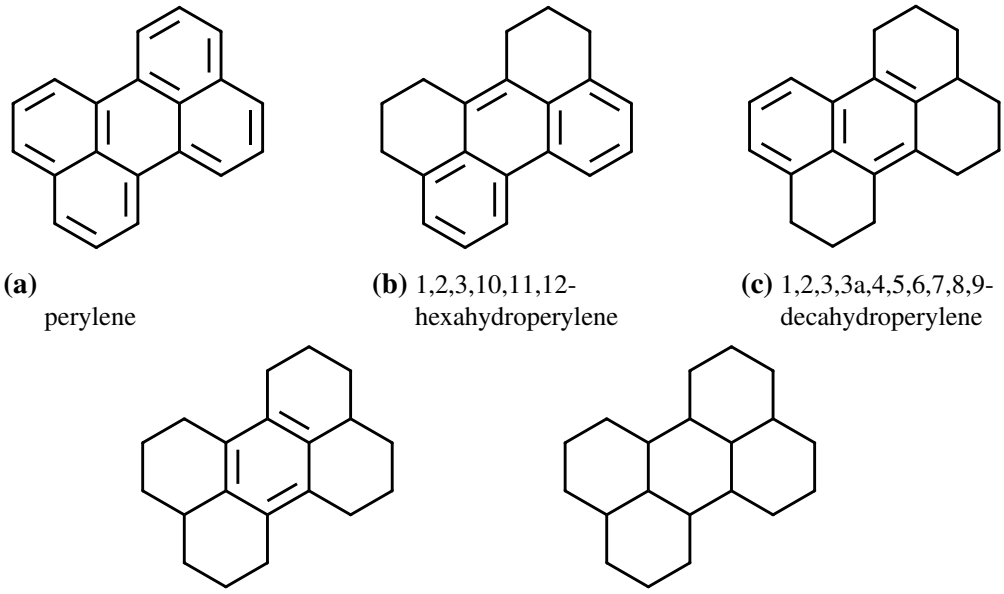

(a) perylene

(b) 1,2,3,10,11,12-hexahydroperylene

(c) 1,2,3,3a,4,5,6,7,8,9-decahydroperylene

(d) 1,2,3,3a,4,5,6,7,8,9,9a,10,11,12-tetradecahydroperylene

(e) eicocosahydroperylene

Figure A.2.: Perylene analouges

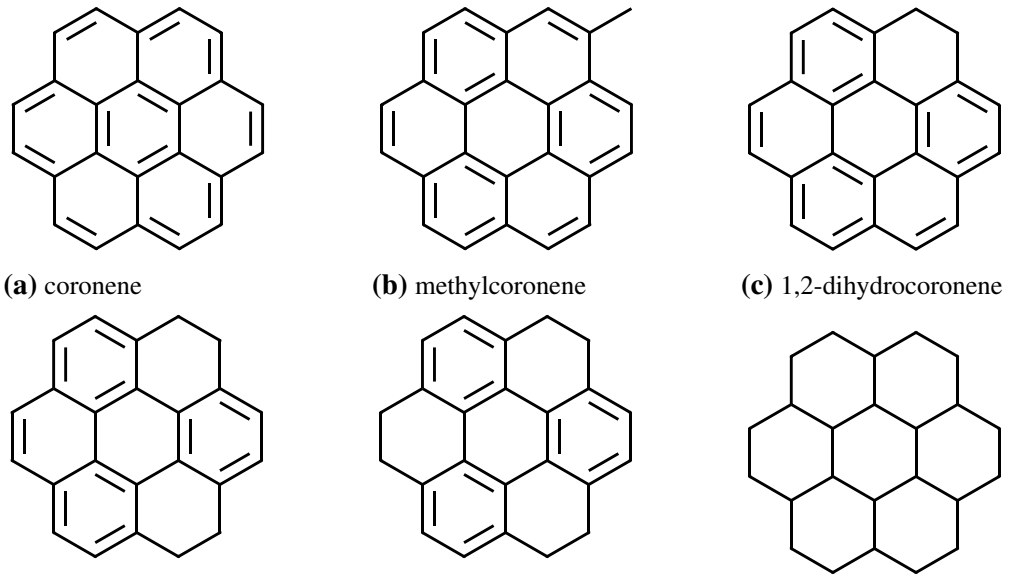

(a) coronene

(b) methylcoronene

(c) 1,2-dihydrocoronene

(d) 1,2,5,6-tetrahydrocoronene

(e) 1,2,5,6,9,10-hexahydrocoronene

(f) tetracosahydrocoronene

Figure A.3.: Coronene analouges

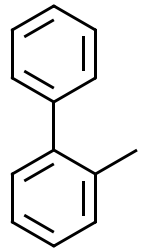

(a) 2-methyl-1,1'-biphenyl

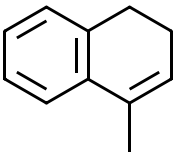

(b) 1,2-dihydro-4-methyl-naphthalene

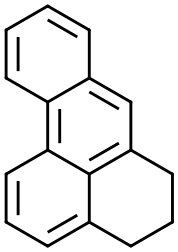

(c) 5,6-dihydro-4H-benz[*de*]anthracene

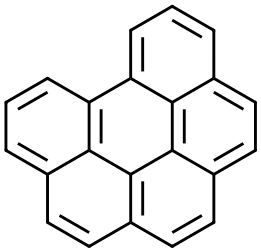

(d) benzo[*ghi*]perylene

Figure A.4.: Other PAHs

3. δ^{34}S processing of ICP-MS data

Hendrik Grotheer

3.1. Introduction

The continuous flow CSIA of the stable $\delta^{34}S$ composition of OSCs is a relatively new technique now available to the organic geochemical community. Amrani *et al.* (2009) first introduced the method by using a gas chromatograph to separate OSCs and then measure their S-isotope abundance with a Thermo Neptune^{+} multicollector inductively coupled mass spectrometer (GS-MC-ICP-MS). The Faraday collectors of the ICP-MS were set for simultaneous detection of $^{32}S^{+}$ and $^{34}S^{+}$, from which isotope ratios (e.g., $\delta^{34}S$) can be calculated. The ICP-MS measured signals of ^{34}S and ^{32}S can be converted to $\delta^{34}S$ values by normalising the ratio to the international isotope scale standard Vienna Canyon Diablo Troilite (VCDT) using a calibration equation (see below).

The Multicollector software (3.2.1.15 preview 4) supports the collection of transient $^{32}S^{+}$ and $^{34}S^{+}$ signals, but is unable to further process the data to directly yield $\delta^{34}S$ values. Rather, the raw Neptune^{+} data can be converted in ASCII format and imported into Microsoft Excel where $\delta^{34}S$ values can be calculated. However, manual processing of the raw S data in Excel is a very laborious process and susceptible to user bias. Worksheet macros applied to predetermined data point sequences might be somewhat helpful, but are limited in their use if acquisition parameters are frequently varied such is typical with analytical methods such as GC and ICP-MS. For instance, a change of GC conditions such as carrier gas flow rates, oven temperature profile or different capillary columns, would change peak retention time requiring manual redefinition of integrated peak and baseline location. In particular, peak start and end point can significantly impact the measured $\delta^{34}S$ values, and their manual designation is prone to subjectivity thus limiting data reproducibility. The example shown in Table 3.1 and Figure 3.1 for several standard and sample peaks processed by i) the candidate and ii) a supervisor using different and independently defined start and end points gave values differing by up to 9 ‰ (i.e., -26.1 Cf. -35.2 ‰). The processing speed and measurement reproducibility of $\delta^{34}S$ values might both be aided by the use of appropriate data processing algorithms.

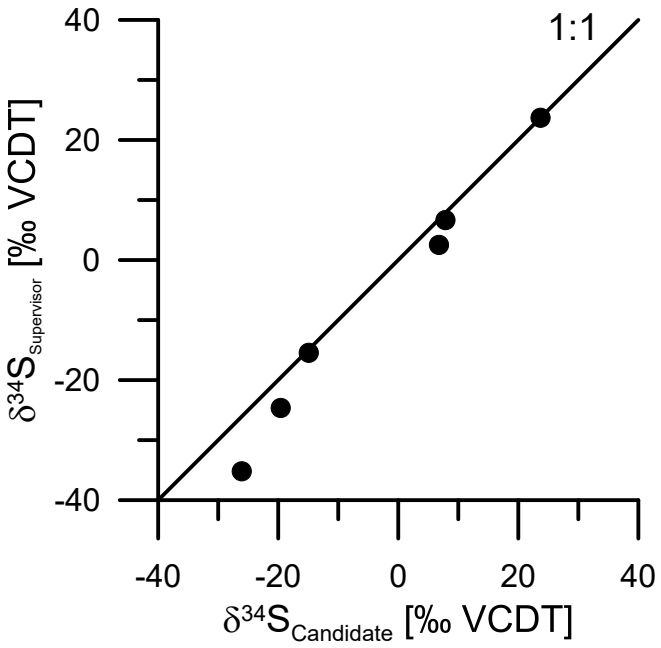

Figure 3.1.: Comparison of $\delta^{34}S_{DBT}$ values processed manually by i) the candidate and ii) a supervisor, independently assigning peak start and end slope for two standards and 4 natural samples. Straight line represents a 1:1 relationship.

Table 3.1.: Comparison of $\delta^{34}S_{DBT}$ values processed manually by i) the candidate and ii) a supervisor with independently assigning peak start and end slope, difference of their results and the true value of the DBT standard.

	$\delta^{34}S_{DBT}$ [‰ VCDT]			
	Candidate	Supervisor	Difference	True
Standard	6.8	2.5	4.3	13.7
Standard	7.9	6.7	1.2	13.7
Sample 1	23.7	23.7	0	
Sample 2	-26.1	-35.2	9.1	
Sample 3	-19.6	-24.6	5.1	
Sample 4	-4.9	-15.5	0.5	

In the seminal δ^{34}S study by Amrani *et al.* (2009) the raw ICP-MS data was processed within Excel using algorithms originally developed for GC-combustion-IRMS by Ricci *et al.* (1994), that were implemented as Visual Basic codes (Sessions *et al.*, 2001). The Visual Basic code supported the precise integration of peaks defined by pre-specified parameters (e.g., start and end slope; sections of baseline used for background subtraction). Such algorithms can considerably speed δ^{34}S processing times, however, their use typically requires a level of experience in programming with Visual Basic, hence may be beyond many analysts.

A user friendly automated processing package would ideally minimise the potential for user introduced bias to enhance the reproducibility of δ^{34}S measurements. More established and commercially available CSIA technologies (i.e., δ^{13}C and δD) include sophisticated processing algorithms easily used by most operators. For instance, Thermo IsoDat (v.3.1) is a common software package used on Thermo isotope instruments. It provides a graphical user interface and allows batch processing following pre-defined peak detection parameters, background subtraction and direct calculation of isotope ratios, essentially following algorithms defined by Ricci *et al.* (1994). Raven *et al.* (2015) recently reported the use of IsoDat to process compound specific δ^{34}S data, but provided few details about the key steps (i.e., data correction; normalisation) of their method.

The current chapter explores and documents the IsoDat based processing of raw $^{32}S^{+}$ and $^{34}S^{+}$ ion data, measured by GC-ICP-MS. Optimal values were also sought for key processing and integration parameters, including data correction and normalisation.

3.2. Data processing with IsoDat

3.2.1. Configuration of IsoDat software

Importing the raw Neptune^{+} data into IsoDat (ASCII, tap delimetered format obtained using Excel or batch wise with MatLab) requires the transformation into an IsoDat configuration (using the IsoDat Configurator application) so that it can be processed using the standard flow through configuration of a Thermo Delta V. The Thermo Delta V does not have the gas configuration or corresponding pre-defined settings associated with δ^{34}S analysis, but the required information can be assigned as follows: Cup 1 mass 32, Cup2 mass 33 and Cup 3 mass 34 and Ratio Groups to mass34/mass32. In this way IsoDat is configured to read and process the imported files to calculate δ^{34}S values.

The settings of the Neptune^{+} files used in the current process included a header with general meta data followed by 8 data columns: 1) Analysis Cycle; 2) Analysis Time; 3) mass 32; 4) mass 33; 5) mass 33.447; 6) mass 34; 7) mass33/mass32 (ratio of signal

V) and 8) mass34/mass32 (Table 3.2). Columns 5 and 7 were then omitted as IsoDat processing of $\delta^{34}S$ values required the following column format 1) Analysis Cycle;2) Analysis Time; 3) mass 32; 4) mass 33; 5) mass 34 and 6) mass34/mass32 to be able to successfully calculate $\delta^{34}S$ values (Table 3.3).

Table 3.2.: Illustration of raw Neptune^{+} result file

Header							
Cycle	Time	32	33	33.45	34	33/32	34/32
1	1459819794.83	3.91E-02	1.69E-04	-1.13E-04	1.50E-03	4.31E-03	3.84E-02

Table 3.3.: Illustration of altered Neptune^{+} result file fit to process in IsoDat

Header					
Cycle	Time	32	33	34	34/32
1	1459819794.83	3.91E-02	1.69E-04	1.50E-03	3.84E-02

3.2.2. IsoDat data processing

IsoDat offers a variety of options to define peak and background subtraction for $\delta^{34}S$ calculation. The primary parameters are "Start slope [mV/s]"; "End slope [mV/s]"; "Peak min Height [mV]"; "Background subtraction type and time"; and "Timeshift". The larger signal intensity of the *m/z* 32 chromatogram was used to define peak locations for both the mass 32 and mass 34 data – possible since there is no chromatographic separation of the S isotopologues (Amrani *et al.*, 2009). Therefore, a time shift, which usually corrects for the isotope chromatographic effect of lighter isotopes (e.g., D and ^{13}C), was no required. Due to varying background levels and the complex signal obtained from natural samples a section of background adjacent to each peak was separately used for signal subtraction and the minimum peak height was constantly defined as 500 mV. A series of parameter values were tested on laboratory standards of known $\delta^{34}S$ to identify optimal conditions for most precise $\delta^{34}S$ measurement. The standards used were 1) dodecanthiol ($C_{12}H_{25}SH$), $\delta^{34}S$ =-7.1 ‰; 2) octadecanethiol ($C_{18}H_{37}SH$), $\delta^{34}S$ = 11.7 ‰; 3) benzothiophene (C_8H_6S), $\delta^{34}S$ = 4.5 ‰; and dibenzothiophene ($C_{12}H_8S$), $\delta^{34}S$ = 13.7 ‰; their $\delta^{34}S$ values were previously measured by EA-IRMS, and ‰ values were calibrated against the International Vienna Canyon Diablo Troilite (VCDT). To avoid any effect of matrix or potentially limited concentration range the standards were each dissolved in equal volumes of hexane and used as the laboratory standard mix.

The parameters to most influence the reliability and precision of the calculated $\delta^{34}S$

values were peak start and end slope as well as definition of the background detection time. A matrix was developed to test the different parameters for their effect on the accuracy and precision of the measured $\delta^{34}S$ value. In the first series the background detection time and peak end slope were kept constant while the peak start slope was changed in subsequent processing steps. The start slope value which showed the smallest difference between the measured and the true $\delta^{34}S$ values ($\Delta\delta^{34}S_{M\text{-}T}$) of the standards, was thus identified. Optimal values for background detection time and end slope parameter were subsequently determined in a similar fashion. This procedure was conducted for six analyses of the 4-standard compound mixture. The complete results for one analysis of the standard mixture are illustrated in Figure 3.2 A-C.

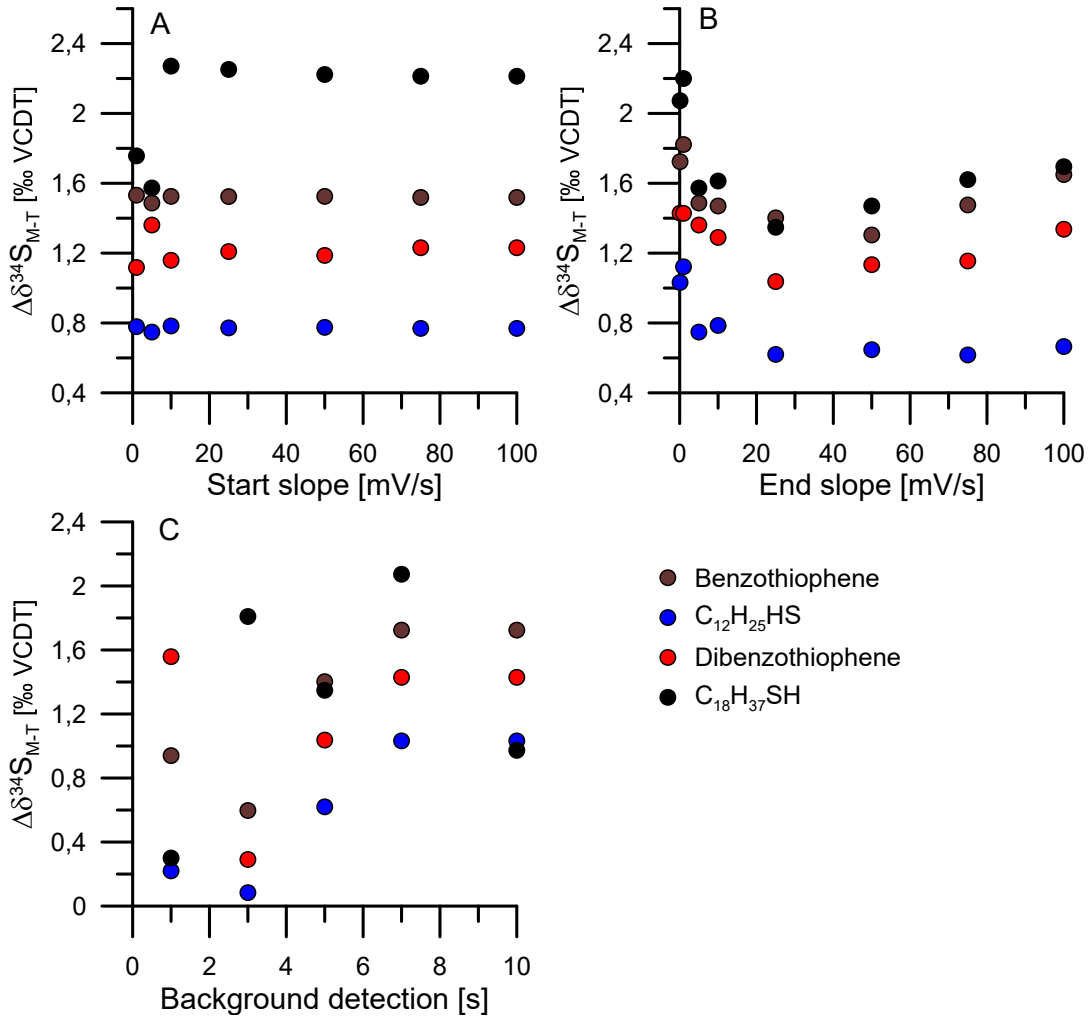

Figure 3.2.: Results for the matrix determining A) best start; B) end slope; and C) background detection time. Plots show the difference between calculated and true $\delta^{34}S$ values of four standard compounds. The optimal parameter gave lowest differences between measured and true $\delta^{34}S$ values.

These analyses revealed the best parameters for the calculation of $\delta^{34}S$ values using IsoDat. Best results for the lowest differences between measured and true $\delta^{34}S$ values, were typically obtained with a starting slope of 5 mV/s, end slope of 25 mV/s and a background detection time of 3s. These numbers vary significantly to the manually determined parameters (i.e., starting slope 0.2 mV/s, end slope 0.4 mV/s) used by Amrani *et al.* (2009) – demonstrating the varied nature of separately acquired S-CSIA data. Starting slopes of <1 mV/s were not possible with the present data due to frequent inability of distinguishing analyte peaks from background noise. This resulted in numerous positive detections of noise and often poor definition of real analyte peaks. End slopes of < 25 mV/s also proved problematic. The reason for this was not clear but may have related to the quite low *m/z* 34 analyte signals.

Correction and Normalisation

Isotope ratio mass spectrometry commonly provides very precise isotopic measurements, but not necessarily accurate measurements. To correct for accuracy stable isotopic values are expressed relative to a reference material rather than being given as absolute values. In this case, the $\delta^{34}S$ values are calculated (automatically by the software) relative to the isotopic composition of the laboratory reference gas (SF_6) following eq. (3.1):

$$\delta^{T}_{Sample} = \delta^{M}_{Sample} + \delta^{T}_{ReferenceGas} + \frac{\delta^{M}_{Sample}\delta^{T}_{ReferenceGas}}{1000} \tag{3.1}$$

Where T represents the true value and M represents the raw ICP-MS measured value (versus the reference gas).

The accuracy of the δ-values obtained is hence dependent on the $\delta^{34}S$ stability of the reference gas. Reference gases are vulnerable to fractionation with pressure or temperature changes, which is the case for CO_2 or H_2 used as references gases for the determination of $\delta^{13}C$ and δD (Skrzypek, 2013). The reference gas should be frequently calibrated against secondary standards to help maintain accuracy.

For the present study a pre-calibrated reference gas was not available. Compared to the common practice of using single reference gases for the calibration of $\delta^{34}S$ values, the accuracy of the $\delta^{34}S$ measurements can be enhanced by use of a multipoint linear regression normalisation curve established from the frequent analysis of multiple standard compounds of known $\delta^{34}S$ composition. This approach was used by comparison of the raw and true $\delta^{34}S$ of 4 standards analysed as a mixture (Figure 3.3). For the resulting regression line eq. (3.2) the slope (a) is expected to be close to unity (1.00 ±0.05) and the intercept (b) primarily dependent on the $\delta^{34}S$ value of the reference gas:

$$\delta^T = a \times \delta^M + b \tag{3.2}$$

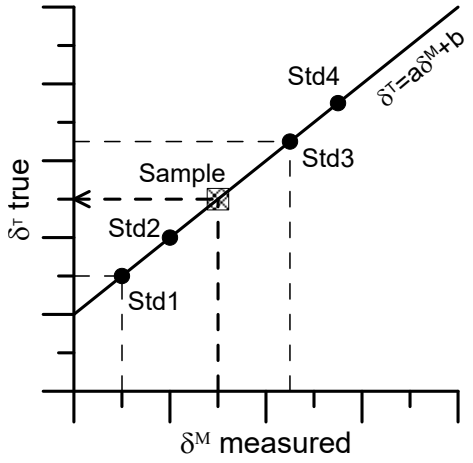

Figure 3.3.: Concept of a multipoint normalisation method using linear regression, based on the known δ^{34}S values of 4 authentic standards (Std1 - Std 4).

During the normalisation of an analysed sample, the raw δ^{34}S value of the sample is multiplied by the slope, then the value of the intercept was added. Normalisation with well-established δ^{34}S of authentic standards thus removes the uncertainties associated with the variables of any specific reference gas.

The δ^{34}S values of analytes in all samples within this thesis were measured at least in duplicates and the average of the raw measurements was then normalised relative to the four laboratory standards. The calibration mixture containing the four authentic OSCs with established δ^{34}S values was analysed at the commencement of each day's analysis. The δ^{34}S values of the standards over a weekly period were averaged to recalculate the normalisation curve/equation (Figure 3.4).

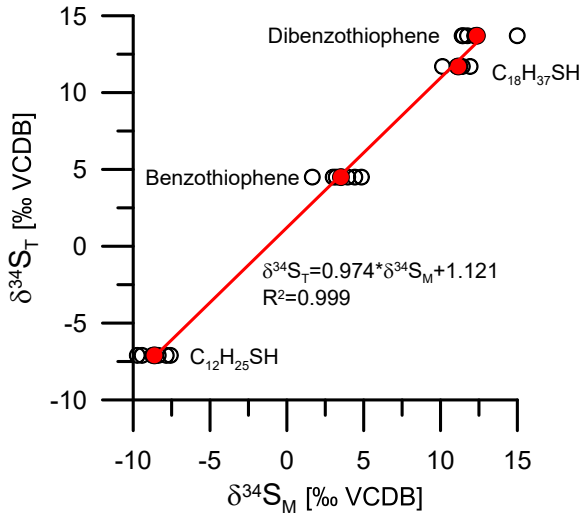

Figure 3.4.: Multipoint normalisation using the four well known laboratory standards. Open black circles show all raw results, red circles the average of these raw results for the period of one week. The linear regression line and equation is based on the averaged raw results.

References

Amrani, Alon, Sessions, AL, & Adkins, JF. 2009. Compound-specific δ34S analysis of volatile organics by coupled GC/multicollector-ICPMS. *Analytical Chemistry*, **81**(21), 9027–9034.

Raven, Morgan Reed, Adkins, Jess F., Werne, Josef P., Lyons, Timothy W., & Sessions, Alex L. 2015. Sulfur isotopic composition of individual organic compounds from Cariaco Basin sediments. *Organic Geochemistry*, **80**, 53–59.

Ricci, M. P., Merritt, D. A., Freeman, K. H., & Hayes, J. M. 1994. Acquisition and processing of data for isotope-ratio-monitoring mass spectrometry. *Organic Geochemistry*, **21**(6-7), 561–571.

Sessions, A. L., Burgoyne, T. W., & Hayes, J. M. 2001. Determination of the H Factor in Hydrogen Isotope Ratio Monitoring Mass Spectrometry. *Analytical Chemistry*, **73**(2), 200–207.

Skrzypek, G. 2013. Normalization procedures and reference material selection in stable HCNOS isotope analyses: an overview. *Analytical and Bioanalytical Chemistry*, **405**(9), 2815–23.

4. δ^{34}S character of organosulfur compounds in kerogen and bitumen fractions of sedimentary rocks

Hendrik Grotheer, Paul F. Greenwood, Malcolm T. McCulloch, Michael E. Böttcher, and Kliti Grice

Organic Geochemistry 2017, 110, pp 60 -64

Abstract

Hydropyrolysis (HyPy) of S-containing oil mature rock samples from two geologic settings each produced much higher concentrations of organosulfur compounds (OSCs) compared to their free occurrence in the bitumen. The $\delta^{34}S$ values of the most abundant OSCs from the kerogen and in the bitumen, were measured by gas chromatography inductively coupled plasma mass spectrometry (GC-ICP-MS). DBT and mDBTs from the HyPy processed kerogen fractions showed a distinct ^{34}S depletion, with $\delta^{34}S$ values up to 12 ‰ lighter than their bitumen occurrence. The different $\delta^{34}S$ values of OSCs from the kerogen and bitumen fractions is likely reflective of differences in timing of production, reduced sulfur sources or organic sulfurisation mechanism.

4.1. Introduction

The emerging capability of compound specific S isotope analysis (CS-S-IA; Amrani *et al.* 2009; Greenwood *et al.* 2014) presents an opportunity to gain a much better understanding of the organic S-cycle and the nature of different S-pools in the Earth's system and may help distinguish different pathways of organic sulfurisation. The distributions and $\delta^{34}S$ character of different sedimentary S-pools has helped identify pathways of organic sulfurisation (e.g., Sinninghe Damste & de Leeuw, 1990; Raven *et al.*, 2015). Compound specific $\delta^{34}S$ data is also attractive for being free of any inorganic S contribution, which can be problematic for bulk $\delta^{34}S$ analysis of sedimentary rocks or fractions due to difficulties in exhaustively removing all pyrite (Cai *et al.*, 2009). Paleoenvironmental reconstructions using compound specific $\delta^{34}S$ of OSCs in sedimentary rocks requires knowledge about timing of organic matter (OM) deposition and its sulfurisation, the identity and $\delta^{34}S$ values of primary S-sources and the molecular and $\delta^{34}S$ fractionation of OSCs during diagenesis and thermal maturation. We measured the $\delta^{34}S$ values of OSCs generated from kerogens by hydropyrolysis (HyPy) treatment and compared them to free OSCs in the corresponding bitumen fractions for several different aged sediments from two geological settings. HyPy has been shown to release indigenous covalently bound hydrocarbons from the kerogen matrix of rock samples (e.g., Love *et al.*, 1995).

4.2. Materials and Methods

Four Permian or Triassic shales recovered from the Hovea-3 well (Perth Basin, Western Australia; e.g., Thomas *et al.*, 2004; Dawson *et al.*, 2005) and calcareous shale samples from three separate wells of the Lower Cretaceous Toolebuc Formation (Queensland, Australia; Boreham & Powell, 1987; Woltering *et al.*, 2016) were selected for

this study. The Toolebuc rocks were much richer in organic matter and generally had slightly higher total sulfur (TS) content (Table 4.1). All samples had thermal maturities within the oil window (Table 4.1; R_c=0.7 – 0.8 %, calculated from MPI-1 index after Radke & Welte (1983); and C_{31} 22*S*/(22*S*+22*R*) homohopane ratio approaching equilibrium, Peters *et al.* (2005)).

Using established procedures (Robert *et al.*, 2016) powdered rocks were Soxhlet-extracted (9:1 DCM: MeOH; 72 hours) to separate the solvent-soluble bitumen and solvent-insoluble kerogen fraction; elemental S (found to be negligible) was removed from the bitumen fraction with activated (HCl) copper (Robert *et al.*, 2016). Column chromatography of the bitumen fraction on silica gel yielded aliphatic, aromatic and polar fractions. To further concentrate OSCs, aromatic fractions were fractionated over aluminum oxide (Type 507C neutral; Fluka); using solutions of *n*-hexane:DCM (99:01 v/v), *n*-hexane:DCM (90:10 v/v) and DCM in a refined procedure outlined by Jiang *et al.* (2013) – the OSCs exclusively eluted in the third sub-fraction. Remnant carbonates were removed from the kerogen fraction by treatment with concentrated HCl at ~ 60 °C for 24 h.

The kerogen (~1 g) and a DBT standard (Aldrich, 50 µl of 100 ppm solution on 0.5 g silica gel) were individually pyrolysed using a STRATA Technology Ltd Hydropyrolyser with standard operating conditions (e.g., Grotheer *et al.*, 2015; Robert *et al.*, 2016) and the exclution of a sulfide catalyst to avoid cross-reactions between sample and catalyst S. The total HyPy products (from the kerogen) were separated into polarity based fractions by column chromatography and activated copper was again used to remove any elemental S as described above.

All fractions were analysed on a HP 6890 gas chromatograph (GC) coupled to an Agilent 5975 mass selective detector (MSD). Separation was achieved on a DB-5MS capillary column (60 m × 0.25 mm i.d. × 0.25 µm) with He carrier gas (ultra-high purity, constant flow: 1.3 ml/min) and the following temperature program: 40 °C (2 min), then ramped to 325 °C at 3°C/min and held for 30 min. Full scan (*m/z* 30-530) spectra were acquired with 70 eV at a scan rate of ~4 scans per second. OSC identification was based on mass spectral and GC elution position correlated to published data (e.g., Asif *et al.*, 2009). Quantification was measured from base ion abundances (dibenzothiophene (DBT) *m/z* 184; methyl dibenzothiophene (mDBTs) *m/z* 198) relative to an external calibration curve established with pure DBT standards.

OSC $\delta^{34}S$ values were measured with a Thermo Neptune Plus multi-collector ICP-MS coupled to an Agilent 6890 GC inlet system (GC-ICP-MS; Greenwood *et al.*, 2014) and are reported in permil (‰) relative to Vienna Canyon Diablo Troilite (VCDT). Analytical precision was assessed by daily analyses of a mixture of OSCs with a standard deviation better than 1.6 ‰. $\delta^{34}S_{OSC}$ values reported for Hovea-3 and Toolebuc rocks represent the average of at least duplicate analyses.

4. $\delta^{34}S$ character of OSCs in kerogen and bitumen fractions of sedimentary rocks

The total S content and bulk $\delta^{34}S$ of the untreated rock and the subsequently isolated kerogen fraction (following inorganic sulfur removal *via* Cr(II) distillation; Fossing & Jørgensen, 1989; Passier *et al.*, 1999) were measured *via* combustion-isotope ratio monitoring mass spectrometry (C-irmMS) in a Thermo Flash 2000 connected to a Thermo Finnigan MAT 253 *via* a Thermo Conflow III interface (C-irmMS; Böttcher & Schnetger, 2004; Böttcher *et al.*, 2006). $\delta^{34}S$ was calibrated to the VCDT scale following Mann *et al.* (2009).

Table 4.1.: Sample information and key compositional parameters of native sediment samples from the Hovea-3 core (Perth Basin, Western Australia) and the Toolebuc Formation (Queensland, Australia).

Sample Number	Sample Name	Age	TOC [wt.%]	TS [µmolS/g Rock]	C_{31} 22*S*/(22*S*+22*R*) Homohopane[a]	MPI-1[a, b]	R_c[c]
H1	Hovea-3 1975.6m	Triassic	2.1	218.8	0.59	0.64	0.83
H2	Hovea-3 1980.05m	Triassic	0.9	n.a.	0.56	0.56	0.79
H3	Hovea-3 1980.9375m	Permian/Triassic	4.6	1062.5	0.57	0.55	0.78
H4	Hovea-3 1990.2m	Permian	2.1	312.5	0.58	0.58	0.80
T1	Boulia-10B 43.35m	Cretaceous	28.8	1125	0.40	0.55	0.73
T2	Jericho-11 60.78m	Cretaceous	15.6	531.3	0.38	0.50	0.70
T3	Crydon-1 101m	Cretaceous	46.2	1156.3	0.44	0.66	0.80

[a]Determined in bitumen extract

[b]Methyl phenanthrene index after Cassani *et al.* (1988); calculated from base ion abundances (phenanthrene *m/z* 178; methyl phenanthrene *m/z* 192)

[c]Calculated vitrinite reflectance (R_c); calculated from MPI-1 index after Radke & Welte (1983)

4.3. Results

DBT Standard: HyPy fully consumed the DBT with a 77 ± 8 wt.% recovery in the pyrolysate, where losses are likely due to condensation within the HyPy reactor or transfer line (Grotheer *et al.*, 2015). No other reaction products were detected. The $\delta^{34}S$ of the pure DBT standard was +5.5 ‰ (± 1.1 ‰). Following HyPy treatment the DBT pyrolysate had a $\delta^{34}S$ of +6.6 ‰ (± 0.3 ‰), representing a very minor enrichment (Table 4.2).

Hovea-3 and Toolebuc rocks: The Hovea-3 sedimentary rocks bitumen extracts contained very low concentrations of OSCs, which principally consisted of DBT and C_1-C_3 alkyl DBTs. The bitumen concentrations of S bound to DBT and mDBT (sum of four isomers) ranged from 0.44 – 0.98 nmolS/gRock and 1.81 – 8.19 nmolS/gRock, respectively with DBT/mDBTs ratios between 0.3 and 1.3. Much higher concentrations of OSCs (4-12x bitumen levels; Table 4.2;Figure 4.1) with DBT/mDBT ratios of 0.3-0.6 were generally detected following HyPy treatment of the kerogen fractions. The Toolebuc rocks had a relatively high S content, but the bitumen extracted from these rocks contained very low DBT and mDBT concentrations (0.01 - 0.24 nmolS/gRock and 0.04 - 0.87 nmolS/gRock). HyPy treatment of the Toolebuc kerogens generated significantly higher concentrations of OSCs, as much as 3 orders of magnitude above bitumen levels (Table 4.2).

$\delta^{34}S$ values of DBT and mDBT were measured from all bitumen and kerogen fractions (Table 4.2; Figure 4.2), but lower concentration of C_2- and C_3- DBTs prevented their $\delta^{34}S$ analysis. $\delta^{34}S$ values of DBT in the Hovea-3 bitumens ranged from -16.8 to -10.7 ‰. The $\delta^{34}S$ values of kerogen OSCs produced by HyPy were consistently lower, with DBT up to 12.2 ‰ and mDBTs up to 9.4 ‰ lighter than their bitumen values (Table 4.2). $\delta^{34}S$ of mDBTs (average of 4 isomers) were usually depleted (by up to 4 ‰) relatively to co-occurring DBT, which seems a common feature of the $\delta^{34}S$ profile of methylated DBTs from oils (Greenwood *et al.*, 2014).

$\delta^{34}S$ data from the Toolebuc sediments showed similar trends with DBT and mDBT from the kerogen being significantly lighter than in the bitumens (by up to 8.8 ‰) and mDBT values being slightly lighter (up to 3.3 ‰) than co-occurring DBT.

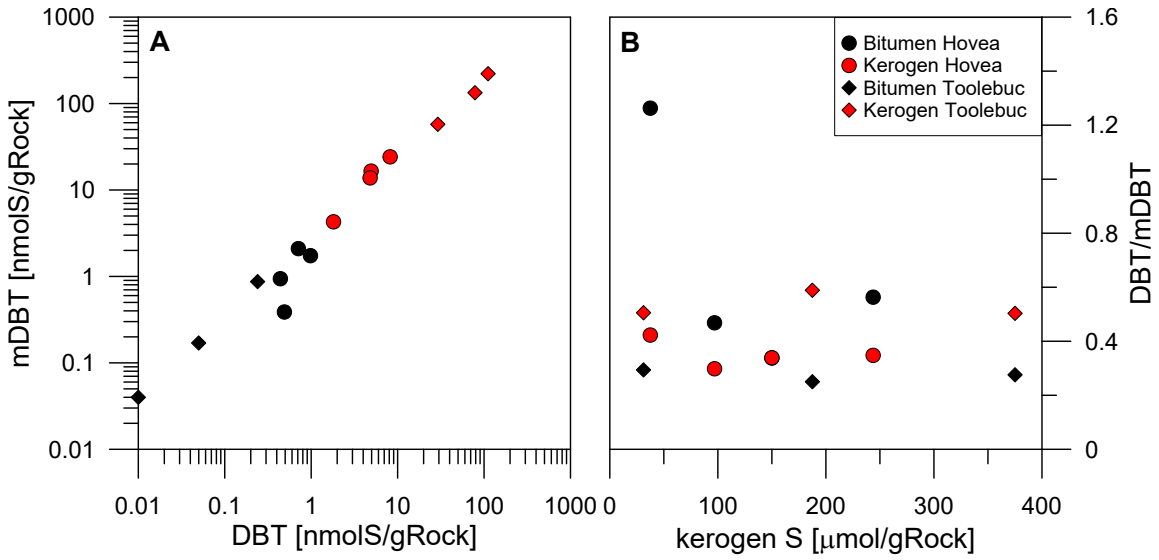

Figure 4.1.: Concentration cross-plots of (A) of bitumen (black) and kerogen (red) DBT over mDBT showing a close abundance correlation; and (B) DBT/mDBT ratio over kerogen S showed no obvious relationship between the distribution of OSCs and kerogen S concentration.

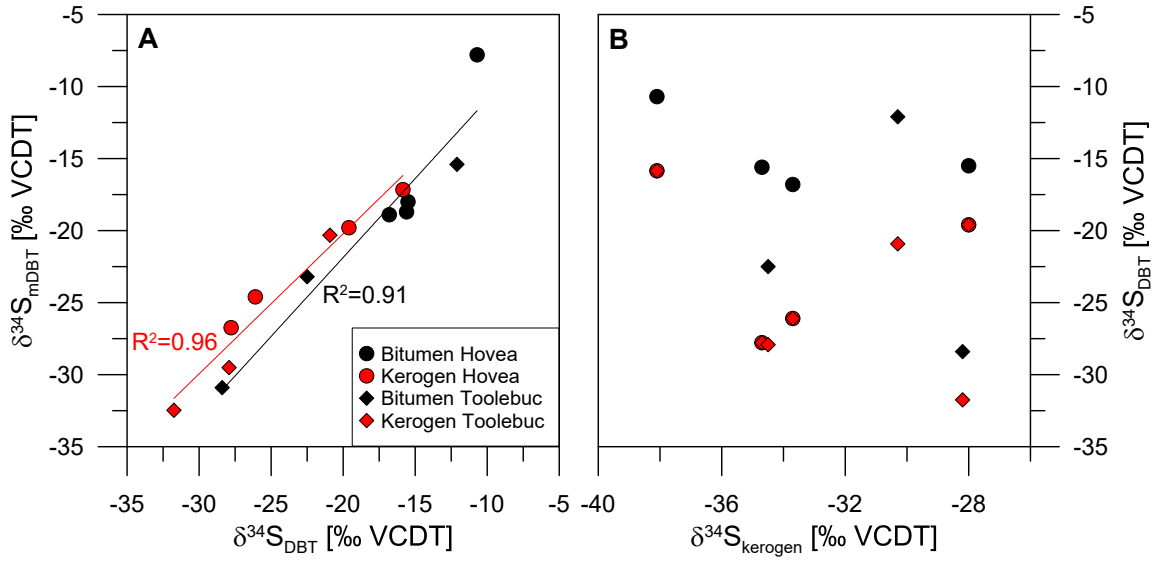

Figure 4.2.: $\delta^{34}S$ cross-plot (A) of bitumen (black) and kerogen (red) of DBT over mDBT which showed a close isotopic correlation and implied a generic link of OSCs in each fraction, as well that kerogen bound OSCs were generally ^{34}S depleted relative to bitumen OSCs; and (B) $\delta^{34}S_{DBT}$ over bulk $\delta^{34}S_{kerogen}$ showed no apparent isotopic relationship.

Table 4.2.: Quantification, δ^{34}S values and relative abundances (DBT/mDBTs) of bitumen and kerogen OSCs.

Sample Number		Kerogen S [μmolS/g Rock]	C DBT [nmolS/g Rock]	C mDBTs [nmolS/g Rock]	DBT/mDBTs	δ^{34}S Kerogen [‰VCDT]	δ^{34}S DBT [‰VCDT]	SV ±	δ^{34}S mDBTs [‰VCDT]	SV ±	$\Delta\delta^{34}$S DBT (Ker-Bit)	$\Delta\delta^{34}$S mDBTs (Ker-Bit)
DBT	native						5.5	1.1				
	HyPy						6.6	0.3				
H1	Bitumen		0.71	2.1	0.34		-15.5	0.1	-18.0	1.0		
	Kerogen	150	8.19	24.17	0.34	-28.0	-19.6	0.3	-19.8	1.1	-4.1	-1.8
H2	Bitumen		0.44	0.94	0.47		-16.8	0.3	-18.9	1.1		
	Kerogen	96.9	4.93	16.54	0.30	-33.7	-26.1	0.0	-24.6	0.0	-9.3	-5.7
H3	Bitumen		0.98	1.74	0.56		-15.6	0.8	-18.7	0.1		
	Kerogen	243.8	4.8	13.81	0.35	-34.7	-27.8	0.3	-26.7	0.8	-12.2	-8.1
H4	Bitumen		0.49	0.39	1.26		-10.7	0.4	-7.8	1.1		
	Kerogen	37.5	1.81	4.28	0.42	-38.1	-15.8	1.4	-17.2	0.8	-5.1	-9.4
T1	Bitumen		0.01	0.04	0.25		-12.1	0.3	-15.4	0.5		
	Kerogen	187.5	78.63	133.54	0.59	-30.3	-20.9	0.1	-20.3	1.0	-8.8	-4.9
T2	Bitumen		0.05	0.17	0.29		-28.4	1.6	-30.9	1.1		
	Kerogen	31.3	29.13	57.63	0.51	-28.2	-31.8	2.0	-32.5	1.2	-3.4	-1.6
T3	Bitumen		0.24	0.87	0.28		-22.5	0.1	-23.2	0.3		
	Kerogen	375	111.54	221.45	0.50	-34.5	-27.9		-29.5		-5.4	-6.3

4.4. Discussion

HyPy treatment of kerogens produced much higher concentrations of OSCs than were present in the corresponding bitumen fractions. Enhanced hydrocarbon yields are typical of the HyPy treatment of carbonaceous materials (e.g., Love *et al.*, 1998).

DBT and mDBTs from the kerogen were significantly depleted in ^{34}S, with $\delta^{34}S$ values up to 12 ‰ lower than their occurrence in the bitumen fraction of the rocks. This differential was much greater than the small ~1 ‰ $\delta^{34}S$ enrichment observed with the HyPy treatment of the DBT standard, which implied the HyPy procedure contributed minimal ^{34}S fractionation.

The lower kerogen $\delta^{34}S$ values is opposite to the common $\delta^{13}C$ trend of heavier values from the kerogen hydrocarbon compounds compared to bitumen hydrocarbons of sedimentary rocks. The kerogen enrichment in ^{13}C arises from preferential cleavage of ^{12}C bonds during diagenesis and thermal cracking (e.g., Tang *et al.*, 2000), although the respective $\delta^{13}C$ values can also be influenced by the varied bitumen and kerogen contribution of different sources (Love *et al.*, 1998). The $\delta^{34}S$ differencesobserved in the kerogen and bitumen fractions may similarly be due to a different representation of S-sources or sulfurisation pathways.

The OSCs in immature sediments from the Cariaco Basin formed during early diagenesis were proposed to form *via* multiple sulfurisation pathways characterised by distinct $\delta^{34}S$ values, with two main organic sulfurisation mechanisms supported (Raven *et al.*, 2015):

i) Reaction of dissolved HS^- with OM resulting in the intramolecular addition of S. This kinetically favours incorporation of ^{32}S ($\delta^{34}S$ light organic S), and difficulties in releasing intramolecularly bound S make this a relatively irreversible reaction.

ii) Intermolecular addition of polysulfides (S_x^{2-}) between different organic units. A reverse of this process could subsequently release the S_x-bridges from the organic moiety, and the equilibrium status of these reactions determines the $\delta^{34}S$ of this organic S.

Raven *et al.* (2015) considered pathway ii most likely responsible for the relative ^{34}S enrichment traditionally attributed to the organic incorporation of reduced S sources during diagenesis and measured in previous laboratory experiments (e.g., Amrani & Aizenshtat, 2004).

Catagenetic (i.e., temperature and pressure driven) cleavage reactions of the kerogens within the oil window maturity Hovea and Toolebuc rocks most likely contributed the OSCs. The S of these compounds may derive from diagenetically incorporated intra- (C-S-C) or inter-molecularly (C-S_x-C) bound kerogen S. S-aromatic forming

reactions during diagenesis or upon maturation would favour ring-closure with the smaller ^{32}S atom resulting in OSCs more depleted in ^{34}S than the initial S-source. On this basis, the bitumen OSCs might be expected to be more depleted than the S-structures remaining in the kerogen fraction. Further fractionation, however, may be encountered with subsequent geologic processes such as secondary cracking of the bitumen OSCs to form H_2S. This process would also kinetically favour the release of ^{32}S enriched H_2S, such that the residual liquid phase OSCs become heavier in $\delta^{34}S$.

Alternatively, the bitumen fraction may subsequently incorporate or isotopically exchange with a relatively heavy S source. Raven *et al.* (2015) cautioned the possibility of $\delta^{34}S$ equilibration between different (organic and inorganic) S-pools within the immature Cariaco Bay basin sediments. A previous $\delta^{34}S$ comparison of the whole bitumen and kerogen fractions of Monterey Formation sediments also showed a trend of kerogen fractions being depleted in ^{34}S relative to corresponding bitumen (Idiz *et al.*, 1990). These authors suggested that isotopically heavy, non-reacted pore water H_2S, may have been preferentially incorporated into the asphaltene fraction of free bitumens after kerogen formation, reflecting a varied timing and mode of organic sulfurisation and different pathways of bitumen formation. The kerogen moiety of the rock might also have continued to develop after bitumen expulsion contributing to a change in the relative abundance or $\delta^{34}S$ nature of the main bound organic-S structures. S_x^{2-}-bridges can link organic functionalities to promote geo-polymerisation. The abundance of these S-linkages may have increased with kerogen development over geologic time and their later formation may have been from a relatively ^{34}S depleted source of S or involved reactions favouring the lighter isotope. The kerogen S of these rocks may thus have evolved into a more ^{34}S depleted form than from which bitumen was earlier released. The bulk $\delta^{34}S$ of the kerogen fraction (Table 4.2; Figure 4.2) were generally even more depleted than the $\delta^{34}S_{OSC}$ values measured, reflecting the presence of other isotopically lighter S-species within the kerogen matrix.

4.5. Conclusions

HyPy treatment of the kerogen fractions released significantly higher concentrations of OSCs that had also been detected in the solvent extractable bitumen fractions. The $\delta^{34}S$ composition of DBT and mDBTs in the HyPy produced kerogen fractions were significantly lighter (by up to 12 ‰) compared to their structurally free bitumen occurrence, indicating that the kerogen and bitumen of sedimentary rocks contain isotopically distinct pools of organic S. There are several possible causes of this isotopic difference including different processes, sources or timing of generation. Further $\delta^{34}S$ evaluation of the OSCs in sedimentary OM may help to resolve the relative importance of different organic sulfurisation pathways and their contribution to hydrocarbon

biomarker preservation.

Acknowledgments

This study was conducted as part of the CSIRO Flagship Collaboration Fund Cluster for Organic Geochemistry of Mineral Systems. HG thanks CSIRO and Curtin University (scholarships) and KG the ARC (DP150102235) for funding support. Geoff Chidlow, Peter Hopper and Iris Schmiedinger provided analytical support. Chris Boreham (Geoscience Australia) kindly provided the Toolebuc Formation rocks. We thank the journal reviewers (Morgan Raven and two anonymous) and Editors (D. Strapoc and E. Idiz) for their constructive advice which improved earlier versions of our study.

References

Amrani, A., & Aizenshtat, Z. 2004. Reaction of polysulfide anions with α, β unsaturated isoprenoid aldehydes in aquatic media: Simulation of oceanic conditions. *Organic Geochemistry*, **35**(8), 909–921.

Amrani, A., Sessions, A. L., & Adkins, J. F. 2009. Compound-specific δ34S analysis of volatile organics by coupled GC/multicollector-ICPMS. *Analytical Chemistry*, **81**(21), 9027–9034.

Asif, M., Alexander, R., Fazeelat, T., & Pierce, K. 2009. Geosynthesis of dibenzothiophene and alkyl dibenzothiophenes in crude oils and sediments by carbon catalysis. *Organic Geochemistry*, **40**(8), 895–901.

Boreham, C. J., & Powell, T. G. 1987. Sources and preservation of organic matter in the Cretaceous Toolebuc Formation, eastern Australia. *Organic Geochemistry*, **11**(6), 433–449.

Böttcher, M. E., & Schnetger, B. 2004. Direct measurement of the content and isotopic composition of sulfur in black shales by means of combustion-isotope-ratio-monitoring mass spectrometry (C-irmMS). *Pages 597–603 of:* de Groot, P. (ed), *Handbook of Stable Isotope Analytical Techniques, Vol. I.* Elsevier.

Böttcher, M. E., Hetzel, A., Brumsack, H. J., & Schipper, A. 2006. Sulfur-iron-carbon geochemistry in sediments of the Demerara Rise. *Proceedings of the Ocean Drilling Program Scientific Results*, **207**(December 2005), 23pp.

Cai, C., Li, K., Anlai, M., Zhang, C., Xu, Z., Worden, R. H., Wu, Guanhui, Zhang, Baoshou, & Chen, Lixin. 2009. Distinguishing Cambrian from Upper Ordovician source rocks: Evidence from sulfur isotopes and biomarkers in the Tarim Basin. *Organic Geochemistry*, **40**(7), 755–768.

Cassani, F., Gallango, O., Talukdar, S., Vallejos, C., & Ehrmann, U. 1988. Methylphenanthrene maturity index of marine source rock extracts and crude oils from the Maracaibo Basin. *Organic Geochemistry*, **13**, 73–80.

Dawson, D., Grice, K., & Alexander, R. 2005. Effect of maturation on the indigenous δD signatures of individual hydrocarbons in sediments and crude oils from the Perth Basin (Western Australia). *Organic Geochemistry*, **36**(1), 95–104.

Fossing, H., & Jørgensen, B. B. 1989. Measurement reduction of a single-step chromium method Evaluation. *Biogeochemistry*, **8**(3), 205–222.

Greenwood, P. F., Amrani, A., Sessions, A., Raven, M. R., Holman, A., Dror, G., Grice, K., McCulloch, M. T., & Adkins, J. F. 2014. Development and Initial Biogeochemical Applications of Compound-Specific Sulfur Isotope Analysis. *Chap. 10, pages 285–312 of:* Grice, K. (ed), *Principles and Practice of Analytical Techniques in Geosciences*. UK: Royal Society of Chemistry.

Grotheer, H., Robert, A. M., Greenwood, P. F., & Grice, K. 2015. Stability and hydrogenation of polycyclic aromatic hydrocarbons during hydropyrolysis (HyPy) – Relevance for high maturity organic matter. *Organic Geochemistry*, **86**, 45–54.

Idiz, E. F., Tannenbaum, E., & Kaplan, I. R. 1990. Pyrolysis of High-Sulfur Monterey Kerogens. *Pages 575–591 of:* Orr, W. L., & White, C. M. (eds), *Geochemistry of Sulfur in Fossil Fuels*, vol. 429. Washington D.C.: American Chemical Society.

Jiang, A., Zhou, P., Sun, Y., & Xie, L. 2013. Rapid column chromatography separation of alkylnaphthalenes from aromatic components in sedimentary organic matter for compound specific stable isotope analysis. *Organic Geochemistry*, **60**, 1–8.

Love, G. D, Snape, C. E., Carr, A. D., & Houghton, R. C. 1995. Release of covalently-bound alkane biomarkers in high yields from kerogen via catalytic hydropyrolysis. *Organic Geochemistry*, **23**(10), 981–986.

Love, G. D., Snape, C. E., & Fallick, A. E. 1998. Differences in the mode of incorporation and biogenicity of the principal aliphatic constituents of a type I oil shale. *Organic Geochemistry*, **28**(12), 797–811.

Mann, J. L., Vocke, R. D., & Kelly, W. R. 2009. Revised δ 34 S reference values for IAEA sulfur isotope reference materials S-2 and S-3. *Rapid Communications in Mass Spectrometry*, **23**(8), 1116–1124.

Passier, H. F., Bosch, H.-J., Nijenhuis, I. A., Lourens, L. J., Böttcher, M. E., Leenders, A., Damsté, J. S. S., de Lange, G. J., & de Leeuw, J. W. 1999. Sulphidic Mediterranean surface waters during Pliocene sapropel formation. *Nature*, **397**(6715), 146–149.

Peters, K. E., Walters, C. C., & Moldowan, J. M. 2005. *The biomarker guide, Volume 2. Biomarkers and isotopes in petroleum exploration and Earth history*. Cambridge University Press.

Radke, M., & Welte, D. H. 1983. The methylphenanthrene index (MPI): a maturity parameter based on aromatic hydrocarbons. *Pages 504–512 of: Advances in Organic Geochemistry 1981*.

Raven, M. R., Adkins, J. F., Werne, J. P., Lyons, T. W., & Sessions, A. L. 2015. Sulfur isotopic composition of individual organic compounds from Cariaco Basin sediments. *Organic Geochemistry*, **80**, 53–59.

Robert, A. M., Grotheer, H., Greenwood, P. F., McCuaig, T. C., Bourdet, J., & Grice, K. 2016. The hydropyrolysis (HyPy) release of hydrocarbon products from a high maturity kerogen associated with an orogenic Au deposit and their relationship to the mineral matrix. *Chemical Geology*, **425**(may), 127–144.

Sinninghe Damste, J. S., & de Leeuw, J. W. 1990. Analysis, structure and geochemical significance of organically-bound sulphur in the geosphere: State of the art and future research. *Organic Geochemistry*, **16**(4-6), 1077–1101.

Tang, Y., Perry, J. K., Jenden, P. D., & Schoell, M. 2000. Mathematical modeling of stable carbon isotope ratios in natural gases. *Geochimica et Cosmochimica Acta*, **64**(15), 2673–2687.

Thomas, B. M., Willink, R. J., Grice, K., Twitchett, R. J., Purcell, R. R., Archbold, N. W., George, A. D., Tye, S., Alexander, R., Foster, C. B., & Barber, C. J. 2004. Unique marine Permian-Triassic boundary section from Western Australia. *Australian Journal of Earth Sciences*, **51**(3), 423–430.

Woltering, M., Tulipani, S., Boreham, C. J., Walshe, J., Schwark, L., & Grice, K. 2016. Simultaneous quantitative analysis of Ni, VO, Cu, Zn and Mn geoporphyrins by liquid chromatography-high resolution multistage mass spectrometry: Method development and validation. *Chemical Geology*, **441**(nov), 81–91.

5. Global significance of the sulfur isotope composition of sedimentary inorganic and organic sulfur phases across the Permian-Triassic transition

Hendrik Grotheer, Paul F. Greenwood,
Malcolm T. McCulloch, Michael E. Böttcher,
Roger E. Summons, and Kliti Grice

The present chapter forms the initial basis for an intended publication. The publication will include additional Fe speciation data for the Hovea-3 core to be provided in the near future by external colleagues, dependent on instrument availability.

Abstract

The Permian Triassic mass extinction, the greatest of such events of the Phanerozoic with 95 % of all life wiped out, was caused by catastrophic environmental stress involving major changes to the global C- and S-cycles. Here, the S-cycle of the Permian Triassic (P-Tr) transition is investigated by measurement of the abundance and $\delta^{34}S$ values of inorganic S (total reducible inorganic sulfur; TRIS), organic S (kerogen bound sulfur) pools and individual organosulfur compounds (OSCs) recorded in P-Tr sedimentary sequences from the Global Stratotype and Point Section (GSSP) in Meishan-1 (South China) and Hovea-3 (Perth Basin, Western Australia). The $\delta^{34}S$ values of solvent extractable OSCs were measured by gas chromatography inductively coupled plasma mass spectrometry (GC-ICP-MS).

Distinct S-isotopic variations between kerogen S and solvent extractable OSCs (e.g., DBTs) reflect the occurrence of multiple pools of isotopically distinct organic sulfur within the macromolecular kerogen network. The Meishan-1 profile of $\delta^{34}S_{DBT}$ seemed unrelated to $\delta^{34}S_{KerS}$ but did show a correlation with the redox sensitive TRIS/(TRIS+KerS) ratio suggesting a kinetic relationship between some of the organic sulfurisation and inorganic sulfidisation processes during times of low S-flux. In contrast, at Hovea-3 the $\delta^{34}S$ values of TRIS and kerogen S were very similar suggesting isotopic exchange between the main organic and inorganic S-pools when S-flux was high.

This further suggests TRIS and OSCs were sensitive to water column conditions or local basin environmental controls. At Meishan-1 fluctuation in $\delta^{34}S$ values of TRIS and DBT indicate the onset of a event horizon caused by a complex combination of geologic processes leading up to the Permian-Triassic extinction. Whereas in Hovea-3 S isotopic variations were related to progressive oxygen depletion during the end Permian.

5.1. Introduction

The P-Tr extinction and subsequent recovery has received considerable attention as it is the most severe of such Phanerozoic events, when up to 95% of all species on Earth vanished (e.g., Benton & Twitchett, 2003; Grice *et al.*, 2005c; Foster & Twitchett, 2014; Whiteside & Grice, 2016; Grotheer *et al.*, 2017). Still there has been little con-

sensus about the cause, or causes of the P-Tr extinction, with two of the most supported explanations being volcanic activity, namely the Siberian flood basalts (e.g., Bowring *et al.*, 1998; Jin *et al.*, 2000; Wignall, 2001); global anoxia and eutrophic oceans (e.g., Hallam & Wignall, 1997; Benton & Twitchett, 2003; Grice *et al.*, 2005c; Bond & Wignall, 2008; Nabbefeld *et al.*, 2010a).

These events would all have had a significant impact on the global sulfur (S) cycle which has traditionally been traced *via* evaporates and carbonate associated sulfides (CAS) in the geologic record (e.g., Newton *et al.*, 2004; Kaiho *et al.*, 2006a,b). During the Permian, seawater sulfate had $\delta^{34}S$ values between 9 and 12 ‰ (Claypool *et al.*, 1980; Cortecci *et al.*, 1981) representing its minimum level through the entire Phanerozoic. Following the Permian Triassic Boundary (PTB) $\delta^{34}S_{SeawaterSulfate}$ showed a rapid rise to peak at ~28 ‰ during the Triassic (Claypool *et al.*, 1980; Chen & Chu, 1988) reflecting major changes to the S cycle and probably also the linked global oxygen (O) and iron (Fe) cycles (Newton *et al.*, 2004). Evaporate deposits, were non-continuous, poorly time constrained and thus unreliable in accurately investigating S cycle changes associated with relatively short term events like the P-Tr extinction (Newton *et al.*, 2004). Carbonate associated sulfides (CAS), however, provided a much higher temporal resolution and have been widely used to investigate the P-Tr extinction (Kaiho *et al.*, 2002, 2006a; Gorjan & Kaiho, 2007). More detailed information on water column redox conditions, the organic matter (OM) associated burial of reduced sulfur and changes to regional and global sulfur cycles can often be obtained from the concentrations and sulfur isotope composition of pyrite and its textures (Berner & Raiswell, 1983; Wilkin *et al.*, 1996; Wignall & Newton, 1998). These data have been widely used to decipher complex S-cycle variations during the PTB (e.g., Wignall *et al.*, 2005; Jiang *et al.*, 2006; Gorjan *et al.*, 2007; Shen *et al.*, 2007, 2011; Zhang *et al.*, 2011).

Changes observed in the inorganic S-cycle across the PTB might also be evident in sedimentary organic S. The emerging capability of compound specific S isotope analysis (CS-S-IA; Amrani *et al.*, 2009; Greenwood *et al.*, 2014), presents an opportunity to gain an insight into the $\delta^{34}S$ nature of different organosulfur compounds (OSCs) during the dynamic global S-cycle at this time.

Here we investigated the dynamics of different organic and inorganic S-pools across PTB horizons from the GSSP in Meishan-1, South China and the Hovea-3 core, Perth Basin, Western Australia. $\delta^{34}S_{OSC}$ data is complemented with the total sulfur (TS) and $\delta^{34}S$ values of kerogen-bound S and total reduced inorganic sulfur (TRIS, typically pyrite). This geochemical data acquired was subsequently correlated with water column redox conditions based on Fe speciation data for the two PTB sections.

5.2. Materials and Methods

5.2.1. Studied sections

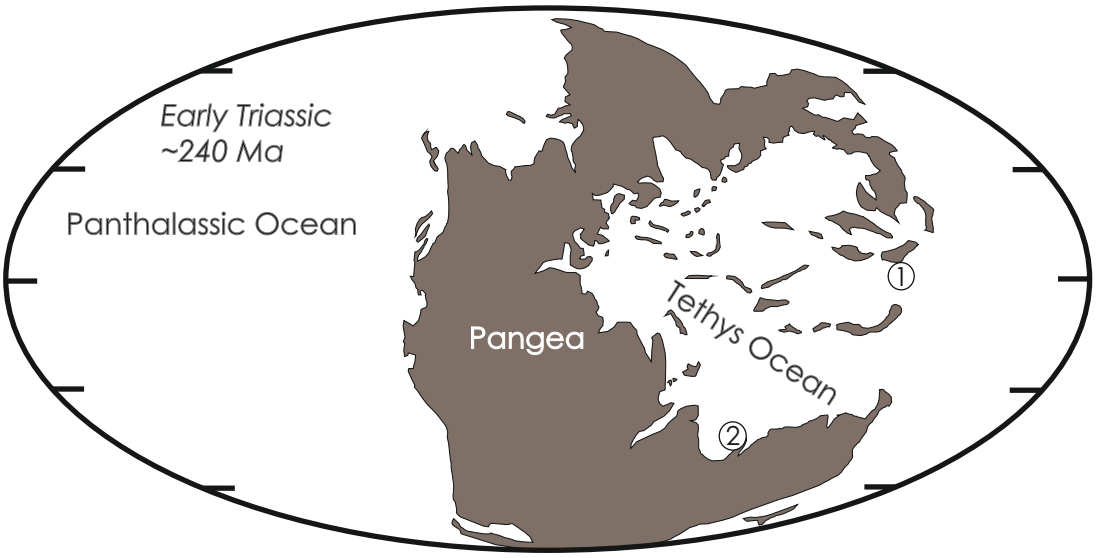

Figure 5.1.: Reconstruction of global paleogeography at the end of the Permian ca. 240 million years ago (modified after Grice *et al.*, 2005b). Numbers indicate the two sample locations: 1, Meishan-1, South China; 2, Hovea-3, Perth Basin, Western Australia.

Meishan-1 (South China)

The GSSP at Meishan (South China) has been thoroughly investigated for the paleontology and geochemistry of the Permian-Triassic mass extinction (Jin *et al.*, 2000; Yin *et al.*, 2001; Cao *et al.*, 2002, 2009; Cao & Zheng, 2009). The Meishan-1 core was drilled near the quarry Meishan Section D, comprised of sediments containing the transition, the entire Changhsingian Stage and post-extinction Early Triassic Induan Stage (Cao *et al.*, 2009). The Changhsingian Formation represents slope-to-basin facies comprised of graded beds of organic-rich calcarenite, marly micrite and radiolarian chert (Wignall & Hallam, 1993; Jin *et al.*, 2000). The limestone in bed 24e is overlain by a pale-colored alternating ash clay bed (bed 25) underlying a laminated organic-rich calcareous claystone (bed 26) and a lime mud bed (bed 27) (Jin *et al.*, 2000). Biostratigraphically, the first occurrence of the conodont *H. parvus* in bed 27c marks the P-T boundary (Yin *et al.*, 2001).

Bed 24 was most likely deposited within a carbonate periplatform ramp under a stratified and anoxic water column that experienced periodic disturbances by storm currents (Cao & Zheng, 2009). The main extinction took place in as little as 100,000 years beginning at the ash clay bed (Bed 25) (Bowring *et al.*, 1999) containing lacerated-shaped volcanic hyaline clasts which suggest direct precipitation of volcanic ejects. Clay beds

in bed 24 possibly originate from weathered and reworked continental silicic volcanic sediments, suggesting intensive volcanism and weathering during the latest Permian and during the PTB (Cao & Zheng, 2009).

Hovea-3 (Perth Basin, Western Australia

The Hovea-3 core was drilled through the organic matter rich source rocks of the Hovea Member in the northern part of the Perth Basin (Thomas *et al.*, 2004). Located at mid-southern paleolatitudes (Figure 5.1), in the south of the Tethys ocean, the shallow marine Hovea Member is comprised of a lower "Inertinitic Interval" with bioturbated sand- and mudstones, and an overlying "Sapropelic Interval" with laminated mudstone and oil-prone source rocks (Thomas *et al.*, 2004). An abrupt facies change between the two intervals is eminent at a depth of 1980.95 m and suggests a hiatus, possibly due to non-deposition during the End Permian (Grice *et al.*, 2005a,b). The facies change coincides with a major palynological change, that has been used to define the PTB in the absence of conodonts (Thomas *et al.*, 2004). Conventionally, in less condensed PTB sections, the palynological change occurs prior to the PTB (e.g., Looy *et al.*, 2001), but due to the low sedimentation rate and the condensed nature of the later section the PTB and extinction are indistinguishable. Just 20 cm above the horizon, the Early Triassic bivalve *Claraia* indicative of low oxygen levels in the depositional environment first appears giving further evidence about the condensed nature of this section.

5.2.2. Methods

Sample preperation

Approximately 5-25 g of finely ground sample were either Soxhlet (Hovea-3) or microwave extracted (Meishan-1) in DCM: MeOH (9:1 v/v). Soxhlet extraction was performed for 72 h in the presence of HCl activated copper turnings to remove elemental sulfur from the extracts obtained by microwave extraction. Microwave extraction was performed twice at 80 °C, and the two aliquots were combined. Cu was then added to remove any elemental sulfur. In Meishan-1 and Hovea-3 samples elemental S was found to be present in negligible concentrations. The extract was subsequently fractionated by column chromatography over activated silica gel (120 °C) into aliphatic, aromatic and polar fractions using *n*-hexane, *n*-hexane:DCM (7:3; v/v) and DCM:MeOH (1:1; v/v). To further concentrate the OSCs, the aromatic fraction was chromatographically separated into sub-fractions over aluminum oxide (AlO_2; Type 507C neutral; Fluka) using solutions of *n*-hexane:DCM (99:01 v/v), *n*-hexane:DCM (90:10 v/v) and DCM (Nb. Refinement of the procedure outlined by Jiang *et al.*,

2013); GC-MS analysis confirmed the isolation of all OSCs in the third/DCM fraction (Grotheer *et al.*, in review).

GC-MS

All fractions were analysed by gas chromatography-mass spectrometry (GC-MS). The gas chromatograph was a HP 6890 GC fitted with a DB-5MS capillary column (60 m × 0.25 mm i.d. × 0.25 µm film thickness). The carrier gas (ultra-high purity helium; BOC Group) was held at a constant flow rate (1.3 ml/min) and the GC oven temperature was increased from an initial 40 °C (held 2 min) to 325 °C (held for 30 min) at a rate of 3 °C/min. An Agilent 5975 mass selective detector (MSD) operated at a source temperature of 230 °C was used to acquire full scan (*m/z* 30-530 Da) 70eV mass spectra at a rate of ~4 scans per second. The OSCs were identified based on correlation of the mass spectral and GC analyses to published data (e.g., Asif *et al.*, 2009). Quantification was measured from parent/base ion abundances (i.e., DBT = *m/z* 184; mDBTs = *m/z* 198) relative to an external calibration curve established by measuring DBT standards at several different concentrations (Grotheer *et al.*, in review).

GC-ICP-MS

The $\delta^{34}S$ values of OSCs in the S concentrated aromatic fraction were analysed using a Thermo Neptune Plus multi-collector ICP-MS coupled with an Agilent 6890 GC (Greenwood *et al.*, 2014; Grotheer *et al.*, in review). The OSCs were separated on the GC with a DB-5 MS column (30 m × 0.25 mm i.d. × 0.1 µm film thickness). The GC oven was heated from 100 °C (held for 0.5 min) to an end temperature of 300 °C (held for 15 min) at a rate of 8 °C/min. The argon gas for the plasma torch was pre-heated to assist the transfer of analytes from the GC. An SF_6 gas standard of known $\delta^{34}S$ value was used for tuning and calibration of the ICP-MS. $\delta^{34}S$ results were reported as permil (‰) relative to the international sulfur isotope standard Vienna Canyon Diablo Troilite (VCDT), following multi-point linear regression normalisation. The precision of the $\delta^{34}S$ measurements was assessed by daily analyses of a mixture comprising three OSCs. Sample $\delta^{34}S$ values represent the average of at least duplicate analyses and their variance expressed as standard variation (SV±).

The S-aromatic fractions of most samples typically contained series of benzothiophenes and dibenzothiophene products. However, only higher MW C_0-C_3 alkyl-dibenzothiophenes (Figure 5.2) were of sufficient abundance for $\delta^{34}S$ measurement, and the poor resolution of the larger polymethyl-DBTs impacted the precision of their $\delta^{34}S$ measurements. As such $\delta^{34}S$ data will only be reported for DBT and mDBT (measured as an average by the co-integration of the three closely eluting mDBT peaks; corresponding to 4-, 3+2- and 1-mDBT isomers).

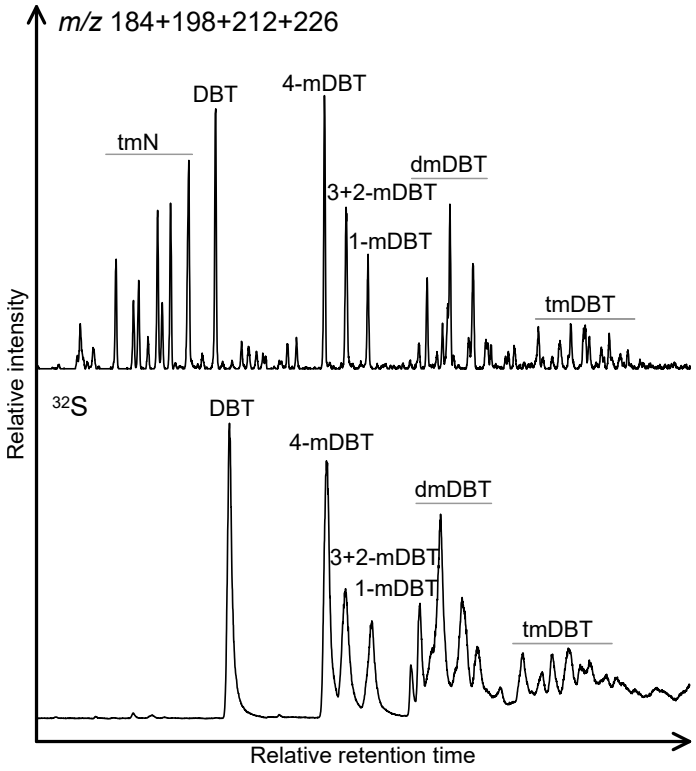

Figure 5.2.: GC-MS (top) and GC-ICP-MS (bottom) chromatograms highlighting separation of OSCs present in the aromatic fraction of sample H6. Key: tmN = tetramethylnapthalene (*m/z* 184); DBT = dibenzothiophene (*m/z* 184); mDBT = methyldibenzothiophene (*m/z* 198); dmDBT = dimethyldibenzothiophen (*m/z* 212); tmDBT = trimethyldibenzothiophene (*m/z* 226).

Sulfur isotopes (C-irmMS)

The sedimentary TRIS (total reducible inorganic sulfur, largely consisting of pyrite) fraction was separated from sediments according to a single-step hot acidic Cr(II) distillation method following Fossing & Jørgensen (1989). Generated H_2S was trapped in a Zn acetate solution and measured spectrophotometrically (Specord 40, Analytical Jena) following Cline (1969). For stable isotope measurements, ZnS was transferred into Ag_2S using an $AgNO_3$ solution. The concentration and stable isotope composition of total sedimentary sulfur was measured using combustion-isotope ratio monitoring mass spectrometry (C-irmMS) following the method of Böttcher & Schnetger (2004). The kerogen-bound organic sulfur fraction was measured following the approach of Passier *et al.* (1999a) and Böttcher *et al.* (2006). Washed and dried residues from the Cr(II) distillation were combusted in a Thermo Flash 2000 elemental analyser, connected to a Thermo Finnigan MAT 253 gas mass spectrometer *via* a Thermo Conflow III interface. The measured intensities at masses 66 and 64 were calibrated to the $^{34}S/^{32}S$ VCDT scale using international standards following Mann *et al.* (2009).

Fe speciation

The pyrite-associated iron fraction (Fe_{Py}) was calculated assuming ideal FeS_2 stoichiometry from the analytical TRIS amounts. Total iron (Fe_T) was measured *via* ICP-OES (Thermo Icap 6300 DUO) after complete acid digestion in a pressure digestion system PDS-6 (Loftfield Analytical Solutions; Heinrichs *et al.*, 1986; Kowalski *et al.*, 2012). Still remaining reactive sedimentary Fe was extracted with 1M HCl (Fe_{HCl}) or buffered Na dithonite solution (Fe_D) and measured spectrophotometrically (Specord 40, Analytical Jena). The highly reactive iron fraction (Fe_{HR}) was calculated as the sum of dominating Fe_{Py} and Fe_{HCl} or Fe_D.

5.3. Results

5.3.1. Meishan-1

Sulfur pools

The concentration and stable isotopic composition of main sulfur species in the P-Tr horizon in Meishan-1 are shown in Figure 5.3 and listed in Table 5.1. These data show major fluctuation during an event horizon beginning near the top of conodont bed 22 and peaking at the top of bed 24 just prior to the proposed P-Tr extinction horizon marked as the base of the pyrite ash layer in bed 25 (Zhang *et al.*, 2007). The two samples above the extinction horizon were taken from Bed 26 ~ 0.2 m below the proposed PTB (Bed 27c-d; Zhang *et al.*, 2007).

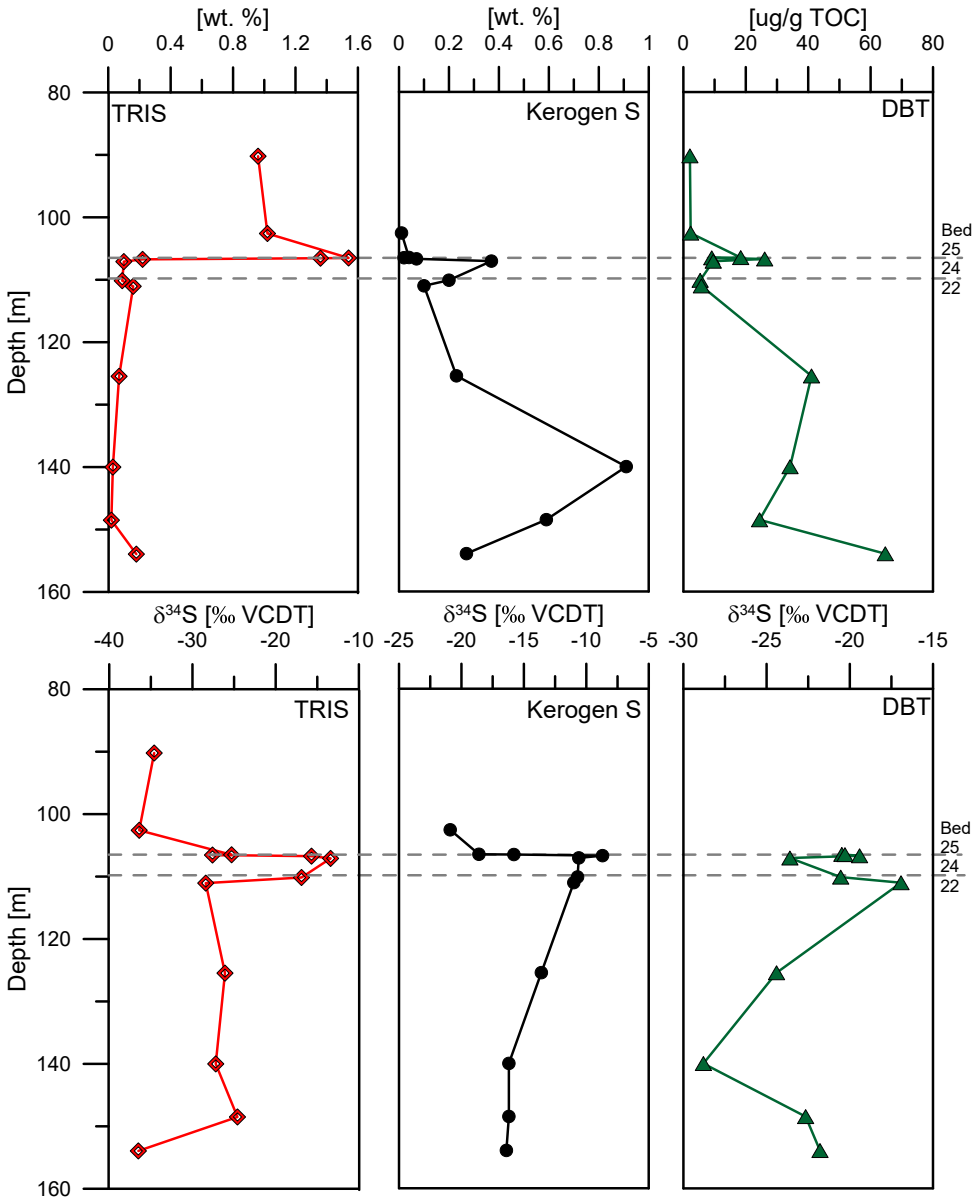

Figure 5.3.: Concentration (top) and $\delta^{34}S$ values (bottom) of TRIS (red line), kerogen S (black line) and DBT (green line) measured from the Meishan-1 section. Dashed lines indicate boundaries between bed 25 to 24 and 24 to 22. Conodont Beds after Cao *et al.*, (2009), Bed 25 marks proposed P-Tr extinction interval.

The TRIS content is very low below Bed 25 (i.e., average 0.11 ±0.07 wt.%) and shows a local minimum in the event horizon. It increases significantly following the P-Tr extinction reaching 1.5 ± 0.1 wt.% early in the horizon, but slightly decreases in the Early Triassic (average 1 ± 0.1 wt.%). Below Bed 24 the $\delta^{34}S_{TRIS}$ was relatively stable at ~ -26.6 ‰ with the exception of the deepest Permian sample which was more depleted in ^{34}S ($\delta^{34}S_{TRIS}$ = -36.5 ‰). In the event horizon $\delta^{34}S_{TRIS}$ suddenly becomes heavier by over 10 ‰ to ~ -15.3 ‰ with highest ^{34}S abundance ~60 cm below the P-Tr extinction horizon. Following the extinction $\delta^{34}S_{TRIS}$ recedes to lighter, near pre-event values (average -26.5 ± 1.6 ‰) and continues to lighter value of ~ -35.5 ‰ in the Early Triassic. The concentration of kerogen S shows some fluctuation through the Permian prior to the event horizon (average 0.5 wt.%) with a distinct maximum of 0.9 wt.% at 140 m. In the event horizon kerogen S concentration gradually increases from a minimum of 0.1 to a maximum of 0.4 wt.% 60 cm below the extinction horizon, followed by a decrease to 0.1 wt. % at the top of bed 24. Lower concentrations were then detected following the extinction (< 0.1 wt.%). The isotopic composition of kerogen S was relatively stable at ~ -16 ‰ below 140 m, but then showed a slight increase to -8.7 ‰ at the top of bed 24. Following the extinction $\delta^{34}S_{KerS}$ had decreased to -18.6 ‰ just prior to the PTB and further to -20.9 ‰ in the Early Triassic. The $\delta^{34}S_{kerS}$ and $\delta^{34}S_{TRIS}$ trends were generally similar, but the event horizon enrichment of $\delta^{34}S_{kerS}$ was not as distinct.

DBT and mDBTs showed similar isotopic and concentration trends, so for simplicity data will be reported for just DBT. The concentration of DBT was at its highest in the lowest Permian sample (64.7 μg/g TOC) and had decreased to 5.4 μg/g TOC at the top of Bed 22. Within the event horizon, concentration increases to 26.1 μg/g TOC at the top of Bed 24, followed by a decrease to 13.7 ± 6.6 μg/ TOC following the extinction. Thereafter in the Triassic, DBT concentrations were very low (~2 μg/g TOC). $\delta^{34}S_{DBT}$ decreased from ~ 22 ‰ in the deep Permian to a low of -28.9 ‰ at 140 m. There was then a progressive enrichment in ^{34}S to a $\delta^{34}S_{DBT}$ value of -17 ‰ at the top of bed 22. Through the event horizon there was a pronounced dip to a $\delta^{34}S_{DBT}$ value of -24 ‰ at ~60 cm below bed 25 then a closely matching increase to -19 ‰ just before the end of the horizon and -20 ‰ just prior to the PTB. Triassic samples were unfortunately too lean in OSCs for their $\delta^{34}S$ measurement. The OSCs were generally more depleted in ^{34}S than total kerogen S, but their distinct $\delta^{34}S$ profiles through the Meishan section reflected no obvious connection. Intriguingly however, the $\delta^{34}S_{DBT}$ incursion through the event horizon was the inverse of a closely coincident $\delta^{34}S_{kerS}$ (and $\delta^{34}S_{TRIS}$) incursion.

Table 5.1.: Summary of Meishan-1 core results

Sample Number	Depth [m]	Bed Number	TOC [wt.%]	TRIS [wt.%]	$\delta^{34}S_{TRIS}$ [‰VCDT]	KerS [wt.%]	$\delta^{34}S_{KerS}$ [‰VCDT]	DBT [μg/g TOC]	$\delta^{34}S_{DBT}$ [‰VCDT]	ΣmDBTs [μg/g TOC]	$\delta^{34}S_{mDBTs}$ [‰VCDT]	TOC/TRIS	TRIS/(TRIS+KerS)	DOP	Fe_{HR}/Fe_T	Fe_{Py}/Fe_{HR}	Redox milieu after Li *et al.* 2010
M1	90.22	37	1.14	0.96	-34.6	n.d.	n.d.	2.1	...	11.7	...	1.19	n.d.	0.81	0.29	0.82	oxic
M2	102.59	34	0.61	1.02	-36.4	0.01	-20.9	2.4	...	3.2	...	0.60	0.99	0.86	0.26	0.87	oxic
M3	106.52	26	0.81	1.54	-25.3	0.04	-18.6	18.4	-20.5	67.3	-17.4	0.53	0.97	0.95	0.39	0.95	oxic/euxinic
M4	106.56	26	0.72	1.36	-27.6	0.02	-15.8	9.1	-20.3	35.0	-21.5	0.53	0.99	0.95	0.39	0.95	oxic/euxinic
M5	106.75	24	0.67	0.22	-15.7	0.07	-8.7	26.1	-19.4	107.2	-20.3	3.05	0.76	0.59	0.54	0.56	ferruginous
M6	107.10	24	0.30	0.10	-13.4	0.37	-10.6	9.6	-23.6	31.1	-24.4	3.00	0.21	0.64	0.64	0.65	ferruginous
M7	110.15	22	0.50	0.09	-16.9	0.20	-10.7	5.4	-20.5	15.7	-19.9	5.56	0.31	0.80	0.53	0.80	euxinic/ferruginous
M8	111.04	22	1.27	0.16	-28.4	0.10	-11.0	5.8	-16.9	25.5	-19.9	7.94	0.62	0.90	0.42	0.90	euxcinic
M9	125.46	16-8	0.54	0.07	-26.1	0.23	-13.6	41.1	-24.4	303.2	-22.5	7.71	0.23	0.97	0.42	0.97	euxcinic
M10	140.01	16-8	0.32	0.03	-27.2	0.91	-16.2	34.2	-28.8	145.5	-28.5	10.67	0.03	0.94	0.48	0.94	euxcinic
M11	148.50	16-8	0.31	0.02	-24.6	0.59	-16.2	24.4	-22.7	139.0	-22.8	15.50	0.03	0.91	0.36	0.92	oxic
M12	153.95	16-8	1.22	0.18	-36.5	0.27	-16.4	64.7	-21.8	412.7	-22.9	6.78	0.40	0.94	0.46	0.95	euxcinic

Redox conditions

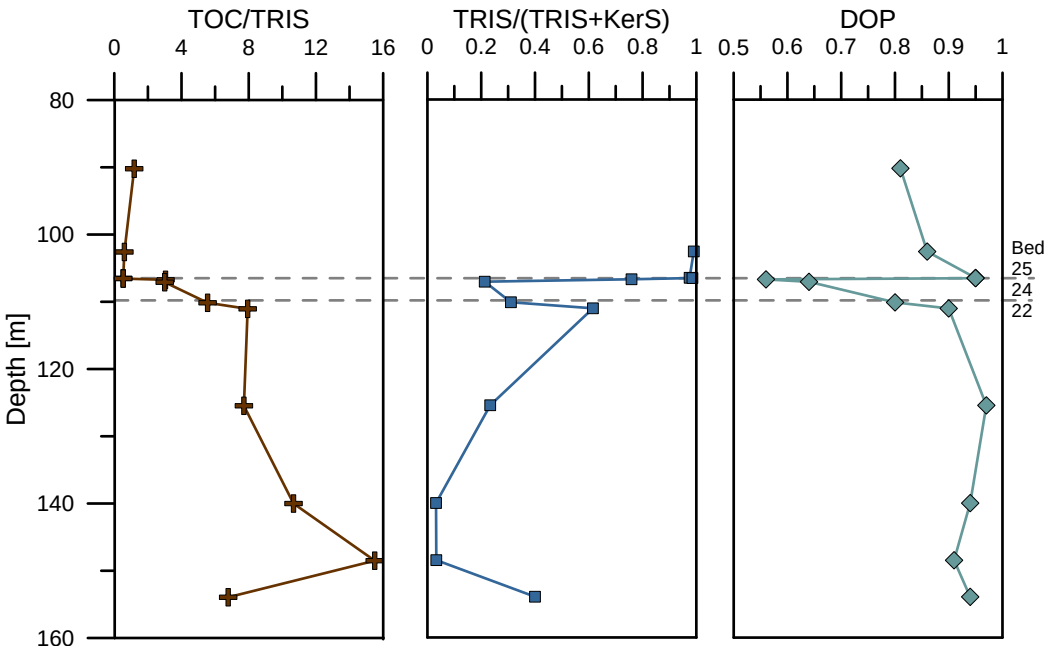

Figure 5.4.: Compositional data of the Meishan-1 section: ratio of TOC/TRIS (brown crosses); ratio of TRIS/(TRIS+KerS) (blue squares); degree of pyritisation (DOP; green diamonds).

Major changes during the event horizon in the relative abundance of inorganic an organic S was evident from the TOC/TRIS ratio, fractional abundance of TRIS (TRIS/(TRIS+KerS) and degree of pyritisation (DOP; Figure 5.4). The TOC/TRIS ratio was very high through the Permian (8-16) indicative of oxygenated marine conditions. TOC/TRIS showed a sharp and consistent decline from 8 to 0.5 through the event horizon with just a slight recovery to ~ 2 during the Early Triassic. The decline in TOC/TRIS values during the extinction horizon reflects a change to anoxic/euxinic water column conditions (Berner & Raiswell, 1983). Below the extinction horizon TRIS is present in much lower abundance than the organic S indicated by high concentrations of kerogen S. This translated to very low TRIS/(TRIS+KerS) values (< 0.1) during the Permian. An increase in this ratio prior to the event horizon reflects an enrichment of TRIS relative to kerogen S. Above bed 22 the TRIS/(TRIS+KerS) ratio showed a sharp drop from 0.6 to 0.2 suggesting preferential OM sulfurisation over pyritisation during the event horizon. From the extinction to the PTB TRIS/(TRIS+KerS) values were close to 1 indicating a dominance of reduced S in the system. Degree of pyritisation (DOP = $Fe_{Py}/(Fe_{Py}+Fe_{HCl})$) was consistently above 0.9 for most of the Permian and Triassic sections, indicating the persistence of anoxic conditions (Raiswell *et al.*, 1988). However, the DOP value drops to < 0.7 during the event horizon reflecting a

change in S mineralisation, and was coincident with significant δ^{34}S variations in all S fractions analysed and changes in TOC/TRIS. Further information about the water column redox conditions can be inferred from the distribution of Fe species. A relatively high proportion of highly reactive Fe-minerals (Fe_{HR}) such as pyrite (Fe_{Py}), Fe(III) oxides, magnetite and Fe-carbonates minerals relative to the total Fe (Fe_T) content indicates anoxic conditions (Raiswell & Canfield, 1998). Further, the Fe_{Py}/Fe_{HR} ratio can separate anoxic settings into ferruginous (Fe(II) enriched water column; low Fe_{Py}/Fe_{HR}) or euxinic (H_2S enriched water column; high Fe_{Py}/Fe_{HR}) conditions (Raiswell & Canfield, 1998; Canfield *et al.*, 2008).

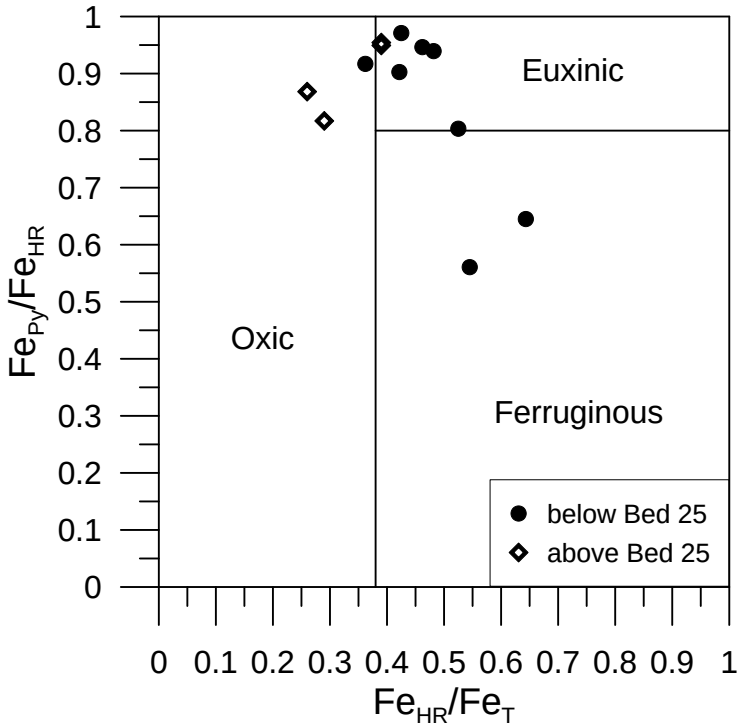

Figure 5.5.: Fe_{Py}/Fe_{HR} over Fe_{HR}/Fe_T plot of Meishan-1 data reflecting the redox conditions of the water column during deposition (Li *et al.*, 2010) from Meishan-1. Samples below bed 25 (prior to extinction) in black circles and above bed 25 in black diamonds.

A plot of Fe_{Py}/Fe_{HR} over Fe_{HR}/Fe_T (Li *et al.*, 2010) indicates the water column redox conditions of the Meishan-1 section were predominantly euxinic (Figure 5.5), consistent with the high DOP values measured. Two samples from the end of the event horizon (bed 24) had more moderate Fe_{Py}/Fe_{HR} and high Fe_{HR}/Fe_T values than the other samples, and plot in the ferruginous region of Figure 5.5. These data suggest a change to ferruginous conditions during the peak of the event horizon, just before the extinction. Following the extinction oxic/euxinic conditions prevail and became more consistently oxic during the Triassic.

5.3.2. Hovea-3

Sulfur Pools

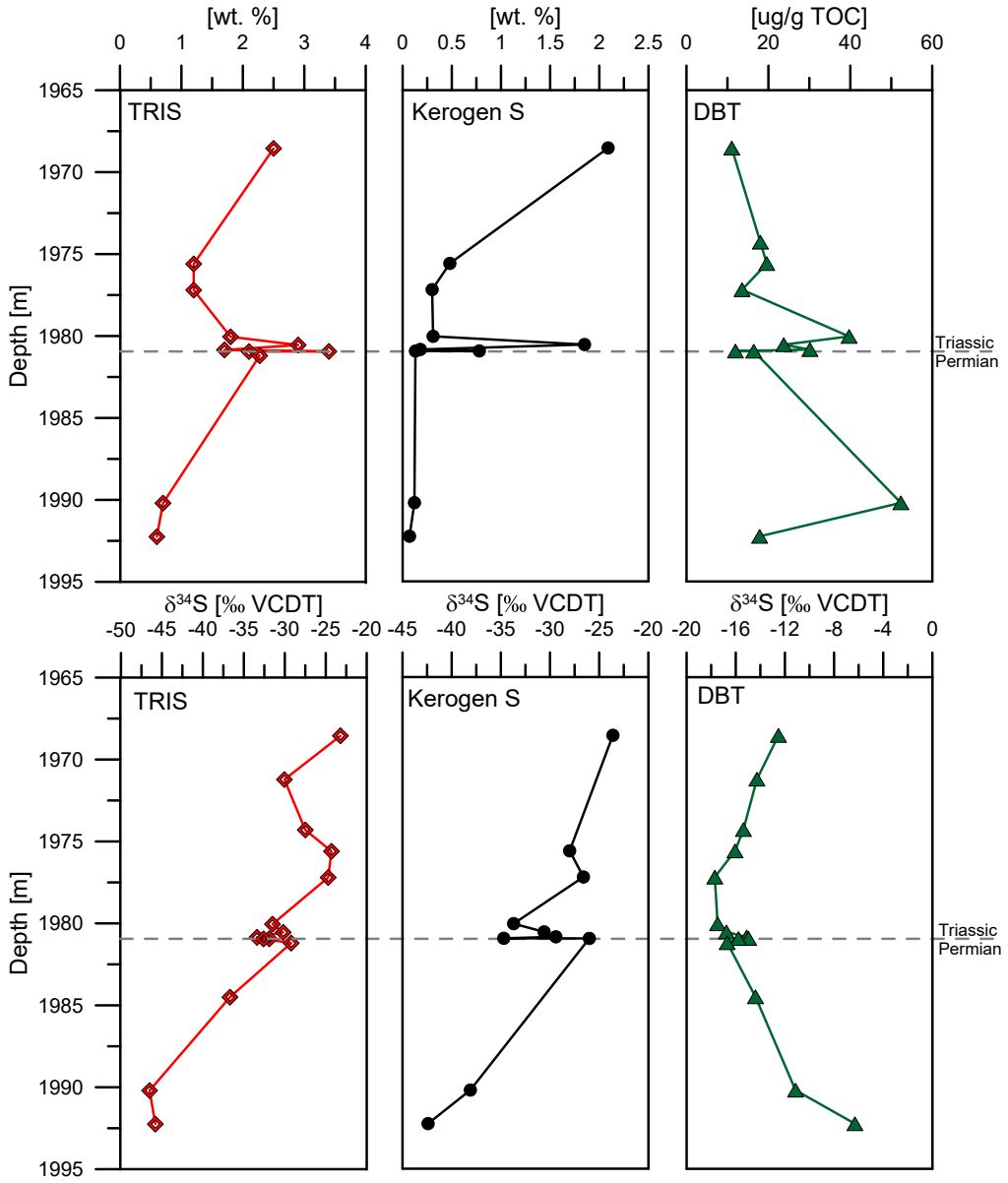

Figure 5.6.: Concentration (top) and $\delta^{34}S$ values (bottom) of TRIS (red line), kerogen S (black line) and DBT (green line) from the Hovea-3 section. Dashed line marks PTB.

Concentration and $\delta^{34}S$ values of the main S species of the P-Tr section in Hovea-3 are shown in Figure 5.6 and listed in Table 5.2. Major fluctuation in content and isotopic composition can be observed within a sharp interval corresponding to the extinction horizon, which can be considered equivalent to the PTB due to either a hiatus or non-sedimentation (Grice *et al.*, 2005a).

TRIS concentrations (> 0.5 wt.%) are generally much higher than in Meishan-1. TRIS increased steadily from 0.6 wt.% in the lowest Permian sample to 2.1 wt.% prior to the PTB. A large jump to 3.1 wt.% was evident at the P-Tr transition for the following 90 cm TRIS values fluctuate significantly within the range of 1.7 to 3.4 wt.%. Early in the Triassic it had decreased to 1.2 but subsequently increased to 2.5 wt.%. The $\delta^{34}S$ of TRIS was very light in the oldest Permian sample (-46.5 ‰) but then became progressively heavier to a value of -29.2 ‰ just 25 cm below the PTB. At the PTB there was then a sharp decline to -33.4 ‰ and in the next 90 cm section of the lower Triassic $\delta^{34}S_{TRIS}$ fluctuated between -32.6 and -30.2 ‰. The decline in $\delta^{34}S_{TRIS}$ at the PTB coincides with a similarly sharp negative shift in $\delta^{13}C_{Ker}$ previously reported by (Nabbefeld *et al.*, 2010b). The apparent synchronicity of $\delta^{34}S_{TRIS}$ and $\delta^{13}C_{Ker}$ excursions may be due to low sedimentation rates and thus the very condensed nature of the P-Tr transition (Grice *et al.*, 2005a). $\delta^{34}S_{TRIS}$ of the later Triassic was relatively heavy with a maximum value of -23.2 ‰ in the highest sample analysed. The kerogen S content of the Permian section was very low (~0.1 wt.%) but distinctive increases to 0.8 wt.% at the PTB interval and further to 1.9 wt.% 40 cm above the PTB were evident. Kerogen S retreated to 0.3 wt.% in the Early Triassic then showed a steady increase through the Triassic to a maximum of 2.1 wt.%. $\delta^{34}S_{KerS}$ was generally similar to the $\delta^{34}S_{TRIS}$ trend of $\delta^{34}S$ enrichment through the Permian, large (-42.4 to -26 ‰) fluctuations just prior to the PTB then increased to heavier values (i.e., -23.6 ‰) through the Triassic.

DBT concentration through the Permian ranged from 52.1 to 16.4 μg/g TOC. Its concentration was lowest at the PTB (11.9 μg/g TOC) and in the first 90 cm of the Triassic showed a relatively sharp increase to 39.7 μg/g TOC. There was a gradual decrease in the later Triassic samples to 11 μg/g TOC. $\delta^{34}S_{DBT}$ was heaviest in the lowest Permian (-6.3 ‰). By the latest Permian, 25 cm below the P-Tr transition, it had a value of -16.7 ‰ reflecting a progressive $\delta^{34}S$ depletion over this part of the section. $\delta^{34}S_{DBT}$ showed a light but sharp increase to -15 ‰ 1cm above the PTB. For the next 90 cm $\delta^{34}S$ was measured in a range of -17 to -15 ‰. Triassic $\delta^{34}S_{DBT}$ values become progressively enriched from the -17 ‰ minimum to a high of -12.5 ‰ at the top of the section. The $\delta^{34}S_{DBT}$ profile of the Hovea-3 section was almost the direct inverse of the $\delta^{34}S_{TRIS}$ data.

Table 5.2.: Summary of Hovea-3 core results.

Sample Number	Depth [m]	TOC [wt.%]	TRIS [wt.%]	$\delta^{34}S_{TRIS}$ [‰VCDT]	KerS [wt.%]	$\delta^{34}S_{KerS}$ [‰VCDT]	DBT [µg/g TOC]	$\delta^{34}S_{DBT}$ [‰VCDT]	ΣmDBTs [µg/g TOC]	$\delta^{34}S_{mDBTs}$ [‰VCDT]	TOC/TRIS	TRIS/(TRIS+KerS)	DOP	Fe_{HR}/Fe_T	Fe_{Py}/Fe_{HR}	Redox milieu after Li *et al.* 2010
H1	1968.55	2.3	2.5	-23.3	2.1	-23.6	11.1	-12.5	43.2	-18.0	0.9	0.5	n.d.	n.d.	n.d.	n.d.
H2	1971.22	2.5	n.d.	-30.1	n.d.	n.d.	n.d.	-14.3	n.d.	-16.7	n.d.	n.d.	n.d.	n.d.	n.d.	n.d.
H3	1974.30	1.7	n.d.	-27.5	n.d.	n.d.	18.0	-15.4	69.8	-18.3	n.d.	n.d.	n.d.	n.d.	n.d.	n.d.
H4	1975.60	2.1	1.2	-24.3	0.5	-28.0	19.6	-16.1	63.0	-18.7	1.7	0.7	n.d.	n.d.	n.d.	n.d.
H5	1977.20	3.8	1.2	-24.7	0.3	-26.6	13.6	-17.7	61.1	-17.2	3.1	0.8	n.d.	n.d.	n.d.	n.d.
H6	1980.05	0.9	1.8	-31.5	0.3	-33.7	39.7	-17.5	92.5	-19.6	0.5	0.9	n.d.	n.d.	n.d.	n.d.
H7	1980.55	1.6	2.9	-30.2	1.9	-30.6	23.7	-16.8	59.3	-19.1	0.5	0.6	n.d.	n.d.	n.d.	n.d.
H8	1980.85	1.5	1.7	-33.4	0.2	-29.4	30.1	-15.1	62.8	-14.6	0.9	0.9	n.d.	n.d.	n.d.	n.d.
H9	1980.94	4.6	3.4	-31.9	0.8	-34.7	11.9	-15.0	22.8	-18.0	1.4	0.8	n.d.	n.d.	n.d.	n.d.
H10	1980.95	5.5	2.1	-32.6	0.1	-26.0	16.4	-15.8	29.9	-19.5	2.6	0.9	n.d.	n.d.	n.d.	n.d.
H11	1981.20	2.0	2.3	-29.2	n.d.	n.d.	n.d.	-16.7	n.d.	-19.2	0.9	n.d.	n.d.	n.d.	n.d.	n.d.
H12	1984.50	1.8	n.d.	-36.7	n.d.	n.d.	n.d.	-14.4	n.d.	-15.7	n.d.	n.d.	n.d.	n.d.	n.d.	n.d.
H13	1990.20	2.1	0.7	-46.5	0.1	-38.1	52.3	-11.1	44.4	-8.1	3.0	0.9	n.d.	n.d.	n.d.	n.d.
H14	1992.25	1.8	0.6	-45.8	0.1	-42.4	17.9	-6.3	28.6	-3.1	3.0	0.9	n.d.	n.d.	n.d.	n.d.

Redox conditions

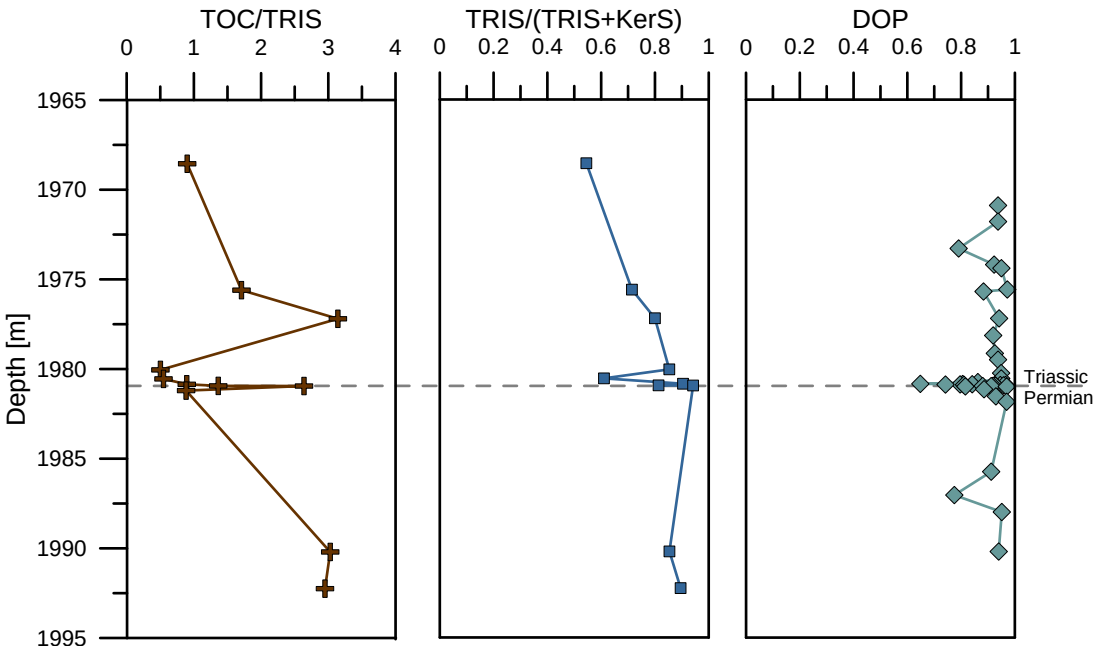

Figure 5.7.: Compositional data of the Hovea-3 section: ratio of TOC/TRIS (brown crosses); ratio of TRIS/(TRIS+KerS) (blue squares); degree of pyritisation (DOP; green diamonds).

Variations of TOC and TRIS in the Hovea-3 PTB section did not coincide with major sulfur isotopic changes of TRIS or OSCs as they did in the Meishan section. The TOC/TRIS ratio was high in the Permian (~3) and decreased to 0.9 prior to the PTB (Figure 5.7). The PTB was marked by a sharp increase in TOC/TRIS to 2.6 then a similarly sharp decrease to a minimum value of 0.5 90 cm above the PTB. TOC/TRIS was < 2 in the Triassic, apart from a measurement of ~3 at 1977.2 m. This data is in general agreement with a change from oxic conditions in the Permian to euxinic conditions in the Triassic reported from a previous study of Hovea-3 (Grice *et al.*, 2005c). The TRIS/(TRIS+KerS) ratios (Figure 5.7) from the Permian to early Triassic was generally high (0.9) indicating a predominance of inorganic S over organic S. Just above the P-Tr transition this ratio dropped suddenly to < 0.5 indicating greater organic sulfurisation immediately after the P-Tr transition. The DOP was consistently very high (ave = 0.9 ± 0.1) through the section, although it showed a drop at the P-Tr transition slightly prior to the decrease in TRIS/(TRIS+KerS). High DOP values typically implies a persistence of anoxic water column conditions. However, this is in contradiction to our TOC/TRIS measurements and previous measurements of elevated isorenieratane, a biomarker for photic zone euxinia (Grice *et al.*, 2005c), which have pointed to the prevalence of oxic conditions during the Permian. Nb. The biomarker

data reported by Grice *et al.* (2005c) was from a different sample set to those for which the current sulfur isotope data was measured.

An oxic water column during the Permian was further supported by the Fe speciation (Figure 5.8) and widespread benthic fauna in Permian sediments (Thomas *et al.*, 2004). The Fe speciation data was consistent with primarily euxinic conditions during the Triassic.

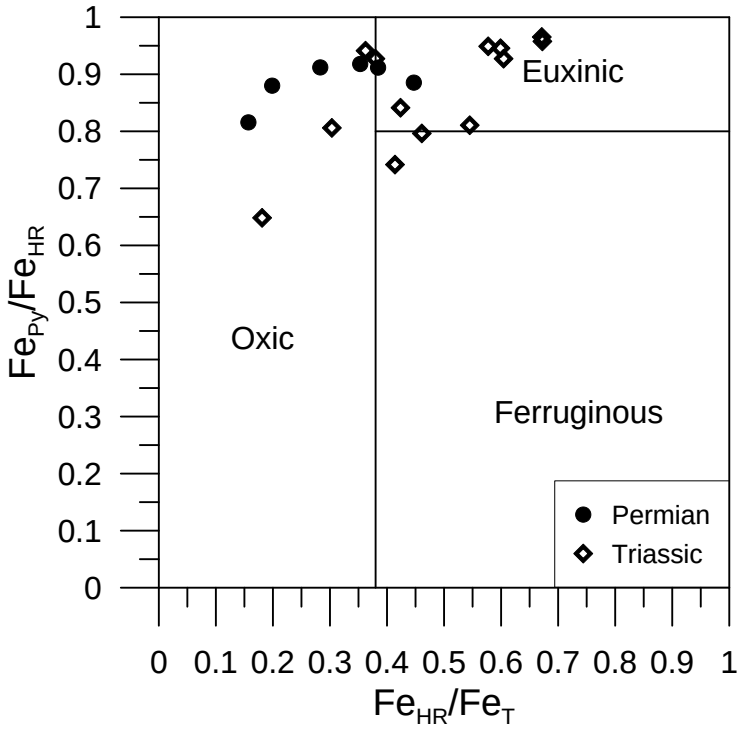

Figure 5.8.: Fe_{Py}/Fe_{HR} over Fe_{HR}/Fe_T plot of Hovea-3 data reflecting the redox conditions of the water column during deposition (Li *et al.*, 2010). Permian samples (prior to extinction) in black circles and Triassic samples in black diamonds.

5.4. Discussion

5.4.1. Organic sulfurisation and inorganic sulfidisation

The sulfur isotopic composition of sedimentary inorganic (TRIS) and organic (kerogen) S is controlled primarily by the isotopic composition of H_2S formed by sulfate reduction. However, it may also be influenced by sulfide oxidation including the production of highly reactive sulfur intermediates (Canfield & Thamdrup, 1994; Böttcher *et al.*, 2001). The rate of sulfate reduction is dependent on availability of reactive organic matter and has been inversely correlated with the isotopic fractionation between

seawater sulfate and H_2S (Goldhaber & Kaplan, 1980). Sulfate reduction is often slower in normal oxygenated marine settings where OM is limited and the isotopic fractionation between seawater sulfate and formed H_2S is very large due to disproportionation reactions (Berner, 1985; Canfield & Thamdrup, 1994; Cypionka *et al.*, 1998; Passier *et al.*, 1999a; Böttcher *et al.*, 2001). The $\delta^{34}S$ of inorganic S and organic S is also likely to be quite similar. The S-isotopic fractionation between H_2S and the pyrite it produces is usually less than 1 ‰ (Price & Shieh, 1979; Böttcher *et al.*, 1998; Butler *et al.*, 2004). Organic S is formed from reduced S *via* S-intermediates typically with a slight increase in $\delta^{34}S$ of a few ‰ (Amrani & Aizenshtat, 2004). Conversely, under euxinic conditions there is often an ample supply of reactive OM and hence H_2S resulting in less disproportionation of the sulfur isotopes and relatively small $\delta^{34}S$ fractionation between sea water sulfate and its reduced forms (i.e., H_2S, pyrite, organic S) (Thamdrup *et al.*, 1993). In a closed system, the $\delta^{34}S$ fractionation between seawater sulfate and H_2S would be less with the progression of the sulfate reduction. These conditions can lead to inorganic S and organic S with relatively heave $\delta^{34}S$ values (Berner, 1985). Pyrite formation is kinetically favored over organic sulfurisation (Berner, 1980), but can be limited by the availability of reactive Fe species (Berner, 1985).

Organic S is formed by the diagenetic reaction of reduced inorganic sulfur species (HS^- or polysulfides S_x^{2-}) with functionalised organic molecules (Sinninghe Damste & de Leeuw, 1990). The S may form discrete OSCs (intramolecular addition of HS^- (Kohnen *et al.*, 1990; Raven *et al.*, 2015) or be incorporated into organic macromolecules (i.e., kerogen) as S_x^{2-} linkages between different organic units (intermolecular addition of S_x^{2-}; kerogen S). Raven *et al.* (2016) reported $\delta^{34}S$ depleted pyrite in the euxinic Cariaco Basin, which they suggested may have derived from microbial sulfate reduction in sediment pores. In such a circumstance the $\delta^{34}S$ of pyrite would be controlled by the redox conditions of the water column rather than sulfur disproportionation of sea water sulfate (Raven *et al.*, 2016). Raven *et al.* (2016) also suggested low pore-water concentrations of non-mineralised H_2S may isotopically exchange with organic S.

5.4.2. Meishan-1

Coincident isotopic variations in TRIS and DBT through the event horizon began at the top of bed 22 and peak at the top of bed 24 prior to the P-Tr extinction (Figure 5.9). The concentrations of TRIS (Permian < 0.2 wt.%; Triassic < 1.6 wt.%; Figure 5.3) and kerogen S (< 1 wt.% throughout; Figure 5.3) were low through the section suggesting low S flux during deposition. The concentration and $\delta^{34}S$ profile of DBT was quite distinct from kerogen S. Kerogen S must contain distinct pools of OSCs, one of which

was represented by the DBTs, with varied isotopic composition. The relatively light $\delta^{34}S$ values of the DBTs indicate they must have been a quantitatively low component of the heavier kerogen S. Other S-pools within the kerogen may include polar S compounds or macromolecular S_x- linkages (Grotheer *et al.*, in review). Furthermore, at the top of bed 24 $\delta^{34}S_{DBT}$ and $\delta^{34}S_{KerS}$ each show isotopic excursions but in opposing directions, which suggests an S-isotope disproportionation between the DBTs and other kerogen-S sources.

Within the event horizon the $\delta^{34}S$ compositions of DBTs were a mirror image to $\delta^{34}S_{TRIS}$. These trends, which also showed a close correlation to TRIS/(TRIS+KerS), suggest a kinetic relationship between organic sulfurisation (i.e., represented by DBTs) and inorganic sulfidisation (i.e., TRIS; Figure 5.9). The apparent redox coupling of the DBT and TRIS pools of S suggest they are sensitive to water column conditions or other local basin environmental controls.

The corresponding $\delta^{34}S$ and concentration data of kerogen S was very different to the DBTs, suggesting the occurrence of other major modes of organic sulfurisation. Furthermore, the opposite direction of the Raven *et al.* (2015) distinguished organic sulfurisation pathways from contrasting $\delta^{34}S_{OSC}$ and $\delta^{34}S_{bulk}$ values in recent Cariaco Bay Basin sediments. The preferential intramolecular incorporation of the smaller ^{32}S gave rise to aromatic OSCs with relatively low $\delta^{34}S$ values (Cf. pyrite and kerogen S Raven *et al.*, 2015). The heavier $\delta^{34}S$ of kerogen S in the Meishan-1 section may be influenced by the intermolecular incorporation of S_x-bridging with a greater ^{34}S bias potentially arising from the equilibrium status of their production or extraction (e.g., thermal cracking) reactions. Field observations (Aycard *et al.*, 2003) and laboratory controlled experiments (Amrani & Aizenshtat, 2004) have both demonstrated the combined influence of different reaction kinetics on the $\delta^{34}S$ of S rich organic sediments.

Raven *et al.* (2016) also suggested OSCs detected in immature Cariaco Bay basin sediments may be vulnerable to isotopic exchange with inorganic S-sources (i.e., porewater H_2S) in a S limited system. Such processes in the low S depositional environment of Meishan might contribute to the contrasting $\delta^{34}S$ profiles of TRIS and DBTs (organic S).

The entire Meishan-1 section was of similar thermal maturity (Cao *et al.*, 2009) so thermal cracking, which can impact more on the smaller ^{32}S, is not likely to have influenced the $\delta^{34}S$ variances observed.

The sensitivity of $\delta^{34}S_{TRIS}$ and $\delta^{34}S_{DBT}$ to environmental change is supported by the Fe speciation data. The event horizon was characterised by a transition from euxinic to ferruginous conditions. The development of ferruginous water column conditions would have required the massive influx of Fe(II) such as from hydrothermal vents or the mineralisation and depletion of vast amounts of H_2S. Both scenarios would result

in the deposition of large quantities of pyrite, by initial reaction and buffering of Fe(II) by the H_2S abundant in euxinic waters. However, the Meishan section contains no such pyrite enriched strata prior to the PTB. The event horizon is marked by a reduction of the Fe_{Py}/Fe_{HR} ratio, low TRIS, elevated kerogen S concentrations and consequently a notable drop in the TRIS/(TRIS+KerS) ratio. During the event horizon, the available reduced S reacted with OM in preference to Fe(II) reducing pyritisation, in agreement with the observed reduction in DOP (Table 5.1).

Above the extinction event TRIS abundance increases significantly becoming the dominant S pool coincident with a ^{34}S depletion in both TRIS and kerogen S. This behavior reflects a change in preference for pyritisation over OM sulfurisation.

The event horizon in the Meishan section has previously been identified from the concentrations and stable isotopic values of mercury (Grasby *et al.*, 2016) and zinc (Liu *et al.*, 2017). Elevated concentrations and distinct variations in the isotopic composition of Hg and Zn in bed 24 prior to the extinction inferred intensified volcanic activity. Our data, however, suggests the event horizon commenced prior i.e., top of bed 22, to the volcanic activity. Nevertheless, the sharp isotopic incursions of TRIS and DBT in bed 24 are likely due in part to the increased volcanism and eruption of the Siberian Flood Basalts. A holistic assessment of our data however, supports previous assertions that the rapid and intensive change to the S-cycle during the extinction horizon was due to a complex involvement and combination of geologic processes (e.g., continental volcanism, weathering; Cao & Zheng, 2009) and related chemical and redox changes to the water column. Multiple controls were also previously thought responsible for a negative shift in $\delta^{34}S_{sulfate}$ beginning at the top of bed 24 (Kaiho *et al.*, 2006b), since the magnitude of the shift was too large for any known volcanic or terrestrial sources. Kaiho *et al.* (2006b) concluded that a $\delta^{34}S_{sulfate}$ depletion may have arisen from the overturning of a stratified H_2S dominated ocean due to a meteorite impact or volcanic induced long-term cooling. Such scenarios could possibly account for the $\delta^{34}S_{sulfate}$ shift beginning at the top of bed 24, but would not also explain the $\delta^{34}S$ trends of TRIS and OSCs observed here to begin at the top of bed 22. Furthermore, a decrease of $\delta^{34}S_{sulfate}$ would normally be mirrored by the ^{34}S depletion of TRIS.

5.4.3. Hovea-3

In Hovea-3, kerogen S and TRIS showed very similar $\delta^{34}S$ values, whereas the $\delta^{34}S$ of DBT showed an almost inverse trend through the section and had consistently heavier values (Figure 5.6). The close $\delta^{34}S$ relationship apparent between the main inorganic and organic (i.e., kerogen) S pools suggests an ample supply of reduced S species and negligible isotopic fractionation between reduced HS^- and kerogen S. The $\delta^{34}S$ profiles of TRIS and kerogen S were not as similar as through the Meishan-1 event

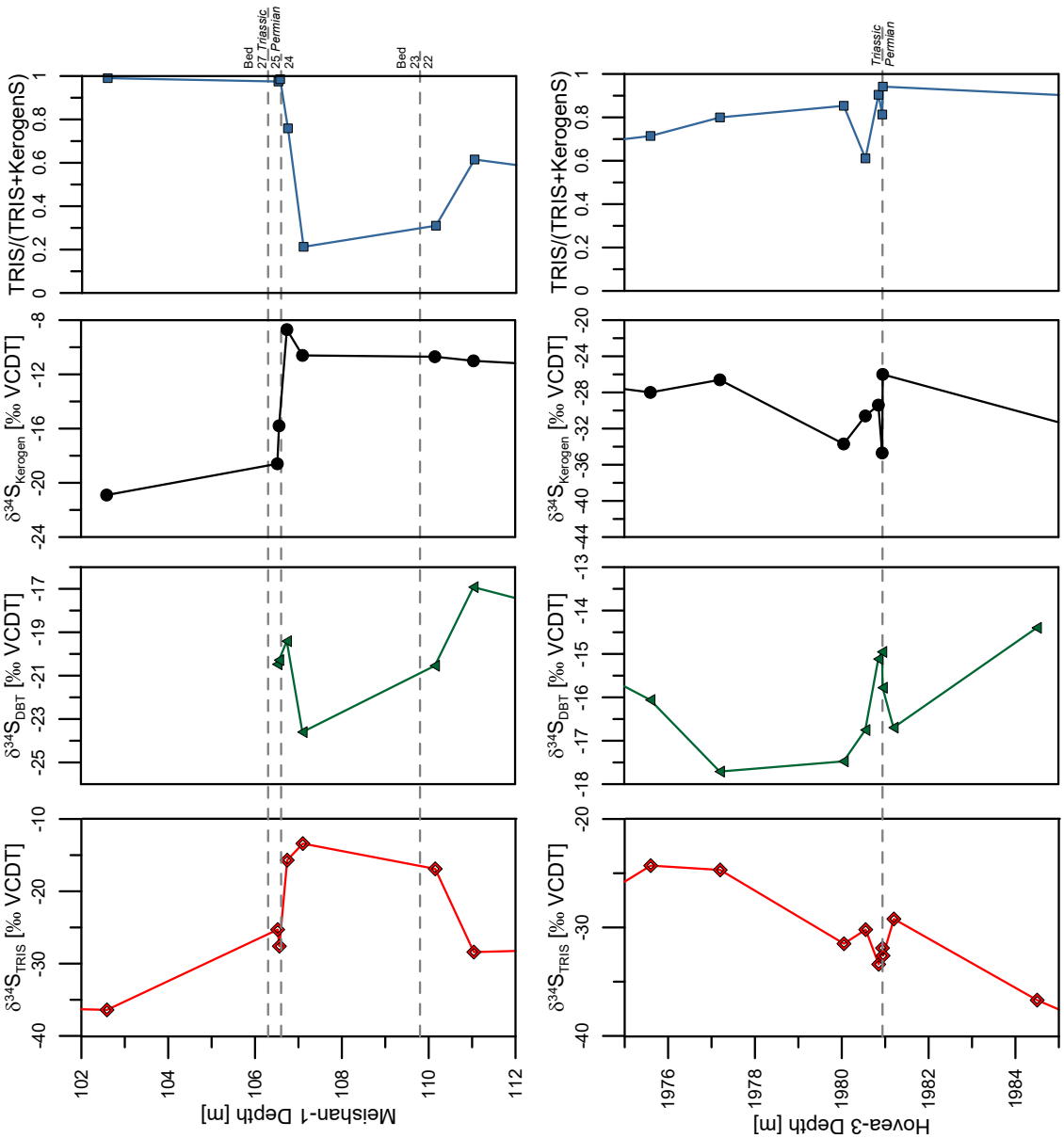

Figure 5.9.: Comparison of $\delta^{34}S$ data and relative abundance of inorganic and organic S pool through the (expanded) P-T extinction horizons of Meishan-1 (top; dashed lines between bed 25 and 27 marks PTB, between bed 25 and 24 extinction event) and Hovea-3 (bottom; dashed line marks PTB). $\delta^{34}S$ profiles shown for TRIS (red diamonds), DBT (green triangles) and bulk kerogen S (black circles) and variations in TRIS/(TRIS+KerS) (blue squares).

horizon (Figure 5.9 top), possibly due to a more limited availability of reduced S. A greater availability of reduced S at Hovea-3 may be implied from the higher concentrations of TRIS, in particular, and kerogen S in this section.

A sharp increase in the $\delta^{34}S_{TRIS}$ value just prior to the PTB may reflect an increase in the rate of sulfate reduction due to changing biochemical conditions. The $\delta^{34}S$ of seawater sulfate was relatively stable (~ 10 ‰) during the Late Permian (Claypool *et al.*, 1980) so was not likely a factor in the $\delta^{34}S$ dynamics measured here in Hovea-3. Sulfate reduction, and subsequent organic sulfurisation and inorganic sulfidisation occurs in the top layer of the sediment at the sediment water interface. The rates of these processes would have increased with the development of anoxic conditions and the increased supply of reactive organic matter to the sediment. TOC in the Hovea-3 section increased sharply towards the PTB (Figure 5.7). This was matched by an increase in the Fe_{HR}/Fe_T ratio, inferring increased oxygen depletion, possibly related to enhanced primary production in response to elevated nutrient flux from increased terrestrial weathering during the End Permian transgression (e.g., Hallam & Wignall, 1999). The incorporation of reduced S into both organic and inorganic S pools typically occurs with little isotopic fractionation under normal marine oxygenated conditions. However, Fe(II) is more reactive with HS^- than OM, so an excess of reduced S species relative to available Fe(II) would be necessary for their incorporation into OM. A limitation in Fe(II) could result in a isotopic enrichment of kerogen S relative to TRIS (Idiz *et al.*, 1990), as non-mineralised reduced S, enriched in ^{34}S, can be incorporated into the kerogen matrix. This could lead to a ^{34}S enrichment of DBT such as observed in Hovea-3. DBT shows a slight $\delta^{34}S$ convergence with TRIS and kerogen S through the late Permian, diverges sharply at the P-Tr transition and is more constant during the Early Triassic (Figure 5.9). The relative heavy $\delta^{34}S$ values of the DBTs and their contrasting extinction event behavior to kerogen S reinforces their characterisation as a minor sub-fraction of the organic S pool in the Hovea-3 sediments.

The slight $\delta^{34}S$ convergence of $\delta^{34}S_{DBT}$ with $\delta^{34}S_{KerS}$ and $\delta^{34}S_{TRIS}$ at the end Permian may be related to increasing anoxia and the enhanced availability of reactive OM fueling sulfate reduction. In turn, the increasing supply of reduced S may decrease the kinetic fractionation between different S-pools (i.e., mineral sulfides/FeS_2 with organic S/DBT). In the Triassic, the $\delta^{34}S$ values of TRIS, kerogen S and DBT were generally stable, suggesting more steady-state reaction conditions persisted under euxinic conditions.

The $\delta^{34}S$ profiles of three S-pools show sharp incursions at the PTB which intriguingly were in the exact opposite direction to the corresponding incursions of Meishan-1. In Hovea-3 the PTB $\delta^{34}S$ incursion of TRIS and DBT diverge and do not directly correlate with the TRIS/(TRIS+KerS) incursion as they did in the Meishan-1 horizon (Figure 5.9). This was likely due to neither TRIS nor organic S being limited

in Hovea-3 as their generally high concentrations imply. However, the contrasting behavior of DBTs suggests the sensitivity of different organic sulfurisation processes to biogeochemical change can vary quite markedly. Furthermore, sub-fractions, even quantitatively minor fractions such as represented by DBT might be sensitive to certain environmental dynamics even when the major organic S substances are not.

5.5. Conclusions

Distinct variations between kerogen S and individual OSCs (e.g., DBTs) indicate that i) kerogen S contains distinct pools of organic sulfur with varied isotopic composition; and ii) the OSCs represent a quite small proportion of kerogen S. Other more quantitatively significant organic S-pools may include polar compounds unamenable to GC separation or S_x-bridges tightly bound within the kerogen macromolecular network.

Further, the abundance and $\delta^{34}S$ composition of OSCs and their relationship with kerogen S and total inorganic S through two geographically distinct Permian Triassic extinction horizons revealed their potential sensitivity to water column conditions and local basin environmental controls. The $\delta^{34}S$ profile of DBT in the two P-Tr sections studied were either controlled by progressive oxygen depletion in developing euxinic water column conditions (Hovea-3) or by a complex combination of geologic processes including terrestrial volcanism and related changes to the basins water chemistry (Meishan-1). These observations highlight the potential of compound-specific sulfur isotope analysis as an additional tool to reconstruct the global S-cycle and illuminate the drivers behind the large environmental fluxes and ecological stresses associated with extinction events.

Acknowledgments

This study was conducted as part of the CSIRO Flagship Collaboration Fund Cluster for Organic Geochemistry of Mineral Systems. HG thanks CSIRO and Curtin University (scholarships) and KG the ARC (DP150102235) for funding support. Alex I. Holman, Geoff Chidlow, Peter Hopper and Iris Schmiedinger provided analytical support.

References

Amrani, A., & Aizenshtat, Z. 2004. Mechanisms of sulfur introduction chemically controlled: δ34S imprint. *Organic Geochemistry*, **35**(11-12), 1319–1336.

Amrani, A., Sessions, A. L., & Adkins, J. F. 2009. Compound-specific δ34S analysis of volatile organics by coupled GC/multicollector-ICPMS. *Analytical Chemistry*, **81**(21), 9027–9034.

Asif, M., Alexander, R., Fazeelat, T., & Pierce, K. 2009. Geosynthesis of dibenzothiophene and alkyl dibenzothiophenes in crude oils and sediments by carbon catalysis. *Organic Geochemistry*, **40**(8), 895–901.

Aycard, Mylène, Derenne, Sylvie, Largeau, Claude, Mongenot, Thierry, Tribovillard, Nicolas, & Baudin, François. 2003. Formation pathways of proto-kerogens in Holocene sediments of the upwelling influenced Cariaco Trench, Venezuela. *Organic Geochemistry*, **34**(6), 701–718.

Benton, M. J., & Twitchett, R. J. 2003. How to kill (almost) all life: the end-Permian extinction event. *Trends in Ecology & Evolution*, **18**(7), 358–365.

Berner, R. A. 1980. *Early diagenesis: A theoretical approach*. No. 1 edn. Princeton University Press.

Berner, R. A. 1982. *Burial of organic carbon and pyrite sulfur in the modern ocean: Its geochemical and environmental significance*.

Berner, R. A. 1985. Sulphate reduction, organic matter decomposition and pyrite formation. *Philosophical Transactions of the Royal Society of London. Series A, Mathematical and Physical Sciences*, **315**(1531), 25–38.

Berner, R. A., & Raiswell, R. 1983. Burial of organic carbon and pyrite sulfur in sediments over phanerozoic time: a new theory. *Geochimica et Cosmochimica Acta*, **47**(5), 855–862.

Bond, D. P. G., & Wignall, P. B. 2008. The role of sea-level change and marine anoxia in the Frasnian-Famennian (Late Devonian) mass extinction. *Palaeogeography, Palaeoclimatology, Palaeoecology*, **263**(3-4), 107–118.

Bowring, S. A., Erwin, D. H., Jin, Y. G., Martin, M. W., Davidek, K., & Wang, W. 1998. U/Pb Zircon Geochronology and Tempo of the End-Permian Mass Extinction. *Science*, **280**, 1039–1045.

Bowring, S. A, Erwin, D. H., & Isozaki, Y. 1999. The tempo of mass extinction and recovery: the end-Permian example. *Proceedings of the National Academy of Sciences of the United States of America*, **96**, 8827–8828.

Böttcher, M. E., & Schnetger, B. 2004. Direct measurement of the content and isotopic composition of sulfur in black shales by means of combustion-isotope-ratio-monitoring mass spectrometry (C-irmMS). *Pages 597–603 of:* de Groot, P. (ed), *Handbook of Stable Isotope Analytical Techniques, Vol. I*. Elsevier.

Böttcher, M. E., Smock, A. M., & Cypionka, H. 1998. Sulfur isotope fractionation during experimental precipitation of iron(II) and manganese (II) sulfide at room temperature. *Chemical Geology*, **146**(3-4), 127–134.

Böttcher, M. E., Thamdrup, B., & Vennemann, T. W. 2001. Oxygen and sulfur isotope fractionation during anaerobic bacterial disproportionation of elemental sulfur. *Geochimica et Cosmochimica Acta*, **65**(10), 1601–1609.

Böttcher, M. E., Hetzel, A., Brumsack, H. J., & Schipper, A. 2006. Sulfur-iron-carbon geochemistry in sediments of the Demerara Rise. *Proceedings of the Ocean Drilling Program Scientific Results*, **207**.

Butler, I. B., Böttcher, M. E., Rickard, D., & Oldroyd, A. 2004. Sulfur isotope partitioning during experimental formation of pyrite via the polysulfide and hydrogen sulfide pathways: Implications for the interpretation of sedimentary and hydrothermal pyrite isotope records. *Earth and Planetary Science Letters*, **228**(3-4), 495–509.

Canfield, D. E., & Thamdrup, B. 1994. The production of 34S-depleted sulfide during bacterial disproportionation of elemental sulfur. *Science*, **266**, 1973–1975.

Canfield, D. E., Poulton, S. W., Knoll, A. H., Narbonne, G. M., Ross, G., Goldberg, T., & Strauss, H. 2008. Ferruginous conditions dominated later neoproterozoic deep-water chemistry. *Science*, **321**(5891), 949–952.

Cao, C., & Zheng, Q. 2009. Geological event sequences of the Permian-Triassic transition recorded in the microfacies in Meishan section. *Science in China, Series D: Earth Sciences*, **52**(10), 1529–1536.

Cao, C., Wang, W., & Jin, Y. 2002. Carbon isotope excursions across the Permian-Triassic bound- ary in the Meishan section, Zhejiang Province, China. *Chinese Science Bulletin*, **47**(13), 1125.

Cao, C., Love, G. D., Hays, L. E., Wang, W., Shen, S., & Summons, R. E. 2009. Biogeochemical evidence for euxinic oceans and ecological disturbance presaging

the end-Permian mass extinction event. *Earth and Planetary Science Letters*, **281**(3-4), 188–201.

Chen, J.-S., & Chu, X.-L. 1988. Sulfur isotope composition of triassic marine sulfates of South China. *Chemical Geology: Isotope Geoscience Section*, **72**(2), 155–161.

Claypool, G. E., Holser, W. T., Kaplan, I. R., Sakai, H., & Zak, I. 1980. The age curves of sulfur and oxygen isotopes in marine sulfate and their mutual interpretation. *Chemical Geology*, **28**(C), 199–260.

Cline, J. D. 1969. Spectrophotometric Determination of Hydrogen Sulfide in Natural Waters. *Limnology and Oceanography*, **14**(3), 454–458.

Cortecci, G., Reyes, E., Berti, G., & Casati, P. 1981. Sulfur and oxygen isotopes in Italian marine sulfates of Permian and Triassic ages. *Chemical Geology*, **34**(1-2), 65–79.

Cypionka, H., Smock, A. M., & Böttcher, M. E. 1998. A combined pathway of sulfur compound disproportionation in Desulfovibrio desulfuricans. *FEMS Microbiology Letters*, **166**, 181–186.

Fossing, H., & Jørgensen, B. B. 1989. Measurement reduction of a single-step chromium method Evaluation. *Biogeochemistry*, **8**(3), 205–222.

Foster, W. J., & Twitchett, R. J. 2014. Functional diversity of marine ecosystems after the Late Permian mass extinction event. *Nature Geoscience*, **7**(3), 233–238.

Goldhaber, M. B., & Kaplan, I. R. 1980. Mechanisms of sulfur incorporation and isotope fractionation during early diagenesis in sediments of the gulf of California. *Marine Chemistry*, **9**(2), 95–143.

Gorjan, P., & Kaiho, K. 2007. Correlation and comparison of seawater δ34Ssulfate records at the permian-triassic transition. *Chemical Geology*, **243**(3-4), 275–285.

Gorjan, P., Kaiho, K., Kakegawa, T., Niitsuma, S., Chen, Z. Q., Kajiwara, Y., & Nicora, A. 2007. Paleoredox, biotic and sulfur-isotopic changes associated with the end-Permian mass extinction in the western Tethys. *Chemical Geology*, **244**(3-4), 483–492.

Grasby, S. E., Shen, W., Yin, R., Gleason, J. D., Blum, J. D., Lepak, R. F., Hurley, James P., & Beauchamp, Benoit. 2016. Isotopic signatures of mercury contamination in latest Permian oceans. *Geology*, **45**(1).

Greenwood, P. F., Amrani, A., Sessions, A., Raven, M. R., Holman, A., Dror, G., Grice, K., McCulloch, M. T., & Adkins, J. F. 2014. Development and Initial Biogeochemical Applications of Compound-Specific Sulfur Isotope Analysis. *Chap. 10, pages 285–312 of:* Grice, K. (ed), *Principles and Practice of Analytical Techniques in Geosciences*. UK: Royal Society of Chemistry.

Grice, K., Twitchett, R. J., Alexander, R., Foster, C. B., & Looy, C. 2005a. A potential biomarker for the Permian–Triassic ecological crisis. *Earth and Planetary Science Letters*, **236**(1-2), 315–321.

Grice, K., Summons, R. E., Grosjean, E., Twitchett, R. J., Dunning, W., Wang, S. X., & Böttcher, Michael E. 2005b. Depositional conditions of the northern onshore Perth Basin (basal Triassic). *APPEA Journal*, **45**(1), 263–274.

Grice, K., Cao, C., Love, G. D., Böttcher, M. E., Twitchett, R. J., Grosjean, E., Summons, R. E., Turgeon, S. C., Dunning, W., & Jin, Y. 2005c. Photic zone euxinia during the Permian-triassic superanoxic event. *Science*, **307**, 706–709.

Grotheer, H., Le Métayer, P., Piggott, M. J., Lindeboom, E. J., Holman, A. I., Twitchett, R. J., & Grice, K. 2017. Occurrence and significance of phytanyl arenes across the Permian-Triassic boundary interval. *Organic Geochemistry*, **104**, 42–52.

Grotheer, H., Greenwood, P. F., McCulloch, M. T., Böttcher, M. E., & Grice, K. in review. d34S character of organosulfur compounds in kerogen and bitumen fractions of organic sediments. *Organic Geochemistry*.

Hallam, A., & Wignall, P. B. 1997. *Mass Extinctions and their Aftermath*. Oxford University Press.

Hallam, A., & Wignall, P. B. 1999. Mass extinctions and sea-level changes. *Earth-Science Reviews*, **48**(4), 217–250.

Heinrichs, H., Brumsack, H. J., Loftfield, N., & König, N. 1986. Verbessertes Druckaufschlußsystem für biologische und anorganische Materialien. *Zeitschrift für Pflanzenernährung und Bodenkunde*, **149**(3), 350–353.

Idiz, E. F., Tannenbaum, E., & Kaplan, I. R. 1990. Pyrolysis of High-Sulfur Monterey Kerogens. *Pages 575–591 of:* Orr, W. L., & White, C. M. (eds), *Geochemistry of Sulfur in Fossil Fuels*, vol. 429. Washington D.C.: American Chemical Society.

Jiang, A., Zhou, P., Sun, Y., & Xie, L. 2013. Rapid column chromatography separation of alkylnaphthalenes from aromatic components in sedimentary organic matter for compound specific stable isotope analysis. *Organic Geochemistry*, **60**, 1–8.

Jiang, Y .-F., Tang, Y .-G., & Chou, C.-L. 2006. Research on genesis of pyrite near the Permian-Triassic boundary in meishan, Zhejiang, China. *Journal of China University of Mining and Technology*, **16**(4), 457–460.

Jin, Y. G., Wang, Y., Wang, W., Shang, Q. H., Cao, C. Q., & Erwin, D. H. 2000. Pattern of marine mass extinction near the Permian-Triassic boundary in South China. *Science*, **289**(5478), 432–436.

Kaiho, K., Kajiwara, Y., Nakano, T., Miura, Y., Kawahata, H., Tazaki, K., Ueshima, M. Masato, Chen, Zhongqiang, & Shi, Guang R. 2002. End-Permian catastrophe by a bolide impact: Evidence of a gigantic release of sulfur from the mantle. *Geology*, **29**(9), 815–818.

Kaiho, K., Kajiwara, Y., Chen, Z.-Q., & Gorjan, P. 2006a. A sulfur isotope event at the end of the Permian. *Chemical Geology*, **235**(1-2), 33–47.

Kaiho, K., Chen, Z. Q., Kawahata, H., Kajiwara, Y., & Sato, H. 2006b. Close-up of the end-Permian mass extinction horizon recorded in the Meishan section, South China: Sedimentary, elemental, and biotic characterization and a negative shift of sulfate sulfur isotope ratio. *Palaeogeography, Palaeoclimatology, Palaeoecology*, **239**(3-4), 396–405.

Kohnen, M. E. L., Sinninghe Damsté, J. S., Kock-Van Dalen, A. C., Ten Havens, H. L., Rullkötter, J., & de Leeuw, J. W. 1990. Origin and diagenetic transformations of C 25 and C 30 highly branched isoprenoid sulphur compounds: Further evidence for the formation of organically bound sulphur during early diagenesis. *Geochimica et Cosmochimica Acta*, **54**, 3053–3063.

Kowalski, N., Dellwing, O., Beck, M., Grunwald, M., Badewien, T., Brumsack, H. J., van Beusekom, J. E. E., & Böttcher, M. E. 2012. A comparative study of manganese dynamics in pelagic and benthic parts of two tidal systems of the North Sea. *Estuarine, Coastal and Shelf Science*, **100**, 3–17.

Li, C., Love, G. D., Lyons, T. W., Fike, D. A., Sessions, A. L., & Chu, X. 2010. A Stratified Redox Model for the Ediacaran Ocean. *Science*, **328**(5974), 80–83.

Liu, S.-A., Wu, H., Shen, S., Jiang, G., Zhang, S., Lv, Y., Zhang, H., & Li, S. 2017. Zinc isotope evidence for intensive magmatism immediately before the end-Permian mass extinction. *Geology*.

Looy, C. V., Twitchett, R. J., Dilcher, D. L., Van Konijnenburg-Van Cittert, J. H., & Visscher, H. 2001. Life in the end-Permian dead zone. *Proceedings of the National Academy of Sciences*, **98**(14), 7879–83.

Mann, J. L., Vocke, R. D., & Kelly, W. R. 2009. Revised δ 34 S reference values for IAEA sulfur isotope reference materials S-2 and S-3. *Rapid Communications in Mass Spectrometry*, **23**(8), 1116–1124.

Nabbefeld, B., Grice, K., Twitchett, R. J., Summons, R. E., Hays, L., Böttcher, M. E., & Asif, M. 2010a. An integrated biomarker, isotopic and palaeoenvironmental study through the Late Permian event at Lusitaniadalen, Spitsbergen. *Earth and Planetary Science Letters*, **291**(1-4), 84–96.

Nabbefeld, B., Grice, K., Schimmelmann, A., Sauer, P. E., Böttcher, M. E., & Twitchett, R. 2010b. Significance of δDkerogen, δ13Ckerogen and δ34Spyrite from several Permian/Triassic (P/Tr) sections. *Earth and Planetary Science Letters*, **295**(1-2), 21–29.

Newton, R. J., Pevitt, E. L., Wignall, P. B., & Bottrell, S. H. 2004. Large shifts in the isotopic composition of seawater sulphate across the Permo-Triassic boundary in northern Italy. *Earth and Planetary Science Letters*, **218**(3-4), 331–345.

Passier, H. F., Bosch, H.-J., Nijenhuis, I. A., Lourens, L. J., Böttcher, M. E., Leenders, A., Damsté, J. S. S., de Lange, G. J., & de Leeuw, J. W. 1999a. Sulphidic Mediterranean surface waters during Pliocene sapropel formation. *Nature*, **397**(6715), 146–149.

Passier, H. F., Böttcher, M. E., & De Lange, G. J. 1999b. Sulphur enrichment in organic matter of eastern Mediterranean sapropels: A study of sulphur isotope partitioning. *Aquatic Geochemistry*, **5**(1), 99–118.

Price, F. T., & Shieh, Y. N. 1979. Fractionation of sulfur isotopes during laboratory synthesis of pyrite at low temperatures. *Chemical Geology*, **27**(3), 245–253.

Raiswell, R., & Canfield, D. E. 1998. *Sources of iron for pyrite formation in marine sediments*.

Raiswell, R., Buckley, F., Berner, R. A., & Anderson, T. F. 1988. Degree of pyritization of iron as a paleoenvironmental indicator of bottom-water oxygenation. *Journal of Sedimentary Research*, **58**(5), 812–819.

Raven, M. R., Adkins, J. F., Werne, J. P., Lyons, T. W., & Sessions, A. L. 2015. Sulfur isotopic composition of individual organic compounds from Cariaco Basin sediments. *Organic Geochemistry*, **80**, 53–59.

Raven, M. R., Sessions, A. L., Fischer, W. W., & Adkins, J. F. 2016. Sedimentary pyrite δ34S differs from porewater sulfide in Santa Barbara Basin: Proposed role of organic sulfur. *Geochimica et Cosmochimica Acta*, **186**, 120–134.

Shen, W., Lin, Y., Xu, L., Li, J., Wu, Y., & Sun, Y. 2007. Pyrite framboids in the Permian-Triassic boundary section at Meishan, China: Evidence for dysoxic deposition. *Palaeogeography, Palaeoclimatology, Palaeoecology*, **253**(3-4), 323–331.

Shen, Y., Farquhar, J., Zhang, H., Masterson, A., Zhang, T., & Wing, B. A. 2011. Multiple S-isotopic evidence for episodic shoaling of anoxic water during Late Permian mass extinction. *Nature Communications*, **2**, 210.

Sinninghe Damste, J. S., & de Leeuw, J. W. 1990. Analysis, structure and geochemical significance of organically-bound sulphur in the geosphere: State of the art and future research. *Organic Geochemistry*, **16**(4-6), 1077–1101.

Thamdrup, B., Finster, K., Hansen, J. W., & Bak, F. 1993. Bacterial disproportionation of elemental sulfur coupled to chemical reduction of iron or manganese. *Applied and Environmental Microbiology*, **59**(1), 101–108.

Thomas, B. M., Willink, R. J., Grice, K., Twitchett, R. J., Purcell, R. R., Archbold, N. W., George, A. D., Tye, S., Alexander, R., Foster, C. B., & Barber, C. J. 2004. Unique marine Permian-Triassic boundary section from Western Australia. *Australian Journal of Earth Sciences*, **51**(3), 423–430.

Whiteside, J. H., & Grice, K. 2016. Biomarker Records Associated with Mass Extinction Events. *Annual Review of Earth and Planetary Sciences*, **44**, 581–612.

Wignall, P. B. 2001. Large igneous provinces and mass extinctions. *Earth Science Reviews*, **53**(1-2), 1–33.

Wignall, P. B., & Hallam, A. 1993. Griesbachian (Earliest Triassic) palaeoenvironmental changes in the Salt Range, Pakistan and southeast China and their bearing on the Permo-Triassic mass extinction. *Palaeogeography, Palaeoclimatology, Palaeoecology*, **102**(3-4), 215–237.

Wignall, P. B., & Newton, R. 1998. Pyrite framboid diameter as a measure of oxygen deficiency in ancient mudrocks. *American Journal of Science*, **298**(7), 537–552.

Wignall, P. B., Newton, R., & Brookfield, M. E. 2005. Pyrite framboid evidence for oxygen-poor deposition during the Permian-Triassic crisis in Kashmir. *Palaeogeography, Palaeoclimatology, Palaeoecology*, **216**(3-4), 183–188.

Wilkin, R. T., Barnes, H. L., & Brantley, S. L. 1996. The size distribution of framboidal pyrite in modern sediments: An indicator of redox conditions. *Geochimica et Cosmochimica Acta*, **60**(20), 3897–3912.

Yin, H. F., Zhang, K. X., Tong, J. N., Yang, Z. Y., & Wu, S. B. 2001. The Global Stratotype Section and Point (GSSP) of the Permian-Triassic Boundary. *Episodes*, **24**(2), 102–114.

Zhang, J., Liang, H., He, X., Yang, Y., & Chen, B. 2011. Sulfur Isotopes of Framboidal Pyrite in the Permian-Triassic Boundary Clay at Meishan Section. *Acta Geologica Sinica - English Edition*, **85**(3), 694–701.

Zhang, Kexin, Tong, Jinnan, Shi, G. R., Lai, Xulong, Yu, Jianxin, He, Weihong, Peng, Yuanqiao, & Jin, Yali. 2007. Early Triassic conodont-palynological biostratigraphy of the Meishan D Section in Changxing, Zhejiang Province, South China. *Palaeogeography, Palaeoclimatology, Palaeoecology*, **252**(1-2), 4–23.

6. Occurrence and significance of phytanyl arenes across the Permian-Triassic boundary interval

Hendrik Grotheer, Pierre LeMétayer,
Matthew J. Piggott, Erik J. Lindeboom,
Alex I. Holmann, Richard J. Twitchett
and Kliti Grice

Organic Geochemistry 2017, 104, pp 42-52

Abstract

Phytanyl benzene and phytanyl toluene occur in mudstones from several key Permian-Triassic Boundary (PTB) sections from mid-northern palaeolatitudes (Spitsbergen and Eastern Greenland), as well as mid-southern palaeolatitudes (Western Australia). The occurrence of these compounds through the different PTB sections is related to the occurrence of the previously identified C_{33} *n*-alkyl cyclohexane, suggesting their parent organism shared a similar unique ecological niche and are associated with the extinction horizon. Further, the lack of these compounds in the carbonate-dominated palaeoequatorial, Global Stratotype Section and Point (GSSP), Meishan-1 (South China) section possibly points to their source being temperature and climate controlled.

6.1. Introduction

Long chain alkyl benzenes and alkyl toluenes are common constituents of crude oils and sedimentary organic matter (Albaigés *et al.*, 1986; Williams *et al.*, 1988; Radke & Willsch, 1993; Sinninghe Damsté *et al.*, 1993; Hartgers *et al.*, 1994). Homologous series of long chain alkyl benzenes have been reported in a number of different geological samples (e.g., Solli *et al.*, 1980; Gallegos, 1981). The first tentative identifications were later confirmed by co-injection with authentic standards (e.g., Albaigés *et al.*, 1986). The presence of alkyl benzenes with isoprenoid side chains is also well documented (Schaeflé *et al.*, 1977; Summons & Powell, 1987; Sinninghe Damsté *et al.*, 1988). However, the origin of most of these biomarkers is not well established and various formation pathways have been proposed. For example, alkyl benzenes and ring-methylated homologues may be formed either by direct biosynthesis by specific communities of archaea (Holzer *et al.*, 1979; Sinninghe Damsté *et al.*, 1988, 1993), diagenetic conversion of isoprenoid quinones (Connan *et al.*, 1986; Sinninghe Damsté *et al.*, 1988), cyclisation and aromatisation of fatty acids and alcohols (Dong *et al.*, 1993; Ellis *et al.*, 1995, 1999) or by diagenetic degradation (Killops *et al.*, 2014), for instance of specific carotenoids such as isorenieratene (Summons & Powell, 1987). Despite their ambiguous origin, the differences in their distributions (e.g., Connan *et al.*, 1986; Sinninghe Damsté *et al.*, 1993) indicate that alkyl benzenes, like other unambiguous biomarkers, can be characteristic of specific microbial communities or associated with particular depositional conditions (Holzer *et al.*, 1979; Connan *et al.*, 1986; Sinninghe Damsté *et al.*, 1993; Killops *et al.*, 2014).

Here we report the appearance (Scheme 6.1) of 3,7,11,15-tetramethylhexadecylbenzene (phytanyl benzene, **4a**) and 1-methyl-3-(3,7,11,15-tetramethylhexadecyl)benzene (phytanyl toluene, **4b**) in mudstones from three sections that span the Permian/Triassic Boundary (PTB): the Hovea-3 core (northern onshore Perth Basin, Western Australia),

the Fiskegrav section (Schuchert-Dal, Jameson Land, East Greenland) and Lusitaniadalen (Spitsbergen, Svalbard). The first unambiguous assignment of phytanyl benzene and phytanyl toluene in sediments and oils is credited to Sinninghe Damsté *et al.* (1988). These biomarkers were subsequently only reported in a few case studies, including a number of evaporitic systems (Sinninghe Damsté *et al.*, 1988, 1993; Grimalt *et al.*, 1991). It has been proposed that they are related to specific halophilic archaea, based in particular on correlation between the relative concentration of these biomarkers and the chroman ratios (as defined by Sinninghe Damsté *et al.*, 1993).

Globally, rocks spanning the Permian-Triassic interval have received considerable attention because they record the Late Permian extinction event, the most severe crisis of the Phanerozoic, and the subsequent Early Triassic recovery (e.g., Benton & Twitchett, 2003; Grice *et al.*, 2005a,b; Foster & Twitchett, 2014). Biomarkers such as those related to isorenieratane have provided critical paleoenvironmental information, indicating the presence of photic zone euxinic conditions in the extinction aftermath (Grice *et al.*, 2005b; Fenton *et al.*, 2007; Hays *et al.*, 2007; Nabbefeld *et al.*, 2010b). The biomarker *n*-heptacosylcyclohexane (C_{33} *n*-alkyl cyclohexane; C_{33} *n*-ACH) (McIldowie & Alexander, 2005; Grice *et al.*, 2005a; Nabbefeld *et al.*, 2010b) may also have stratigraphic value in providing a proxy for the mass extinction horizon. C_{33} *n*-ACH has only been reported from early Triassic source rocks and related oils in the northern Perth Basin (Western Australia), and PTB sections in East Greenland (Grice *et al.*, 2005a) and Spitsbergen (Nabbefeld *et al.*, 2010b). It was postulated that its appearance is related to the specific environmental conditions during and following the major ecological crisis, which supported a phytoplankton community uniquely adapted to these conditions (Grice *et al.*, 2005a; Nabbefeld *et al.*, 2010b). The aims of this study were to synthesise 3,7,11,15-tetramethylhexadecylbenzene (**4a**), 1-methyl-3-(3,7,11,15-tetramethylhexadecyl)benzene (**4b**) and 2-(3,7,11,15-tetramethylhexadecyl)naphthalene (**4c**; Scheme 6.1) and to use them as standards to confirm their presence in or absence from PTB sections and thereby their significance (temperature and climate) in sections around the world.

6.2. Materials and methods

6.2.1. Samples

Samples containing phytanyl benzene and phytanyl toluene came from three PTB sections in the Perth Basin (Western Australia), Fiskegrav (Jameson Land, East Greenland) and Lusitaniadalen (central Spitsbergen, Svalbard). The shallow marine lithofacies of these three sections are broadly similar, recording local expressions of the latest Permian marine transgression and a transition from well-bioturbated fine sandstones and siltstones of Changhsingian age to finer, deep water, and more laminated, less bioturbated mudstones with occasional thin, distal tempestites around the PTB.

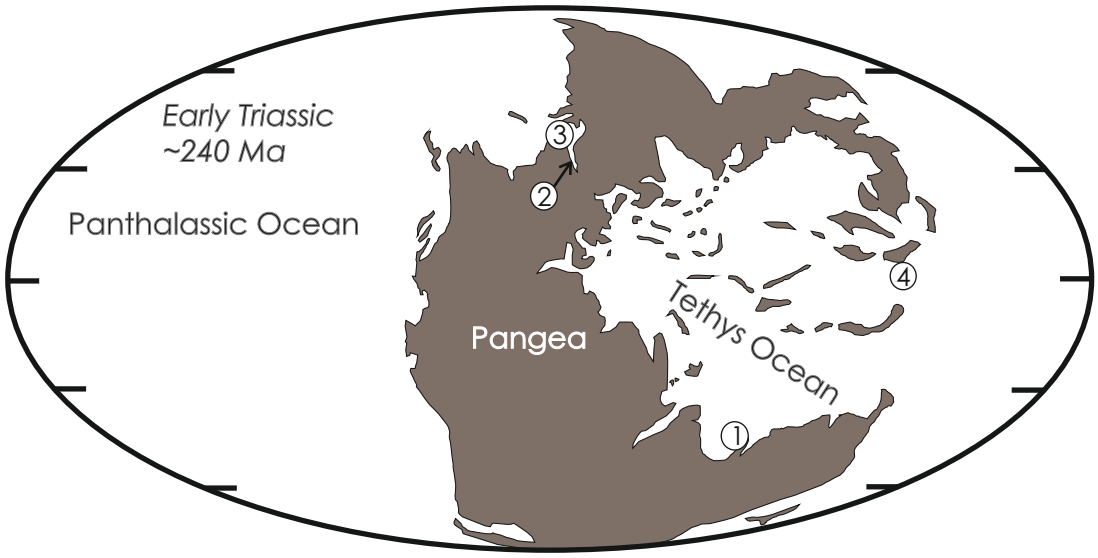

Figure 6.1.: Reconstruction of global palaeogeography at the end of the Permian ca. 240 million years ago (modified after Grice et al., 2005b). Numbers indicate sampled locations: 1, Hovea-3, Perth Basin, Western Australia; 2, Fishgrav, Jameson Land, East Greenland; 3, Lusitaniadalen, Spitsbergen, Svalbard; 4, Meishan, South China.

Hovea -3 core (Perth Basin, Western Australia)

The core was drilled in the northern Perth Basin through the source rocks of the organic-rich Hovea Member (Thomas *et al.*, 2004). The mid-southern palaeolatitude (Figure 6.1) Hovea Member was deposited in a marine shelf environment, with a lower 'Inertinitic Interval' of bioturbated sandstones and mudstones, and an upper 'Sapropelic Interval' of laminated mudstones, including oil-prone source rocks (Thomas *et al.*, 2004). The abrupt facies change at the boundary between these two intervals (at a depth of 1980.95 m) implies the presence of a hiatus, due to non-deposition during the transgression. A major palynological change occurs at this surface, which Thomas

et al. (2004) used to define the local PTB in the absence of conodonts. In more complete sections elsewhere, similar palynological changes record the extinction event, which occurred prior to the PTB (e.g., Looy *et al.*, 2001), but due to the condensed nature of this section the extinction and PTB are indistinguishable. The Early Triassic bivalve *Claraia* first appears just 20 cm above this horizon, which provides additional evidence that this section is the most condensed of the three studied. Forty-five samples from the core were studied, spanning both the lower inertinitic and upper sapropelic intervals. The maturity of the sampled section is relatively low, with vitrinite reflectance (R_e) values of 0.68% or lower (Dawson *et al.*, 2005) for samples from the uppermost Permian. The methyl phenanthrene maturity index (MPI-1) ranges between 0.47 and 0.96 (Grice *et al.*, 2007), with the highest values recorded for the Lower Triassic. The lack of coal and vitrinite in the early Triassic likely influenced the high MPI-1 values (Cassani *et al.*, 1988) and the low maturity values reported for the Upper Permian can be assumed to span the entire studied section.

Fiskegrav section (Jameson Land, Eastern Greenland)

The mid-northern palaeolatitude (Figure 6.1) Eastern Greenland PTB section was described by Twitchett *et al.* (2001) and comprises ca. 40 m of the uppermost Schuchert Dal Formation and overlying lowermost Wordie Creek Formation. The rocks comprise mudstones and siltstones deposited in a shallow marine embayment and contain a marine fauna and flora, as well as terrestrial spores and pollen (Looy *et al.*, 2001). Due to the abundance of fish in the Wordie Creek Formation, this location is known as Fiskegrav (Stemmerik *et al.*, 2001). Elevens samples from this section were analysed here, spanning the Upper Permian and Lower Triassic.

The PTB is defined by the first appearance of *Hindeodus parvus* in the Meishan-1 section of South China (Yin *et al.*, 2001). Locally at Fiskegrav, *H. parvus* first appears ca. 23.5 m above the base of the Wordie Creek Formation (Twitchett *et al.*, 2001). However, as noted by Twitchett *et al.* (2001), it is likely that the actual PTB horizon is lower in the Wordie Creek Formation because the bivalve *Claraia*, which indicates basal Triassic strata elsewhere, occurs ca. 10 m below the appearance of *H. parvus*, and the intervening rocks have not been sampled for conodonts. The local expression of the late Permian extinction event is recorded in the uppermost part of the underlying Schuchert Dal Formation and has been identified by the disappearance of bioturbation, changes in the acritarch record and the disappearance of Permian macro- and microfossils (Looy *et al.*, 2001; Twitchett *et al.*, 2001). These changes all occur within a marine transgression, but notably the facies change is not as sharp as in the Hovea-3 core, with bioturbation disappearing over ca. 0.5 m.

MPI-1 values for the analysed samples ranged between very immature (0.07) for the Schuchert Dal Formation up to onset of oil generation (0.52) for the Wordie Creek For-

mation, equating to a calculated vitrinite reflectance (R_c) of 0.44 – 0.71% (Nabbefeld *et al.*, 2010a). As in the Hovea-3 core the MPI-1 values in the Lower Triassic (lowermost Wordie Creek Formation) possibly overestimate the maturity due to the absence of coal and vitrinite. The colour and exceptional preservation of palynomorphs (Looy *et al.*, 2001) and the very low colour alteration index (CAI = 1) of Wordie Creek Formation conodonts indicate unequivocally that the entire section is immature.

Vikinghøgda section (Lusitaniadalen, Spitsbergen (Svalbard))

The site exposed at Lusitaniadalen, Spitsbergen (Svalbard) records shallow marine, mid-palaeolatitude deposition at a site a few degrees north of Fiskegrav (Figure 6.1), and was described by Mørk *et al.* (1999) and Nabbefeld *et al.* (2010b). The studied samples come from the lower ca. 12 m of the Deltadalen Member of the Vikinghøgda Formation. This interval was described in detail by Nabbefeld *et al.* (2010b) and records a transition from glauconitic, bioturbated fine-medium sandstones to predominantly laminated, dark grey mudstones, followed by the return of small-sized burrows and benthic invertebrates in the upper part (Nabbefeld *et al.*, 2010b). The later authors followed the approach of Twitchett *et al.* (2001) and identified the horizon at which Permian marine ecosystems collapsed as the last occurrence of abundant, high diversity of large Permian trace fossils, just before the top of the glauconitic sandstones, 1.53 m above the base of the Vikinghøgda Formation. Marine ecosystem collapse occurred after the onset of a marine transgression and the first evidence of anoxia (Nabbefeld *et al.*, 2010b).

The exact location of the PTB at the Lusitaniadalen site is unclear since the conodont *H. parvus* does not occur in the area. Mørk *et al.* (1999) originally placed the PTB at the base of the Vikinghøgda Formation while, more recently, Hounslow *et al.* (2008) shifted the boundary 12 m above, based on magnetostratigraphic data, whereas Nakrem *et al.* (2008) placed the PTB in-between on the basis of conodonts. The sediments are slightly more mature than the other sections, with MPI-1 values ranging from 0.46 – 0.69 (R_c 0.68 – 0.82%; Nabbefeld *et al.* (2010a)).

6.2.2. Extraction and fractionation

Crushed sediment (ca. 80 g) was extracted using automated accelerated solvent extraction (DIONEX ASE 200) with dichloromethane (DCM)/MeOH (9:1, v/v) at 100 °C and 1000 psi. The extraction procedure was repeated 3x. The extract was fractionated with silica gel column chromatography using *n*-pentane for eluting aliphatic hydrocarbons, 30 % DCM/pentane (v/v) for aromatic hydrocarbons and 50 % DCM/MeOH (v/v) for the polar compounds. Solvents were carefully removed under N_2.

6.2.3. Gas chromatography–mass spectrometry (GC–MS)

GC–MS was carried out with a HP 6890 gas chromatograph coupled to a HP 5973 mass spectrometer operating in electron impact ionization mode (70 eV). Separation was achieved using a 60 m × 0.25 mm i.d. WCOT fused silica column coated with 0.25 µm film (DB-5, J&W Scientific) and He as carrier gas at 1 ml/min. Samples were dissolved in *n*-hexane and 1 µl was injected using a HP 6890 auto-sampler. The GC oven temperature programme was 40–325 °C (at 3 °C/min; final temperature held 45 min). Chromatographic peaks were integrated using the HP ChemStation data analysis program.

6.2.4. Synthesis of phytanyl benzene and phytanyl toluene

Although we considered a combinatorial synthesis for the three target compounds along the lines of those described previously (Greenwood *et al.*, 2009; Lengkeek *et al.*, 2010), in this case traditional synthesis was not overly onerous, due to the limited number of reactions entailed. Thus, the phytanyl arene standards **4a-c** were prepared in three steps, as depicted in Scheme 6.1. Oxidation of phytol (**1**; Aldrich, mixture of isomers) with MnO_2 gave phytal (**2**) as a ca. 2:1 mixture of E and Z isomers, respectively (Kulkarni *et al.*, 1988; Knierzinger *et al.*, 1990). Addition of aryl Grignard reagents to **2** provided the secondary allylic alcohols **3a-c**. Similar reactions have been used in the synthesis of α-tocopherol (Hübscher & Barner, 1990) and vitamin K epoxide analogues (Ryall *et al.*, 1990). Hydrogenation/hydrogenolysis (Lengkeek *et al.*, 2010) of **3a-c** afforded the target hydrocarbons **4a-c**.

Phytanyl benzene (**4a**) and ring-methylated congeners have been synthesised previously *via* a Barbier reaction of aryl bromides with phytal, prepared in four steps from phytol (**1**), followed by reductive deoxygenation with triethylsilane/trifluoroacetic acid (Sinninghe Damsté *et al.*, 1988); the approach used here is more succinct.

General experimental details

^{1}H NMR spectra were acquired in $CDCl_3$ at 25 °C on a Varian Inova 300 (^{1}H, 300 MHz, ^{13}C 75 MHz) spectrometer. Rapid silica filtration (RSF) refers to chromatography on a short column of silica gel in a sintered glass funnel, in which the eluent is sucked through the column under vacuum. Other general experimental details are as previously described Gandy & Piggott (2008).

Phytal (**2**; Kulkarni *et al.*, 1988; Knierzinger *et al.*, 1990). MnO_2 (29 g, 0.33 mol) was added to a solution of phytol (**1**; 5.00 g, 16.7 mmol, mixture of isomers) in *n*-hexane (350 ml) under Ar and the suspension was stirred for 3 h. The reaction mixture

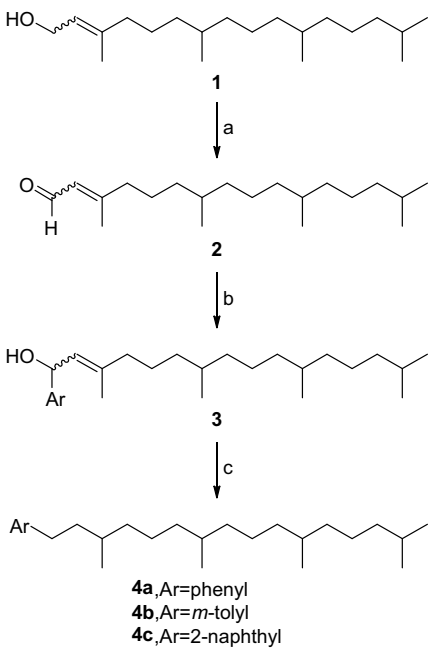

Scheme 6.1: Synthesis of phytanyl arene standards. Reagents, conditions and yields: (a) MnO_2, hexanes, 81%; (b) ArMgBr, Et_2O, then 10% H_2SO_4 (**3a**, Ar = phenyl - 80%, **3b**, Ar = *m*-tolyl - 76%, **3c**, Ar = 2-naphthyl - 69%); (c) H_2, Pd/C, AcOH, EtOH (**4a** - 89%, **4b** - 60%, **4c** - 59%).

was vacuum filtered and the filter cake washed with *n*-hexane (2 × 100 ml). The filtrate was evaporated and the residue was subjected to RSF. Elution with *n*-hexane provided **2** as a colourless oil (4.0 g, 81%). ^{1}H NMR (300 MHz): δ 9.94–10.00 (^{1}H, m, CHO) 5.86–5.89 (^{1}H, m, =CH) 2.15 (3H, br s), 1.05–1.54 (21 H, m), 0.83–0.87 (12 H, m). The ^{1}H NMR data are slightly different from those reported by Upadhyay *et al.* (2014).

3,7,11,15-Tetramethyl-1-phenylhexadec-2-en-1-ol (**3a**). Bromobenzene (450 μl, 4.3 mmol) was added dropwise to a suspension of Mg (207 mg, 8.52 mmol) in anhydrous Et_2O (2 ml) under Ar, and the reaction mixture was heated under reflux for 30 min. The solution of the Grignard reagent was cooled to 0 °C and a solution of phytal (**2**; 940 mg, 3.2 mmol) in Et_2O (2 ml) was added dropwise. The reaction mixture was allowed to warm to room temperature and stirred for another 30 min, then cooled to 0 °C, quenched with 10 % H_2SO_4 (10 ml), and extracted with Et_2O (3 × 30 ml). The extract was dried ($MgSO_4$) and the solvent evaporated, and the residue was subjected to RSF. Elution with 5% EtOAc/hexane provided **3a** as a colourless oil (950 mg, 80%). IR (ν, cm^{-1}): 3443, br (OH). ^{1}H NMR (300 MHz): δ 7.24–7.42 (5H, m, Ar), 5.41–5.51 (2H, m, vinylic/benzylic), 1.75–1.80 (3H, m), 1.04–1.56 (22H, m), 0.84–0.90 (12H, m); ^{13}C NMR (75 MHz): δ 144.4, 139.3, 128.57, 128.56, 128.0, 127.41, 127.36, 127.33, 126.1, 126.0, 70.8, 70.5, 40.03, 40.00, 39.5, 37.56, 37.53, 37.46, 37.43, 36.9, 36.8, 32.9, 32.84, 32.81, 32.79, 32.77, 32.75, 28.1, 25.8, 25.25, 25.23, 25.0, 24.6, 23.6, 22.9, 22.8, 19.9, 19.8, 16.8.

3,7,11,15-Tetramethyl-1-m-tolylhexadec-2-en-1-ol (**3b**). Prepared as described above from *m*-bromotoluene (520 μL, 4.3 mmol), giving **3b** as a colourless oil (1.00 g, 76%). IR (ν, cm^{-1}): 3448, br (OH). ^{1}H NMR (300 MHz): δ 7.11–7.31 (4H, m, Ar), 5.48 (2H, m, vinylic/benzylic), 2.41 (3H, s) 1.84 (3H, m), 1.11–1.65 (22H, m), 0.88–0.93 (12H, m); ^{13}C NMR (75 MHz): δ 144.4, 139.3, 138.2, 128.53, 128.52, 128.21, 128.16, 127.4, 126.8, 126.7, 123.13, 123.08, 70.8, 70.6, 40.1, 39.5, 37.6, 37.5, 36.9, 36.8, 32.9, 32.84, 32.82, 28.1, 25.0, 24.62, 24.61, 23.7, 22.9, 22.8, 21.9, 21.65, 21.63, 19.9, 19.8, 16.8.

3,7,11,15-Tetramethyl-1-(naphthalen-2-yl)hexadec-2-en-1-ol (**3c**). Prepared as described above from 2-bromonaphthalene (880 mg, 4.3 mmol), giving **3c** as a colourless oil (990 mg, 69%). IR (ν, cm^{-1}): 3458, br (OH). ^{1}H NMR (300 MHz): δ 7.82–7.85 (4H, m, Ar), 7.45–7.53 (3H, m, Ar), 5.48–5.67 (2H, m, vinylic/benzylic), 1.78–1.85 (3H, m), 1.07–1.58 (22H, m), 0.83–0.89 (12H, m); ^{13}C NMR (75 MHz): δ 141.8, 139.7, 133.5, 132.9, 128.4, 128.11, 128.10, 127.8, 127.2, 126.2, 125.8, 124.6, 124.3, 71.0, 70.7, 40.07, 40.04, 39.5, 37.5, 37.4, 36.8, 32.9, 32.8, 28.1, 25.2, 25.0, 24.6, 23.7, 22.9, 22.8, 19.9, 19.8, 16.9.

3,7,11,15-Tetramethylhexadecylbenzene (phytanyl benzene; **4a**). A suspension of **3a** (810 mg, 2.2 mmol) and 10% Pd/C (0.24 g) in 1:9 AcOH/EtOH (50 ml) was stirred overnight under a balloon of H_2. The reaction mixture was vacuum-filtered through a pad of Celite and rinsed with EtOH (100 ml). The filtrate was evaporated to give **4a** as a colourless oil (694 mg, 89%). ^{1}H NMR (300 MHz): δ 7.14–7.31 (5H, m, Ar), 2.56–2.69 (2H, m), 1.08–1.75 (25H, m), 0.93 (2H, m), 0.86 (12H, m); ^{13}C NMR (75 MHz): δ 143.4 (Ar), 128.5 (ArH), 128.4 (ArH), 125.7 (ArH), 39.5, 39.2, 39.1, 37.60, 37.55, 37.44, 37.41, 37.37, 33.7, 32.94, 32.92, 32.7, 28.1, 25.0, 24.6, 24.5, 22.9, 22.8, 19.89, 19.85, 19.81, 19.75.

1-Methyl-3-(3,7,11,15-tetramethylhexadecyl)benzene (*m*-phytanyl toluene; **4b**). Hydrogenation/hydrogenolysis of **3b** (1.00 g, 2.57 mmol) as described for **3a** provided **4b** as a colourless oil (582 mg, 60%). ^{1}H NMR (300 MHz): δ 6.98–7.20 (4H, m), 2.52–2.63 (2H, m), 2.34 (3H, s) 1.09–1.80 (25H, m), 0.96 (2H, d), 0.86 (12H, t); ^{13}C NMR (75 MHz): δ 143.3, 143.2, 138.0, 129.32, 129.26, 128.4, 128.3, 126.5, 126.4, 125.5, 125.4, 40.1, 39.5, 38.7, 37.6, 37.5, 37.43, 37.41, 37.37, 33.6, 32.94, 32.89, 32.7, 30.1, 28.1, 25.0, 24.63, 24.61, 24.5, 23.5, 22.9, 22.8, 21.55, 21.54, 19.89, 19.88, 19.81, 19.76, 16.3.

2-(3,7,11,15-Tetramethylhexadecyl)naphthalene (phytanyl naphthalene; **4c**). Hydro-

genation/hydrogenolysis of **3c** (990 mg, 2.3 mmol) as described for **3a** provided **4c** as a colourless oil (562 mg, 59%). ^{1}H NMR (300 MHz): δ 7.33–7.86 (7H, m), 2.77–2.80 (2H, m), 1.10–1.56 (25H, m), 0.97 (2H, d, J = Hz), 0.87 (12H, t, J = Hz); ^{13}C NMR (75 MHz): δ 140.9, 140.8, 133.86, 133.84, 132.08, 132.06, 128.1, 128.0, 127.9, 127.8, 127.61, 127.56, 127.53, 127.51, 127.49, 126.36, 126.35, 126.30, 126.24, 126.04, 126.00, 125.97, 125.20, 125.12, 40.0, 39.6, 39.1, 39.0, 38.8, 37.6, 37.58, 37.52, 37.48, 37.43, 33.8, 33.97, 32.96, 32.72, 32.71, 30.4, 28.1, 25.00, 24.98, 24.67, 24.64, 24.57, 24.56, 23.6, 22.9, 22.8, 19.97, 19.94, 19.91, 19.88, 19.81, 16.32.

6.3. Results and discussion

6.3.1. Identification

A striking feature of almost all 'post-extinction' samples is the presence of phytanyl toluene (**4b**; Figure 6.2 A-C) in the aromatic fraction. It is the major component of samples from Greenland, whereas samples from Spitsbergen and Hovea-3 are dominated by phenanthrene and methylated phenanthrene analogue. The identification is based on comparison with mass spectra and relative retention time described by Sinninghe Damsté *et al.* (1988) and with our authentic standard. The mass spectrum of **4b** displays M^+ at *m/z* 372 ($C_{27}H_{48}$) and a base peak at *m/z* 106 resulting from γ-hydrogen transfer and a dimethylbenzene moiety (Figure 6.4b; Sinninghe Damsté *et al.* (1988)). The *m/z* 106/*m/z* 105 ratio is ca. 5, as described by Sinninghe Damsté *et al.* (1988). The retention time relative to that of the homologous series of *n*-alkyl toluenes (Figure 6.3 D-F) is also in agreement with the retention behaviour reported by Sinninghe Damsté *et al.* (1988), with phytanyl toluene eluting just after C_{24}- and before C_{25} *n*-alkyl toluene, confirming the isoprenoid phytanyl side chain (Figure 6.3 D-F). The identification was confirmed by co-injection of the synthesised standard.

Phytanyl benzene (**4a**), previously identified by Sinninghe Damsté *et al.* (1988), was also detected in most 'post-extinction' samples. It was assigned here from the summed chromatogram of *m/z* 91+92 (Figure 6.3 A-C), with a base peak at *m/z* 92 and a M^+ at *m/z* 358 ($C_{26}H_{46}$; Figure 6.4a). Again, the dominance of even *m/z* 92 over odd *m/z* 91 is suggestive of γ-hydrogen transfer and the presence of a benzene moiety. Relative retention time compared with the homologous *n*-alkyl benzene series confirms the isoprenoid phytanyl side chain. Phytanyl benzene also co-eluted with the synthesised standard.

Phytanyl naphthalene (**4c**) was detected in very low abundance in only five of the samples, so does not appear to be a useful biomarker associated with specific conditions during PTB intervals. The mass spectrum of the standard is shown in Figure 6.4c and displays a base peak at *m/z* 142, with M^+ at *m/z* 408 ($C_{30}H_{48}$).

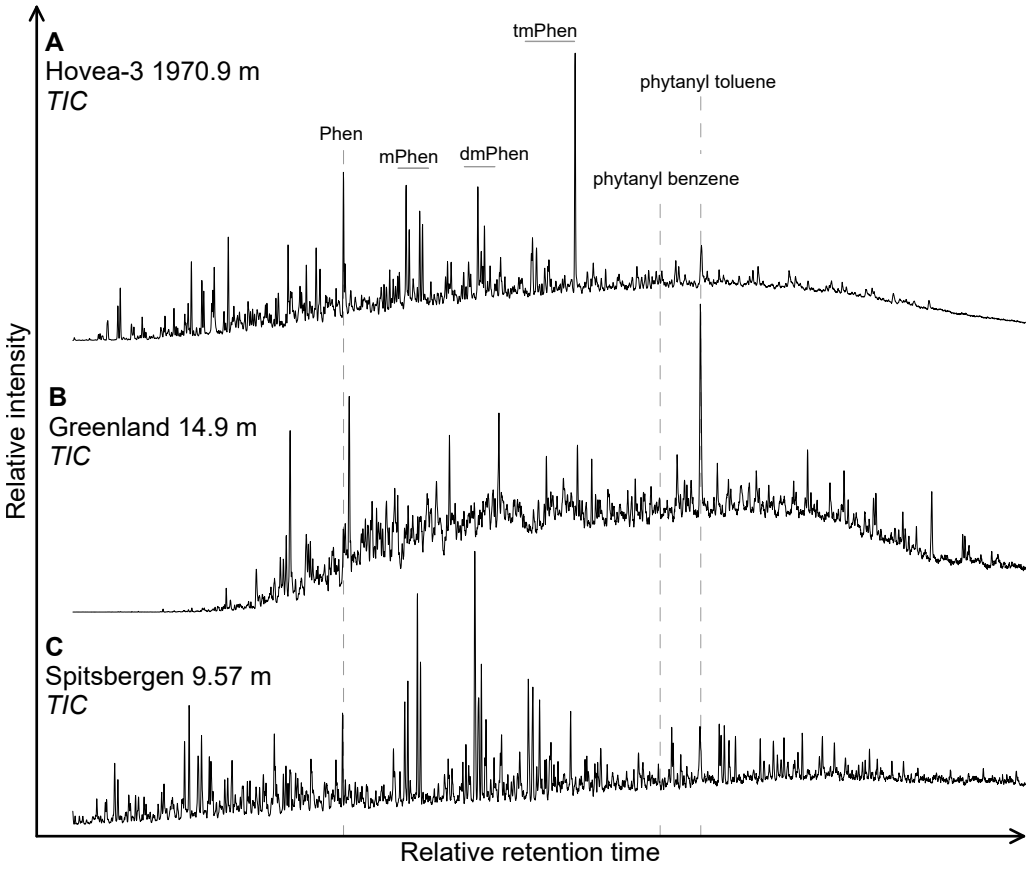

Figure 6.2.: Total ion chromatograms of aromatic fractions of the three sections from depths above the marine collapse.

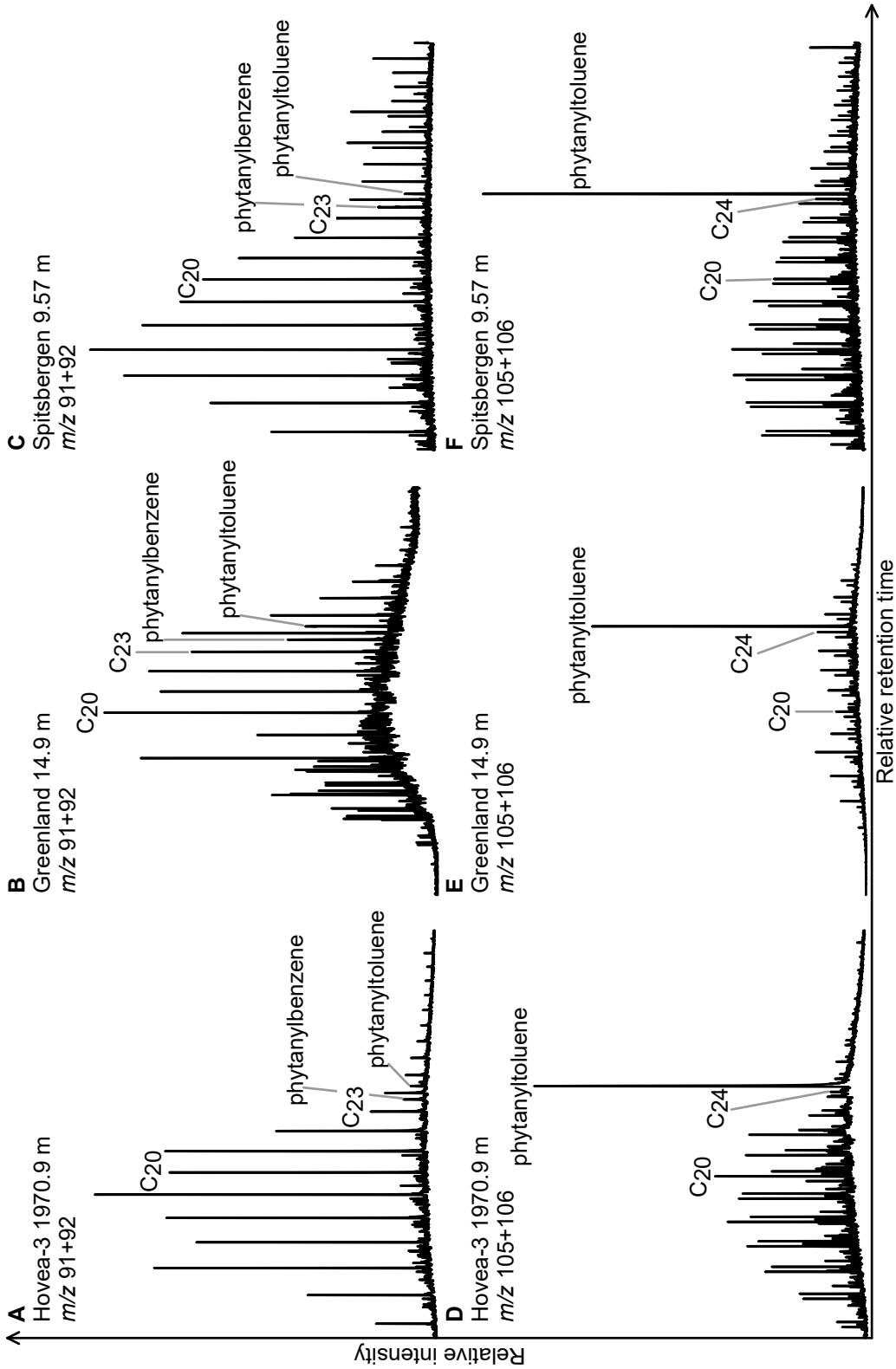

Figure 6.3.: Summed ion chromatograms for alkyl benzenes (*m/z* 91+92, top) and alkyl toluenes (*m/z* 105+106, bottom) from the three sections from depths above the marine collapse.

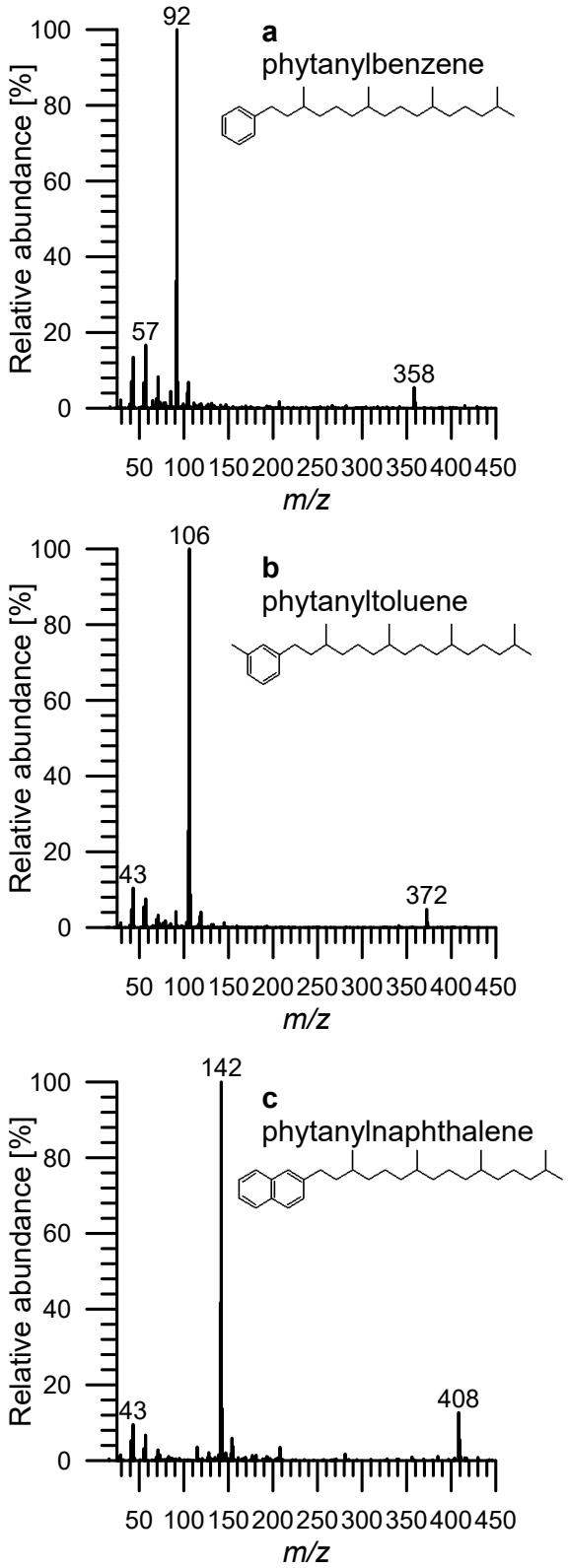

Figure 6.4.: Mass spectra (corrected for background) of synthetic (a) 3,7,11,15-tetramethylhexadecylbenzene (phytanyl benzene, **4a**), (b) 1-methyl-3-(3,7,11,15-tetramethylhexadecyl)benzene (phytanyl toluene, **4b**) and (c) 2-(3,7,11,15-tetramethylhexadecyl)naphthalene (phytanyl naphthalene, **4c**).

6.3.2. Occurence

Hovea-3 core

The local PTB in the Hovea -3 core was identified at a depth of 1980.95 m by Thomas *et al.* (2004) but, due to a likely hiatus, this horizon also corresponds to the level at which the Permian fauna and spores/pollen disappear (Grice *et al.*, 2005a). Phytanyl benzene and phytanyl toluene were present in samples from 1980.92 m and above, corresponding to the Lower Triassic upper Sapropelic Interval of the Hovea Member, but not in any Permian sample. Figure 6.3A+D show the GC–MS extracted ion chromatograms of the alkyl benzenes (*m/z* 91+92) and alkyl toluenes (*m/z* 105+106) from the 1970.9 m sample, showing the occurrence of phytanyl benzene and phytanyl toluene. The far greater relative abundance of phytanyl toluene than phytanyl benzene is common to every sample in which these biomarkers appear. The phytanyl toluene/phytanyl benzene ratio ranges from 12.5 to 36.7 (based on integration of the *m/z* 92 and 106 chromatograms).

To illustrate the presence of phytanyl benzene and phytanyl toluene through the core the ratio of each compound relative to phenanthrene is shown in Figure 6.5 (based on integration of the *m/z* 92 and 106 relative to 178 chromatograms). Phenanthrene is present in all samples analysed but can be associated with variation in source (e.g., terpenoids or pyrolytic compounds), however, concentration does not change significantly in Hovea-3, suggesting no major source change. Phenanthrene was therefore chosen as the most suitable PAH to show the appearance of the phytanyl arenes. Although phytanyl benzene and phytanyl toluene appear suddenly and synchronously immediately above the local extinction/PTB horizon, maximum abundance does not occur until 11 m higher in the section (Figure 6.5). In comparison, the peak abundance of C_{33} *n*-ACH identified in the same section by Grice *et al.* (2005a) occurs immediately after the local extinction/PTB horizon.

Fiskegrav section

Of the eleven samples, phytanyl toluene was present in seven and phytanyl benzene in four (Figure 6.6). As in the Hovea-3 core, where the two co-occur, phytanyl toluene is present in greater relative abundance than phytanyl benzene. The maximum abundance of the two biomarkers occurs ca. 6.4 m above the local extinction horizon (i.e. “marine ecosystem collapse” of Twitchett *et al.* (2001); Figure 6.6) but low abundances occur just above the marine collapse. The maximum abundance of the two occurs during a macrofaunal “dead zone” that extends from the level of marine collapse until 14 m above the base of the Wordie Creek Formation, characterised by the total absence of bioturbation and benthic macrofossils and inferred to be the result of benthic anoxia (Looy *et al.*, 2001; Twitchett *et al.*, 2001). Even after the reappearance of benthic

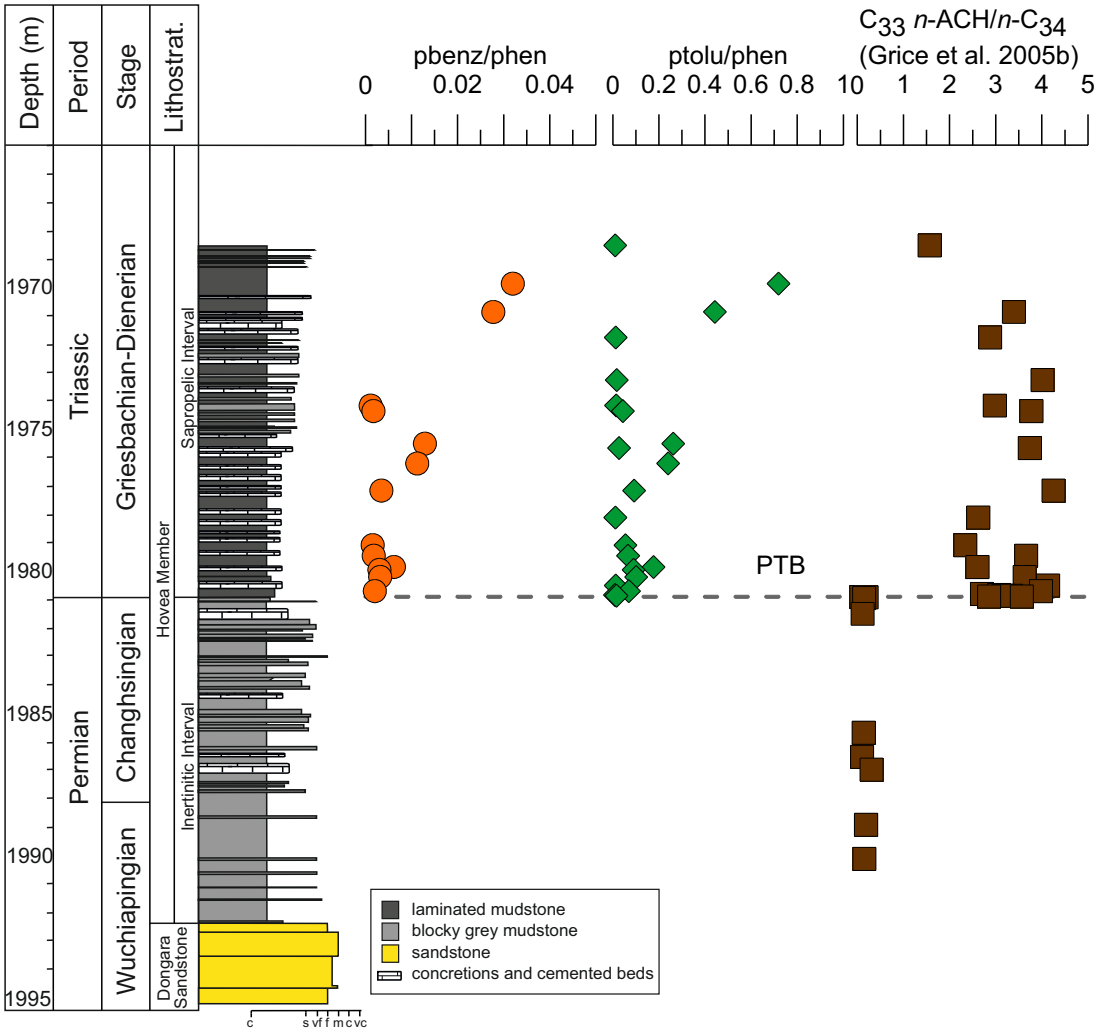

Figure 6.5.: Abundance of phytanyl benzene (pbenz) and phytanyl toluene (ptolu) relative to phenanthrene (phen) and C_{33} *n*-ACH relative to *n*-C_{34} (from Grice et al., 2005b). Stratigraphic log of the Hovea-3 core, Perth Basin, Western Australia is redrawn from Thomas et al. (2004). Permian/Triassic boundary (PTB) as defined by Thomas et al. (2004). Lithological scale comprises claystone (c), siltstone (s), very fine- (vf), fine- (f), medium- (m), coarse-, and very coarse-grained sandstone (vc).

macrofossils (i.e. the bivalve *Claraia*), phytanyl toluene and phytanyl benzene remain absent until just above the first appearance of *H. parvus*. Biomarker relative abundance remains low vs. samples from shortly after the marine ecosystem collapse. C_{33} *n*-ACH appears with the onset of the marine collapse (Grice *et al.*, 2005a), preceding the first occurrence of phytanyl toluene and phytanyl benzene, but is similarly absent throughout the remaining "dead zone", before reappearing above the first appearance of *H. parvus*.

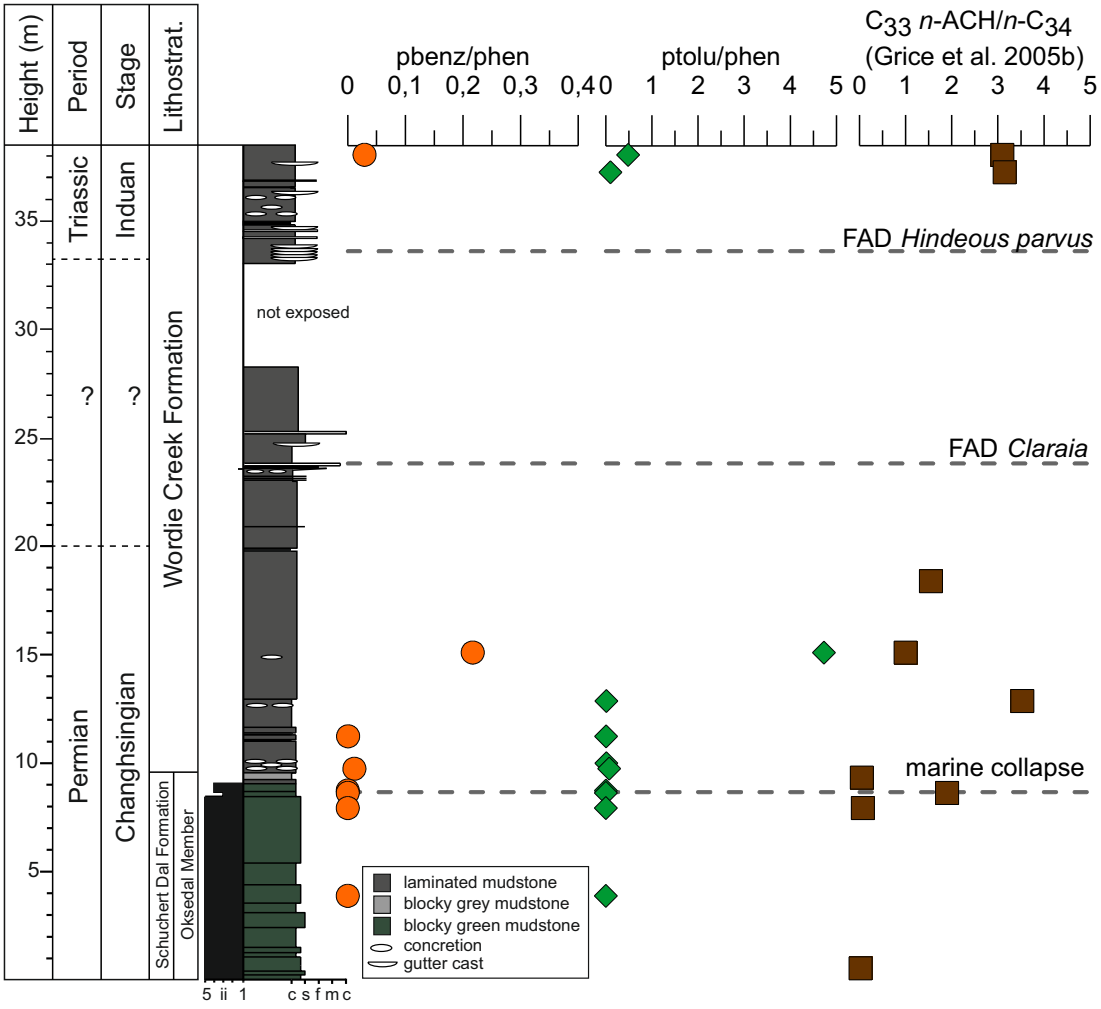

Figure 6.6.: Abundance of phytanyl benzene (pbenz) and phytanyl toluene (ptolu) relative to phenanthrene (phen) and C_{33} *n*-ACH relative to *n*-C_{34} (from Grice et al., 2005b). Stratigraphic log of the Schuchert Dal and Wordie Creek formations, Fishgrav, Jameson Land, East Greenland is redrawn from Twitchett et al. (2001). Marine collapse, first appearances date (FAD) of *Claraia* and *H. parvus* as defined by Twitchett et al. (2001). ii, ichnofabric index; lithological scale comprises claystone (c), siltstone (s), fine- (f), medium- (m), and coarse-grained sandstone (c). Dashed horizontal lines and question marks indicate two alternative positions of the Permian/Triassic boundary (see Twitchett et al. (2001), for discussion).

Spitsbergen section

Phytanyl toluene was present in seven and phytanyl benzene in five of the ten samples from the lower Vikinghøgda Formation. Similar to the other two sections phytanyl toluene is present in much greater relative abundance than phytanyl benzene, as shown in Figure 6.3 C+F based on the extracted ion chromatograms. The maximum abundance of both occurs 4.3 m above the base of the Vikinghøgda Formation and ca. 2.7 m above the collapse of the marine ecosystem (Figure 6.7), but low abundance occurs just above the ecosystem collapse. The shallowest sample analysed, of unequivocal basal Induan age, did not contain any phytanyl benzene or phytanyl toluene. C_{33} *n*-ACH first appears after the onset of the marine transgression and anoxia, reaches maximum abundance following the marine collapse, and remains present throughout the entire sampled section. Similar to Hovea-3 and the East Greenland section the first appearance of C_{33} *n*-ACH precedes the appearance of phytanyl benzene and phytanyl toluene.

6.3.3. Origin & Significance

The biomarker distribution and trends from the sampled PTB sections show some similarities. In all three sections the abundance of phytanyl benzene correlates well with the abundance of phytanyl toluene (Figure 6.8), suggesting similar origin/source or similar environmental conditions that allowed the source organism to flourish under stressed environmental conditions. Both compounds appear in low abundance shortly after the marine ecosystem collapse, with maximum abundance reached just above in East Greenland and Spitsbergen, and they almost vanish with the onset of the Triassic. In Western Australia, however, the compounds only occur above the palynologically-defined local PTB. The apparent hiatus in Hovea-3 makes a direct comparison with the other two sections difficult as the interval from the marine collapse to the PTB is not resolved and the extent of the missing record remains unclear.

The first appearance and maximum abundance of C_{33} *n*-ACH precedes the first detection of phytanyl benzene and phytanyl toluene in all three sections and coincides with the onset of the marine ecosystem collapse in the PTB sections from Greenland and Spitsbergen. Although simultaneously elevated abundances of both groups of biomarkers are evident in all three sections, suggesting origin from source organisms similarly adapted to environmental stress, C_{33} *n*-ACH does not correlate with phytanyl toluene (Figure 6.8).

The origin of ring-methylated phytanyl benzenes has not yet been determined. Sinninghe Damsté *et al.* (1988) suggested the formation of methylated phytanyl benzenes by diagenetic conversion of isoprenoid quinones. They also proposed a direct biosynthetic origin from specific archaea, halophilic ones living in hypersaline environments,

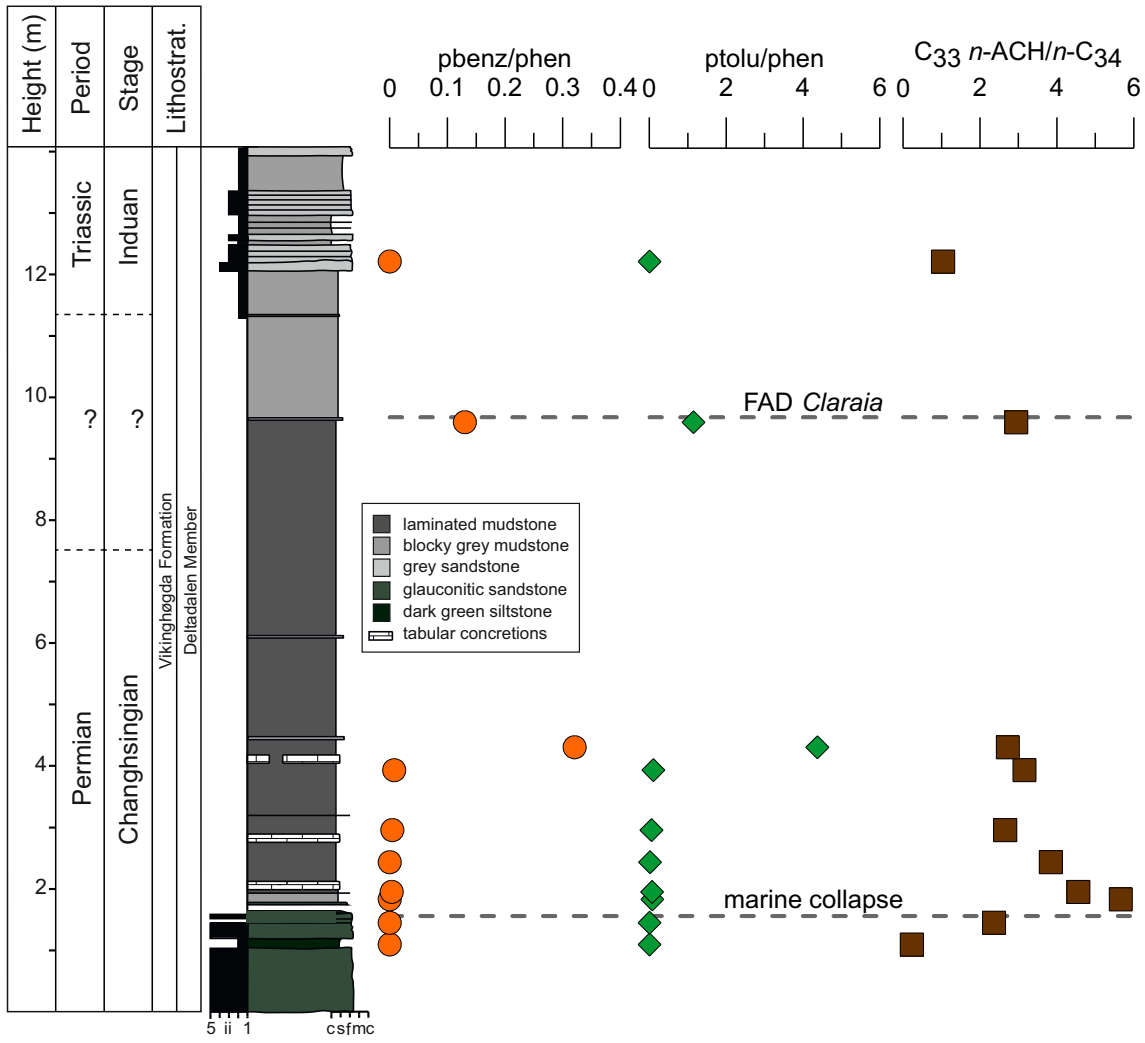

Figure 6.7.: Abundance of phytanyl benzene (pbenz) and phytanyl toluene (ptolu) relative to phenanthrene (phen) and C_{33} *n*-ACH relative to *n*-C_{34}. Stratigraphic log of the Vikinghøgda Formation, Lusitaniadalen, Spitsbergen, Svalbard is redrawn from Nabbefeld et al. (2010b). Marine collapse and first appearance date (FAD) of *Claraia* as defined by Nabbefeld et al. (2010b). ii, ichnofabric index; lithological scale comprises claystone (c), siltstone (s), fine- (f), medium- (m), and coarse-grained sandstone (c). Dashed horizontal lines and question marks indicate two alternative positions of the Permian/Triassic boundary (see Nabbefeld et al. (2010b), for discussion).

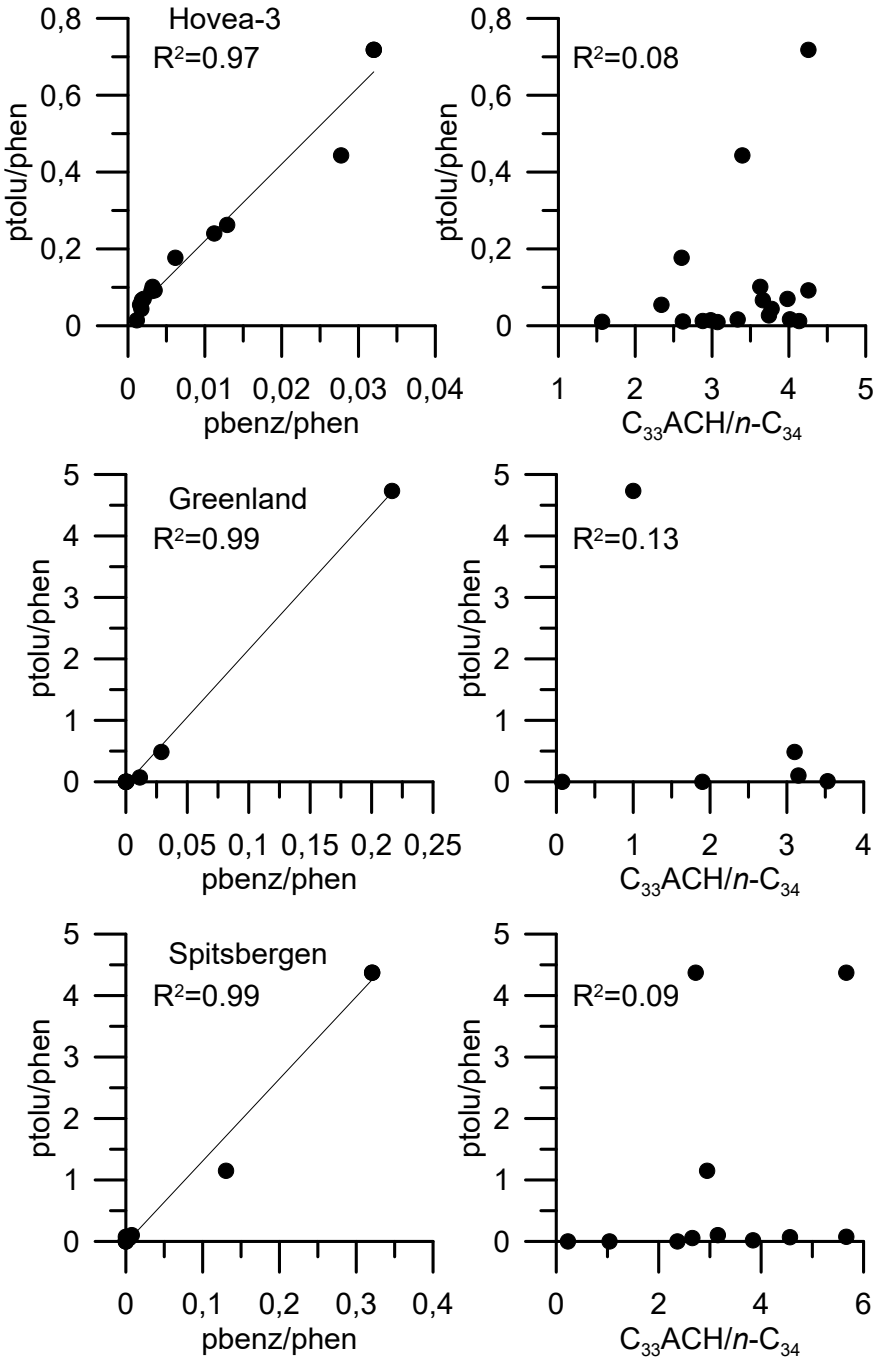

Figure 6.8.: Cross plots of relative abundances of phytanyl toluene (ptolu)/phenanthrene (phen) vs. phytanyl benzene (pbenz)/phen and ptolu/phen vs. C_{33} *n*-ACH/*n*-C_{34} from the three investigated sections from depths above the marine collapse

and Sinninghe Damsté *et al.* (1993) showed the distribution of phytanyl benzene to be biologically controlled and paleosalinity driven, at least in hypersaline environments. Although Nabbefeld *et al.* (2010b) have reported increased concentrations of C_{21} regular isoprenoid (*i*-C_{21}) at the onset of the marine ecosystem collapse in the Spitsbergen section, its maximum abundance clearly precedes the maximum abundance of phytanyl toluene. The concentration declines immediately to pre-collapse levels (Nabbefeld *et al.*, 2010b), indicating that any change in palaeosalinity, if it occurred at all, was only temporary and not related to the appearance of phytanyl toluene. This suggests here that, ring-methylated phytanyl benzenes do not originate from halophilic archaea.

The source of C_{33} *n*-ACH has also not yet been positively identified. Nabbefeld *et al.* (2010b) supported the proposal of Grice *et al.* (2005a) that it might be a molecular marker for the Late Permian biotic crisis. Under this hypothesis, the source for C_{33} *n*-ACH is proposed to be a post-event phytoplankton bloom that developed from the specific environmental conditions that triggered marine collapse and continued afterwards, such as global warming, sea level rise, spreading hypoxia, elevated run-off and flux of terrestrial-derived nutrients to shallow shelf seas (Grice *et al.*, 2005a; Nabbefeld *et al.*, 2010b).

The lack of a positive correlation between the abundance of C_{33} *n*-ACH and phytanyl toluene in any of the three PTB sections (Figure 6.8) indicates that these biomarkers do not originate from the same source, but are from organisms that could live under stressed conditions. In the Spitsbergen and East Greenland PTB sections, the ring-methylated phytanyl benzene occurs after the maximum abundance of C_{33} *n*-ACH (Figure 6.5–Figure 6.7). Hence, it is possible that environmental conditions that followed, or were created by, those that stimulated the phytoplankton bloom that generated the C_{33} *n*-ACH, provided ideal conditions for the appearance of a specific group of organisms that produced the ring-methylated phytanyl toluene.

Thus far, the three sections are the formations known to yield phytanyl benzene, phytanyl toluene and C_{33} *n*-ACH. Samples from the carbonate-dominated lithofacies of the Global Stratotype Section and Point (GSSP) at Meishan, South China, located near the equator during the Late Permian (Figure 6.1), have been specifically investigated but did not yield any trace of phytanyl benzene, phytanyl toluene or C_{33} *n*-ACH. Marked lithological differences exist between the mid-latitudinal shale deposits and the equatorial carbonate deposit in Meishan, so differences in biomarker abundance could be related to preferential preservation of these compounds in siliclastic mudrocks compared to carbonates. Selective preservation can occur if the site dependent depositional conditions (e.g., redox conditions) or diagenetic/catagenetic reactions (e.g., acid or transition metal catalysis) promote biomarker decomposition. Preferential preservation cannot easily be proven or rejected and usually requires biomarker-specific laboratory simulations and hence remains a possibility in this case. However, general biomarker

preservation appears to be favoured in carbonates compared to shales (French *et al.*, 2015). French *et al.* (2015) found significantly higher abundance of biomarkers in Archean carbonates than in shales of similar age. Further post-depositional catalytic reactions, e.g., acid or transition metal catalysis have been shown to occure primarily in shales and would not affect acidic mineral-free carbonates (Mango, 1990, 1992; Mango *et al.*, 1994).

Based on current data, the global record of phytanyl benzene, phytanyl toluene and C_{33} *n*-ACH shows an apparent latitudinal distribution, suggesting that the community of phytoplankton/organisms responsible for their occurrence may have been climate and/or temperature controlled. If so, then we predict that they should be present in PTB samples from other locations that record marine deposition in mid-palaeolatitudes

6.4. Conclusions

Phytanyl benzene and phytanyl toluene were identified in mudstones from several key Permian-Triassic Boundary (PTB) sections from mid-northern palaeolatitudes and mid-southern palaeolatitudes. The occurrence of these compounds is related to the occurrence of the previously identified C_{33} *n*-alkyl cyclohexane, suggesting they share a similar unique ecological niche and are associated with the extinction horizon. Their absence from the palaeoequatorial, GSSP, Meishan-1 (South China), of carbonate lithology possibly points to their origin to be further controlled by local temperature and climate.

Acknowledgments

This study was conducted by the Australian Research Council (ARC) and Discovery Outstanding Research Award project (KG DP130100577) and ARC LIEFP (LE110100119). H. G. thanks CSIRO and the Department of Chemistry, Curtin University, for a joint PhD scholarship as well as WA-OIGC for a part of the tuition fees and TIGeR for top-up scholarships. G. Chidlow is thanked for providing technical support for GC-MS. We thank the two anonymous reviewers for their helpful and constructive comments.

References

Albaigés, J., Algaba, J., Clavell, E., & Grimalt, J. 1986. Petroleum geochemistry of the Tarragona Basin (Spanish mediterranean off–shore). *Organic Geochemistry*, **10**, 441–450.

Benton, M. J., & Twitchett, R. J. 2003. How to kill (almost) all life: the end-Permian extinction event. *Trends in Ecology & Evolution*, **18**(7), 358–365.

Cassani, F., Gallango, O., Talukdar, S., Vallejos, C., & Ehrmann, U. 1988. Methylphenanthrene maturity index of marine source rock extracts and crude oils from the Maracaibo Basin. *Organic Geochemistry*, **13**, 73–80.

Connan, J., Bouroullec, J., Dessort, D., & Albrecht, P. 1986. The microbial input in carbonate-anhydrite facies of a sabkha palaeoenvironment from Guatemala: A molecular approach. *Organic Geochemistry*, **10**, 29–50.

Dawson, D., Grice, K., & Alexander, R. 2005. Effect of maturation on the indigenous δD signatures of individual hydrocarbons in sediments and crude oils from the Perth Basin (Western Australia). *Organic Geochemistry*, **36**(1), 95–104.

Dong, J.-Z., Vorkink, W. P., & Lee, M. L. 1993. Origin of long-chain alkylcyclohexanes and alkylbenzenes in a coal-bed wax. *Geochimica et Cosmochimica Acta*, **57**(4), 837–849.

Ellis, L., Singh, R. K, Alexander, R., & Kagi, R. I. 1995. Geosynthesis of organic compounds: III. Formation of alkyltoluenes and alkylxylenes in sediments. *Geochimica et Cosmochimica Acta*, **59**(24), 5133–5140.

Ellis, L., Fisher, S. J., Singh, R. K., Alexander, R., & Kagi, R. I. 1999. Identification of alkenylbenzenes in pyrolyzates using GC-MS and GC-FTIR techniques: Evidence for kerogen aromatic moieties with various binding sites. *Organic Geochemistry*, **30**(7), 651–665.

Fenton, S., Grice, K., Twitchett, R., Bottcher, M., Looy, C., & Nabbefeld, B. 2007. Changes in biomarker abundances and sulfur isotopes of pyrite across the Permian–Triassic (P/Tr) Schuchert Dal section (East Greenland). *Earth and Planetary Science Letters*, **262**(1-2), 230–239.

Foster, W. J., & Twitchett, R. J. 2014. Functional diversity of marine ecosystems after the Late Permian mass extinction event. *Nature Geoscience*, **7**(3), 233–238.

French, K. L., Hallmann, C., Hope, J. M., Schoon, P. L., Zumberge, J. A., Hoshino, Y., Peters, C. A., George, S. C., Love, G. D., Brocks, J. J., Buick, R., & Summons,

R. E. 2015. Reappraisal of hydrocarbon biomarkers in Archean rocks. *Proceedings of the National Academy of Sciences*, **112**(19), 5915–5920.

Gallegos, E. J. 1981. Alkylbenzenes derived from carotenes in coals by GC/MS. *Journal of Chromatographic Science*, **19**, 177–182.

Gandy, M. N., & Piggott, M. J. 2008. Synthesis of kalasinamide, a putative plant defense phototoxin. *Journal of Natural Products*, **71**(5), 866–8.

Greenwood, P. F., Lengkeek, N. A., Piggott, M. J., & Pierce, K. 2009. Structural identification and mass spectral interpretation of C3n highly branched alkanes in sediment and aquatic extracts and evidence for their anthropogenic origin. *Organic Geochemistry*, **40**(10), 1055–1062.

Grice, K., Twitchett, R. J., Alexander, R., Foster, C. B., & Looy, C. 2005a. A potential biomarker for the Permian–Triassic ecological crisis. *Earth and Planetary Science Letters*, **236**(1-2), 315–321.

Grice, K., Cao, C., Love, G. D., Böttcher, M. E., Twitchett, R. J., Grosjean, E., Summons, R. E., Turgeon, S. C., Dunning, W., & Jin, Y. 2005b. Photic zone euxinia during the Permian-triassic superanoxic event. *Science*, **307**, 706–709.

Grice, K., Nabbefeld, B., & Maslen, E. 2007. Source and significance of selected polycyclic aromatic hydrocarbons in sediments (Hovea-3 well, Perth Basin, Western Australia) spanning the Permian–Triassic boundary. *Organic Geochemistry*, **38**, 1795–1803.

Grimalt, J. O., Grifoll, M., Solanas, A. M., & Albaiges, J. 1991. Microbial degradation of marine evaporitic crude oils. *Geochimica et Cosmochimica Acta*, **55**, 1903–1913.

Hartgers, W. A., Sinninghe-Damste, J. S., & de Leeuw, J. W. 1994. Geochemical significance of alkylbenzene distributions in flash pyrolysates of kerogens, coals and asphaltenes. *Geochimica et Cosmochimica Acta*, **58**(7), 1759–1775.

Hays, L. E., Beatty, T., Henderson, C. M., Love, G. D., & Summons, R. E. 2007. Evidence for photic zone euxinia through the end-Permian mass extinction in the Panthalassic Ocean (Peace River Basin, Western Canada). *Palaeoworld*, **16**(1-3), 39–50.

Holzer, G., Oro, J., & Tornabene, T. G. 1979. Gas chromatographic-mass spectrometric analysis of neutral lipids from methanogenic and thermoacidophilic bacteria. *Journal of Chromatography*, **186**, 795–809.

Hounslow, M. W., Peters, C., Mørk, A., Weitschat, W., & Vigran, J. O. 2008. Biomagnetostratigraphy of the Vikinghøgda formation, Svalbard (Arctic Norway), and the geomagnetic polarity timescale for the lower Triassic. *Bulletin of the Geological Society of America*, **120**(9), 1305–1325.

Hübscher, J, & Barner, R. 1990. Totalsynthese von natülichem α-Tocopherol. 5. Mitteilung. Asymmetrische Alkylierung und asymmetrische Epoxidierung als Methoden zur Einführung der (R)-Konfiguration an C(2) des Chroman-Systems. *Helvetica Chimica Acta*, **73**, 1068–1086.

Killops, S., Stoddart, D., & Mills, N. 2014. Inferences for sources of oils from the Norwegian Barents Sea using statistical analysis of biomarkers. *Organic Geochemistry*, **76**, 157–166.

Knierzinger, A, Walther, W, Weber, B, Müller, R K, & Netscher, T. 1990. Eine neue Methode zur stereochemischen Analyse offenkettiger terpenoider Carbonyl-Verbindungen. *Helvetica Chimica Acta*, **73**, 1087–1107.

Kulkarni, S. N., Phadke, A. S., Rangaishenvi, M. V., & Kamath, S. V. 1988. Synthesis of phytol isomers - 7,11,15-trimethyl-3-methylenehexadecanol and 3,7,11,15-tetramethylhexadec-3-en-1-ol and their conversion into vitamin-E. *Indian Journal of Chemistry Section B-Organic Chemistry Including Medicinal Chemistry*, **27**, 65–66.

Lengkeek, N. A., Greenwood, P. F., Nguyen, B., Koutsantonis, G. A., & Piggott, M. J. 2010. Making mixtures to solve structures: structural elucidation via combinatorial synthesis. *Journal of Combinatorial Chemistry*, **12**(1), 141–150.

Looy, C. V., Twitchett, R. J., Dilcher, D. L., Van Konijnenburg-Van Cittert, J. H., & Visscher, H. 2001. Life in the end-Permian dead zone. *Proceedings of the National Academy of Sciences*, **98**(14), 7879–83.

Mango, F. D. 1990. The origin of light hydrocarbons in petroleum: A kinetic test of the steady-state catalytic hypothesis. *Geochimica et Cosmochimica Acta*, **54**(5), 1315–1323.

Mango, F. D. 1992. Transition metal catalysis in the generation of petroleum: A genetic anomaly in Ordovician oils. *Geochimica et Cosmochimica Acta*, **56**(10), 3851–3854.

Mango, F. D., Hightower, J. W., & James, A. T. 1994. Role of transition-metal catalysis in the formation of natural gas. *Nature*, **368**(6471), 536–538.

McIldowie, M., & Alexander, R. 2005. Identification of a novel C33 n-alkylcyclohexane biomarker in Permian-Triassic sediments. *Organic Geochemistry*, **36**(10), 1454–1458.

Mørk, A., Elvebakk, G., Forsberg, A. W., Hounslow, M. W., Vigran, J. O., & Weitschat, W. 1999. The Vikinghogda Formation - a new Lower Triassic type section for Central and Eastern Svalbard. *Polar Research*, **18**(1), 51–82.

Nabbefeld, B., Grice, K., Schimmelmann, A., Summons, R. E., Troitzsch, U., & Twitchett, R. J. 2010a. A comparison of thermal maturity parameters between freely extracted hydrocarbons (Bitumen I) and a second extract (Bitumen II) from within the kerogen matrix of Permian and Triassic sedimentary rocks. *Organic Geochemistry*, **41**(2), 78–87.

Nabbefeld, B., Grice, K., Twitchett, R. J., Summons, R. E., Hays, L., Böttcher, M. E., & Asif, M. 2010b. An integrated biomarker, isotopic and palaeoenvironmental study through the Late Permian event at Lusitaniadalen, Spitsbergen. *Earth and Planetary Science Letters*, **291**(1-4), 84–96.

Nakrem, H. A., Orchard, M. J., Weitschat, W., Hounslow, M. W., Beatty, T. W., & Mørk, A. 2008. Triassic conodonts from Svalbard and their Boreal correlations. *Polar Research*, **27**(3), 523–539.

Radke, M., & Willsch, H. 1993. Generation of alkylbenzenes and benzo[b]thiophenes by artificial maturation of sulfur-rich coal. *Fuel*, **72**(8), 1103–1108.

Ryall, R. P., Nandi, D. L., & Silverman, R. B. 1990. Substituted vitamin K epoxide analogues. New competitive inhibitors and substrates of vitamin K1 epoxide reductase. *Journal of Medicinal Chemistry*, **33**(6), 1790–1797.

Schaeflé, J., Ludwig, B., Albrecht, P., & Ourisson, G. 1977. Hydrocarbures aromatiques d'origine geologique. II : Nouveaux carotanoïdes aromatiques fossiles. *Tetrahedron Letters*, **18**(41), 3673–3676.

Sinninghe Damsté, J. S., Kock-van Dalen, A. C., & de Leeuw, J. W. 1988. Identification of long-chain isoprenoid alkylbenzenes in sediments and crude oils. *Geochimica et Cosmochimica Acta*, **52**(11), 2671–2677.

Sinninghe Damsté, J. S., Keely, B. J., Betts, S. E., Baas, M., Maxwell, J. R., & de Leeuw, J. W. 1993. Variations in abundances and distributions of isoprenoid chromans and long-chain alkylbenzenes in sediments of the Mulhouse Basin: a molecular sedimentary record of palaeosalinity. *Organic Geochemistry*, **20**(8), 1201–1215.

Solli, H., Larter, S. R., & Douglas, A. G. 1980. Analysis of kerogens by pyrolysis-gas chromatography-mass spectrometry using selective ion monitoring. III. Long-chain alkylbenzenes. *Physics and Chemistry of the Earth*, **12**(jan), 591–597.

Stemmerik, L., Bendix-Almgreen, S. E., & Piasecki, S. 2001. The Permian-Triassic boundary in central East Greenland: Past and present views. *Bulletin of the Geological Society of Denmark*, **48**(2), 159–167.

Summons, R. E., & Powell, T. G. 1987. Identification of aryl isoprenoids in source rocks and crude oils: biological markers for the green sulphur bacteria. *Geochimica et Cosmochimica Acta*, **51**, 557–566.

Thomas, B. M., Willink, R. J., Grice, K., Twitchett, R. J., Purcell, R. R., Archbold, N. W., George, A. D., Tye, S., Alexander, R., Foster, C. B., & Barber, C. J. 2004. Unique marine Permian-Triassic boundary section from Western Australia. *Australian Journal of Earth Sciences*, **51**(3), 423–430.

Twitchett, R. J., Looy, C. V., Morante, R., Visscher, H., & Wignall, P. B. 2001. Rapid and synchronous collapse of marine and terrestrial ecosystems during the end-Permian biotic crisis. *Geology*, **29**(4), 351–354.

Upadhyay, H. C., Dwivedi, G. R., Roy, S., Sharma, A., Darokar, M. P., & Srivastava, S. K. 2014. Phytol derivatives as drug resistance reversal agents. *ChemMedChem*, **9**(8), 1860–1868.

Williams, J. A., Dolcater, D. L., Torkelson, B. E., & Winters, J. C. 1988. Anomalous concentrations of specific alkylaromatic and alkylcycloparaffin components in west Texas and Michigan basin crude Oils. *Organic Geochemistry*, **13**(1-3), 47–60.

Yin, H. F., Zhang, K. X., Tong, J. N., Yang, Z. Y., & Wu, S. B. 2001. The Global Stratotype Section and Point (GSSP) of the Permian-Triassic Boundary. *Episodes*, **24**(2), 102–114.

7. Conclusions

Hendrik Grotheer

This PhD project has researched several novel applications of new organic geochemical analytical techniques. Hydropyrolysis (HyPy) and compound specific sulfur isotope analysis (CS-S-IA). HyPy applied to authentic PAHs was used to test the authenticity of aromatic hydrocarbons detected in HyPy fractions of metamorphosed rocks associated with orogenic Au-deposits (**Chapter 2**). HyPy was further evaluated for its capacity to release kerogen bound OSCs from two oil mature S-rich sediments (**Chapter 4**). CS-S-IA was used to investigate S fractionation between different organic S-pools (e.g., kerogen, bitumen) in sedimentary rocks (**Chapter 4**) and to elucidate the potential of $\delta^{34}S_{OSCs}$ as a paleoenvironmental proxie to trace global S-cycle dynamics (**Chapter 5**). The aim of this thesis was to investigate the applicability, reliability and potential biases of the novel techniques which offer much potential to exploration for valuable commodities and deciphering environmental conditions favourable to the formation of petroleum deposits.

7.1. Hydropyrolysis

Previous HyPy treatment of metamorphosed, OM rich rocks associated with orogenic Au-deposits released high concentrations of parent and hydrogenated polycyclic aromatic hydrocarbons (PAH; Robert *et al.*, 2016, in review). The application of HyPy to pure PAHs (**Chapter 2**) established that hydrogenation of aromatics is an artefact of the HyPy procedure, largely dependent on the catalyst load, and the authenticity of condensed PAHs in the pyrolysate. These outcomes help to accurately interpret the origin and reaction history of the HyPy product distributions from complex natural materials. The results of this research imply that the parent and hydrogenated PAHs detected from the metamorphosed rocks of orogenic Au-deposits (Robert *et al.*, 2016) are derived (*via* cleavage) from their graphitic like kerogen fraction. The results further enabled Robert *et al.* (in review) to identify at least two different phases of OM potentially involved in the Au mineralisation process, based on varying molecular and stable carbon isotopic compositions of PAHs released by HyPy. HyPy was thus proven a useful procedure to characterise the molecular structure of overmature OM and has also recently been applied on a mine scale investigation to identify key organic geochemical proxies (e.g., molecular and $\delta^{13}C$ composition) that could potentially be used as pathfinders in Au-deposit exploration (Robert *et al.*, unpublished results).

7.2. Compound specific sulfur isotope analysis

CS-S-IA of OSCs promises to provide great advancements in the field of S-biogeochemistry and paleoenvironmental reconstructions. In order to improve the processing speed

and precision of ICP-MS measured $\delta^{34}S$ data, previously performed by tedious manual integration and calibration, **Chapter 3** describes a routine procedure for the auto-processing of raw Neptune^{+} signals using IsoDat (v. 3.1) and subsequent multipoint regression normalisation against the international sulfur isotope standard Vienna Canyon Diablo Troilite (VCDT). Optimum peak integration (starting and end slope) and background subtraction parameters were defined on standard laboratory samples and substantially increased both reproducibility and accuracy of measured values. The defined optimum settings for peak integration and background subtraction varied significantly from previously published parameters (Amrani *et al.*, 2009) – demonstrating the varied nature of separately acquired CS-S-IA data. It is thus advisable that optimum processing parameters are determined for individual analytical conditions and are frequently tested and revised.

The use of $\delta^{34}S$ for paleoenvironmental reconstructions is enhanced with knowledge about the timing of organic matter deposition and its sulfurisation processes, the identity and $\delta^{34}S$ values of primary S-sources and the molecular and $\delta^{34}S$ fractionation during diagenesis and catagenesis. Qualitative information about S-sources and secondary alteration processes (e.g., diagenesis or thermal maturation) can be obtained by separate analysis of the OSCs from different organic sulfur fractions (e.g., kerogen, bitumen). Kerogen bound OSCs are not readily accessible to molecular and isotopic analyses, but can be released by HyPy (**Chapter 4**). HyPy applied to pure dibenzothiophene (DBT) confirmed the stability and S-isotopic authenticity of OSCs during the hydropyrolysis procedure and imply that HyPy generated OSCs provide a reliable isotopic representation of kerogen S. Further, HyPy of several rock kerogens produced significantly higher concentrations of OSCs compared to their free occurrence in the bitumen fraction. The OSCs detected in the bitumen (**Chapter 4 + 5**) or HyPy (**Chapter 4**) released fractions represent quantitatively small portions of total kerogen S. The largest fraction of organic S species likely comprises polar compounds or S_x-bridged moieties within the kerogen macromolecular network, unamenable to GC separation. Distinct pools of organic S may reflect varied sources of sulfur, timing of generation and mechanisms of sulfurisation (e.g., formation of discrete OSCs with intramolecular S; or intermolecular S_x-bridging between different organic functionalities). HyPy has the potential to differentiate and separate the individual organic S pools and thus can potentially help decipher complex kerogen formation processes and also help to exploit the biomarker preservation potential of S-rich sedimentary rocks. **Chapter 4** provides a case study highlighting the capability of HyPy, but further data is required to fully understand the geologic fractionations of organic S. To strengthen our understanding of S-biogeochemistry samples covering a variety of defined depositional settings and thermal maturities should be investigated.

7.3. Permian-Triassic extinction

The Permian-Triassic extinction was the greatest mass extinction event during the Phanerozoic. The extinction was caused by catastrophic environmental stress involving major changes to the global C- and S-cycle. To date, direct isotopic investigations of S-cycle dynamics at this time have largely been limited to measuring the $\delta^{34}S$ of inorganic S-species. **Chapter 5** combined the bulk S isotopic analysis of inorganic S (total reducible inorganic sulfur; TRIS) and organic S (kerogen bound S) fractions with S isotopic analysis of individual OSCs in two P-Tr sequences. The abundance and $\delta^{34}S$ composition of OSCs and their relationship with kerogen and total inorganic S implied a sensitivity to water column chemistry and local basin environmental controls (e.g., progressive oxygen depletion, terrestrial weathering induced primary production, volcanism). This study demonstrated the potential of CS-S-IA to reconstruct S-cycles of the past and specifically illuminated some of the global drivers behind the large environmental fluxes and ecological stresses associated with extinction events. However, $\delta^{34}S_{OSCs}$ should not be considered a stand alone paleoproxy. OSC data should still be evaluated with other traditional data from different elements of the S-system and independent environmental proxies. Extending the CS-S-IA approach to additional extinction events and other significant S-cycle dynamics will help establish $\delta^{34}S_{OSCs}$ as important analytical tool for paleoenvironmental studies.

The severe environmental stresses during the Permian Triassic extinction and consequential decline in biodiversity supported the emergence of unique microbial communities (with distinct biomarkers) during the subsequent phase of recovery. The identification and interpretation of source diagnostic compounds has helped to further illuminate the ecosystem and evolutionary boost following the extinction. In **Chapter 6**, two microbial biomarkers (phytanyl benzene and phytanyl toluene) were identified in mudstones from three key P-Tr horizons from mid-northern and southern paleolatitudes. These compounds, unambiguously identified by analytical correlation to previously synthesised standards, were closely related to C_{33} *n*-alkyl cyclohexane, suggesting their parent organisms shared a similar ecological niche. The widespread geographic distribution, but noteworthy absence from a paleoequatorial P-Tr section, implies a temperature and climate sensitivity of these microbes. The combination of C_{33} *n*-alkyl cyclohexane and phytanyl arenes have the potential to serve as stratigraphic biomarkers for the Early Triassic phase of recovery where trace fossils (e.g., conodonts) are absent.

7.4. Limitations and future work

With further technological maturity, the novel analytical methods and applications developed in this PhD project will almost certainly enjoy wider use and acceptance by the organic geochemical and related earth science research communities. The use of $\delta^{34}S_{OSCs}$ values in a paleoenvironmental context still requires a better understanding of the isotopic fractionation of organic S compounds and major S-fractions during diagenesis and other geologic processes. As observed in **Chapter 4 + 5**, GC amenable OSCs detected from several sedimentary rocks had a different S-isotopic signature to kerogen S, indicating they represent only a small fraction of sedimentary organic S. Most organic S is likely bound to the kerogen matrix or present as polar compounds and thus difficult to chromatographically resolve. Consequently, we should acknowledge a naïve understanding of the molecular and isotopic character of these pools. Further, the OSCs observed (DBTs) represent thermodynamically stable products of not fully understood reaction mechanisms. Fractionating processes may dissipate the $\delta^{34}S$ signature of primary S sources or the organic S formed during sedimentation or early diagenesis. To fully and reliably interpret $\delta^{34}S$ data in ancient sediments a thorough investigation of the molecular and isotopic fractionation of OSCs and organic S-pools beginning at their formation in recent sediments or water column through early diagenesis and geologic processes is required. The capacity of HyPy to release kerogen bound OSCs (**Chapter 4**) to hydrogenate and defunctionalise polar compounds (**Chapter 2**), with negligible alteration of their $\delta^{34}S$ character, makes it a useful compliment to CS-S-IA by GC-ICP-MS. As observed by Raven *et al.* (2015) the kerogen fraction of recent sediments in the S-rich Cariaco Basin contained a significantly high S content that was isotopically distinct from free OSCs in the bitumen fractions. Subsequent geological transformation of diagenetically incorporated organic S, such as the advance of thermal maturity, has the potential for additional separation and isotopic fractionation of sub-pools of organic S. The capacity of HyPy to release OSCs from the intractable kerogen fraction of sedimentary rocks should prove invaluable to the future study of these complex processes.

As observed in **Chapter 2 + 4** the HyPy procedure adopted did not allow for a proper mass balance. One major limitation was the incomplete transfer of pyrolysates from the reactor chamber to the trap due to condensation along the transfer line. Unfortunately, the Strata manufactured apparatus does not readily allow modifications to the reactor-trap assemblage. Volatile products (e.g., H_2S, CH_4, CO_2, etc.) are also not trapped with this commercial set-up. S-rich samples typically released large amounts of H_2S on HyPy treatment (noticeable by smell!). C-S and S-S bonds (within S_x-bridges) are susceptible to thermal cracking, but the H_2S product escapes the HyPy system and is thus not accounted for. Further, mineralogical studies have shown that

under pyrolysis conditions, comparable to HyPy, pyrite can be reduced to elemental Fe and release H_2S that might react with the pyrolysates. It is therefore highly recommended that further application of HyPy treatment on organic sediments incorporate a trapping system to capture all volatile products. For instance, redirecting the exhaust stream through a series of gas traps would help to quantify and isotopically characterise the volatiles and incorporate this data into mass balance approaches to account for all S pools in the system.

References

Amrani, A., Sessions, A. L., & Adkins, J. F. 2009. Compound-specific δ34S analysis of volatile organics by coupled GC/multicollector-ICPMS. *Analytical Chemistry*, **81**(21), 9027–9034.

Raven, M. R., Adkins, J. F., Werne, J. P., Lyons, T. W., & Sessions, A. L. 2015. Sulfur isotopic composition of individual organic compounds from Cariaco Basin sediments. *Organic Geochemistry*, **80**, 53–59.

Robert, A. M., Grotheer, H., Greenwood, P. F., McCuaig, T. C., Bourdet, J., & Grice, K. 2016. The hydropyrolysis (HyPy) release of hydrocarbon products from a high maturity kerogen associated with an orogenic Au deposit and their relationship to the mineral matrix. *Chemical Geology*, **425**, 127–144.

Robert, A. M., Grotheer, H., Bourdet, J., Suvorova, A., Grice, K., McCuaig, T. C., & Greenwood, P. F. in review. Evidence and origin of the different types of sedimentary organic matter and its implications on Paleoproterozoic orogenic gold mineralisation. *Precambrian Research*.

Robert, A. M., Grotheer, H., Grice, K., McCuaig, T. C., & Greenwood, P. F. unpublished results. The role of organic matter in orogenic gold mineralisation.

Literature

Abbott, G. D., Bennett, B., & Petch, G. S. 1995. The thermal degradation of 5a (H)-cholestane during closed-system pyrolysis. *Geochimica et Cosmochimica Acta*, **59**(11), 2259–2264.

Aboglila, S., Grice, K., Trinajstic, K., Snape, C., & Williford, K. H. 2011. The significance of 24-norcholestanes, 4-methylsteranes and dinosteranes in oils and source-rocks from East Sirte Basin (Libya). *Applied Geochemistry*, **26**(9-10), 1694–1705.

Albaigés, J., Algaba, J., Clavell, E., & Grimalt, J. 1986. Petroleum geochemistry of the Tarragona Basin (Spanish mediterranean off–shore). *Organic Geochemistry*, **10**, 441–450.

Algeo, T., Shen, Y., Zhang, T., Lyons, T., Bates, S., Rowe, H., & Nguyen, T. K T. 2008. Association of 34S-depleted pyrite layers with negative carbonate d13C excursions at the Permian-Triassic boundary: Evidence for upwelling of sulfidic deep-ocean water masses. *Geochemistry, Geophysics, Geosystems*, **9**(4), 1–10.

Algeo, T. J., & Twitchett, R. J. 2010. Anomalous early Triassic sediment fluxes due to elevated weathering rates and their biological consequences. *Geology*, **38**(11), 1023–1026.

Amrani, A. 2014. Organosulfur Compounds: Molecular and Isotopic Evolution from Biota to Oil and Gas. *Annual Review of Earth and Planetary Sciences*, **42**(1), 733–768.

Amrani, A., & Aizenshtat, Z. 2004a. Mechanisms of sulfur introduction chemically controlled: δ34S imprint. *Organic Geochemistry*, **35**(11-12), 1319–1336.

Amrani, A., & Aizenshtat, Z. 2004b. Reaction of polysulfide anions with α, β unsaturated isoprenoid aldehydes in aquatic media: Simulation of oceanic conditions. *Organic Geochemistry*, **35**(8), 909–921.

Amrani, A., Deev, A., Sessions, A. L., Tang, Y., Adkins, J. F., Hill, R. J., Moldowan, M. J., & Wei, Z. 2012. The sulfur-isotopic compositions of benzothiophenes and dibenzothiophenes as a proxy for thermochemical sulfate reduction. *Geochimica et Cosmochimica Acta*, **84**, 152–164.

Amrani, A., Said-Ahmad, W., Shaked, Y., & Kiene, R. P. 2013a. Sulfur isotope homogeneity of oceanic DMSP and DMS. *Proceedings of the National Academy of Sciences*, **110**(46), 18413–8.

Amrani, A., Dror, G., Said-Ahmad, W., Feinstein, S., & Reznik, I. J. 2013b. The distribution and sulfur isotope ratios of specific organic sulfur compounds during pyrolysis of thermally immature kerogen. *Pages 561–562 of: 26th International Meeting of Organic Geochemistry, Book of Abstracts*.

Amrani, Alon, Sessions, AL, & Adkins, JF. 2009. Compound-specific δ34S analysis of volatile organics by coupled GC/multicollector-ICPMS. *Analytical Chemistry*, **81**(21), 9027–9034.

Anderson, T. F., & Pratt, L. M. 1995. Isotopic evidence for the origin of organic sulfur and elemental sulfur in marine sediments. *Pages 378–396 of: Geochemical Transformations of Sedimentary Sulfur*. Washington D. C.: ACS Symposium Series 612.

Ascough, P., Bird, M.I., Meredith, W., Wood, R.E., Snape, C.E., Brock, F., Higham, T.F., Large, D.J., & Apperley, D.C. 2010. Hydropyrolysis: implications for radiocarbon pre-treatment and characterization of Black Carbon. *Radiocarbon*, **52**(2), 1336–1350.

Asif, M., Alexander, R., Fazeelat, T., & Pierce, K. 2009. Geosynthesis of dibenzothiophene and alkyl dibenzothiophenes in crude oils and sediments by carbon catalysis. *Organic Geochemistry*, **40**(8), 895–901.

Aycard, Mylène, Derenne, Sylvie, Largeau, Claude, Mongenot, Thierry, Tribovillard, Nicolas, & Baudin, François. 2003. Formation pathways of proto-kerogens in Holocene sediments of the upwelling influenced Cariaco Trench, Venezuela. *Organic Geochemistry*, **34**(6), 701–718.

Bambach, R. K. 2006. Phanerozoic Biodiversity Mass Extinctions. *Annual Review of Earth and Planetary Sciences*, **34**(1), 127–155.

Becker, L., Poreda, R. J., & Bunch, T. E. 2000. Fullerenes: an extraterrestrial carbon carrier phase for noble gases. *Proceedings of the National Academy of Sciences*, **97**(7), 2979–83.

Benton, M. J., & Twitchett, R. J. 2003. How to kill (almost) all life: the end-Permian extinction event. *Trends in Ecology & Evolution*, **18**(7), 358–365.

Berner, R. A. 1980. *Early diagenesis: A theoretical approach*. No. 1 edn. Princeton University Press.

Berner, R. A. 1982. *Burial of organic carbon and pyrite sulfur in the modern ocean: Its geochemical and environmental significance*.

Berner, R. A. 1985. Sulphate reduction, organic matter decomposition and pyrite formation. *Philosophical Transactions of the Royal Society of London. Series A, Mathematical and Physical Sciences*, **315**(1531), 25–38.

Berner, R. A. 1989. Biogeochemical cycles of carbon and sulfur and their effect on atmospheric oxygen over phanerozoic time. *Global and Planetary Change*, **1**(1-2), 97–122.

Berner, R. A. 2005. The carbon and sulfur cycles and atmospheric oxygen from middle Permian to middle Triassic. *Geochimica et Cosmochimica Acta*, **69**(13), 3211–3217.

Berner, R. A., & Raiswell, R. 1983. Burial of organic carbon and pyrite sulfur in sediments over phanerozoic time: a new theory. *Geochimica et Cosmochimica Acta*, **47**(5), 855–862.

Bishop, A. N., Love, G. D., McAulay, A. D., Snape, C. E., & Farrimond, P. 1998. Release of kerogen-bound hopanoids by hydropyrolysis. *Organic Geochemistry*, **29**(4), 989–1001.

Bolton, C., Riemer, C., Snape, C. E., Derbushire, F. J., & Terrer, M.T. 1988. Effect of low temperature catalytic hydrogenation on pyrolysis and hydropyrolysis of a bituminous coal. *Fuel*, **67**, 901–905.

Bolton, C., Snape, C. E., & Stephens, H. P. 1989. Hydrocracking of hydropyrolysis tar with hydrous titanium oxide catalysts. *Fuel*, **68**(2), 161–167.

Bond, D. P. G., & Wignall, P. B. 2008. The role of sea-level change and marine anoxia in the Frasnian-Famennian (Late Devonian) mass extinction. *Palaeogeography, Palaeoclimatology, Palaeoecology*, **263**(3-4), 107–118.

Bond, D. P. G., & Wignall, P. B. 2010. Pyrite framboid study of marine Permian-Triassic boundary sections: A complex anoxic event and its relationship to contemporaneous mass extinction. *Bulletin of the Geological Society of America*, **122**(7-8), 1265–1279.

Boreham, C. J., & Powell, T. G. 1987. Sources and preservation of organic matter in the Cretaceous Toolebuc Formation, eastern Australia. *Organic Geochemistry*, **11**(6), 433–449.

Böttcher, M. E., & Schnetger, B. 2004. Direct measurement of the content and isotopic composition of sulfur in black shales by means of combustion-isotope-ratio-monitoring mass spectrometry (C-irmMS). *Pages 597–603 of:* de Groot, P. (ed), *Handbook of Stable Isotope Analytical Techniques, Vol. I*. Elsevier.

Böttcher, M. E., Hetzel, A., Brumsack, H. J., & Schipper, A. 2006. Sulfur-iron-carbon geochemistry in sediments of the Demerara Rise. *Proceedings of the Ocean Drilling Program Scientific Results*, **207**(December 2005), 23pp.

Bottrell, S. H., & Raiswell, R. 2000. Sulphur isotopes and microbial sulphur cycling in sediments. *Pages 96–104 of:* Riding, R., & Awramik, S. (eds), *Microbial Sediments*. Springer Berlin / Heidelberg.

Bowden, S. A., Farrimond, P., Snape, C. E., & Love, G. D. 2006. Compositional differences in biomarker constituents of the hydrocarbon, resin, asphaltene and kerogen fractions: An example from the Jet Rock (Yorkshire, UK). *Organic Geochemistry*, **37**(3), 369–383.

Bowring, S. A., Erwin, D. H., Jin, Y. G., Martin, M. W., Davidek, K., & Wang, W. 1998. U/Pb Zircon Geochronology and Tempo of the End-Permian Mass Extinction. *Science*, **280**, 1039–1045.

Bowring, S. A, Erwin, D. H., & Isozaki, Y. 1999. The tempo of mass extinction and recovery: the end-Permian example. *Proceedings of the National Academy of Sciences of the United States of America*, **96**, 8827–8828.

Brocks, J. J., & Grice, K. 2011. Biomarkers (molecular fossils). *Pages 147–167 of:* Reitner, J., & Thiel, V. (eds), *Encyclopedia of Geobiology*. Dordrecht, The Netherlands: Springer.

Brocks, J. J., & Summons, R. E. 2013. Sedimentary Hydrocarbons, Biomarkers for Early Life. *Pages 61–103 of:* Holland, H., & Turekian, K. (eds), *Treatise on Geochemistry: Second Edition*, vol. 10. Elsevier Ltd.

Brocks, J. J., Love, G. D., Snape, C. E., Logan, G. A., Summons, R. E., & Buick, R. 2003. Release of bound aromatic hydrocarbons from late Archean and Mesoproterozoic kerogens via hydropyrolysis. *Geochimica et Cosmochimica Acta*, **67**(8), 1521–1530.

Brunner, B., & Bernasconi, S. M. 2005. A revised isotope fractionation model for dissimilatory sulfate reduction in sulfate reducing bacteria. *Geochimica et Cosmochimica Acta*, **69**(20), 4759–4771.

Böttcher, M. E., Smock, A. M., & Cypionka, H. 1998. Sulfur isotope fractionation during experimental precipitation of iron(II) and manganese (II) sulfide at room temperature. *Chemical Geology*, **146**(3-4), 127–134.

Böttcher, M. E., Thamdrup, B., & Vennemann, T. W. 2001. Oxygen and sulfur isotope fractionation during anaerobic bacterial disproportionation of elemental sulfur. *Geochimica et Cosmochimica Acta*, **65**(10), 1601–1609.

Burgess, S. D., Bowring, S. A., & Shen, S. Z. 2014. High-precision timeline for Earth's most severe extinction. *Proceedings of the National Academy of Sciences*, **111**(9), 3316–3321.

Butler, I. B., Böttcher, M. E., Rickard, D., & Oldroyd, A. 2004. Sulfur isotope partitioning during experimental formation of pyrite via the polysulfide and hydrogen sulfide pathways: Implications for the interpretation of sedimentary and hydrothermal pyrite isotope records. *Earth and Planetary Science Letters*, **228**(3-4), 495–509.

Cai, C., Li, K., Anlai, M., Zhang, C., Xu, Z., Worden, R. H., Wu, Guanhui, Zhang, Baoshou, & Chen, Lixin. 2009. Distinguishing Cambrian from Upper Ordovician source rocks: Evidence from sulfur isotopes and biomarkers in the Tarim Basin. *Organic Geochemistry*, **40**(7), 755–768.

Canfield, D. E. 2001. Biogeochemistry of Sulfur Isotopes. *Reviews in Mineralogy and Geochemistry*, **43**(1), 607–636.

Canfield, D. E., & Teske, A. 1996. Late Proterozoic rise in atmospheric oxygen concentration inferred from phylogenetic and sulphur-isotope studies. *Nature*, **382**(6587), 127–132.

Canfield, D. E., & Thamdrup, B. 1994. The production of 34S-depleted sulfide during bacterial disproportionation of elemental sulfur. *Science*, **266**, 1973–1975.

Canfield, D. E., Habicht, K. S., & Thamdrup, B. 2000. The Archean Sulfur Cycle and the early history of Atmospheric Oxygen. *Science*, **288**(5466), 658–661.

Canfield, D. E., Poulton, S. W., Knoll, A. H., Narbonne, G. M., Ross, G., Goldberg, T., & Strauss, H. 2008. Ferruginous conditions dominated later neoproterozoic deep-water chemistry. *Science*, **321**(5891), 949–952.

Canfield, D. E., Stewart, F. J., Thamdrup, B., De Brabandere, L., Dalsgaard, T., Delong, E. F., Revsbech, N. P., & Ulloa, O. 2010. A cryptic sulfur cycle in oxygen-minimum-zone waters off the Chilean coast. *Science*, **330**(6009), 1375–1378.

Cao, C., & Zheng, Q. 2009. Geological event sequences of the Permian-Triassic transition recorded in the microfacies in Meishan section. *Science in China, Series D: Earth Sciences*, **52**(10), 1529–1536.

Cao, C., Wang, W., & Jin, Y. 2002. Carbon isotope excursions across the Permian-Triassic bound- ary in the Meishan section, Zhejiang Province, China. *Chinese Science Bulletin*, **47**(13), 1125.

Cao, C., Love, G. D., Hays, L. E., Wang, W., Shen, S., & Summons, R. E. 2009. Biogeochemical evidence for euxinic oceans and ecological disturbance presaging the end-Permian mass extinction event. *Earth and Planetary Science Letters*, **281**(3-4), 188–201.

Cassani, F., Gallango, O., Talukdar, S., Vallejos, C., & Ehrmann, U. 1988. Methylphenanthrene maturity index of marine source rock extracts and crude oils from the Maracaibo Basin. *Organic Geochemistry*, **13**, 73–80.

Chen, J.-S., & Chu, X.-L. 1988. Sulfur isotope composition of triassic marine sulfates of South China. *Chemical Geology: Isotope Geoscience Section*, **72**(2), 155–161.

Clar, E. 1972. *The Aromatic Sextet*. London: J. Wiley.

Clar, E., Guye-Vuillème, J. F., McCallum, S., & Macpherson, I. A. 1963. Annellation effects in the pyrene series and the classification of absorption spectra. *Tetrahedron*, **19**(1954), 2185–2197.

Clar, E., Sanigök, Ü., & Zander, M. 1968. NMR studies of perylene and coronene derivatives. *Tetrahedron*, **24**, 2817–2823.

Claypool, G. E., Holser, W. T., Kaplan, I. R., Sakai, H., & Zak, I. 1980. The age curves of sulfur and oxygen isotopes in marine sulfate and their mutual interpretation. *Chemical Geology*, **28**(C), 199–260.

Cline, J. D. 1969. Spectrophotometric Determination of Hydrogen Sulfide in Natural Waters. *Limnology and Oceanography*, **14**(3), 454–458.

Connan, J., Bouroullec, J., Dessort, D., & Albrecht, P. 1986. The microbial input in carbonate-anhydrite facies of a sabkha palaeoenvironment from Guatemala: A molecular approach. *Organic Geochemistry*, **10**, 29–50.

Cortecci, G., Reyes, E., Berti, G., & Casati, P. 1981. Sulfur and oxygen isotopes in Italian marine sulfates of Permian and Triassic ages. *Chemical Geology*, **34**(1-2), 65–79.

Cross, M. M., Manning, D. A. C., Bottrell, S. H., & Worden, R. H. 2004. Thermochemical sulphate reduction (TSR): Experimental determination of reaction kinetics and implications of the observed reaction rates for petroleum reservoirs. *Organic Geochemistry*, **35**(4), 393–404.

Cypionka, H., Smock, A. M., & Böttcher, M. E. 1998. A combined pathway of sulfur compound disproportionation in Desulfovibrio desulfuricans. *FEMS Microbiology Letters*, **166**, 181–186.

Dawson, D., Grice, K., & Alexander, R. 2005. Effect of maturation on the indigenous δD signatures of individual hydrocarbons in sediments and crude oils from the Perth Basin (Western Australia). *Organic Geochemistry*, **36**(1), 95–104.

de Leeuw, J. W., & Sinninghe Damsté, J. S. 1990. Organic sulphur compounds and other biomarkers as indicators of Palaeosalinity: A critical evaluation. *Pages 417–443 of:* Orr, W L., & White, C. M. (eds), *Geochemistry of sulfur in fossil fuels*. Washington, D.C.: American Chemical Society Symposium Series 249.

Des Marais, D. J. 1997. Long-term evolution of the biogeochemical carbon cycle. *Reviews in Mineralogy and Geochemistry*, **35**, 429–448.

Detmers, J., Brüchert, V., Habicht, K. S., & Kuever, J. 2001. Diversity of sulfur isotope fractionations by sulfate reducing prokaryotes. *Applied and Environmental Microbiology*, **67**(2), 888–894.

Dick, J. M., Evans, K. A., Holman, A. I., Jaraula, C. M. B., & Grice, K. 2013. Estimation and application of the thermodynamic properties of aqueous phenanthrene and isomers of methylphenanthrene at high temperature. *Geochimica et Cosmochimica Acta*, **122**(dec), 247–266.

Dong, J.-Z., Vorkink, W. P., & Lee, M. L. 1993. Origin of long-chain alkylcyclohexanes and alkylbenzenes in a coal-bed wax. *Geochimica et Cosmochimica Acta*, **57**(4), 837–849.

Ellis, L., Singh, R. K, Alexander, R., & Kagi, R. I. 1995. Geosynthesis of organic compounds: III. Formation of alkyltoluenes and alkylxylenes in sediments. *Geochimica et Cosmochimica Acta*, **59**(24), 5133–5140.

Ellis, L., Fisher, S. J., Singh, R. K., Alexander, R., & Kagi, R. I. 1999. Identification of alkenylbenzenes in pyrolyzates using GC-MS and GC-FTIR techniques: Evidence for kerogen aromatic moieties with various binding sites. *Organic Geochemistry*, **30**(7), 651–665.

Erwin, D. H. 1994. The Permo-Triassic Extinction. *Nature*, **367**(6460), 231–236.

Erwin, D. H., Bowring, S. A., & Yugan, J. 2002. End-Permian mass extinctions: A review. *Geological Society of America Special Paper*, **365**, 363–383.

Feder, H. M., & Halpern, J. 1975. Mehanism of the cobalt carbonyl-catalyzed homogenous hydrogenation of aromatic hydrocarbons. *Journal of the American Chemical Society*, **97**, 7186–7188.

Fenton, S., Grice, K., Twitchett, R., Bottcher, M., Looy, C., & Nabbefeld, B. 2007. Changes in biomarker abundances and sulfur isotopes of pyrite across the Permian–Triassic (P/Tr) Schuchert Dal section (East Greenland). *Earth and Planetary Science Letters*, **262**(1-2), 230–239.

Fike, D. A., Grotzinger, J. P., Pratt, L. M., & Summons, R. E. 2006. Oxidation of the Ediacaran ocean. *Nature*, **444**(7120), 744–7.

Finn, M. J., Fynes, G., Ladner, W. R., & Newman, J. O. H. 1980. Light aromatics from the hydropyrolysis of coal. *Fuel*, **59**(6), 397–404.

Fossing, H., & Jørgensen, B. B. 1989. Measurement reduction of a single-step chromium method Evaluation. *Biogeochemistry*, **8**(3), 205–222.

Foster, W. J., & Twitchett, R. J. 2014. Functional diversity of marine ecosystems after the Late Permian mass extinction event. *Nature Geoscience*, **7**(3), 233–238.

Francois, R. 1987. A study of sulfur enrichment in the humic fraction of marine sediments during early diagenesis. *Geochimica et Cosmochimica Acta*, **51**(1), 17–27.

Freeman, K. H., Hayes, J. M., Trendel, J.-M., & Albrecht, P. 1990. Evidence from carbon isotope measurements for diverse origins of sedimentary hydrocarbons. *Nature*, **343**.

French, K. L., Hallmann, C., Hope, J. M., Schoon, P. L., Zumberge, J. A., Hoshino, Y., Peters, C. A., George, S. C., Love, G. D., Brocks, J. J., Buick, R., & Summons, R. E. 2015. Reappraisal of hydrocarbon biomarkers in Archean rocks. *Proceedings of the National Academy of Sciences*, **112**(19), 5915–5920.

Fry, B., Ruf, W., Gest, H., & Hayes, J. M. 1988. Sulphur isotope effects associated with oxidation of sulphide by O2 in aqueous solution. *Chemical Geology*, **73**, 205–210.

Fu, P. P., Lee, H. M., & Harvey, R. G. 1980. Regioselective catalytic hydrogenation of polycyclic aromatic hydrocarbons under mild conditions. *Journal of Organic Chemistry*, **45**, 2797–2803.

Fynes, G., Ladner, W. R., & Newman, J. O. H. 1980. The hydropyrolysis of coal to BTX. *Progress in Energy and Combustion Science*, **6**(3), 223–232.

Gallegos, E. J. 1981. Alkylbenzenes derived from carotenes in coals by GC/MS. *Journal of Chromatographic Science*, **19**, 177–182.

Gandy, M. N., & Piggott, M. J. 2008. Synthesis of kalasinamide, a putative plant defense phototoxin. *Journal of Natural Products*, **71**(5), 866–8.

Gelin, F., Sinninghe Damsté, J. S., Harrison, W. N., Reiss, C., Maxwell, J. R., & De Leeuw, J. W. 1996. Variations in origin and composition of kerogen constituents as revealed by analytical pyrolysis of immature kerogens before and after desulphurization. *Organic Geochemistry*, **24**(6-7), 705–714.

Goldhaber, M. B. 2004. Sulfur-rich sediments. *Pages 257–288 of: Sediments, Diagenesis, and Sedimentary Rocks*. Elsevier.

Goldhaber, M. B., & Kaplan, I. R. 1980. Mechanisms of sulfur incorporation and isotope fractionation during early diagenesis in sediments of the gulf of California. *Marine Chemistry*, **9**(2), 95–143.

Gorjan, P., & Kaiho, K. 2007. Correlation and comparison of seawater δ34Ssulfate records at the permian-triassic transition. *Chemical Geology*, **243**(3-4), 275–285.

Gorjan, P., Kaiho, K., Kakegawa, T., Niitsuma, S., Chen, Z. Q., Kajiwara, Y., & Nicora, A. 2007. Paleoredox, biotic and sulfur-isotopic changes associated with the end-Permian mass extinction in the western Tethys. *Chemical Geology*, **244**(3-4), 483–492.

Grasby, S. E., Shen, W., Yin, R., Gleason, J. D., Blum, J. D., Lepak, R. F., Hurley, James P., & Beauchamp, Benoit. 2016. Isotopic signatures of mercury contamination in latest Permian oceans. *Geology*, **45**(1).

Greenwood, P. F., Lengkeek, N. A., Piggott, M. J., & Pierce, K. 2009. Structural identification and mass spectral interpretation of C3n highly branched alkanes in sediment and aquatic extracts and evidence for their anthropogenic origin. *Organic Geochemistry*, **40**(10), 1055–1062.

Greenwood, P. F., McCulloch, M., Grice, K., Holman, A., Hong, L., Ling, H., & Jin, S. 2013. Compound specific d34S analysis - Development and applications. *Pages 146–147 of: 26th International Meeting of Organic Geochemistry, Book of Abstracts*.

Greenwood, P. F., Amrani, A., Sessions, A., Raven, M. R., Holman, A., Dror, G., Grice, K., McCulloch, M. T., & Adkins, J. F. 2014. Development and Initial Biogeochemical Applications of Compound-Specific Sulfur Isotope Analysis. *Chap. 10,*

pages 285–312 of: Grice, K. (ed), *Principles and Practice of Analytical Techniques in Geosciences*. UK: Royal Society of Chemistry.

Greenwood, P. F., Schwark, L., Mohammed, L., Zhu, G., Grice, K., & McCulloch, M. 2015. Compound-specific sulfur isotope analysis of oils using GC-MC-ICPMS. *Pages 113–114 of: 27th International Meeting of Organic Geochemistry, Book of Abstracts*.

Grice, K., & Brocks, J. J. 2011. Biomarkers (organic, compound specific isotopes). *Pages 167–182 of:* Reitner, J., & Thiel, V. (eds), *Encyclopedia of Geobiology*. Dordrecht, The Netherlands: Springer.

Grice, K., Twitchett, R. J., Alexander, R., Foster, C. B., & Looy, C. 2005a. A potential biomarker for the Permian–Triassic ecological crisis. *Earth and Planetary Science Letters*, **236**(1-2), 315–321.

Grice, K., Summons, R. E., Grosjean, E., Twitchett, R. J., Dunning, W., Wang, S. X., & Böttcher, Michael E. 2005b. Depositional conditions of the northern onshore Perth Basin (basal Triassic). *APPEA Journal*, **45**(1), 263–274.

Grice, K., Cao, C., Love, G. D., Böttcher, M. E., Twitchett, R. J., Grosjean, E., Summons, R. E., Turgeon, S. C., Dunning, W., & Jin, Y. 2005c. Photic zone euxinia during the Permian-triassic superanoxic event. *Science*, **307**, 706–709.

Grice, K., Nabbefeld, B., & Maslen, E. 2007. Source and significance of selected polycyclic aromatic hydrocarbons in sediments (Hovea-3 well, Perth Basin, Western Australia) spanning the Permian–Triassic boundary. *Organic Geochemistry*, **38**, 1795–1803.

Grice, K., Lu, H., Atahan, P., Asif, M., Hallmann, C., Greenwood, P., Maslen, E., Tulipani, S., Williford, K., & Dodson, J. 2009. New insights into the origin of perylene in geological samples. *Geochimica et Cosmochimica Acta*, **73**(21), 6531–6543.

Grimalt, J. O., Grifoll, M., Solanas, A. M., & Albaiges, J. 1991. Microbial degradation of marine evaporitic crude oils. *Geochimica et Cosmochimica Acta*, **55**, 1903–1913.

Grotheer, H., Robert, A. M., Greenwood, P. F., & Grice, K. 2015. Stability and hydrogenation of polycyclic aromatic hydrocarbons during hydropyrolysis (HyPy) – Relevance for high maturity organic matter. *Organic Geochemistry*, **86**, 45–54.

Grotheer, H., Le Métayer, P., Piggott, M. J., Lindeboom, E. J., Holman, A. I., Twitchett, R. J., & Grice, K. 2017. Occurrence and significance of phytanyl arenes across the Permian-Triassic boundary interval. *Organic Geochemistry*, **104**, 42–52.

Grotheer, H., Greenwood, P. F., McCulloch, M. T., Böttcher, M. E., & Grice, K. in review. d34S character of organosulfur compounds in kerogen and bitumen fractions of organic sediments. *Organic Geochemistry*.

Gvirtzman, Z., Said-Ahmad, W., Ellis, G. S., Hill, R. J., Moldowan, J. M., Wei, Z., & Amrani, A. 2015. Compound-specific sulfur isotope analysis of thiadiamondoids of oils from the Smackover Formation, USA. *Geochimica et Cosmochimica Acta*, **167**, 144–161.

Hallam, A., & Wignall, P. B. 1997. *Mass Extinctions and their Aftermath*. Oxford University Press.

Hallam, A., & Wignall, P. B. 1999. Mass extinctions and sea-level changes. *Earth-Science Reviews*, **48**(4), 217–250.

Hartgers, W. A., Sinninghe-Damste, J. S., & de Leeuw, J. W. 1994. Geochemical significance of alkylbenzene distributions in flash pyrolysates of kerogens, coals and asphaltenes. *Geochimica et Cosmochimica Acta*, **58**(7), 1759–1775.

Hays, L. E., Beatty, T., Henderson, C. M., Love, G. D., & Summons, R. E. 2007. Evidence for photic zone euxinia through the end-Permian mass extinction in the Panthalassic Ocean (Peace River Basin, Western Canada). *Palaeoworld*, **16**(1-3), 39–50.

Hedges, J. I. 1992. Global biogeochemical cycles: progress and problems. *Marine Chemistry*, **39**(1-3), 67–93.

Heinrichs, H., Brumsack, H. J., Loftfield, N., & König, N. 1986. Verbessertes Druckaufschlußsystem für biologische und anorganische Materialien. *Zeitschrift für Pflanzenernährung und Bodenkunde*, **149**(3), 350–353.

Hiteshue, R. W., Anderson, R. B., & Schlesinger, M. D. 1957. Hydrogenating Coal at 800 C. *Industrial & Engineering Chemistry*, 1–3.

Hoefs, J. 2009. *Stable isotope geochemistry*. 9th edn. Springer Berlin.

Holman, A. I., Greenwood, P. F., Brocks, J. J., & Grice, K. 2014. Effects of sulfide minerals on aromatic maturity parameters: Laboratory investigation using micro-scale sealed vessel pyrolysis. *Organic Geochemistry*, **76**, 270–277.

Holser, W. T., Schönlaub, H. P., Attrep Jr, M., Boeckelmann, K., Klein, P., Magaritz, M., Orth, C. J., Fenninger, A., Jenny, C., Kralik, M., Mauritsch, H., Pak, E., Schramm, J. M., Stattegger, K., & Schmöller, R. 1989. A unique geochemical record at the Permian/Triassic boundary. *Nature*, **337**(5), 39–44.

Holzer, G., Oro, J., & Tornabene, T. G. 1979. Gas chromatographic-mass spectrometric analysis of neutral lipids from methanogenic and thermoacidophilic bacteria. *Journal of Chromatography*, **186**, 795–809.

Hounslow, M. W., Peters, C., Mørk, A., Weitschat, W., & Vigran, J. O. 2008. Biomagnetostratigraphy of the Vikinghøgda formation, Svalbard (Arctic Norway), and the geomagnetic polarity timescale for the lower Triassic. *Bulletin of the Geological Society of America*, **120**(9), 1305–1325.

Hübscher, J, & Barner, R. 1990. Totalsynthese von natülichem α-Tocopherol. 5. Mitteilung. Asymmetrische Alkylierung und asymmetrische Epoxidierung als Methoden zur Einführung der (R)-Konfiguration an C(2) des Chroman-Systems. *Helvetica Chimica Acta*, **73**, 1068–1086.

Hurtgen, M. T. 2012. The Marine Sulfur Cycle, Revisited. *Science*, **337**(6092), 305–306.

Idiz, E. F., Tannenbaum, E., & Kaplan, I. R. 1990. Pyrolysis of High-Sulfur Monterey Kerogens. *Pages 575–591 of:* Orr, W. L., & White, C. M. (eds), *Geochemistry of Sulfur in Fossil Fuels*, vol. 429. Washington D.C.: American Chemical Society.

Jiang, A., Zhou, P., Sun, Y., & Xie, L. 2013. Rapid column chromatography separation of alkylnaphthalenes from aromatic components in sedimentary organic matter for compound specific stable isotope analysis. *Organic Geochemistry*, **60**, 1–8.

Jiang, Y .-F., Tang, Y .-G., & Chou, C.-L. 2006. Research on genesis of pyrite near the Permian-Triassic boundary in meishan, Zhejiang, China. *Journal of China University of Mining and Technology*, **16**(4), 457–460.

Jin, Y. G., Wang, Y., Wang, W., Shang, Q. H., Cao, C. Q., & Erwin, D. H. 2000. Pattern of marine mass extinction near the Permian-Triassic boundary in South China. *Science*, **289**(5478), 432–436.

Jørgensen, B. B. 1982. Mineralization of organic matter in the sea bed - the role of sulphate reduction. *Nature*, **296**(5858), 643–645.

Kaiho, K., Kajiwara, Y., Nakano, T., Miura, Y., Kawahata, H., Tazaki, K., Ueshima, M. Masato, Chen, Zhongqiang, & Shi, Guang R. 2002. End-Permian catastrophe by a bolide impact: Evidence of a gigantic release of sulfur from the mantle. *Geology*, **29**(9), 815–818.

Kaiho, K., Kajiwara, Y., Chen, Z.-Q., & Gorjan, P. 2006a. A sulfur isotope event at the end of the Permian. *Chemical Geology*, **235**(1-2), 33–47.

Kaiho, K., Chen, Z. Q., Kawahata, H., Kajiwara, Y., & Sato, H. 2006b. Close-up of the end-Permian mass extinction horizon recorded in the Meishan section, South China: Sedimentary, elemental, and biotic characterization and a negative shift of sulfate sulfur isotope ratio. *Palaeogeography, Palaeoclimatology, Palaeoecology*, **239**(3-4), 396–405.

Kajiwara, Y., Yamakita, S., Ishida, K., Ishiga, H., & Imai, A. 1994. Development of a largely anoxic stratified ocean and its temporary massive mixing at the Permian/Triassic boundary supported by the sulfur isotopic record. *Palaeogeography, Palaeoclimatology, Palaeoecology*, **111**(3-4), 367–379.

Kamo, S. L., Czamanske, G. K., Amelin, Y., Fedorenko, V. A., Davis, D. W., & Trofimov, V. R. 2003. Rapid eruption of Siberian flood-volcanic rocks and evidence for coincidence with the Permian-Triassic boundary and mass extinction at 251 Ma. *Earth and Planetary Science Letters*, **214**(1-2), 75–91.

Kaplan, I. R., & Rittenberg, S. C. 1964. Microbiological Fractionation of Sulphur Isotopes. *Journal of general Microbiology*, **34**(1958), 195–212.

Killops, S., Stoddart, D., & Mills, N. 2014. Inferences for sources of oils from the Norwegian Barents Sea using statistical analysis of biomarkers. *Organic Geochemistry*, **76**, 157–166.

Killops, S. D., & Killops, V. J. 2005. *Introduction to Organic Geochemistry*. Oxford: Blackwell Publishing.

Knierzinger, A, Walther, W, Weber, B, Müller, R K, & Netscher, T. 1990. Eine neue Methode zur stereochemischen Analyse offenkettiger terpenoider Carbonyl-Verbindungen. *Helvetica Chimica Acta*, **73**, 1087–1107.

Koeberl, C., Farley, K. A., Peucker-Ehrenbrink, B., & Sephton, M. A. 2004. Geochemistry of the end-Permian extinction event in Austria and Italy: No evidence for an extraterrestrial component. *Geology*, **32**(12), 1053–1056.

Kohnen, M. E. L., Sinninghe Damsté, J. S., Kock-Van Dalen, A. C., Ten Havens, H. L., Rullkötter, J., & de Leeuw, J. W. 1990. Origin and diagenetic transformations of C 25 and C 30 highly branched isoprenoid sulphur compounds: Further evidence for the formation of organically bound sulphur during early diagenesis. *Geochimica et Cosmochimica Acta*, **54**, 3053–3063.

Kohnen, M. E. l., Sinninghe Damsté, J. S., Kock-van Dalen, A. c., & de Leeuw, J. W. 1991. Di- or polysulphide-bound biomarkers in sulphur-rich geomacromolecules as revealed by selective chemolysis. *Geochimica et Cosmochimica Acta*, **55**(5), 1375–1394.

Korte, C., Kozur, H. W., Joachimski, M. M., Strauss, H., Veizer, J., & Schwark, L. 2004. Carbon, sulfur, oxygen and strontium isotope records, organic geochemistry and biostratigraphy across the Permian/Triassic boundary in Abadeh, Iran. *International Journal of Earth Sciences*, **93**(4), 565–581.

Kowalski, N., Dellwing, O., Beck, M., Grunwald, M., Badewien, T., Brumsack, H. J., van Beusekom, J. E. E., & Böttcher, M. E. 2012. A comparative study of manganese dynamics in pelagic and benthic parts of two tidal systems of the North Sea. *Estuarine, Coastal and Shelf Science*, **100**, 3–17.

Kring, D. A. 2007. The Chicxulub impact event and its environmental consequences at the Cretaceous-Tertiary boundary. *Palaeogeography, Palaeoclimatology, Palaeoecology*, **255**(1-2), 4–21.

Krull, E. S., & Retallack, G. J. 2000. d13C depth profiles from paleosols across the Permian-Triassic boundary: Evidence for methane release. *Bulletin of the Geological Society of America*, **112**(9), 1459–1472.

Kulkarni, S. N., Phadke, A. S., Rangaishenvi, M. V., & Kamath, S. V. 1988. Synthesis of phytol isomers - 7,11,15-trimethyl-3-methylenehexadecanol and 3,7,11,15-tetramethylhexadec-3-en-1-ol and their conversion into vitamin-E. *Indian Journal of Chemistry Section B-Organic Chemistry Including Medicinal Chemistry*, **27**, 65–66.

Le Métayer, P., Grice, K., Chow, C. N., Caccetta, L., Maslen, E., Dawson, D., & Fusetti, L. 2014. The effect of origin and genetic processes of low molecular weight aromatic hydrocarbons in petroleum on their stable carbon isotopic compositions. *Organic Geochemistry*, **72**, 23–33.

Lengkeek, N. A., Greenwood, P. F., Nguyen, B., Koutsantonis, G. A., & Piggott, M. J. 2010. Making mixtures to solve structures: structural elucidation via combinatorial synthesis. *Journal of Combinatorial Chemistry*, **12**(1), 141–150.

Li, C., Love, G. D., Lyons, T. W., Fike, D. A., Sessions, A. L., & Chu, X. 2010. A Stratified Redox Model for the Ediacaran Ocean. *Science*, **328**(5974), 80–83.

Li, S., Amrani, A., Pang, X., Yang, H., Said-Ahmad, W., Zhang, B., & Pang, Q. 2015. Origin and quantitative source assessment of deep oils in the Tazhong Uplift, Tarim Basin. *Organic Geochemistry*, **78**, 1–22.

Littke, R., Baker, D. R., & Rullkötter, J. 1997. Deposition of petroleum source rocks. *Pages 271–333 of:* Welte, D. H, Horsfield, B., & Baker, D. R. (eds), *Petroleum and basin evolution.*

Liu, S.-A., Wu, H., Shen, S., Jiang, G., Zhang, S., Lv, Y., Zhang, H., & Li, S. 2017. Zinc isotope evidence for intensive magmatism immediately before the end-Permian mass extinction. *Geology*.

Lockhart, R. S., Meredith, W., Love, G. D., & Snape, C. E. 2008. Release of bound aliphatic biomarkers via hydropyrolysis from Type II kerogen at high maturity. *Organic Geochemistry*, **39**(8), 1119–1124.

Lockhart, R. S., Berwick, L. J., Greenwood, P. F., Grice, K., Kraal, P., & Bush, R. 2013. Analytical pyrolysis for determining the molecular composition of contemporary monosulfidic black ooze. *Journal of Analytical and Applied Pyrolysis*, **104**, 640–652.

Looy, C. V., Twitchett, R. J., Dilcher, D. L., Van Konijnenburg-Van Cittert, J. H., & Visscher, H. 2001. Life in the end-Permian dead zone. *Proceedings of the National Academy of Sciences*, **98**(14), 7879–83.

Love, G. D, Snape, C. E., Carr, A. D., & Houghton, R. C. 1995. Release of covalently-bound alkane biomarkers in high yields from kerogen via catalytic hydropyrolysis. *Organic Geochemistry*, **23**(10), 981–986.

Love, G. D., Snape, C. E., Carr, A. D., & Houghton, R. C. 1996. Changes in Molecular Biomarker and Bulk Carbon Skeletal Parameters of Vitrinite Concentrates as a Function of Rank. *Energy & Fuels*, **10**(1), 149–157.

Love, G. D., McAulay, A., Snape, C. E., & Bishop, A. N. 1997. Effect of Process Variables in Catalytic Hydropyrolysis on the Release of Covalently Bound Aliphatic Hydrocarbons from Sedimentary Organic Matter. *Energy & Fuels*, **11**(3), 522–531.

Love, G. D., Snape, C. E., & Fallick, A. E. 1998. Differences in the mode of incorporation and biogenicity of the principal aliphatic constituents of a type I oil shale. *Organic Geochemistry*, **28**(12), 797–811.

Machel, H. G. 2001. Bacterial and thermochemical sulfate reduction in diagenetic settings – old and new insights. *Sedimentary Geology*, **140**, 143–175.

Machel, H. G., Krouse, H. R., & Sassen, R. 1995. Products and distinguishing criteria of bacterial and thermochemical sulfate reduction. *Applied Geochemistry*, **10**(4), 373–389.

Mango, F. D. 1990. The origin of light hydrocarbons in petroleum: A kinetic test of the steady-state catalytic hypothesis. *Geochimica et Cosmochimica Acta*, **54**(5), 1315–1323.

Mango, F. D. 1992. Transition metal catalysis in the generation of petroleum: A genetic anomaly in Ordovician oils. *Geochimica et Cosmochimica Acta*, **56**(10), 3851–3854.

Mango, F. D., Hightower, J. W., & James, A. T. 1994. Role of transition-metal catalysis in the formation of natural gas. *Nature*, **368**(6471), 536–538.

Mann, J. L., Vocke, R. D., & Kelly, W. R. 2009. Revised δ 34 S reference values for IAEA sulfur isotope reference materials S-2 and S-3. *Rapid Communications in Mass Spectrometry*, **23**(8), 1116–1124.

Manzano, B. K., Fowler, M. G., & Machel, H. G. 1997. The influence of thermochemical sulphate reduction on hydrocarbon composition in Nisku reservoirs, Brazeau river area, Alberta, Canada. *Organic Geochemistry*, **27**(7-8), 507–521.

Marshall, C. P., Love, G. D., Snape, C. E., Hill, A. C., Allwood, A. C., Walter, M. R., Van Kranendonk, M. J., Bowden, S. A., Sylva, S. P., & Summons, R. E. 2007. Structural characterization of kerogen in 3.4Ga Archaean cherts from the Pilbara Craton, Western Australia. *Precambrian Research*, **155**(1-2), 1–23.

Matthaei, S. K., Henley, R. W., & Heinrich, C. A. 1995a. Gold precipitation by fluid mixing in bedding-parallel fractures near carbonaceous slates at the Cosmopolitan Howley gold deposit, northern Australia. *Economic Geology*, **90**, 2123–2142.

Matthaei, S. K., Henley, R. W., Bacigalupo-Rose, S., Binns, R. A., Andrew, A. S., Carr, G. R., French, DH, McAndrew, J, & Kananagh, M. 1995b. Intrusion-related, high-temperature gold quartz veining in the Cosmopolitan Howley metasedimentary rock-hosted gold deposit, Northern Territory, Australia. *Economic Geology*, **90**, 1012–1045.

McCollom, T. M., Simoneit, B. R. T., & Shock, E. L. 1999. Hydrous pyrolysis of polycyclic aromatic hydrocarbons and implications for the origin of PAH in hydrothermal petroleum. *Energy and Fuels*, **13**(6), 401–410.

McIldowie, M., & Alexander, R. 2005. Identification of a novel C33 n-alkylcyclohexane biomarker in Permian-Triassic sediments. *Organic Geochemistry*, **36**(10), 1454–1458.

Meredith, W., Russell, C. A., Cooper, M., Snape, C. E., Love, G. D., Fabbri, D., & Vane, C. H. 2004. Trapping hydropyrolysates on silica and their subsequent thermal desorption to facilitate rapid fingerprinting by GC-MS. *Organic Geochemistry*, **35**(1), 73–89.

Meredith, W., Sun, C.-G., Snape, C. E., Sephton, M. A., & Love, G. D. 2006. The use of model compounds to investigate the release of covalently bound biomarkers via hydropyrolysis. *Organic Geochemistry*, **37**(12), 1705–1714.

Meredith, W., Ascough, P. L., Bird, M. I., Large, D. J., Snape, C. E., Song, J., Sun, Y., & Tilston, E. L. 2013. Direct evidence from hydropyrolysis for the retention of long alkyl moieties in black carbon fractions isolated by acidified dichromate oxidation. *Journal of Analytical and Applied pyrolysis*, **103**, 232–239.

Meredith, W., Snape, C. E., & Love, G. D. 2014. Development and use of catalytic hydropyrolysis (HyPy) as an analytical tool for organic geochemical application. *Chap. 6, pages 171–203 of:* Grice, Kliti (ed), *Principles and Practice of Analytical Techniques in Geosciences*. UK: Royal Society of Chemistry.

Meyer, K. M., Kump, L. R., & Ridgwell, A. 2008. Biogeochemical controls on photic-zone euxinia during the end-Permian mass extinction. *Geology*, **36**(9), 747–750.

Mitchell, S. C., Lafferty, C. J., Garcia, R., Snape, C. E., Buchanan, A. C., Britt, P. F., & Klavetter, E. 1993. Silica-Immobilized Compounds As Models For Probing Coal Pyrolysis and Hydropyrolysis Phenomena. *Energy & Fuels*, **7**(11), 331–333.

Moodley, L., Middelburg, J. J., Herman, P. M. J., Soetaert, K. E. R., & de Lange, G. J. 2005. Oxygenation and organic-matter preservation in marine sediments: direct experimental evidence from ancient organic carbon-rich deposits. *Geology*, **33**, 889–892.

Mørk, A., Elvebakk, G., Forsberg, A. W., Hounslow, M. W., Vigran, J. O., & Weitschat, W. 1999. The Vikinghogda Formation - a new Lower Triassic type section for Central and Eastern Svalbard. *Polar Research*, **18**(1), 51–82.

Mukherjee, J., Sarofim, A. F., & Longwell, J. P. 1994. Polycyclic aromatic hydrocarbons from the high-temperature pyrolysis of pyrene. *Combustion and Flame*, **96**, 191–200.

Murray, I. P., Love, G. D., Snape, C. E., & Bailey, N. J. L. 1998. Comparison of covalently-bound aliphatic biomarkers released via hydropyrolysis with their solvent-extractable counterparts for a suite of Kimmeridge clays. *Organic Geochemistry*, **29**(5-7), 1487–1505.

Nabbefeld, B., Grice, K., Schimmelmann, A., Summons, R. E., Troitzsch, U., & Twitchett, R. J. 2010a. A comparison of thermal maturity parameters between freely extracted hydrocarbons (Bitumen I) and a second extract (Bitumen II) from within the kerogen matrix of Permian and Triassic sedimentary rocks. *Organic Geochemistry*, **41**(2), 78–87.

Nabbefeld, B., Grice, K., Twitchett, R. J., Summons, R. E., Hays, L., Böttcher, M. E., & Asif, M. 2010b. An integrated biomarker, isotopic and palaeoenvironmental study through the Late Permian event at Lusitaniadalen, Spitsbergen. *Earth and Planetary Science Letters*, **291**(1-4), 84–96.

Nabbefeld, B., Grice, K., Schimmelmann, A., Sauer, P. E., Böttcher, M. E., & Twitchett, R. 2010c. Significance of δDkerogen, δ13Ckerogen and δ34Spyrite from several Permian/Triassic (P/Tr) sections. *Earth and Planetary Science Letters*, **295**(1-2), 21–29.

Nakrem, H. A., Orchard, M. J., Weitschat, W., Hounslow, M. W., Beatty, T. W., & Mørk, A. 2008. Triassic conodonts from Svalbard and their Boreal correlations. *Polar Research*, **27**(3), 523–539.

Needham, R. S., Stuart-Smith, P. G., & Page, R. W. 1988. Tectonic evolution of the Pine Creek Inlier, Northern Territory. *Precambrian Research*, **41**, 543–564.

Newton, R. J., Pevitt, E. L., Wignall, P. B., & Bottrell, S. H. 2004. Large shifts in the isotopic composition of seawater sulphate across the Permo-Triassic boundary in northern Italy. *Earth and Planetary Science Letters*, **218**(3-4), 331–345.

Nissenbaum, A., Baedecker, M. J., & Kaplan, I. R. 1972. Organic geochemistry of Dead Sea sediments. *Geochimica et Cosmochimica Acta*, **36**(7), 709–727.

Nkansah, M. A., Christy, A. A., & Barth, T. 2011. The use of anthracene as a model compound in a comparative study of hydrous pyrolysis methods for industrial waste remediation. *Chemosphere*, **84**(4), 403–408.

Parnell, J., Boyce, A. J., Mark, D., Bowden, S., & Spinks, S. 2010. Early oxygenation of the terrestrial environment during the Mesoproterozoic. *Nature*, **468**(7321), 290–293.

Passier, H. F., Bosch, H.-J., Nijenhuis, I. A., Lourens, L. J., Böttcher, M. E., Leenders, A., Damsté, J. S. S., de Lange, G. J., & de Leeuw, J. W. 1999a. Sulphidic Mediterranean surface waters during Pliocene sapropel formation. *Nature*, **397**(6715), 146–149.

Passier, H. F., Böttcher, M. E., & De Lange, G. J. 1999b. Sulphur enrichment in organic matter of eastern Mediterranean sapropels: A study of sulphur isotope partitioning. *Aquatic Geochemistry*, **5**(1), 99–118.

Peters, K. E., Walters, C. C., & Moldowan, J. M. 2005a. *The biomarker guide Volume 1: biomarkers and isotopes in the environment and human history*. Cambridge: Cambridge University Press.

Peters, K. E., Walters, C. C., & Moldowan, J. M. 2005b. *The biomarker guide, Volume 2. Biomarkers and isotopes in petroleum exploration and Earth history*. Cambridge University Press.

Peterson, B. J. 1999. Stable isotopes as tracers of organic matter input and transfer in benthic food webs: A review. *Acta Oecologica*, **20**(4), 479–487.

Price, F. T., & Shieh, Y. N. 1979. Fractionation of sulfur isotopes during laboratory synthesis of pyrite at low temperatures. *Chemical Geology*, **27**(3), 245–253.

Racki, G., & Wignall, P. B. 2005. Late permian double-phased mass extinction and volcanism: an oceanographic perspective. *Developments in Palaeontology and Stratigraphy*, **20**, 263–297.

Radke, M., & Welte, D. H. 1983. The methylphenanthrene index (MPI): a maturity parameter based on aromatic hydrocarbons. *Pages 504–512 of: Advances in Organic Geochemistry 1981*.

Radke, M., & Willsch, H. 1993. Generation of alkylbenzenes and benzo[b]thiophenes by artificial maturation of sulfur-rich coal. *Fuel*, **72**(8), 1103–1108.

Radke, M., Willsch, H., Leythaeuser, D., & Teichmüller, M. 1982. Aromatic components of coal: relation of distribution pattern to rank. *Geochimica et Cosmochimica Acta*, **46**, 1831–1848.

Raiswell, R., & Canfield, D. E. 1998. *Sources of iron for pyrite formation in marine sediments*.

Raiswell, R., Buckley, F., Berner, R. A., & Anderson, T. F. 1988. Degree of pyritization of iron as a paleoenvironmental indicator of bottom-water oxygenation. *Journal of Sedimentary Research*, **58**(5), 812–819.

Rasmussen, J. A. 2013. Polycyclic aromatic hydrocarbons: Trends for bonding hydrogen. *Journal of Physical Chemistry A*, **117**, 4279–4285.

Raven, M. R., Sessions, A. L., Adkins, J. F., & Thunell, R. C. 2016a. Rapid organic matter sulfurization in sinking particles from the Cariaco Basin water column. *Geochimica et Cosmochimica Acta*, **190**, 175–190.

Raven, M. R., Sessions, A. L., Fischer, W. W., & Adkins, J. F. 2016b. Sedimentary pyrite δ34S differs from porewater sulfide in Santa Barbara Basin: Proposed role of organic sulfur. *Geochimica et Cosmochimica Acta*, **186**, 120–134.

Raven, Morgan Reed, Adkins, Jess F., Werne, Josef P., Lyons, Timothy W., & Sessions, Alex L. 2015. Sulfur isotopic composition of individual organic compounds from Cariaco Basin sediments. *Organic Geochemistry*, **80**, 53–59.

Reichow, M. K., Pringle, M. S., Al'Mukhamedov, A. I., Allen, M. B., Andreichev, V. L., Buslov, M. M., Davies, C. E., Fedoseev, G. S., Fitton, J. G., Inger, S., Medvedev, A. Y., Mitchell, C., Puchkov, V. N., Safonova, I. Y., Scott, R. A., & Saunders, A. D. 2009. The timing and extent of the eruption of the Siberian Traps large igneous province: Implications for the end-Permian environmental crisis. *Earth and Planetary Science Letters*, **277**(1-2), 9–20.

Riccardi, A. L., Arthur, M. A., & Kump, L. R. 2006. Sulfur isotopic evidence for chemocline upward excursions during the end-Permian mass extinction. *Geochimica et Cosmochimica Acta*, **70**(23), 5740–5752.

Ricci, M. P., Merritt, D. A., Freeman, K. H., & Hayes, J. M. 1994. Acquisition and processing of data for isotope-ratio-monitoring mass spectrometry. *Organic Geochemistry*, **21**(6-7), 561–571.

Rickard, D., & Luther, G. W. 2007. Chemistry of iron sulfides. *Chemical Reviews*, **107**, 514–562.

Robert, A. M., Grotheer, H., Lockhart, R., Greenwood, P. F., McCuaig, T.C., Jaraula, C. M.B., Grice, K., Bagas, L., & Schwark, L. 2014. Organics in orogenic gold systems: Characterisation of organic matter associated with gold (Au) deposits. *Page 2092 of: Goldschmidt 2014 Book of Abstracts*.

Robert, A. M., Grotheer, H., Greenwood, P. F., McCuaig, T. C., Bourdet, J., & Grice, K. 2016. The hydropyrolysis (HyPy) release of hydrocarbon products from a high maturity kerogen associated with an orogenic Au deposit and their relationship to the mineral matrix. *Chemical Geology*, **425**(may), 127–144.

Robert, A. M., Grotheer, H., Bourdet, J., Suvorova, A., Grice, K., McCuaig, T. C., & Greenwood, P. F. in review. Evidence and origin of the different types of sedimentary organic matter and its implications on Paleoproterozoic orogenic gold mineralisation. *Precambrian Research*.

Robert, A. M., Grotheer, H., Grice, K., McCuaig, T. C., & Greenwood, P. F. unpublished results. The role of organic matter in orogenic gold mineralisation.

Robinson, N., Eglinton, G., Lafferty, C. J., & Snape, C. E. 1991. Comparison of alkanes released from a bituminous coal via hydropyrolysis and low temperature hydrogenation. *Fuel*, **70**(2), 249–253.

Rooney, M. A. 1996. Carbon isotopic evidence for the accelerated destruction of light hydrocarbons by thermochemical sulfate reduction. *In: Abstract of the NSERC Thermochemical Sulphate Reduction (TSR) and Bacterial Sulphate Reduction (BSR) Workshop*.

Rospondek, M. J., Köster, J., & Sinninghe Damsté, J. S. 1997. Novel C26 highly branched isoprenoid thiophenes and alkane from the menilite formation, outer Carpathians, SE Poland. *Organic Geochemistry*, **26**(5-6), 295–304.

Rushdi, A. I., Ritter, G., Grimalt, J. O., & Simoneit, B. R. T. 2003. Hydrous pyrolysis of cholesterol under various conditions. *Organic Geochemistry*, **34**, 799–812.

Russell, C. A., Snape, C. E., Meredith, W., Love, G. D., Clarke, E., & Moffatt, B. 2004. The potential of bound biomarker profiles released via catalytic hydropyrolysis to reconstruct basin charging history for oils. *Organic Geochemistry*, **35**, 1441–1459.

Ryall, R. P., Nandi, D. L., & Silverman, R. B. 1990. Substituted vitamin K epoxide analogues. New competitive inhibitors and substrates of vitamin K1 epoxide reductase. *Journal of Medicinal Chemistry*, **33**(6), 1790–1797.

Ryskin, G. 2003. Methane-driven oceanic eruptions and mass extinctions. *Geology*, **31**(9), 741–744.

Said-Ahmad, W., & Amrani, A. 2013. A sensitive method for the sulfur isotope analysis of dimethyl sulfide and dimethylsulfoniopropionate in seawater. *Rapid Communications in Mass Spectrometry*, **27**(24), 2789–2796.

Schaeflé, J., Ludwig, B., Albrecht, P., & Ourisson, G. 1977. Hydrocarbures aromatiques d'origine geologique. II : Nouveaux carotanoïdes aromatiques fossiles. *Tetrahedron Letters*, **18**(41), 3673–3676.

Schulz, H. D., & Zabel, M. 2006. *Marine Geochemistry*. Springer.

Sephton, M. A., Love, G. D., Watson, J. S., Verchovsky, A. B., Wright, I. P., Snape, C. E., & Gilmour, I. 2004. Hydropyrolysis of insoluble carbonaceous matter in the Murchison meteorite: new insights into its macromolecular structure. *Geochimica et Cosmochimica Acta*, **68**(6), 1385–1393.

Sephton, M. A., Looy, C. V., Brinkhuis, H., Wignall, P. B., de Leeuw, J. W., & Visscher, H. 2005. Catastrophic soil erosion during the end-Permian biotic crisis. *Geology*, **33**(12), 941–944.

Sepkoski Jr., J. J. 1986. Phanerozoic overview of mass extinction. *Pages 277–295 of: Patterns and Processes in the History of Life*. Springer Berlin / Heidelberg.

Sessions, A. L., Burgoyne, T. W., & Hayes, J. M. 2001. Determination of the H Factor in Hydrogen Isotope Ratio Monitoring Mass Spectrometry. *Analytical Chemistry*, **73**(2), 200–207.

Shen, W., Lin, Y., Xu, L., Li, J., Wu, Y., & Sun, Y. 2007. Pyrite framboids in the Permian-Triassic boundary section at Meishan, China: Evidence for dysoxic deposition. *Palaeogeography, Palaeoclimatology, Palaeoecology*, **253**(3-4), 323–331.

Shen, Y., Farquhar, J., Zhang, H., Masterson, A., Zhang, T., & Wing, B. A. 2011. Multiple S-isotopic evidence for episodic shoaling of anoxic water during Late Permian mass extinction. *Nature Communications*, **2**, 210.

Sinninghe Damste, J. S., & de Leeuw, J. W. 1990. Analysis, structure and geochemical significance of organically-bound sulphur in the geosphere: State of the art and future research. *Organic Geochemistry*, **16**(4-6), 1077–1101.

Sinninghe Damsté, J. S., Kock-van Dalen, A. C., & de Leeuw, J. W. 1988. Identification of long-chain isoprenoid alkylbenzenes in sediments and crude oils. *Geochimica et Cosmochimica Acta*, **52**(11), 2671–2677.

Sinninghe Damsté, J. S., Keely, B. J., Betts, S. E., Baas, M., Maxwell, J. R., & de Leeuw, J. W. 1993. Variations in abundances and distributions of isoprenoid chromans and long-chain alkylbenzenes in sediments of the Mulhouse Basin: a molecular sedimentary record of palaeosalinity. *Organic Geochemistry*, **20**(8), 1201–1215.

Skrzypek, G. 2013. Normalization procedures and reference material selection in stable HCNOS isotope analyses: an overview. *Analytical and Bioanalytical Chemistry*, **405**(9), 2815–23.

Smith, J. W., Batts, B. D., & Gilbert, T. D. 1989. Hydrous pyrolysis of model compounds. *Organic Geochemistry*, **14**(4), 365–373.

Snape, C. E., Bolton, C., Dosch, R. G., & Stephens, H. P. 1989a. High liquid yields from bituminous coal via hydropyrolysis with dispersed catalysts. *Energy & Fuels*, 421–425.

Snape, C. E., Bolton, C., Dosch, R. G., & Stephens, H. P. 1989b. High liquid yields from bituminous coal via hydropyrolysis with dispersed catalysts. *Energy & Fuels*, 421–425.

Snape, C. E., Lafferty, C. J., Eglinton, G., Robinson, N., & Collier, R. 1994. The potential of hydropyrolysis as a route for coal liquefaction. *International Journal of Energy Research*, **18**, 233–242.

Solli, H., Larter, S. R., & Douglas, A. G. 1980. Analysis of kerogens by pyrolysis-gas chromatography-mass spectrometry using selective ion monitoring. III. Long-chain alkylbenzenes. *Physics and Chemistry of the Earth*, **12**(jan), 591–597.

Sonibare, O. O., Snape, C. E., Meredith, W., Uguna, C. N., & Love, G. D. 2009. Geochemical characterisation of heavily biodegraded tar sand bitumens by catalytic hydropyrolysis. *Journal of Analytical and Applied Pyrolysis*, **86**(1), 135–140.

Stein, S. E. 1978. On the High Temperature Chemical Equilibria of Polycyclic Aromatic Hydrocarbons. *The Journal of Physical Chemistry*, **82**(5), 566–571.

Stein, S. E. 1991. Thermal reactions and properties of polycyclic aromatic hydrocarbons. *Accounts of Chemical Research*, **24**(6), 350–356.

Stein, S. E., & Brown, R. L. 1991. Prediction of carbon-hydrogen bond dissociation energies for polycyclic aromatic hydrocarbons of arbitrary size. *Journal of the American Chemical Society*, **113**(12), 787–793.

Stein, S. E., & Fahr, A. 1985. High-Temperature Stabillties of Hydrocarbons. *American Chemical Society*, 3114–3125.

Stemmerik, L., Bendix-Almgreen, S. E., & Piasecki, S. 2001. The Permian-Triassic boundary in central East Greenland: Past and present views. *Bulletin of the Geological Society of Denmark*, **48**(2), 159–167.

Summons, R. E., & Powell, T. G. 1987. Identification of aryl isoprenoids in source rocks and crude oils: biological markers for the green sulphur bacteria. *Geochimica et Cosmochimica Acta*, **51**, 557–566.

Svensen, H., Planke, S., Polozov, A. G., Schmidbauer, N., Corfu, F., Podladchikov, Y. Y., & Jamtveit, B. 2009. Siberian gas venting and the end-Permian environmental crisis. *Earth and Planetary Science Letters*, **277**(3-4), 490–500.

Tang, Y., Perry, J. K., Jenden, P. D., & Schoell, M. 2000. Mathematical modeling of stable carbon isotope ratios in natural gases. *Geochimica et Cosmochimica Acta*, **64**(15), 2673–2687.

Tegelaar, E. W., de Leeuw, J. W., Derenne, S., & Largeau, C. 1989. A reappraisal of kerogen formation. *Geochimica et Cosmochimica Acta*, **53**(11), 3103–3106.

Thamdrup, B., Finster, K., Hansen, J. W., & Bak, F. 1993. Bacterial disproportionation of elemental sulfur coupled to chemical reduction of iron or manganese. *Applied and Environmental Microbiology*, **59**(1), 101–108.

Thomas, B. M., Willink, R. J., Grice, K., Twitchett, R. J., Purcell, R. R., Archbold, N. W., George, A. D., Tye, S., Alexander, R., Foster, C. B., & Barber, C. J. 2004. Unique marine Permian-Triassic boundary section from Western Australia. *Australian Journal of Earth Sciences*, **51**(3), 423–430.

Tissot, B., & Welte, D. 1984. *Petroleum Formation and Occurrence*. 2nd edn. Heidelberg: Springer.

Twitchett, R. J. 2006. The palaeoclimatology, palaeoecology and palaeoenvironmental analysis of mass extinction events. *Palaeogeography, Palaeoclimatology, Palaeoecology*, **232**(2-4), 190–213.

Twitchett, R. J., Looy, C. V., Morante, R., Visscher, H., & Wignall, P. B. 2001. Rapid and synchronous collapse of marine and terrestrial ecosystems during the end-Permian biotic crisis. *Geology*, **29**(4), 351–354.

Upadhyay, H. C., Dwivedi, G. R., Roy, S., Sharma, A., Darokar, M. P., & Srivastava, S. K. 2014. Phytol derivatives as drug resistance reversal agents. *ChemMedChem*, **9**(8), 1860–1868.

Vandenbroucke, M., & Largeau, C. 2007. Kerogen origin, evolution and structure. *Organic Geochemistry*, **38**(5), 719–833.

Werne, J. P., Hollander, D. J., Lyons, T. W., & Sinninghe Damsté, J. S. 2004. Organic sulfur biogeochemistry: Recent advances and future research directions. *Pages 135–150 of: Special paper 379: Sulfur biogeochemistry - past and present*. Geological Society of America.

Werne, J. P., Lyons, T. W., Hollander, D. J., Schouten, S., Hopmans, E. C., & Sinninghe Damsté, J. S. 2008. Investigating pathways of diagenetic organic matter sulfurization using compound-specific sulfur isotope analysis. *Geochimica et Cosmochimica Acta*, **72**(14), 3489–3502.

Werner, R. A., & Brand, W. A. 2001. Referencing strategies and techniques in stable isotope ratio analysis. *Rapid Communications in Mass Spectrometry*, **15**(7), 501–519.

Whiteside, J. H., & Grice, K. 2016. Biomarker Records Associated with Mass Extinction Events. *Annual Review of Earth and Planetary Sciences*, **44**, 581–612.

Wiese, F., & Reitner, J. 2011. Critical intervals in Earth's history. *In: Encyclopedia of geobiology*. Springer Netherlands.

Wignall, P. B. 2001. Large igneous provinces and mass extinctions. *Earth Science Reviews*, **53**(1-2), 1–33.

Wignall, P. B., & Hallam, A. 1993. Griesbachian (Earliest Triassic) palaeoenvironmental changes in the Salt Range, Pakistan and southeast China and their bearing on the Permo-Triassic mass extinction. *Palaeogeography, Palaeoclimatology, Palaeoecology*, **102**(3-4), 215–237.

Wignall, P. B., & Newton, R. 1998. Pyrite framboid diameter as a measure of oxygen deficiency in ancient mudrocks. *American Journal of Science*, **298**(7), 537–552.

Wignall, P. B., Newton, R., & Brookfield, M. E. 2005. Pyrite framboid evidence for oxygen-poor deposition during the Permian-Triassic crisis in Kashmir. *Palaeogeography, Palaeoclimatology, Palaeoecology*, **216**(3-4), 183–188.

Wilkin, R. T., Barnes, H. L., & Brantley, S. L. 1996. The size distribution of framboidal pyrite in modern sediments: An indicator of redox conditions. *Geochimica et Cosmochimica Acta*, **60**(20), 3897–3912.

Williams, J. A., Dolcater, D. L., Torkelson, B. E., & Winters, J. C. 1988. Anomalous concentrations of specific alkylaromatic and alkylcycloparaffin components in west Texas and Michigan basin crude Oils. *Organic Geochemistry*, **13**(1-3), 47–60.

Woltering, M., Tulipani, S., Boreham, C. J., Walshe, J., Schwark, L., & Grice, K. 2016. Simultaneous quantitative analysis of Ni, VO, Cu, Zn and Mn geoporphyrins by liquid chromatography-high resolution multistage mass spectrometry: Method development and validation. *Chemical Geology*, **441**(nov), 81–91.

Wortmann, U. G., Bernasconi, S. M., & Böttcher, M. E. 2001. Hypersulfidic deep biosphere indicates extreme sulfur isotope fractionation during single-step microbial sulfate reduction. *Geology*, **29**(7), 647–650.

Yin, H. F., Zhang, K. X., Tong, J. N., Yang, Z. Y., & Wu, S. B. 2001. The Global Stratotype Section and Point (GSSP) of the Permian-Triassic Boundary. *Episodes*, **24**(2), 102–114.

Zhang, J., Liang, H., He, X., Yang, Y., & Chen, B. 2011. Sulfur Isotopes of Framboidal Pyrite in the Permian-Triassic Boundary Clay at Meishan Section. *Acta Geologica Sinica - English Edition*, **85**(3), 694–701.

Zhang, Kexin, Tong, Jinnan, Shi, G. R., Lai, Xulong, Yu, Jianxin, He, Weihong, Peng, Yuanqiao, & Jin, Yali. 2007. Early Triassic conodont-palynological biostratigraphy of the Meishan D Section in Changxing, Zhejiang Province, South China. *Palaeogeography, Palaeoclimatology, Palaeoecology*, **252**(1-2), 4–23.

Every reasonable effort has been made to acknowledge the owners of copyright material. I would be pleased to hear from any copyright owner who has been omitted or incorrectly acknowledged.

A. Appendix

The following pages detail the rights granted by Elsevier, to the first author of the publications that form **Chapter 2**, **Chapter 4** and **Chapter 6** of this thesis, to reproduce the full article in a thesis or dissertation.

ELSEVIER LICENSE
TERMS AND CONDITIONS
Dec 12, 2016

This Agreement between Hendrik Grotheer ("You") and Elsevier ("Elsevier") consists of your license details and the terms and conditions provided by Elsevier and Copyright Clearance Center.

License Number	4004661125055
License date	Dec 09, 2016
Licensed Content Publisher	Elsevier
Licensed Content Publication	Organic Geochemistry
Licensed Content Title	Stability and hydrogenation of polycyclic aromatic hydrocarbons during hydropyrolysis (HyPy) – Relevance for high maturity organic matter
Licensed Content Author	Hendrik Grotheer,Aileen M. Robert,Paul F. Greenwood,Kliti Grice
Licensed Content Date	September 2015
Licensed Content Volume Number	86
Licensed Content Issue Number	n/a
Licensed Content Pages	10
Start Page	45
End Page	54
Type of Use	reuse in a thesis/dissertation
Portion	full article
Format	both print and electronic
Are you the author of this Elsevier article?	Yes
Will you be translating?	No
Order reference number	
Title of your thesis/dissertation	Novel Techniques in Organic Geochemistry applied to Australian Resources
Expected completion date	Jan 2017
Estimated size (number of pages)	200
Elsevier VAT number	GB 494 6272 12
Requestor Location	Hendrik Grotheer Ostertorsteinweg 72 Bremen, 28203 Germany Attn: Hendrik Grotheer

Total 0.00 AUD

Terms and Conditions

INTRODUCTION

1. The publisher for this copyrighted material is Elsevier. By clicking "accept" in connection with completing this licensing transaction, you agree that the following terms and conditions apply to this transaction (along with the Billing and Payment terms and conditions established by Copyright Clearance Center, Inc. ("CCC"), at the time that you opened your Rightslink account and that are available at any time at http://myaccount.copyright.com).

GENERAL TERMS

2. Elsevier hereby grants you permission to reproduce the aforementioned material subject to the terms and conditions indicated.

3. Acknowledgement: If any part of the material to be used (for example, figures) has appeared in our publication with credit or acknowledgement to another source, permission must also be sought from that source. If such permission is not obtained then that material may not be included in your publication/copies. Suitable acknowledgement to the source must be made, either as a footnote or in a reference list at the end of your publication, as follows:

"Reprinted from Publication title, Vol /edition number, Author(s), Title of article / title of chapter, Pages No., Copyright (Year), with permission from Elsevier [OR APPLICABLE SOCIETY COPYRIGHT OWNER]." Also Lancet special credit - "Reprinted from The Lancet, Vol. number, Author(s), Title of article, Pages No., Copyright (Year), with permission from Elsevier."

4. Reproduction of this material is confined to the purpose and/or media for which permission is hereby given.

5. Altering/Modifying Material: Not Permitted. However figures and illustrations may be altered/adapted minimally to serve your work. Any other abbreviations, additions, deletions and/or any other alterations shall be made only with prior written authorization of Elsevier Ltd. (Please contact Elsevier at permissions@elsevier.com). No modifications can be made to any Lancet figures/tables and they must be reproduced in full.

6. If the permission fee for the requested use of our material is waived in this instance, please be advised that your future requests for Elsevier materials may attract a fee.

7. Reservation of Rights: Publisher reserves all rights not specifically granted in the combination of (i) the license details provided by you and accepted in the course of this licensing transaction, (ii) these terms and conditions and (iii) CCC's Billing and Payment terms and conditions.

8. License Contingent Upon Payment: While you may exercise the rights licensed immediately upon issuance of the license at the end of the licensing process for the transaction, provided that you have disclosed complete and accurate details of your proposed use, no license is finally effective unless and until full payment is received from

you (either by publisher or by CCC) as provided in CCC's Billing and Payment terms and conditions. If full payment is not received on a timely basis, then any license preliminarily granted shall be deemed automatically revoked and shall be void as if never granted. Further, in the event that you breach any of these terms and conditions or any of CCC's Billing and Payment terms and conditions, the license is automatically revoked and shall be void as if never granted. Use of materials as described in a revoked license, as well as any use of the materials beyond the scope of an unrevoked license, may constitute copyright infringement and publisher reserves the right to take any and all action to protect its copyright in the materials.

9. Warranties: Publisher makes no representations or warranties with respect to the licensed material.

10. Indemnity: You hereby indemnify and agree to hold harmless publisher and CCC, and their respective officers, directors, employees and agents, from and against any and all claims arising out of your use of the licensed material other than as specifically authorized pursuant to this license.

11. No Transfer of License: This license is personal to you and may not be sublicensed, assigned, or transferred by you to any other person without publisher's written permission.

12. No Amendment Except in Writing: This license may not be amended except in a writing signed by both parties (or, in the case of publisher, by CCC on publisher's behalf).

13. Objection to Contrary Terms: Publisher hereby objects to any terms contained in any purchase order, acknowledgment, check endorsement or other writing prepared by you, which terms are inconsistent with these terms and conditions or CCC's Billing and Payment terms and conditions. These terms and conditions, together with CCC's Billing and Payment terms and conditions (which are incorporated herein), comprise the entire agreement between you and publisher (and CCC) concerning this licensing transaction. In the event of any conflict between your obligations established by these terms and conditions and those established by CCC's Billing and Payment terms and conditions, these terms and conditions shall control.

14. Revocation: Elsevier or Copyright Clearance Center may deny the permissions described in this License at their sole discretion, for any reason or no reason, with a full refund payable to you. Notice of such denial will be made using the contact information provided by you. Failure to receive such notice will not alter or invalidate the denial. In no event will Elsevier or Copyright Clearance Center be responsible or liable for any costs, expenses or damage incurred by you as a result of a denial of your permission request, other than a refund of the amount(s) paid by you to Elsevier and/or Copyright Clearance Center for denied permissions.

LIMITED LICENSE

The following terms and conditions apply only to specific license types:

15. **Translation**: This permission is granted for non-exclusive world **English** rights only unless your license was granted for translation rights. If you licensed translation rights you may only translate this content into the languages you requested. A professional translator

must perform all translations and reproduce the content word for word preserving the integrity of the article.

16. **Posting licensed content on any Website**: The following terms and conditions apply as follows: Licensing material from an Elsevier journal: All content posted to the web site must maintain the copyright information line on the bottom of each image; A hyper-text must be included to the Homepage of the journal from which you are licensing at http://www.sciencedirect.com/science/journal/xxxxx or the Elsevier homepage for books at http://www.elsevier.com; Central Storage: This license does not include permission for a scanned version of the material to be stored in a central repository such as that provided by Heron/XanEdu.

Licensing material from an Elsevier book: A hyper-text link must be included to the Elsevier homepage at http://www.elsevier.com . All content posted to the web site must maintain the copyright information line on the bottom of each image.

Posting licensed content on Electronic reserve: In addition to the above the following clauses are applicable: The web site must be password-protected and made available only to bona fide students registered on a relevant course. This permission is granted for 1 year only. You may obtain a new license for future website posting.

17. **For journal authors:** the following clauses are applicable in addition to the above:

Preprints:

A preprint is an author's own write-up of research results and analysis, it has not been peer-reviewed, nor has it had any other value added to it by a publisher (such as formatting, copyright, technical enhancement etc.).

Authors can share their preprints anywhere at any time. Preprints should not be added to or enhanced in any way in order to appear more like, or to substitute for, the final versions of articles however authors can update their preprints on arXiv or RePEc with their Accepted Author Manuscript (see below).

If accepted for publication, we encourage authors to link from the preprint to their formal publication via its DOI. Millions of researchers have access to the formal publications on ScienceDirect, and so links will help users to find, access, cite and use the best available version. Please note that Cell Press, The Lancet and some society-owned have different preprint policies. Information on these policies is available on the journal homepage.

Accepted Author Manuscripts: An accepted author manuscript is the manuscript of an article that has been accepted for publication and which typically includes author-incorporated changes suggested during submission, peer review and editor-author communications.

Authors can share their accepted author manuscript:

- – immediately
    - via their non-commercial person homepage or blog

    - by updating a preprint in arXiv or RePEc with the accepted manuscript
    - via their research institute or institutional repository for internal institutional uses or as part of an invitation-only research collaboration work-group
    - directly by providing copies to their students or to research collaborators for their personal use
    - for private scholarly sharing as part of an invitation-only work group on commercial sites with which Elsevier has an agreement
- – after the embargo period
    - via non-commercial hosting platforms such as their institutional repository
    - via commercial sites with which Elsevier has an agreement

In all cases accepted manuscripts should:

- – link to the formal publication via its DOI
- – bear a CC-BY-NC-ND license - this is easy to do
- – if aggregated with other manuscripts, for example in a repository or other site, be shared in alignment with our hosting policy not be added to or enhanced in any way to appear more like, or to substitute for, the published journal article.

Published journal article (JPA): A published journal article (PJA) is the definitive final record of published research that appears or will appear in the journal and embodies all value-adding publishing activities including peer review co-ordination, copy-editing, formatting, (if relevant) pagination and online enrichment.

Policies for sharing publishing journal articles differ for subscription and gold open access articles:

Subscription Articles: If you are an author, please share a link to your article rather than the full-text. Millions of researchers have access to the formal publications on ScienceDirect, and so links will help your users to find, access, cite, and use the best available version.

Theses and dissertations which contain embedded PJAs as part of the formal submission can be posted publicly by the awarding institution with DOI links back to the formal publications on ScienceDirect.

If you are affiliated with a library that subscribes to ScienceDirect you have additional private sharing rights for others' research accessed under that agreement. This includes use for classroom teaching and internal training at the institution (including use in course packs and courseware programs), and inclusion of the article for grant funding purposes.

Gold Open Access Articles: May be shared according to the author-selected end-user license and should contain a CrossMark logo, the end user license, and a DOI link to the formal publication on ScienceDirect.

Please refer to Elsevier's posting policy for further information.

18. **For book authors** the following clauses are applicable in addition to the above: Authors are permitted to place a brief summary of their work online only. You are not allowed to download and post the published electronic version of your chapter, nor may you scan the printed edition to create an electronic version. **Posting to a repository:** Authors are permitted to post a summary of their chapter only in their institution's repository.

19. **Thesis/Dissertation**: If your license is for use in a thesis/dissertation your thesis may be submitted to your institution in either print or electronic form. Should your thesis be published commercially, please reapply for permission. These requirements include permission for the Library and Archives of Canada to supply single copies, on demand, of the complete thesis and include permission for Proquest/UMI to supply single copies, on demand, of the complete thesis. Should your thesis be published commercially, please reapply for permission. Theses and dissertations which contain embedded PJAs as part of the formal submission can be posted publicly by the awarding institution with DOI links back to the formal publications on ScienceDirect.

Elsevier Open Access Terms and Conditions

You can publish open access with Elsevier in hundreds of open access journals or in nearly 2000 established subscription journals that support open access publishing. Permitted third party re-use of these open access articles is defined by the author's choice of Creative Commons user license. See our open access license policy for more information.

Terms & Conditions applicable to all Open Access articles published with Elsevier:

Any reuse of the article must not represent the author as endorsing the adaptation of the article nor should the article be modified in such a way as to damage the author's honour or reputation. If any changes have been made, such changes must be clearly indicated.

The author(s) must be appropriately credited and we ask that you include the end user license and a DOI link to the formal publication on ScienceDirect.

If any part of the material to be used (for example, figures) has appeared in our publication with credit or acknowledgement to another source it is the responsibility of the user to ensure their reuse complies with the terms and conditions determined by the rights holder.

Additional Terms & Conditions applicable to each Creative Commons user license:

CC BY: The CC-BY license allows users to copy, to create extracts, abstracts and new works from the Article, to alter and revise the Article and to make commercial use of the Article (including reuse and/or resale of the Article by commercial entities), provided the user gives appropriate credit (with a link to the formal publication through the relevant DOI), provides a link to the license, indicates if changes were made and the licensor is not represented as endorsing the use made of the work. The full details of the license are available at http://creativecommons.org/licenses/by/4.0.

CC BY NC SA: The CC BY-NC-SA license allows users to copy, to create extracts, abstracts and new works from the Article, to alter and revise the Article, provided this is

not done for commercial purposes, and that the user gives appropriate credit (with a link to the formal publication through the relevant DOI), provides a link to the license, indicates if changes were made and the licensor is not represented as endorsing the use made of the work. Further, any new works must be made available on the same conditions. The full details of the license are available at http://creativecommons.org/licenses/by-nc-sa/4.0.

CC BY NC ND: The CC BY-NC-ND license allows users to copy and distribute the Article, provided this is not done for commercial purposes and further does not permit distribution of the Article if it is changed or edited in any way, and provided the user gives appropriate credit (with a link to the formal publication through the relevant DOI), provides a link to the license, and that the licensor is not represented as endorsing the use made of the work. The full details of the license are available at http://creativecommons.org/licenses/by-nc-nd/4.0. Any commercial reuse of Open Access articles published with a CC BY NC SA or CC BY NC ND license requires permission from Elsevier and will be subject to a fee.

Commercial reuse includes:

- – Associating advertising with the full text of the Article
- – Charging fees for document delivery or access
- – Article aggregation
- – Systematic distribution via e-mail lists or share buttons

Posting or linking by commercial companies for use by customers of those companies.

20. **Other Conditions**:

v1.9

Questions? customercare@copyright.com or +1-855-239-3415 (toll free in the US) or +1-978-646-2777.

ELSEVIER LICENSE
TERMS AND CONDITIONS

Oct 28, 2017

This Agreement between Hendrik Grotheer ("You") and Elsevier ("Elsevier") consists of your license details and the terms and conditions provided by Elsevier and Copyright Clearance Center.

License Number	4167590501849
License date	Aug 14, 2017
Licensed Content Publisher	Elsevier
Licensed Content Publication	Organic Geochemistry
Licensed Content Title	δ34S character of organosulfur compounds in kerogen and bitumen fractions of sedimentary rocks
Licensed Content Author	Hendrik Grotheer,Paul F. Greenwood,Malcolm T. McCulloch,Michael E. Böttcher,Kliti Grice
Licensed Content Date	Aug 1, 2017
Licensed Content Volume	110
Licensed Content Issue	n/a
Licensed Content Pages	5
Start Page	60
End Page	64
Type of Use	reuse in a thesis/dissertation
Portion	full article
Format	both print and electronic
Are you the author of this Elsevier article?	Yes
Will you be translating?	No
Title of your thesis/dissertation	Novel techniques in Organic Geochemistry applied to Australian Resources
Expected completion date	Oct 2017
Estimated size (number of pages)	250
Requestor Location	Hendrik Grotheer Ostertorsteinweg 72 Bremen, 28203 Germany Attn: Hendrik Grotheer
Publisher Tax ID	GB 494 6272 12
Total	0.00 USD
Terms and Conditions	

INTRODUCTION

1. The publisher for this copyrighted material is Elsevier. By clicking "accept" in connection with completing this licensing transaction, you agree that the following terms and conditions apply to this transaction (along with the Billing and Payment terms and

conditions established by Copyright Clearance Center, Inc. ("CCC"), at the time that you opened your Rightslink account and that are available at any time at http://myaccount.copyright.com).

GENERAL TERMS

2. Elsevier hereby grants you permission to reproduce the aforementioned material subject to the terms and conditions indicated.

3. Acknowledgement: If any part of the material to be used (for example, figures) has appeared in our publication with credit or acknowledgement to another source, permission must also be sought from that source. If such permission is not obtained then that material may not be included in your publication/copies. Suitable acknowledgement to the source must be made, either as a footnote or in a reference list at the end of your publication, as follows:

"Reprinted from Publication title, Vol /edition number, Author(s), Title of article / title of chapter, Pages No., Copyright (Year), with permission from Elsevier [OR APPLICABLE SOCIETY COPYRIGHT OWNER]." Also Lancet special credit - "Reprinted from The Lancet, Vol. number, Author(s), Title of article, Pages No., Copyright (Year), with permission from Elsevier."

4. Reproduction of this material is confined to the purpose and/or media for which permission is hereby given.

5. Altering/Modifying Material: Not Permitted. However figures and illustrations may be altered/adapted minimally to serve your work. Any other abbreviations, additions, deletions and/or any other alterations shall be made only with prior written authorization of Elsevier Ltd. (Please contact Elsevier at permissions@elsevier.com). No modifications can be made to any Lancet figures/tables and they must be reproduced in full.

6. If the permission fee for the requested use of our material is waived in this instance, please be advised that your future requests for Elsevier materials may attract a fee.

7. Reservation of Rights: Publisher reserves all rights not specifically granted in the combination of (i) the license details provided by you and accepted in the course of this licensing transaction, (ii) these terms and conditions and (iii) CCC's Billing and Payment terms and conditions.

8. License Contingent Upon Payment: While you may exercise the rights licensed immediately upon issuance of the license at the end of the licensing process for the transaction, provided that you have disclosed complete and accurate details of your proposed use, no license is finally effective unless and until full payment is received from you (either by publisher or by CCC) as provided in CCC's Billing and Payment terms and conditions. If full payment is not received on a timely basis, then any license preliminarily granted shall be deemed automatically revoked and shall be void as if never granted. Further, in the event that you breach any of these terms and conditions or any of CCC's Billing and Payment terms and conditions, the license is automatically revoked and shall be void as if never granted. Use of materials as described in a revoked license, as well as any use of the materials beyond the scope of an unrevoked license, may constitute copyright infringement and publisher reserves the right to take any and all action to protect its copyright in the materials.

9. Warranties: Publisher makes no representations or warranties with respect to the licensed material.

10. Indemnity: You hereby indemnify and agree to hold harmless publisher and CCC, and their respective officers, directors, employees and agents, from and against any and all claims arising out of your use of the licensed material other than as specifically authorized pursuant to this license.

11. No Transfer of License: This license is personal to you and may not be sublicensed, assigned, or transferred by you to any other person without publisher's written permission.

12. No Amendment Except in Writing: This license may not be amended except in a writing signed by both parties (or, in the case of publisher, by CCC on publisher's behalf).
13. Objection to Contrary Terms: Publisher hereby objects to any terms contained in any purchase order, acknowledgment, check endorsement or other writing prepared by you, which terms are inconsistent with these terms and conditions or CCC's Billing and Payment terms and conditions. These terms and conditions, together with CCC's Billing and Payment terms and conditions (which are incorporated herein), comprise the entire agreement between you and publisher (and CCC) concerning this licensing transaction. In the event of any conflict between your obligations established by these terms and conditions and those established by CCC's Billing and Payment terms and conditions, these terms and conditions shall control.
14. Revocation: Elsevier or Copyright Clearance Center may deny the permissions described in this License at their sole discretion, for any reason or no reason, with a full refund payable to you. Notice of such denial will be made using the contact information provided by you. Failure to receive such notice will not alter or invalidate the denial. In no event will Elsevier or Copyright Clearance Center be responsible or liable for any costs, expenses or damage incurred by you as a result of a denial of your permission request, other than a refund of the amount(s) paid by you to Elsevier and/or Copyright Clearance Center for denied permissions.

LIMITED LICENSE

The following terms and conditions apply only to specific license types:
15. **Translation**: This permission is granted for non-exclusive world **English** rights only unless your license was granted for translation rights. If you licensed translation rights you may only translate this content into the languages you requested. A professional translator must perform all translations and reproduce the content word for word preserving the integrity of the article.
16. **Posting licensed content on any Website**: The following terms and conditions apply as follows: Licensing material from an Elsevier journal: All content posted to the web site must maintain the copyright information line on the bottom of each image; A hyper-text must be included to the Homepage of the journal from which you are licensing at http://www.sciencedirect.com/science/journal/xxxxx or the Elsevier homepage for books at http://www.elsevier.com; Central Storage: This license does not include permission for a scanned version of the material to be stored in a central repository such as that provided by Heron/XanEdu.
Licensing material from an Elsevier book: A hyper-text link must be included to the Elsevier homepage at http://www.elsevier.com . All content posted to the web site must maintain the copyright information line on the bottom of each image.

Posting licensed content on Electronic reserve: In addition to the above the following clauses are applicable: The web site must be password-protected and made available only to bona fide students registered on a relevant course. This permission is granted for 1 year only. You may obtain a new license for future website posting.
17. **For journal authors:** the following clauses are applicable in addition to the above:
Preprints:
A preprint is an author's own write-up of research results and analysis, it has not been peer-reviewed, nor has it had any other value added to it by a publisher (such as formatting, copyright, technical enhancement etc.).
Authors can share their preprints anywhere at any time. Preprints should not be added to or enhanced in any way in order to appear more like, or to substitute for, the final versions of articles however authors can update their preprints on arXiv or RePEc with their Accepted Author Manuscript (see below).

If accepted for publication, we encourage authors to link from the preprint to their formal publication via its DOI. Millions of researchers have access to the formal publications on ScienceDirect, and so links will help users to find, access, cite and use the best available version. Please note that Cell Press, The Lancet and some society-owned have different preprint policies. Information on these policies is available on the journal homepage.
Accepted Author Manuscripts: An accepted author manuscript is the manuscript of an article that has been accepted for publication and which typically includes author-incorporated changes suggested during submission, peer review and editor-author communications.
Authors can share their accepted author manuscript:

- immediately
    - via their non-commercial person homepage or blog
    - by updating a preprint in arXiv or RePEc with the accepted manuscript
    - via their research institute or institutional repository for internal institutional uses or as part of an invitation-only research collaboration work-group
    - directly by providing copies to their students or to research collaborators for their personal use
    - for private scholarly sharing as part of an invitation-only work group on commercial sites with which Elsevier has an agreement
- After the embargo period
    - via non-commercial hosting platforms such as their institutional repository
    - via commercial sites with which Elsevier has an agreement

In all cases accepted manuscripts should:

- link to the formal publication via its DOI
- bear a CC-BY-NC-ND license - this is easy to do
- if aggregated with other manuscripts, for example in a repository or other site, be shared in alignment with our hosting policy not be added to or enhanced in any way to appear more like, or to substitute for, the published journal article.

Published journal article (JPA): A published journal article (PJA) is the definitive final record of published research that appears or will appear in the journal and embodies all value-adding publishing activities including peer review co-ordination, copy-editing, formatting, (if relevant) pagination and online enrichment.
Policies for sharing publishing journal articles differ for subscription and gold open access articles:
Subscription Articles: If you are an author, please share a link to your article rather than the full-text. Millions of researchers have access to the formal publications on ScienceDirect, and so links will help your users to find, access, cite, and use the best available version.
Theses and dissertations which contain embedded PJAs as part of the formal submission can be posted publicly by the awarding institution with DOI links back to the formal publications on ScienceDirect.
If you are affiliated with a library that subscribes to ScienceDirect you have additional private sharing rights for others' research accessed under that agreement. This includes use for classroom teaching and internal training at the institution (including use in course packs and courseware programs), and inclusion of the article for grant funding purposes.
Gold Open Access Articles: May be shared according to the author-selected end-user license and should contain a CrossMark logo, the end user license, and a DOI link to the formal publication on ScienceDirect.

Please refer to Elsevier's posting policy for further information.
18. **For book authors** the following clauses are applicable in addition to the above: Authors are permitted to place a brief summary of their work online only. You are not allowed to download and post the published electronic version of your chapter, nor may you scan the printed edition to create an electronic version. **Posting to a repository:** Authors are permitted to post a summary of their chapter only in their institution's repository.
19. **Thesis/Dissertation**: If your license is for use in a thesis/dissertation your thesis may be submitted to your institution in either print or electronic form. Should your thesis be published commercially, please reapply for permission. These requirements include permission for the Library and Archives of Canada to supply single copies, on demand, of the complete thesis and include permission for Proquest/UMI to supply single copies, on demand, of the complete thesis. Should your thesis be published commercially, please reapply for permission. Theses and dissertations which contain embedded PJAs as part of the formal submission can be posted publicly by the awarding institution with DOI links back to the formal publications on ScienceDirect.

Elsevier Open Access Terms and Conditions
You can publish open access with Elsevier in hundreds of open access journals or in nearly 2000 established subscription journals that support open access publishing. Permitted third party re-use of these open access articles is defined by the author's choice of Creative Commons user license. See our open access license policy for more information.
Terms & Conditions applicable to all Open Access articles published with Elsevier:
Any reuse of the article must not represent the author as endorsing the adaptation of the article nor should the article be modified in such a way as to damage the author's honour or reputation. If any changes have been made, such changes must be clearly indicated.
The author(s) must be appropriately credited and we ask that you include the end user license and a DOI link to the formal publication on ScienceDirect.
If any part of the material to be used (for example, figures) has appeared in our publication with credit or acknowledgement to another source it is the responsibility of the user to ensure their reuse complies with the terms and conditions determined by the rights holder.
Additional Terms & Conditions applicable to each Creative Commons user license:
CC BY: The CC-BY license allows users to copy, to create extracts, abstracts and new works from the Article, to alter and revise the Article and to make commercial use of the Article (including reuse and/or resale of the Article by commercial entities), provided the user gives appropriate credit (with a link to the formal publication through the relevant DOI), provides a link to the license, indicates if changes were made and the licensor is not represented as endorsing the use made of the work. The full details of the license are available at http://creativecommons.org/licenses/by/4.0.
CC BY NC SA: The CC BY-NC-SA license allows users to copy, to create extracts, abstracts and new works from the Article, to alter and revise the Article, provided this is not done for commercial purposes, and that the user gives appropriate credit (with a link to the formal publication through the relevant DOI), provides a link to the license, indicates if changes were made and the licensor is not represented as endorsing the use made of the work. Further, any new works must be made available on the same conditions. The full details of the license are available at http://creativecommons.org/licenses/by-nc-sa/4.0.
CC BY NC ND: The CC BY-NC-ND license allows users to copy and distribute the Article, provided this is not done for commercial purposes and further does not permit distribution of the Article if it is changed or edited in any way, and provided the user gives appropriate credit (with a link to the formal publication through the relevant DOI), provides a link to the license, and that the licensor is not represented as endorsing the use made of the work. The full details of the license are available at http://creativecommons.org/licenses/by-nc-nd/4.0.

Any commercial reuse of Open Access articles published with a CC BY NC SA or CC BY NC ND license requires permission from Elsevier and will be subject to a fee.
Commercial reuse includes:

- Associating advertising with the full text of the Article
- Charging fees for document delivery or access
- Article aggregation
- Systematic distribution via e-mail lists or share buttons

Posting or linking by commercial companies for use by customers of those companies.

20. **Other Conditions**:

v1.9

ELSEVIER LICENSE
TERMS AND CONDITIONS
Jan 03, 2017

This Agreement between Hendrik Grotheer ("You") and Elsevier ("Elsevier") consists of your license details and the terms and conditions provided by Elsevier and Copyright Clearance Center.

License Number	4021211317069
License date	Dec 30, 2016
Licensed Content Publisher	Elsevier
Licensed Content Publication	Organic Geochemistry
Licensed Content Title	Occurrence and significance of phytanyl arenes across the Permian-Triassic boundary interval
Licensed Content Author	H. Grotheer,P. Le Métayer,M.J. Piggott,E.J. Lindeboom,A.I. Holman,R.J. Twitchett,K. Grice
Licensed Content Date	Available online 23 December 2016
Licensed Content Volume Number	n/a
Licensed Content Issue Number	n/a
Licensed Content Pages	1
Start Page	
End Page	
Type of Use	reuse in a thesis/dissertation
Portion	full article
Format	both print and electronic
Are you the author of this Elsevier article?	Yes
Will you be translating?	No
Order reference number	
Title of your thesis/dissertation	Novel Techniques in Organic Geochemistry applied to Australian Resources
Expected completion date	Jan 2017
Estimated size (number of pages)	200
Elsevier VAT number	GB 494 6272 12
Requestor Location	Hendrik Grotheer Ostertorsteinweg 72 Bremen, 28203 Germany Attn: Hendrik Grotheer

Billing Type	Invoice
Billing Address	Hendrik Grotheer Ostertorsteinweg 72 Bremen, Germany 28203 Attn: Hendrik Grotheer
Total	0.00 USD

Terms and Conditions

INTRODUCTION

1. The publisher for this copyrighted material is Elsevier. By clicking "accept" in connection with completing this licensing transaction, you agree that the following terms and conditions apply to this transaction (along with the Billing and Payment terms and conditions established by Copyright Clearance Center, Inc. ("CCC"), at the time that you opened your Rightslink account and that are available at any time at http://myaccount.copyright.com).

GENERAL TERMS

2. Elsevier hereby grants you permission to reproduce the aforementioned material subject to the terms and conditions indicated.

3. Acknowledgement: If any part of the material to be used (for example, figures) has appeared in our publication with credit or acknowledgement to another source, permission must also be sought from that source. If such permission is not obtained then that material may not be included in your publication/copies. Suitable acknowledgement to the source must be made, either as a footnote or in a reference list at the end of your publication, as follows:

"Reprinted from Publication title, Vol /edition number, Author(s), Title of article / title of chapter, Pages No., Copyright (Year), with permission from Elsevier [OR APPLICABLE SOCIETY COPYRIGHT OWNER]." Also Lancet special credit - "Reprinted from The Lancet, Vol. number, Author(s), Title of article, Pages No., Copyright (Year), with permission from Elsevier."

4. Reproduction of this material is confined to the purpose and/or media for which permission is hereby given.

5. Altering/Modifying Material: Not Permitted. However figures and illustrations may be altered/adapted minimally to serve your work. Any other abbreviations, additions, deletions and/or any other alterations shall be made only with prior written authorization of Elsevier Ltd. (Please contact Elsevier at permissions@elsevier.com). No modifications can be made to any Lancet figures/tables and they must be reproduced in full.

6. If the permission fee for the requested use of our material is waived in this instance, please be advised that your future requests for Elsevier materials may attract a fee.

7. Reservation of Rights: Publisher reserves all rights not specifically granted in the combination of (i) the license details provided by you and accepted in the course of this licensing transaction, (ii) these terms and conditions and (iii) CCC's Billing and Payment terms and conditions.

8. License Contingent Upon Payment: While you may exercise the rights licensed immediately upon issuance of the license at the end of the licensing process for the transaction, provided that you have disclosed complete and accurate details of your proposed use, no license is finally effective unless and until full payment is received from you (either by publisher or by CCC) as provided in CCC's Billing and Payment terms and conditions. If full payment is not received on a timely basis, then any license preliminarily granted shall be deemed automatically revoked and shall be void as if never granted. Further, in the event that you breach any of these terms and conditions or any of CCC's Billing and Payment terms and conditions, the license is automatically revoked and shall be void as if never granted. Use of materials as described in a revoked license, as well as any use of the materials beyond the scope of an unrevoked license, may constitute copyright infringement and publisher reserves the right to take any and all action to protect its copyright in the materials.

9. Warranties: Publisher makes no representations or warranties with respect to the licensed material.

10. Indemnity: You hereby indemnify and agree to hold harmless publisher and CCC, and their respective officers, directors, employees and agents, from and against any and all claims arising out of your use of the licensed material other than as specifically authorized pursuant to this license.

11. No Transfer of License: This license is personal to you and may not be sublicensed, assigned, or transferred by you to any other person without publisher's written permission.

12. No Amendment Except in Writing: This license may not be amended except in a writing signed by both parties (or, in the case of publisher, by CCC on publisher's behalf).

13. Objection to Contrary Terms: Publisher hereby objects to any terms contained in any purchase order, acknowledgment, check endorsement or other writing prepared by you, which terms are inconsistent with these terms and conditions or CCC's Billing and Payment terms and conditions. These terms and conditions, together with CCC's Billing and Payment terms and conditions (which are incorporated herein), comprise the entire agreement between you and publisher (and CCC) concerning this licensing transaction. In the event of any conflict between your obligations established by these terms and conditions and those established by CCC's Billing and Payment terms and conditions, these terms and conditions shall control.

14. Revocation: Elsevier or Copyright Clearance Center may deny the permissions described in this License at their sole discretion, for any reason or no reason, with a full refund payable to you. Notice of such denial will be made using the contact information provided by you. Failure to receive such notice will not alter or invalidate the denial. In no event will Elsevier or Copyright Clearance Center be responsible or liable for any costs, expenses or damage incurred by you as a result of a denial of your permission request, other than a refund of the amount(s) paid by you to Elsevier and/or Copyright Clearance Center for denied permissions.

LIMITED LICENSE

The following terms and conditions apply only to specific license types:

15. **Translation**: This permission is granted for non-exclusive world **English** rights only unless your license was granted for translation rights. If you licensed translation rights you may only translate this content into the languages you requested. A professional translator must perform all translations and reproduce the content word for word preserving the integrity of the article.

16. **Posting licensed content on any Website**: The following terms and conditions apply as follows: Licensing material from an Elsevier journal: All content posted to the web site must maintain the copyright information line on the bottom of each image; A hyper-text must be included to the Homepage of the journal from which you are licensing at http://www.sciencedirect.com/science/journal/xxxxx or the Elsevier homepage for books at http://www.elsevier.com; Central Storage: This license does not include permission for a scanned version of the material to be stored in a central repository such as that provided by Heron/XanEdu.

Licensing material from an Elsevier book: A hyper-text link must be included to the Elsevier homepage at http://www.elsevier.com . All content posted to the web site must maintain the copyright information line on the bottom of each image.

Posting licensed content on Electronic reserve: In addition to the above the following clauses are applicable: The web site must be password-protected and made available only to bona fide students registered on a relevant course. This permission is granted for 1 year only. You may obtain a new license for future website posting.

17. **For journal authors:** the following clauses are applicable in addition to the above:

Preprints:

A preprint is an author's own write-up of research results and analysis, it has not been peer-reviewed, nor has it had any other value added to it by a publisher (such as formatting, copyright, technical enhancement etc.).

Authors can share their preprints anywhere at any time. Preprints should not be added to or enhanced in any way in order to appear more like, or to substitute for, the final versions of articles however authors can update their preprints on arXiv or RePEc with their Accepted Author Manuscript (see below).

If accepted for publication, we encourage authors to link from the preprint to their formal publication via its DOI. Millions of researchers have access to the formal publications on ScienceDirect, and so links will help users to find, access, cite and use the best available version. Please note that Cell Press, The Lancet and some society-owned have different preprint policies. Information on these policies is available on the journal homepage.

Accepted Author Manuscripts: An accepted author manuscript is the manuscript of an article that has been accepted for publication and which typically includes author-incorporated changes suggested during submission, peer review and editor-author communications.

Authors can share their accepted author manuscript:

- – immediately
    - via their non-commercial person homepage or blog
    - by updating a preprint in arXiv or RePEc with the accepted manuscript
    - via their research institute or institutional repository for internal institutional uses or as part of an invitation-only research collaboration work-group
    - directly by providing copies to their students or to research collaborators for their personal use
    - for private scholarly sharing as part of an invitation-only work group on commercial sites with which Elsevier has an agreement
- – after the embargo period
    - via non-commercial hosting platforms such as their institutional repository
    - via commercial sites with which Elsevier has an agreement

In all cases accepted manuscripts should:

- – link to the formal publication via its DOI
- – bear a CC-BY-NC-ND license - this is easy to do
- – if aggregated with other manuscripts, for example in a repository or other site, be shared in alignment with our hosting policy not be added to or enhanced in any way to appear more like, or to substitute for, the published journal article.

Published journal article (JPA): A published journal article (PJA) is the definitive final record of published research that appears or will appear in the journal and embodies all value-adding publishing activities including peer review co-ordination, copy-editing, formatting, (if relevant) pagination and online enrichment.

Policies for sharing publishing journal articles differ for subscription and gold open access articles:

Subscription Articles: If you are an author, please share a link to your article rather than the full-text. Millions of researchers have access to the formal publications on ScienceDirect, and so links will help your users to find, access, cite, and use the best available version.

Theses and dissertations which contain embedded PJAs as part of the formal submission can be posted publicly by the awarding institution with DOI links back to the formal publications on ScienceDirect.

If you are affiliated with a library that subscribes to ScienceDirect you have additional private sharing rights for others' research accessed under that agreement. This includes use for classroom teaching and internal training at the institution (including use in course packs and courseware programs), and inclusion of the article for grant funding purposes.

Gold Open Access Articles: May be shared according to the author-selected end-user license and should contain a CrossMark logo, the end user license, and a DOI link to the formal publication on ScienceDirect.

Please refer to Elsevier's posting policy for further information.

18. **For book authors** the following clauses are applicable in addition to the above: Authors are permitted to place a brief summary of their work online only. You are not allowed to download and post the published electronic version of your chapter, nor may you scan the printed edition to create an electronic version. **Posting to a repository:** Authors are permitted to post a summary of their chapter only in their institution's repository.

19. **Thesis/Dissertation**: If your license is for use in a thesis/dissertation your thesis may be submitted to your institution in either print or electronic form. Should your thesis be published commercially, please reapply for permission. These requirements include permission for the Library and Archives of Canada to supply single copies, on demand, of the complete thesis and include permission for Proquest/UMI to supply single copies, on demand, of the complete thesis. Should your thesis be published commercially, please reapply for permission. Theses and dissertations which contain embedded PJAs as part of the formal submission can be posted publicly by the awarding institution with DOI links back to the formal publications on ScienceDirect.

Elsevier Open Access Terms and Conditions

You can publish open access with Elsevier in hundreds of open access journals or in nearly 2000 established subscription journals that support open access publishing. Permitted third

party re-use of these open access articles is defined by the author's choice of Creative Commons user license. See our open access license policy for more information.

Terms & Conditions applicable to all Open Access articles published with Elsevier:

Any reuse of the article must not represent the author as endorsing the adaptation of the article nor should the article be modified in such a way as to damage the author's honour or reputation. If any changes have been made, such changes must be clearly indicated.

The author(s) must be appropriately credited and we ask that you include the end user license and a DOI link to the formal publication on ScienceDirect.

If any part of the material to be used (for example, figures) has appeared in our publication with credit or acknowledgement to another source it is the responsibility of the user to ensure their reuse complies with the terms and conditions determined by the rights holder.

Additional Terms & Conditions applicable to each Creative Commons user license:

CC BY: The CC-BY license allows users to copy, to create extracts, abstracts and new works from the Article, to alter and revise the Article and to make commercial use of the Article (including reuse and/or resale of the Article by commercial entities), provided the user gives appropriate credit (with a link to the formal publication through the relevant DOI), provides a link to the license, indicates if changes were made and the licensor is not represented as endorsing the use made of the work. The full details of the license are available at http://creativecommons.org/licenses/by/4.0.

CC BY NC SA: The CC BY-NC-SA license allows users to copy, to create extracts, abstracts and new works from the Article, to alter and revise the Article, provided this is not done for commercial purposes, and that the user gives appropriate credit (with a link to the formal publication through the relevant DOI), provides a link to the license, indicates if changes were made and the licensor is not represented as endorsing the use made of the work. Further, any new works must be made available on the same conditions. The full details of the license are available at http://creativecommons.org/licenses/by-nc-sa/4.0.

CC BY NC ND: The CC BY-NC-ND license allows users to copy and distribute the Article, provided this is not done for commercial purposes and further does not permit distribution of the Article if it is changed or edited in any way, and provided the user gives appropriate credit (with a link to the formal publication through the relevant DOI), provides a link to the license, and that the licensor is not represented as endorsing the use made of the work. The full details of the license are available at http://creativecommons.org/licenses/by-nc-nd/4.0. Any commercial reuse of Open Access articles published with a CC BY NC SA or CC BY NC ND license requires permission from Elsevier and will be subject to a fee.

Commercial reuse includes:

- – Associating advertising with the full text of the Article

- – Charging fees for document delivery or access
- – Article aggregation
- – Systematic distribution via e-mail lists or share buttons

Posting or linking by commercial companies for use by customers of those companies.

20. **Other Conditions**:

v1.9

Questions? customercare@copyright.com or +1-855-239-3415 (toll free in the US) or +1-978-646-2777.